Journal of METALS

VOL. 188, NO. 12 DECEMBER, 1950

Published to provide a continuing, authoritative, and up-to-date record of technologic, engineering, and economic progress in all branches of the metals industry by the

Metals Branch
American Institute of Mining and
Metallurgical Engineers, Inc.
29 West 39th Street, New York 18

* * *

THOMAS E. LLOYD
Manager of Publications
Editor, Journal of Metals

* * *

JAMES A. STANGARONE
Advertising Manager

* * *

HAROLD N. UNDERHILL, ALVIN S. COHAN, DOROTHY G. GARRETT, MARGARET BAGG, *Assistant Editors:* GRACE PUGSLEY, *Production Manager:* WALTER J. SEWING, *Assistant.*

* * *

OFFICERS, AIME

D. H. McLaughlin	*President*
A. B. Kinzel	*Vice President*
Philip Kraft	*Vice President*
R. W. Thomas	*Vice President*
C. H. Benedict	*Vice President*
C. V. Millikan	*Vice President*
Andrew Fletcher	*VP & Treasurer*

* * *

AIME STAFF

E. H. Robie	*Secretary*
H. A. Maloney	*Asst. Treasurer*
E. J. Kennedy, Jr.	*Asst. Secretary*
Ernest Kirkendall	*Asst. Secretary*
H. Newell Appleton	*Asst. to Secretary*

* * *

Technical Publications Committee

F. B. Foley	*Chairman*
E. J. Kennedy, Jr.	*Secretary*

* * *

Auxiliary Publications Committee Chairmen

F. N. Rhines	*IMD*
F. M. Washburn	*ISD*
Philip T. Stroup	*EMD*

* * *

The AIME Publishes:
Mining Engineering
Journal of Metals
Journal of Petroleum Technology

COVER

Charging scrap into the No. 7, 100-ton electric furnace at the Steel and Tube Division's plant of Timken Roller Bearing Co., Canton. This is the largest electric furnace in the United States, was built in 1929 by Timken and has been in continuous operation since that time. It is oval in shape and is actually two furnaces placed side-by-side with the common wall removed.

FEATURES AND NEWS

Journal of Metals REPORTER **1423**
"Drift of Things" **1425**
Engineering Employment Service **1413**
Authors in This Issue **1411**
New Products and Literature **1418**
Coming Meetings **1514**
Electric Furnace Steel Program **1429**
News of Industry **1427**
AIME News **1509**
Personals and Obituaries **1515**

TECHNICAL ARTICLES

Practical Aspects of Tool Steel Melting *C. F. Sawyer, Jr.* **1433**
Today's Scrap—Availability, Condition and Contamination *R. W. Farly, R. J. McCurdy* **1435**
Deoxidizing in the Ladle With Carbortam *W. O. Igelman, D. A. Finch* **1439**
Control of Refractory Materials *C. E. Sumpter* **1442**
X-ray Examination of Small Parts **1443**
Measurement of Low Order Ductility *N. P. Pinto* **1444**

TRANSACTIONS

Production of Malleable Zirconium on a Pilot-Plant Scale *W. J. Kroll, W. W. Stephens, H. P. Holmes* **1445**
Torsion Texture of Copper *W. A. Backofen* **1454**
Lattice Parameters of Magnesium Alloys *R. S. Busk* **1460**
Effect of Ferrite Grain Structure Upon Impact Properties of 0.80 Pct Carbon Spheroidite *M. Baeyertz, W. F. Craig, Jr., E. S. Bumps* **1465**
Crystal Structures and Transformations in Indium-Thallium Solid Solutions *L. Guttman* **1472**
Crystallography of Cubic-Tetragonal Transformation in the Indium-Thallium System *J. S. Bowles, C. S. Barrett, L. Guttman* **1478**
Alloys of Copper and Iron *C. S. Smith, E. W. Palmer* **1486**
Kinetics of Solid Phase Reactions in Oxide Films on Iron—The Reversible Transformation At or Near 570°C *E. A. Gulbransen, R. Ruka* **1500**

Published the first day of each month by the American Institute of Mining and Metallurgical Engineers, Inc., 29 West 39th Street, New York 18, N. Y. Telephone: PEnnsylvania 6-9220. Subscription $8 per year for non-AIME members in United States and North, South and Central America; $9, foreign; $6 for AIME members, or $4 in combination with a subscription to *Mining Engineering* or the *Journal of Petroleum Technology*. Single copies, 75 cents; special issues, $1.50 . . . The AIME is not responsible for any statement made or opinion expressed in its publications. . . . Copyright 1950 by the American Institute of Mining and Metallurgical Engineers, Inc. . . . Registered cable address, AIME New York . . . Indexed in Engineering Index, Industrial Arts Index and Chemical Abstracts . . . Reentered as second-class matter Sept. 21, 1949, at the post office at New York, N. Y., under the Act of March 3, 1879.

Authors In This Issue

Charles F. Sawyer, Jr. (p. 1433) came to Vanadium Alloys Steel Co., Latrobe, Pa., via a roundabout route. Born in Keokuk, Iowa, he attended high school in Pasadena, Calif., and college at Oklahoma A&M where he graduated with a B.S.

C. F. Sawyer, Jr.

H. P. Holmes (p. 1445), a graduate of Oregon State College with a B.S., is a native of Concord, Neb. He has been with the U. S. Bureau of Mines, Albany, Ore., as metallurgist since 1945; but was with Balatoc Mining Co., in the Philippines prior to that time.

W. W. Stephens (p. 1445), born at Arden, Nev., went to high school at Denver, Colo., and was graduated with an E.Met. from Colorado School of Mines. He worked as metallurgical observer for Colorado Fuel & Iron Corp., Pueblo, Colo.; chemist for American Smelting & Refining Co., Denver; and since 1941 has been with the U. S. Bureau of Mines at Salt Lake City, Utah, Boulder City, Nev., Redding, Calif., and now Albany, Ore. He co-authored with W. J. Kroll on zirconium production, presented at the 1950 AIME annual meeting.

H. P. Holmes

Walter A. Backhofen (p. 1454) is from Rockville in the Nutmeg state. He went to Rockville high school and later was graduated with an Sc.D. from Massachusetts Institute of Technology. He was an instructor, a research associate, and is now assistant professor at MIT.

E. S. Bumps (p. 1465) is a globe-trotter. He was born in Springfield, Mass., went to Rutland, Vt., high school, and got his B.S. at Missouri School of Mines. From 1943 to 1948 he worked as mill metallurgical observer and research metallurgist for Republic Steel Corp., and since 1948 has been in Illinois as associate metallurgist in the ferrous metals section of Armour Research Foundation. He likes golf, bowling, and photography.

W. A. Backofen

J. S. Bowles (p. 1478) was born in Yarrowonga, Victoria, Australia, and graduated from the University of Melbourne with an M.S. He has been lecturer in metallography at University of Melbourne; on a two-year research fellowship at the Institute of Metals, University of Chicago; and is now research officer for the Commonwealth Scientific & Industrial Research Organization at University of Melbourne.

Roswell Ruka (p. 1500) is a native of Wisconsin, born at Boscobel and graduating from University of Wisconsin with a B.S. and an M.S. He worked for two years at Westinghouse Research Labs at East Pittsburgh, and is now at University of Michigan, Ann Arbor. Tennis, golf, and fishing are his hobbies.

Roswell Ruka

Lester Guttman (p. 1472). See Journal of Metals, October, 1949.

C. S. Barrett (p. 1478). See Journal of Metals, September, 1949.

M. Baeyertz (p. 1465). See Journal of Metals, February, 1950.

W. F. Craig, Jr. (p. 1465). See Journal of Metals, February, 1950.

R. S. Busk (p. 1460). See Journals of Metals, July, 1950.

W. J. Kroll (p. 1445). See Journal of Metals, November, 1950.

C. S. Smith (p. 1486). See Journal of Metals, October, 1949.

Earl W. Palmer (p. 1486). See Journal of Metals, December, 1949.

E. A. Gulbransen (p. 1500). See Journal of Metals, October, 1949.

New Products, Services and Information....

Products and services recently announced are described here. Also, new publications offered free by producers servicing the metalworking industry are listed.

For further information on any product or for your copies of the free publications, fill in the coupon below and send it to the *Journal of Metals*.

1—AB MOUNTING PRESS: For the metallurgist comes a streamlined AB mounting press with qualities of precision workmanship, speed, and convenience in the preparation of metallurgical specimens in plastic mounts. Bakelite mounts are produced in 2½ to 3½ min and may be used with 1 in., 1¼ in. or 1½ in. molds. Prices, $380, $400 and $430. *Buehler Ltd.*

2—GLOVE RECONDITIONING: A work glove reconditioning service is offered by the *U. S. Industrial Glove Corp.* It includes complete renovation, sanitizing and packaging of all types of worn fabric and leather gloves and protective clothing. Many gloves can be salvaged several times. Reconditioned gloves are preferred because of their pliability and comfort. A free trial plan is available.

3—AIR-FED HOOD: For lead disking, grinding operations, light sand blasting and paint spraying, the #600 Air-Fed Hood, approved by the U. S. Bureau of Mines under "Class C" Respirator, is available. To eliminate bulk and rigidity and to provide comfort and full freedom of movement, the hood is made of a lightweight, flexible, rubberized fabric. Incoming air is brought in noiselessly. The hood protects the head, shoulders, chest, and back against flying particles. It is also waterproof and acid-resistant. *Chicago Eye Shield Co.*

4—STRETCH METER: Percentage stretch or shrinkage of materials being processed through rolls turning at different speeds is indicated and automatically recorded by the new Tag-Weston recording speed-ratio tachometer offered by *Weston Electrical Instrument Corp.* It provides a continuous record of roll speed ratio for metal-rolling. Various calibration ranges and chart graduations are available.

5—BARREL TILTER: The new GS Safety tilter with pouring spout provides a safe, fast and convenient method of draining acids and other liquids from stainless steel barrels. Flow capacity is 5 gal per min. Tilter #11, complete with the safety air vent pouring spout, costs $34.50, shipped on open account. *General Scientific Equipment Co.*

Journal of Metals December
29 West 39th St.
New York 18, N. Y.

Please send me
More Information ☐
Free Literature ☐
Price Data ☐
on items indicated.

1	2	3	4	5	6	7	8	9	10
11	12	13	14	15	16	17	18	19	20
21	22	23	24	25	26	27	28	29	30
31	32	33	34	35	36	37	38	39	40

Name .... Title................
Company ....
Street ....
City and Zone .... State...............

6—ALUMINUM ROOFING: Greater strength and rigidity than ordinary aluminum are claimed for the New Holland cross-crimp aluminum roofing. The additional crimping prevents sagging and brings strength up to 28 gage galvanized roofing. It has less glare and is more attractive looking. *New Holland Metals Co.*

7—MARKING STAINLESS: *Stainless Ornamentals, Inc.*, announces a method of applying permanent markings and designs on stainless steel. Called Ateen-ate, the process treats stainless steel to produce markings in contrast to the lustrous surface of stainless. Uses are both decorative and utilitarian.

8—STRIP POSITIONERS: *Askania Regulator Co.* offers optimum solutions to web and strip handling problems. A new edge postioning control is a simplified, rugged, efficient, and accurate method of controlling the position of a moving web or strip using Askania hydraulic methods. Installations for metallic and nonmetallic webs have successfully withstood the test of time. Accuracies of ±0.0005 in. have been obtained.

9—ATMOSPHERE CONTROL: For carbon restoration, hardening, annealing, normalizing, and carburizing homogeneously or with controlled surface carbon *Leeds & Northrup Co.* has introduced the new "Series H" Homocarb with Microcarb atmosphere control. The heart of Microcarb control is the Carbohm, a unique primary element located in the work chamber that responds to the carbon potential of the atmosphere as does the steel being heat-treated. To users, it means that closer specs can be met more easily.

10—BRONZE PRODUCTS: To withstand heavy crushing loads and increase wearing life from three to five times, Non-Gran bronze parts are recommended. Non-Gran is an alloy having a non-granular structure, resulting from the use of virgin metals and a special melting process that assures positive amalgamation of the copper and tin. *American Non-Gran Bronze Co.*

11—SELF-CLEANING NOZZLE: Only a push and a pull are necessary to clean the McKinney self-cleaning spray nozzle. Full cone coverage over a pressure range to 150 lb is assured. At higher pressures it produces semi-fog and fog. The nozzle section is heavy cast bronze, with cast bronze moving parts packed in grease and enclosed in a seperate compartment of the body. *S. P. Kinney Engineers, Inc.*

12—PRECISION INDICATOR: The Brown ElectroniK precision indicator provides fast and accurate readings in an indicating type of instrument. When the object measured is subject to low temperatures, the operator switches in the proper measuring circuit and reads the temperature on the lower range scale. When the object reaches the higher temperatures, the other measuring circuit is closed and an accurate reading is obtained on the higher range scale. *Minneapolis-Honeywell Regulator Co.*

13—X-RAY GAGE: *Sheffield Corp.* announces a new simplified "50" Series Measurays X-ray gage for noncontact continuous or intermittent thickness measuring. Two thickness setting dials eliminate the need for gage-setting masters and master indexing mechanisms. The gage does not require an engineer to operate. Thickness setting dials enable it to be applied where frequent and quick changes of gage are necessary. X-ray tubes cost 75 pct less and have longer life.

14—PORTABLE WELDER: A new silicone-insulated, portable ac welder, equipped with automatic Hot Start control has been announced by the *General Electric Co.* Known as 6WK30J series, it is one of the first standard ac welder lines commercially available incorporating silicone insulation. Instant arc striking without any manual adjustment is provided by Hot Start automatic control.

15—HEAVY-DUTY CONTACTOR: *Westinghouse Electric Corp.* announces a new, complete and uniform line of heavy-duty Type M, dc contactors in all standard NEMA ratings 25 to 2500 amp. It is an extension of their 25- and 50-amp sizes. Copper current-carrying parts are silver plated for low contact resistance.

16—STRIP GAGE: A new electronic gage has been developed by *General Electric Co.* for continuously indicating the width of hot strip steel. It is a non-contacting gage with the detector head mounted 15 ft above the stop, and no changes on the mill or mill table are required for installing. Accuracy is within $\pm\frac{1}{8}$ in. of actual strip width, with response within $\frac{1}{4}$ sec after strip passes detector. Strip temperatures of 1500°F or higher are handled, and power requirements are: 550 volt-amp., on 220, 440 or 550 volt, 3 phase, 60 cycle current.

17—SILICON CARBIDE: The chemical and physical properties of silicon carbide make it ideally suited to deoxidizing steel at a fraction of the cost of other agents, according to *Electro Refractories & Alloys Corp.* Price: $140 per ton in 50,000 lb carload or 20,000 lb truckloads; $150 per ton in less than a truckload. Freight allowed east of the Mississippi.

18—ELECTROSTATIC PRECIPITATOR: For applications where space is a problem, or where the precipitator must be mounted on top of a primary tower washer, the cylindrical vertical flow Koppers-Elex Precipitator, manufactured by the *Koppers Co., Inc.* is recommended. The entire cross sectional area of the unit is open to unrestricted gas flow, a modern and efficient design resulting in maximum cleaning per unit of area. Maintenance is minimized by auxiliary sprays provided for periodic total flushing.

* Contrary to accepted furnace lining methods, it has been found that the new "zebra" construction extends the life of furnace areas subject to wear. "Zebra" construction consists of alternate courses of silica and basic brick in wear areas such as roofs and backwalls, and the method is being tried by several large steel companies.

* Belt conveyors have been proposed for speeding up the flow of battlefield supplies. It has been suggested that supply bases be inter-connected with a system of conveyors that will run across countryside, releasing trucks for other uses as well as reducing traffic congestion. Construction speed; simplicity, economy, and speed of operation; increased capacity; and a less visible target are suggested advantages. A 30 mile conveyor manned by 100 men could carry as much as a fleet of 400 trucks manned by 1200 men, it is claimed.

* The first non-Atomic Energy Commission owned and operated nuclear reactor in the United States will be built by the Consolidated University of North Carolina, at Raleigh. It will use nuclear fuel loaned by AEC, and have a water or homogeneous type boiler. A solution of uranium in water will be the fuel.

* A new pressure-fed gun for spraying powdered metals and non-metallics uses an air blast to spray heated powders. The pressure fed system forces the powder into the nozzle, in contrast to present vacuum type guns. Air and propane gas pressures are preset, and the gun has a single lever control. Higher coating densities and no moving parts are claimed, and some 80 substances can be applied.

* Colorado Fuel & Iron Corp. will spend $26,200,000 in expansion of its Pueblo steel plant and nearby coal mines. The program includes two new 225-ton openhearth furnaces, rebuilding a blast furnace, a new high-speed 10-in. merchant mill, and a new coal mine that will be opened about 27 miles from Trinidad, Colo. This expansion is in addition to the $31 million spent on capital improvements at Pueblo during the past 5 years.

* A new resin-sand process for making foundry molds and cores promises to become one of the major markets for phenolic resins. The "Croning," "C," or "shell" process, as it is variously known, involves a resin-sand mixture of about 1:12. A metal pattern is first treated with silicone resin, as in greasing a pan, and then heated. The resin-sand mixture is then dumped on the pattern, a 1/8-in. coating builds up, and excess is shaken off. Mold and coating are then heated to set the plastic, cooled, and the shell is removed, forming a half mold. Cores are made by blowing the mixture into a heated split metal core box.

Two half molds and cores are assembled to make a full mold, embedded in a box of steel shot, and the metal is poured. No special venting is needed, and casting finish is excellent. Metal patterns are used over again. Sections as thin as 0.010 in. can be poured, and tolerances of 0.002 to 0.003 in. can be held on small castings. Sand requirements are reduced as much as 90 pct, and machining and cleaning costs are reduced by up to 80 pct.

* National Production Authority has stopped civilian use of columbium, used frequently in the manufacture of stainless steel welding electrodes and other items. Columbium will be directed into defense goods, particularly jet turbines. The principal sources are Nigeria and Belgian Congo, but the Norwegian Government just announced that it was opening a mine for soevite ores, from which columbium is recovered.

The
Drift of Things . . . . as followed by Edward H. Robie

IN the recent World War the special talents of engineers, like those of many other groups of professional men, to a large extent were wasted. Further, their training in colleges was interrupted, so that the postwar supply was inadequate. Only in the past year has the supply equaled the demand. Members of the national engineering societies often have suggested that some action should be taken looking to a better utilization of their talents in future emergencies. They are not trying to evade service to their country, although few people look forward to taking up a gun and going out to shoot somebody; but feel that it is to the country's interest as well as their own to serve where they can to the best advantage.

With the draft boards again picking up engineers for non-engineering military service, the problem has again become acute. Engineers Joint Council, representing the AIME, ASME, AIEE, ASCE, and AIChE, therefore has set up an Engineering Manpower Commission in which the American Society for Engineering Education also is represented. Its function is to develop "policies and procedures designed to secure the most effective use of engineering skills and experience in industry and government (civilian and military) during the emergency and to take necessary steps within the scope of EJC to put such policies and procedures into practice." Three AIME representatives, one for each Branch of Institute activities, are acting on this Commission: George B. Corless, of the Standard Oil Co. (N.J.); M. W. Lightner, Carnegie-Illinois Steel Corp.; and H. J. O'Carroll, Kennecott Copper Corp.

Similar groups have been working through the American Chemical Society, American Institute of Physics, and National Research Council, and study of the general problem has been undertaken by six committees advisory to General Hershey, director of Selective Service. These groups are reporting to the National Security Resources Board.

One is likely to underestimate the complexities of the problem and perhaps to overlook the political angles. Almost every skilled laborer thinks he can serve his country better than by carrying a gun, and why should any white collar man be deferred? Military service by practically every physically fit man was fundamental in the idea of the Selective Service Act. Even if the idea is accepted that outstanding engineers and scientists be treated differently from others, the problem remains of registering them, finding the proper thing for them to do, and deciding on a cutoff point.

The Commission has made no final report as this is written. but has agreed that fundamentally the long-range problem is twofold: (1) Maintaining an adequate supply of personnel of the necessary abilities, and (2) Assigning this personnel to the maximum advantage. The programs to be recommended also must take account of what is desirable on a large-scale or full mobilization basis, on a partial mobilization basis with medium military forces, and lastly on the present 3,000,000-man military force basis.

To maintain an adequate supply of engineers it is felt that deferment from military service should be granted to those wishing to enter engineering schools who show exceptional promise, and that definite percentages of this group be advanced each year to the sophomore, junior, and senior classes. 80, 85, and 90 pct, respectively, have been suggested, so that 61 pct of a well-selected freshman group would graduate. Fixed survival percentages would prevent any complaints of academic grade juggling.

For all-out mobilization, registration of all scientific and technical personnel, both men and women, between the ages of 18 and 65 has been proposed. Registrants would include those with bachelor or higher degrees in engineering, physics, and chemistry; those enrolled in training programs; those employed in these fields without regard to education; and perhaps highly skilled technicians. Selective Service would handle the registration. The group thus registered, after proper screening, would constitute a "National Technical Reserve" membership, which would be comparable to membership in the armed forces or in the military reserve. Some badge, or other indication of membership, would be desirable because of social pressures.

A "National Technical Manpower Board", with regional and specialized committees, would be set up to assign duties to those registered, including assignment to and withdrawal from the military forces.

For partial mobilization, it is proposed that this plan be adopted on a skeletonized basis, carrying assignments by the Board only to the extent necessary.

Admittedly, all this should have been done some time ago. But better late than never. It is hoped that some action may result, either immediately or after any required legislation can be enacted, which will prevent some of the waste of technological and professional manpower that until now has existed in this country in times of military emergency.

One Sixth Foreign

AIME members living outside of the United States frequently complain of the difficulty of securing American dollars with which to pay their dues. Efforts have been made to devise some means of easing the burden but so far without result. Deposits of foreign currency to the credit of the Institute cannot be utilized, for the expense of conducting the society has to be paid in American dollars.

As late as 1938, 25 pct of the membership resided in foreign lands. The exigencies of the last World War reduced this to 16 pct in 1944, and it has since remained at between 15 and 17 pct. The current figure is 16 pct, and of this group of foreign members, 23 pct are in South America, 21 pct in Canada, 20 pct in Europe, and 9 pct in Mexico. It seems, therefore, that some 2600 AIME members living in foreign countries still can secure American dollars, so the problem cannot be too acute. Many, of course, maintain balances in banks in this country, particularly American engineers employed abroad.

In the last Directory, Toronto has been displaced as the city outside of the United States (we hesitate to call it a foreign city) with the largest number of AIME members. In the 1948 Directory the 1-2-3 rank was Toronto, London, and Caracas. Caracas now takes the lead, with just 100 on the Institute rolls, thanks to the oil and mining activity in Venezuela.

M.I.T. Research Refutes Present Theories of Metal Behavior at Low Temperatures

Extreme cold has been the key to a new understanding of what makes steel really hard, Dr. James R. Killian, Jr., president of the Massachusetts Institute of Technology, told an audience of alumni and friends of the Institute at the University Club in Cleveland recently.

Recent studies at M.I.T. show that the atoms in steel can rearrange themselves in the process that makes steel hard even at the extremely low temperatures of liquid helium, —453°, 6° above absolute zero.

It appears that steel hardening takes place more completely at low temperatures than at any others. The new studies indicate that steel hardening is a cooperative shear-like sliding in which many atoms move in unison. It does not seem to be the result of individual shuffling movements by many atoms.

At extremely low temperatures, research indicates, large groups of atoms in steel participate in this sliding motion, and thus are transformed from austenite to martensite.

In some types of steel, the amount of hardening, measured by the amount of martensite formed, was found to increase from very little at room temperature to nearly 100 pct at the temperature of liquid helium. In other steels, hardening did not begin until the temperature dropped below —240°.

Cold working of steel, the process normally used at room temperature to increase hardness, is still more effective at these extremely low temperatures.

These principles are being applied in the manufacture of stainless steel, where the rolling operations designed to harden the metal are being carried out at temperatures below freezing. The larger implications of the research are in its contributions to the theory on the mechanism of steel hardening. Never before has an adequate understanding of this process been available.

The new theory on steel hardening has made possible, for the first time, quantitative predictions of the behavior of steel treated in specific processes. This, in turn, promises a more scientific approach in future improvements of steel processing.

New Jersey Zinc Starts Operating New Battery of Nine Vertical Retorts

New Jersey Zinc Co. (of Pa.) put into operation nine new vertical retorts at its Palmerton Plant, bringing the total to 43 retorts. The new battery incorporates new design features, which are the outgrowth of over 20 years of operating experience. The retorts are larger and are equipped with splash condensers of the type announced by the company in March, 1949. The result is a substantially increased capacity per retort, in the order of 25 pct, coupled with smoother operation and better condensation efficiency.

Two major improvements have been made in the firing of these retorts. In the old batteries, waste gases from the recuperators were passed through the cokers where the briquetted charge was coked before charging to the retorts. This limited the heavy recovery in the recuperators. The new battery is provided with a new type autogenous coker that permits completely independent operation of the retorts and cokers. A recuperator of new design is used, with a resultant fuel economy of over 15 pct as compared with the old style battery.

The new plant also embodies many other refinements in design, resulting in reduced labor costs and better operation.

Carnegie-Illinois Develops New High Strength Alloy Plate Steel

A group of new alloy steels, to be known as T-steels, has been announced by the Carnegie-Illinois Steel Corp., Pittsburgh. Carilloy T1 is a multiple-alloy plate steel, combining extremely high strength with excellent ductility and toughness, even at subzero temperatures. With almost double the strength of high-strength, low-alloy steels and almost triple that of ordinary welding grade structural steels, Carilloy T1 promises to effect considerable savings in applications of heavy steel members ½ in. thick and greater. It is at least two to three times as resistant to atmospheric corrosion as plain carbon steels.

This plate steel is furnished heat treated to a minimum yield strength of 100,000 psi. It maintains adequate toughness even at this high level of strength, and is suitable for application where extreme high strength and good weldability are required.

Welding does not adversely affect the properties of this steel, which requires no special preheating or postheating treatments in welding or gas-cutting operations beyond those normally used with ordinary structural steels. If low-hydrogen type electrodes are used, Carilloy T1 is not susceptible to underbead cracking. Electrodes that will develop the full strength of the T1 basic metal are available and should be used if 100 pct joint efficiency is needed.

No special equipment and procedures are required for fabrication. Bending or forming may be accomplished cold if sufficient power is available to overcome the high yield strength of Carilloy T1. If hot forming is necessary, the operation must be followed by heat treatment involving liquid quenching and tempering after forming. Necessary heat treatment information for this work is available.

Ordinary room temperature testing procedures will not predict adequately the behavior of welded structures under adverse conditions of restraint or when used at low temperatures. An extensive testing program was initiated, utilizing various tests to determine its tendency toward brittle failure under various conditions. Results of this program indicate that Carilloy T1 possesses excellent toughness under such conditions. This feature gives the user added insurance against brittle failure.

The unique properties of this new steel are obtained by blending multiple alloying elements, coupled with precision heat treatment. Carbon content is restricted to 0.18 pct max to promote ease of welding and gas cutting.

Congress to Act on Martempering Bills

Two bills were recently introduced in Congress to assist Richard F. Harvey in obtaining a patent on the heat treatment now known as Martempering. These are S3918, introduced in the US Senate on July 14, 1950 by Sen. T. F. Green of Rhode Island, and HR 9210, introduced in the US House of Representatives on July 20, 1950 by Congressman J. E. Fogarty of Rhode Island.

A patent application was filed on this heat treatment early in 1940. This relates to work previous to Mr. Harvey's present employment as metallurgist at the Brown & Sharpe Mfg. Co.

Conference Program

Wednesday 6:30 p.m.—Dec. 6 **Rooms 566-68-70**

Electric Furnace Steel Executive and Conference Committee

Annual Dinner and Business Meeting

All Chairmen of technical sessions are invited to attend.

Thursday 9:30 a.m. to 9:45 a.m.—Dec. 7 **Ballroom**

General Session

Welcoming Remarks

T. J. McLoughlin, Chairman, Committee for the Eighth Annual Conference.

Response

J. A. Bowers, Chairman, Electric Furnace Steel Executive Committee.

Announcements and Reports

Thursday 9:45 a.m. to 12:30 p.m.—Dec. 7 **Ballroom**

Acid and Basic Session on Raw Materials

Chairman:* *M. J. Meinen, Universal-Cyclops Steel Corp.
R. H. Frank, Chief Met., Bonney-Floyd Co.

Use of Iron Ore in Steel Making

Paper by John Arthur, Supt. of Melt., Crucible Steel Co. of America.

Formal discussion by A. K. Blough, Supt. No. 2 Melt Shop, Republic Steel Corp., and J. S. Marsh, Res. Engr., Bethlehem Steel Co.

Scrap—Availability, Present Physical Condition, Contamination

Paper by R. W. Farley and R. J. McCurdy, Supt. No. 2 Melt Shop, Republic Steel Corp., Chicago. JOURNAL OF METALS, December.

Formal Discussion by J. J. Green, Asst. Melt. Supt., Universal-Cyclops Steel Corp., and Ray Bromley, M. E. Solomon Co.

Slag Material and Slag Action in Basic Arc Furnaces

Paper by C. B. Post, Met., and D. G. Schoffstall, Melt Shop, Met., Carpenter Steel Co. Preprinted. JOURNAL OF METALS, November.

Formal Discussion by Leland Peterson, Asst. Supt. Melt. Alloy Steels, Timken Roller Bearing Co., and M. V. Healey, Met., General Electric Co.

Thursday 2 p.m. to 5 p.m.—Dec. 7 **Ballroom**

Basic Session On Continuous Casting

Chairmen:* *Norman I. Stotz, Pres., Braeburn Alloy Steel Corp.
E. C. Smith, Chief Met., Republic Steel Corp.

Mold Design, Casting Shape, Melting Practice and Refractories, Control of Process, Quality and Products, Typical Production Layouts

Paper by Isaac Harter, Jr., Engr. in Charge of Continuous Casting, Babcock & Wilcox Tube Co.

Film to be shown, and a Q. and A. period to be held by T. W. Ratcliff and G. G. Zipf, Babcock & Wilcox Tube Co.

Thursday 2 p.m. to 5 p.m.—Dec. 7 **Allegheny Room**

Acid Session On Oxidation Practice (Boil)

Chairman:* *C. W. Briggs, Tech. & Res. Dir., Steel Founders' Society of America

Ore Practice

Paper by F. J. Stanley, Works Mgr., McConway & Torley Corp.

Paper by W. L. Doyle, Fort Pitt Steel Casting Div., Pittsburgh Steel Foundry Corp.

Oxygen Practice

Paper by R. H. Jacoby, Met., Key Co.

Paper by J. H. Garrison, Chief Met., Oklahoma Steel Castings Co., Inc.

ANNUAL DINNER

Thursday, December 7

6:30 p.m.—Urban Room, Reception and Cocktail Party for dinner guests

7:00 p.m.—Ballroom, Annual Dinner

Toastmaster: Gilbert Soler, Vice-president, Mfg. Operations, Atlas Steels, Ltd., Welland, Ont.

Speaker: C. F. Hood, President, Carnegie-Illinois Steel Corp., Pittsburgh

Friday 9:30 a.m. to 12:30 p.m.—Dec. 8 Urban Room

Basic Session On Furnace Maintenance And Rebuilding

Chairmen: *J. H. Eisaman, Supt. No. 2 Electric Furnace Shop, Carnegie-Illinois Steel Corp. J. S. Marsh, Res. Engr., Bethlehem Steel Co.*

Bottom Building and Maintenance

Paper by H. C. Bigge, Supt. Open Hearth, Bethlehem Steel Co.

Top Charging and High Voltages in Lining Life and Repair

Paper by R. J. McCurdy, Supt. No. 2 Melt Shop, Republic Steel Corp.

Types of Roof Construction

Paper by G. C. Olson, Melt. Supt., Atlas Steels, Ltd.

Relining Time

Paper by C. F. Stanley, Supt. Extractive Met. Div., Armco Steel Corp.

Materials Used and Specifications

Paper by Charles Sumpter, Genl. Supvr., Ceramic Div., Carnegie-Illinois Steel Corp. Preprinted. JOURNAL OF METALS, December.

Applications of Resistance Indicator to Electric Arc Furnaces

Paper by Alex Sherman, Prod. Mgr., Sherman Electric Co.

Panel and floor discussion follow each paper.

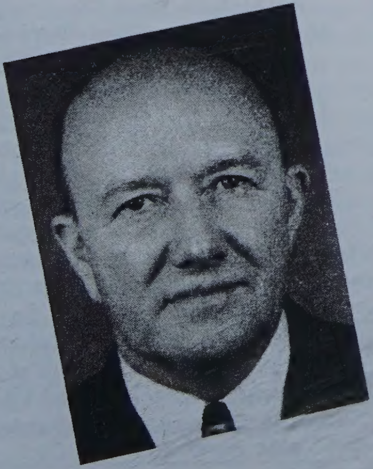

C. F. Hood, Speaker at the Dinner

Gilbert Soler, Toastmaster for the Annual Dinner

Friday 9:30 a.m. to 12:30 p.m.—Dec. 8 Monongahela Room

Acid Sessions On Experience With Special Deoxidizers

Chairmen: *C. E. Sims, Asst. Dir., Battelle Memorial Institute R. H. Jacoby, Met., The Key Co.*

Investigation of New Special Deoxidizers

Paper by C. G. Mickelson, Res. Met., American Steel Foundries. Preprinted. JOURNAL OF METALS, November.

The Effect of Various Deoxidation Treatments Upon Type of Inclusion and Properties of Class B Steel

Paper by Clyde Wyman, Chief Met., Burnside Steel Foundry Co.

Effects of Various Deoxidizers on the Structures of Nonmetallic Inclusions and Mechanical Properties of Cast Steels

Paper by E. A. Loria, Senior Engr., Res. and Dev. Dept., The Carborundum Co.

Further Studies on Higher than Normal Silicon Steels

Paper by J. A. Bowers, Melt. Supt., American Cast Iron Pipe Co.

Use of Carbortam as a Deoxidizer in Acid Electric Furnaces

Paper by W. O. Igelman, Met., and D. A. Finch, Head Melter, National Malleable & Steel Casting Co. Preprinted. JOURNAL OF METALS, December.

Friday 2 p.m. to 5 p.m.—Dec. 8 Urban Room

Basic Session On Melting Practice

Chairmen: *Leland Peterson, Asst. Melt. Supt., Timken Roller Bearing Co. Joseph Mravec, Melt Shop Met., Timken Roller Bearing Co.*

Metallurgy

Paper by Charles Taylor, Supervising Met., Armco Steel Corp.

Tool Steels

Paper by Charles Sawyer, Jr., Mill Met., Vanadium Alloys Steel Corp. Preprinted. JOURNAL OF METALS, December.

Simple and Compound Steels

Paper by Arthur Blough, Melt. Supt., Republic Steel Corp.

Rimming and Carbon Steels

Paper by Paul Lindberg, Jr., Melt. Sup., McLough Steel Corp.

Induction Melting

Paper by Ray Wilcox, Tech. Dir., Michigan Steel Castings Co. Preprinted. JOURNAL OF METALS, November.

Stainless Steels

Paper by Al Ogan, Asst. Melt. Supt., Duquesne Works, Carnegie-Illinois Steel Corp.

Panel and floor discussion follow each paper.

Friday 2 p.m. to 5 p.m.—Dec. 8 **Monongahela Room**

Acid Session On Temperature Control

Chairmen: ***Victor E. Zang, V.P. Res., Unitcast Corp. H. H. Blosjo, Chief Met., Minneapolis Electric Steel Casting Co.***

Production Control of Molten Steel Temperature and Its Effect on Steel Casting Quality

Paper by Charles A. Faist, Res. Met., Burnside Steel Foundry Co. Preprinted.

Formal Discussion by G. A. Lillieqvist, Res. Dir., American Steel Foundries; E. H. Berry, Met., Dodge Steel Co.; Warren Hart, Supt. Electric Furnace Bldg., Ford Motor Co.; J. A. Bowers, Melt. Supt., American Cast Iron Pipe Co.; and H. H. Johnson, Chief Met., National Malleable & Steel Castings Co.

Saturday 9:30 a.m. to 12:30 p.m.—Dec. 9 **Urban Room**

Educational Session

Chairmen: ***H. E. Phelps, Electric Furnace Supt., Rotary Electric Steel Co. C. H. Lorig, Asst. Div., Battelle Memorial Institute.***

Alloy Steels-A Picture of Controlled Production

Motion Picture.

Effect of Residuals and Their Removal

Paper by J. S. Marsh, Res. Engr., Bethlehem Steel Co.

Question Period

Panel of Experts: J. H. Eisaman, Supt. No. 2 Electric, Carnegie-Illinois Steel Corp.; H. E. Phelps, Electric Furnace Supt., Rotary Electric Steel Co.; C. H. Lorig, Asst. Dir., Battelle Memorial Institute; H. H. Blosjo, Chief Met., Minneapolis Electric Steel Castings Co.; W. S. Debenham, Res. Assoc., Carnegie-Illinois Steel Corp.; Samuel Arnold, III, Consult. Engr.; and Gerhard Dirge Prof. Met. Engrg., Carnegie Institute of Technology.

Electric Furnace Steel Executive Committee

J. A. Bowers, Chairman *Melting Supt., American Cast Iron Pipe Co., Birmingham*

Norman I. Stotz, Past Chairman *President, Braeburn Alloy Steel Corp., Braeburn, Pa.*

Ernest Kirkendell, Secretary

H. H. Blosjo, *Metallurgist, Minneapolis Electric Steel Casting Co., Minneapolis*

C. W. Briggs, *Technical & Research Director, Steel Founders Society of America, Cleveland.*

W. M. Farnsworth, *Asst. District Manager, Republic Steel Corp., Massillon, Ohio*

Frank Garratt, *Vice President & Technical Director, Universal - Cyclops Steel Corp., Bridgeville, Pa.*

J. P. Gill, *Exec. Vice President, Vanadium Alloy Steel Co., Latrobe*

M. E. Goetz, *Asst. Vice President, Charge of Operations, Republic Steel Corp., Cleveland*

Charles Locke, *Metallurgical Engineer, Armour Research Foundation, Chicago*

C. E. Sims, *Asst. Director, Battelle Memorial Institute, Columbus*

H. F. Walther, *Melting Superintendent, Timken Roller Bearing Co., Canton*

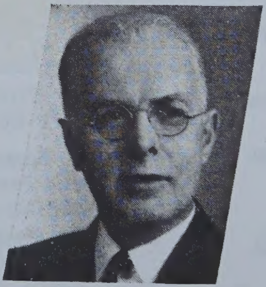

T. J. McLoughlin

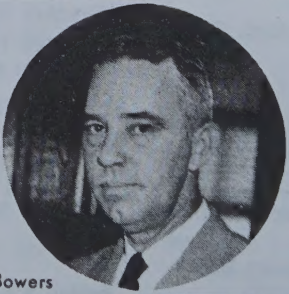

J. A. Bowers

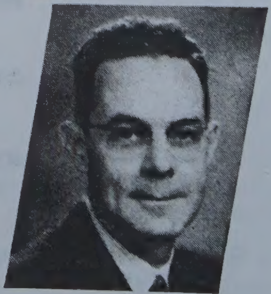

R. H. Frank

Local Committee On Arrangements

D. B. Baxter, Chairman
A. Bickell
G. A. Brunner
J. W. Harvey
R. K. Kulp

Committee for the Eighth Conference

T. J. McLoughlin, Chairman, *Asst. to Vice President, Charge of Operations, Carnegie - Illinois Steel Corp.*

R. H. Frank, Vice-Chairman *Chief Metallurgist, Bonney-Floyd Co.*

J. Alfred Berger, *Molybdenum Corp. of America.*

F. W. Brooke, *Vice-President, Swindell - Dressler Corp.*

Gerhard Derge, *Professor Metals Research Lab., Carnegie Institute of Technology*

J. H. Eisaman, *Superintendent No. 2 Electric Furnace, Carnegie - Illinois Steel Corp.*

John Juppenlatz, *Chief Metallurgist, Lebanon Steel Foundry*

Floyd Lemmon, *Asst. Plant Superintendent, Ohio Steel Foundry Co.*

J. S. Marsh, *Research Engr., Bethlehem Steel Co.*

M. J. Meinen, *Steel Works Superintendent, Crucible Steel Co. of America*

C. B. Post, *Metallurgist, Carpenter Steel Co.*

Alden Safford, *Melter, Chapman Valve Mfg. Co.*

Gilbert Soler, *Vice President Manufacturing Operations, Atlas Steels Ltd., Welland, Ontario*

C. T. Stowe, *Engineer, Lavino & Co., Philadelphia*

R. J. Wilcox, *Chief Met., Michigan Steel Casting Co.*

Clyde Wyman, *Met., Burnside Steel Foundry Co.*

Practical Aspects of Tool Steel Melting

Taking a spoon sample for chemical analysis

by Charles F. Sawyer, Jr.

SINCE the first World War, rapid strides have been made in melting tool steels in the basic electric arc furnace. Prior to that time the crucible melting process was considered to be the only satisfactory method of melting steels of the high quality required for tools used to cut, shape or form other materials. Once the basic arc method was tried, it became apparent that because of its increased flexibility and economy, the arc furnace eventually would displace the crucible process as a means of melting tool steels.

The development of rapid, accurate analytical methods and the evolution of complex, highly alloyed steels for tools and dies now make mandatory a versatile melting unit such as the basic arc furnace. Even plain carbon tool steels are made to such rigid specifications of hardenability, cleanliness, and grain size that melting in the electric arc furnace is almost a necessity.

A well constructed furnace is the first step in melting quality steel of any type. The furnaces at the Vanadium-Alloys Steel Co. are constructed of heavy duty silica brick in the walls and roof with a rammed bottom of rice magdolite mixed with tar and pitch. The oil coated ramming bottom refractories have not given satisfactory service in these furnaces for the original bottom and do not seem to be as suitable for patching as the uncoated bottom refractories. In certain hot spots in the furnace walls, as between the two doors opposite the tap hole, magnesite bricks are used.

These furnaces are completely rebuilt, except for the brickwork under the bottom, each time any one of the three components—bottom, sidewalls or roof—must be replaced. Experience has shown this practice to be the most economical over a period of time. A furnace campaign is from 125 to 175 heats.

Given a basic electric arc furnace and a well trained crew, the first consideration will be the charge. This charge is made up in such a way that melting will be as rapid as possible and the composition on melting will approximate the desired final composition as closely as practicable. To this end it is necessary to know the composition of all the materials used to make up the charge. Scrap is purchased only from known reliable sources so that sampling and analyzing incoming shipments does not involve a disproportionate outlay. Suitable handling facilities must exist in the plant to avoid mixups after the scrap has been properly identified.

The furnace is charged by placing the necessary limestone on the bottom, covering this with the heavy scrap such as hot tops, ingot butts and billet crops, and following with the lighter scrap on top. Any necessary oxides of alloying elements or slag making materials such as burnt lime are placed at about door level so that they will be among the first part of the charge to melt. This gives a slag cover to help prevent undue oxidation during melting. In the grades which are not slagged off, the amount of these slag making constituents cannot be too high a percentage of the charge or else the large volume of slag resulting will unnecessarily prolong the heat time. The oxides of alloying elements, such as molybdenum oxide in the molybdenum types of high speed

---

Charles F. Sawyer, Jr., is Plant Metallurgist for Vanadium-Alloys Steel Co., Latrobe, Pa. This paper will be presented at the Electric Furnace Steel Conference, Pittsburgh, Dec. 7 to 9, 1950.

Bins are used for storing scrap of varying chemical analysis

steels, are always mixed with the reducing materials, calcium carbide and ferrosilicon, in order that the desired metal be reduced into the steel during melting.

Most of the highly alloyed types of tool steel are dead melted. Steels such as M-2 and 18-4-1 of nominal chemical composition, as shown in Table I, are not slagged off after meltdown except for the occasional heat that melts with an excessive slag volume. When this happens, the slag is turned from oxidizing to reducing before removing the excess. Thus the chromium and vanadium which have been oxidized during melting are not lost. Turning more than a normal amount of slag increases the furnace time per heat and should be avoided.

The low carbon highly alloyed hot work die steels of nominal chemical compositions present problems not encountered with the higher carbon grades. The type of slag that results on melting down these steels is thin and oily appearing and it is uneconomical to finish the heat without slagging off and rebuilding a proper slag. These steels are dead melted the same as the high speed types but the carbon content is about 0.35 pct. The charge must be properly calculated to melt at or slightly below the correct carbon content for finishing the heat since boiling down the carbon will result in a substantial loss of tungsten as well as chromium and vanadium. Diluting the bath with low carbon scrap is obviously limited by the capacity of the furnace.

In the finishing slag on these hot work die steels, calcium carbide must be used as the reducing agent because of the carbon pickup associated with the use of coke. The melter will also be cautious in the addition of calcium carbide in order that the slag does not turn past a white into a gray carburizing slag with the attendant chance of carbon pickup.

Table I—Nominal Chemical Compositions of High Speed and Hot Work Die Steels

				Percent			
Grade	C	Si	Mn	W	Mo	Cr	V
High Speed Steels							
18-4-1	0.70	0.32	0.20	18.00	—	4.00	1.00
M-2	0.83	0.30	0.25	6.35	5.00	4.20	1.90
Hot Word Die Steels							
9 Pct W	0.33	0.30	0.20	9.75	—	3.50	0.45
14 Pct W	0.26	0.25	0.25	14.00	—	3.50	0.50
12 Pct W, 12 Pct Cr	0.32	0.50	0.35	12.00	—	12.00	1.05

Some of the high carbon grades, such as the 2.25 pct carbon, 12.0 pct chromium type, must be slagged off only because the amount of carbon addition necessary is too much to be obtained by the use of pig iron. The carbon is added in the form of crushed electrodes and stirred into the bath before the new slag making materials are added. The new slag is made up of burnt lime, sand and fluorspar which is allowed to melt before the reducing agents, coke or carbide are added.

During the refining stage, it is necessary to rabble the heats frequently to lessen the possibility of stratification of the bath and also to bring about an increased contact between the molten metal and the reducing slag. Thus equilibrium conditions between slag and metal are more nearly attained, and spoon tests taken to judge the temperature and chemical analysis of the molten metal are more representative.

Any large additions of alloying elements to the bath such as chromium in the 12 pct chromium grades must be preheated if heat times are to be kept within reason. Final additions of ferrotungsten always present a problem because of the high melting point of the alloy. By preheating, using fines, and allowing as much time as possible between the addition and tapping, the possibility of finding small bits of undissolved ferrotungsten in the finished bars will be obviated. By recovering all possible alloying elements from the charge, final additions are kept as small as possible. Ladle additions of anything but small amounts of deoxidizing alloys are avoided.

The tapping temperature is important but is hard to assess in its relative value with the many other variables affecting quality and recovery. When dealing with steels ranging in carbon content from 0.25 to 2.25 pct and alloy contents as high as 48.0 pct, a considerable range of tapping temperatures is encountered. This range will be from about 2500° to 2850°F as indicated by the blowpipe type of measurement.

The temperature at which the ingots are cast is closely related to the temperature at which the steel is tapped. Holding in the ladle for a temperature drop is limited by the extremely erosive action of the reducing slag on the ladle and stopper rod refractories. In addition, the fluidity of some of the highly alloyed grades decreases rapidly with decreasing temperature. The fluidity depends upon composition and will vary between grades even when teeming is done at the proper temperature for each grade. It is necessary to cast tool steels hot enough to give a good ingot surface or the further processing of the ingots will show unduly low recoveries. The better the ingot surface, the lower the incidence of corner cracking during hammer cogging, and the higher the overall recovery. Casting too hot will increase the occurrence of ingots that stick in the molds and shortens mold life appreciably.

Melting tool steels to obtain the highest quality possible and still maintain a reasonable recovery is an exacting task. The many grades involved, each with its own peculiarities, calls for the closest attention possible to details. Every advantage must be taken to make the melting less of an art and more of a science.

Today's Scrap— Availability, Condition and Contamination

by
Ralph W. Farley
and
Ray J. McCurdy

ALTHOUGH the subject of scrap for electric furnaces often has been discussed at this conference, it is sufficiently important to warrant inclusion again.

To mention, in review, a few of the previous discussions: George A. Barker, Jr.[1] in 1945 gave the definition for the *ideal charge*, and broke down the problem into three main divisions: (a) Segregation of the various analyses; (b) Preparation for charging; (c) Method of charging. Preparation of scrap for fast melting was discussed by Samuel D. Gladding[2] in 1946. He set forth the following objectives: (a) Make the scrap chargeable by proper sizing. (b) Raise the density of the scrap. (c) Remove extraneous or harmful material.

Stanley M. Kaplan[3] in 1947 discussed problems in supplying scrap, pointed out the importance of educating the scrap producer as well as the collector and dealer, and touched upon the efforts then getting under way to bring into the market large tonnages held by divisions of the Federal Government. At the same meeting, Edwin C. Barringer,[4] in a paper read by L. H. Krieger, sketched the recent history of scrap movements, and explained the loss by war of 124,000,000 gross tons of potential scrap between 1941 and 1945. The potential sources of scrap known at that time, and efforts to get it into the market, were further described. It seems particularly fitting that the question of availability should be discussed before this conference after the pattern set by the 1947 papers.

The preparation of scrap in a mill operated yard was discussed by C. F. Staley[5] in 1949. In this paper the importance of scrap density was demonstrated by the close correlation between tons per hour of production and the number of buggies required per charge.

At present, the impact of world events upon the scrap supply is unpredictable. Should the present situation deteriorate into total war, the military effort would require maximum steel production with maximum scrap consumption. Yet, as Barringer pointed out, total war results in the loss of millions of tons of potential scrap.

The electric furnace, its capacity greatly expanded during World War II, stands today in a most critical position. Its unique position in the production of superior quality alloy steels long has been known. Its capabilities in the fast and economical melting of lower quality steels now is perceived, but not realized and developed fully. The goal is to achieve complete versatility as to all grades and qualities, as required in any emergency. The attainment of this goal depends in large measure upon good charging, fast melting, reliable chemical control and meltdown, and freedom from injurious contamination. These factors are all characteristic of the scrap supply.

An attempt will be made to point out some

Ralph W. Farley is Special Mill Metallurgist, and Ray J. McCurdy is Superintendent of No. 2 Melt Shop for the Republic Steel Corp., Chicago, Ill. This paper will be presented at the Electric Furnace Steel Conference, Pittsburgh, Dec 7 to 9, 1950.

Table I—Required Box Density of Scrap for a 70-ton Furnace with Varying Amounts of Crops

Furnace Charge: 170,000 Lb
Capacity of Charging Box: 22 Cu Ft
Number of Boxes in One Charge, Max.: 55

Lb of Crops	Balance of Scrap, Lb	Cu Ft of Scrap in Boxes	Wt per Cu Ft in Box
Case 1. No Back Charge			
none	170,000	1,210	140
25,000	145,000	1,100	132
50,000	120,000	990	121
Case 2. 25,000 Lb Back Charge			
none	145,000	1,210	120
25,000	120,000	1,100	109
50,000	95,000	990	96
Case 3. 50,000 Lb Back Charge			
none	120,000	1,210	99
25,000	95,000	1,100	86
50,000	70,000	990	71

specific requirements of the scrap supply, and some improvements in meeting these requirements. This will be generalized as much as possible to cover the field of electric furnace steel melting, but any figures and estimates apply strictly to one shop in the Chicago area, with one-size furnaces, operating on a charge of about 15 pct hot metal and cold pig combined. It is hoped that this report will indicate trends that may be interpreted for other sizes and methods of operation, under conditions obtaining in other areas.

The main sources of scrap today are: Home scrap, about 15 pct; Purchased scrap, about 85 pct. Home scrap consists chiefly of bloom, billet, and bar crops, there being no flat rolling in this mill. Of the purchased scrap, about 70 pct is waste material coming directly from the fabricators, the direct producers of scrap. This is the most desirable form of purchased scrap from the standpoint of segregation of analysis, density and contamination. An increasing amount of this class is sheet clippings in the form of No. 1 bundles, which are improving in analysis, cleanliness and density. Another good item is punchings and short heavy clippings. Inasmuch as closer control of the scrap analysis is necessary for the electric furnace than for the open hearth, it is increasingly important that the above items from known sources be channeled to the electric furnace. Plate scrap, bar crops, and flashings are desirable, if of known origin, but chemical segregation is often not as good on these as on the other items mentioned.

The other 30 pct of purchased scrap, or about 25 pct of the total, is that which arises through wear, obsolescence and replacement plus small lots of nonsegregated production scrap gathered by the collectors. These items require the greatest amount of segregation and preparation. This job never has been advanced to an adequate proficiency. Boat and locomotive scrap have been in good supply and are good items when properly prepared. But much trouble has been experienced with dealers' bundles and miscellaneous scrap. Dealers' bundles still appear to be a *catch-all* for off grade, low density and nonmetallic *loading*. It is this factor which, if undetected, can poison an entire charge of otherwise good scrap, and render the melt unfit for the grade of steel desired. On altogether too many occasions, production schedules have been disturbed seriously by residual elements and lack of melt control, traceable to this item. On altogether too many occasions, furnaces have been damaged and safety of personnel jeopardized by the contaminants in dealers' bundles and miscellaneous scrap, carelessly prepared.

Table II—Required Box Density of Scrap for a 50-ton Furnace with Varying Amounts of Crops

Furnace Charge: 140,000 Lb
Capacity of Charging Box: 20 Cu Ft
Number of Boxes in One Charge, Max.: 48

Lb of Crops	Balance of Scrap, Lb	Cu Ft of Scrap in Boxes	Wt per Cu Ft in Box
Case 1. No Back Charge			
none	140,000	960	146
20,000	120,000	880	136
40,000	100,000	800	125
Case 2. 20,000 Lb Back Charge			
none	120,000	960	125
20,000	100,000	880	114
40,000	80,000	800	100
Case 3. 40,000 Lb Back Charge			
none	100,000	960	104
20,000	80,000	880	91
40,000	60,000	800	75

It has been repeatedly stressed that the success of the electric furnace in the melting of all grades depends primarily upon fast melting. To achieve this, the density of scrap is all important. There are two main requirements which must be met: (a) The size and weight distribution must be such as to give the maximum heat absorption, concentrating the heat in the charge and permitting high power input without damage to the refractories. (b) The average density of the scrap must be high enough to permit charging with the least possible time lost and number of back charges.

In the shop of origin of this report, the best distribution is approximately equal quantities of crops and heavy scrap on the bottom, medium weight next, and light weight on top. In the absence of sufficient amounts of any one of these three groups, the other groups should be balanced to yield the same average density. For fast melting, sizing and weight of scrap cannot be considered as independent. It is imperative that light scrap be cut into smaller pieces. It permits control of the bulk density of the lighter scrap in the charging box; and, in the furnace, contributes to safety and avoids one important cause of damage to the furnace.

The average bulk density in the box is the chief factor in promoting high production rates. Because the furnace will hold a certain number of boxes, the number of boxes required for the charge controls charging time, number of back charges, and the rate of heat absorption. In a 70-ton furnace to be charged with 170,000 lb total, including 25,000 lb of crops, a balance of scrap having a density of 132 lb per cu ft in the box can be handled in one charge. Material with a density of 109 lb per cu ft will require a back charge of 25,000 lb. These figures appear not unreasonable, considering that with present equipment good sheet scrap can be compressed in No. 1 bundles to a density of close to 200 lb per cu ft. Yet in this shop two or three back charges are not uncommon.

In elaboration of these figures on density requirements, Table I presents data for several charging conditions for a 70-ton furnace to be charged with 170,000 lb, using boxes of 22 cu ft capacity. This furnace will take 55 boxes of scrap in one charge. In each case the figure in the column to the far right, headed "Wt Per Cu Ft in

Box", is the required density of scrap in the box.

Similar density requirements for any size door-charging furnace can be derived from data at hand. Table II gives the density requirements for a 50-ton furnace with a charge of 140,000 lb. The boxes have 20 cu ft capacity, and the furnace will hold 48 boxes in one charge.

In like manner, the melting performance of a top-charging furnace is dependent upon the density and size-weight distribution in the charging bucket. In this shop, one 70-ton furnace has been converted to top charging, but the data on this furnace are not yet sufficient to make any density derivations.

Comparative figures for scrap density for 1947 and 1950 are given in Table III, which shows the total charging box cubage required to make up a charge of 170,000 lb. Note that the average cubage in 1950 is 14 pct lower than in 1947. This is nearly the same as the amount of hot metal and pig in use in 1950. Thus, the change in average density of the scrap is slight. The range, or difference between maximum and minimum cubage, shows a decided improvement, 60 pct lower in 1950. This results in part from education of personnel within the shop, particularly in the stock house. At least a part of this improvement, however, is attributable to better scrap, particularly to more and better No. 1 bundles. These cubage figures may be interpolated in Table I to find the amount of back charge required with a given amount of crops. Thus, the average of 1975 cu ft for 1950 indicates a box density of 94 lb per cu ft, which with 25,000 lb of crops would require a back charge of 42,000 lb.

The matter of segregation is now taking on an unusually serious aspect. Segregation is to be viewed as two separate requirements: (a) Remove nonferrous metals, and (b) Sort the various grades of steel. These requirements must be met with unusual diligence at this time for two reasons.

First, the undesired effects of alloying upon carbon steels and alloy steels not requiring a particular element are to be avoided. Second, the alloying elements at a time when supplies are becoming increasingly critical must be conserved.

The present state of scrap segregation is indicated by statistical study of alloy contents of a series of meltdown tests. Only those melts that were not intentionally charged for an alloy containing the element sought were used in such studies. In the shop of origin of this report, where residuals have been high for several years, and with 15 pct hot metal and pig charged, the residual contents of 553 melts in the month of July, 1950, were:

	Pct, Avg	Pct, Max	Pct, Min
Copper	0.14	0.29	0.07
Nickel	0.15	0.28	0.05
Chromium	0.08	0.25	0.03
Molybdenum	0.03	0.12	0.01
Tin	0.02	0.06	0.01

A considerable amount of alloy scrap and some nonferrous metal has come through unsegregated; and several melts have had to be diverted to unscheduled alloy heats.

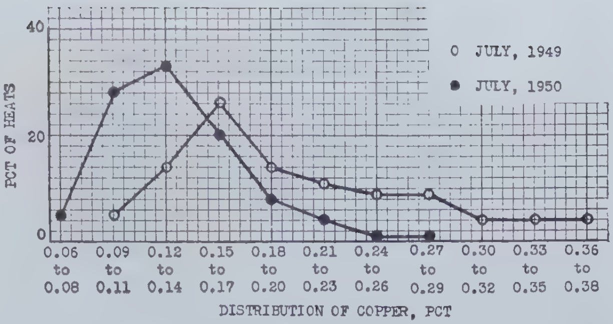

Fig. 1. Distribution of residual copper in electric furnace heats.

The distribution of copper, nickel, chromium, and molybdenum contents of these same melts are shown in Figs. 1 to 4, respectively, with the distribution of these elements in July, 1949 for comparison. It will be noted that copper contents ran considerably lower than a year ago, nickel contents a little higher, and chromium and molybdenum remained unchanged.

High contents of cobalt are occasionally found in the melts. The source has never been traced, in spite of a serious effort to do so; but it is supposed that cobalt originated in the production of high temperature alloy parts used, for example, in jet engines. If this is so, then this item will increase with increased production of these engines, and this kind of scrap must be segregated.

While diligence must be exercised in the segregation of purchased scrap, it is just as important that the same diligence be exercised in the handling of home scrap. If redoubled effort is called for in the case of purchased scrap, then surely it is called for in the case of home scrap. And what melt shop does not face a constant fight for segregation of scrap returned from other departments? Coming closer to home, segregation of scrap entering the stockhouse does not assure success, except by constant vigilance to maintain segregation all the way into the furnace.

The importance of clean scrap hardly needs to be mentioned. Contamination affects steelmaking in many ways: (1) It alters the meltdown composition and may make the melt worthless or at least unsuitable for the grade intended, (2) it introduces materials, bought and paid for at the price of good scrap, which are worthless and add nothing to the product yield of the operation, (3) it is destructive to the furnaces, and (4) above all, it presents some of the most violent hazards to the safety of the men on the job.

Although it is supposed that all concerned are quite familiar with the forms of contamination of scrap and their effects, it may be appropriate to call attention to some things which must be stopped by any available means.

Table III—Scrap Density: 1947 vs. 1950
For 70-ton Electric Furnace

Total Charging Box Cubage Required per 170,000 lb Charge

Cubic Feet	1947	1950
Average	2300	1975
Maximum	4450	2500
Minimum	1600	1450

Improvement: In Average Cubage - 14 Pct
In Range - 60 Pct

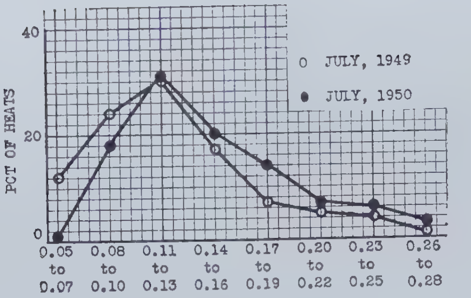

Fig. 2. Distribution of residual nickel in electric furnace heats.

Loading of dealers' bundles with bricks, wood and other worthless waste materials still occurs. In addition to the economic loss, such material may insulate and break an electrode, and the low yield resulting may lead to an off analysis heat.

In miscellaneous scrap, such items as pipe nipples poured with concrete, and not cleaned in preparation, lead to similar results.

Scale, excessive rust, and other oxidizing agents decrease the product yield and cause low carbon meltdown, sometimes leading to diverted heats or adverse effects upon quality. Scale is often found packed in bundles. Assemblies made up of ferrous combined with nonferrous metals, plastics, or ceramics may vitiate the slags, attack and damage the furnace refractories, or introduce residuals sufficient to cause rejection of the heat. Lead, zinc, and their alloys are especially destructive to the furnace. Plated and hot-dip coated steel must be more effectively stripped in preparation, for the same reasons.

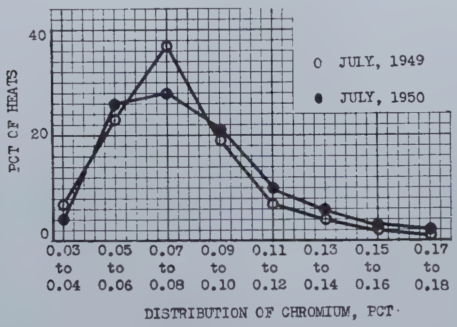

Fig. 3. Distribution of residual chromium in electric furnace heats.

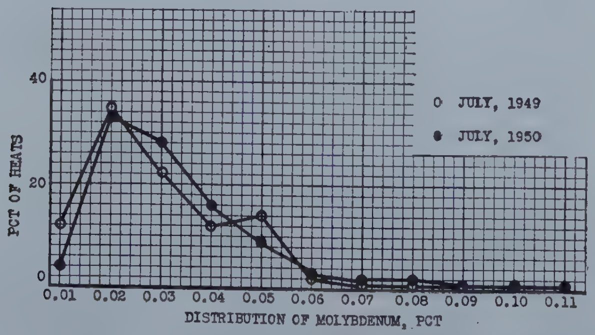

Fig. 4. Distribution of residual molybdenum in electric furnace heats.

Grease packed bearings and journal boxes, and containers not cleaned of their previous contents of paint, oil, or other organic liquids frequently are received. They particularly are to be guarded against, because of the danger to the furnace and equipment, and to the health and safety of the men. Finally, it need hardly be repeated that closed vessels and loaded shells are in a class by themselves, among the most vicious of contaminants.

This is not intended to be a complete list of scrap contaminants. There are others. Undoubtedly, the list of things that give trouble in one area is not the same as that in another area. The method of elimination of scrap contamination is nothing new; but begins with education and ends with enforcement.

Education has been a keynote in many of the papers read before this conference. It is the beginning and essence of any program to improve the scrap supply to the furnaces. It has two branches: Education of the workers in the supply industry, and education of the workers within the mill. The first may be conducted through the broker, by keeping him informed at all times what the requirements are and that they will be strictly enforced. The broker should be kept informed as to the troubles encountered through various defects, and why. He is in a position to pass this information along through the channels of scrap supply, and can enforce the buyer's requirements, especially when he is backed up by rejections when warranted on the part of the buyer.

Workers within the mill must be taught to maintain segregation all the way into the furnaces, to keep a sharp watch for contaminants, to load for maximum density and uniform cubage per charge, and to charge furnaces for maximum melting rate and safety to the equipment and personnel. Education is a never ending effort; more so today because its best results often have been lost by rapid turnover of labor. Be that as may, it remains the inescapable duty of every supervisor to teach—and teach—and teach.

In considering the various aspects of this problem, the close association of each factor with the problem of safety has been pointed out. This is, and must remain, the ultimate test for the suitability of scrap: "Is it safe for the men?" Safety, like education, is a never ending effort, and an effort which must be prosecuted by every means possible.

References

[1] Barker, George A., Jr.: Preparation of Scrap for Fast Melting. *Electric Furnace Steel Proc., AIME,* vol. 3, 1945, pp. 4 to 6.

[2] Gladding, Samuel D.: Preparation of Raw Materials for Fast Melting in an Electric-arc Furnace. *Electric Furnace Steel Proc., AIME,* vol. 4, 1946, pp. 81 to 87.

[3] Kaplan, Stanley M.: Problems in Supplying Scrap for Electric-furnace Requirements. *Electric Furnace Steel Proc., AIME,* vol. 5, 1947, pp. 94 to 97.

[4] Barringer, Edwin C.: The Outlook for Scrap. *Electric Furnace Steel Proc., AIME,* vol. 5, 1947, pp. 97 to 103.

[5] Staley, C. F.: Preparation of Scrap for Armco Electric Furnaces. *Electric Furnace Steel Proc., AIME,* vol. 7, 1949, pp. 18 to 23.

Deoxidizing in the Ladle With Carbortam

by W. O. Igelman
and D. A. Finch

WHEN operation of the acid electric furnaces for production of steel for castings started in 1943 at the Melrose Park plant of National Malleable & Steel Castings Co., previous experience at other company plants indicated that the best deoxidizer consisted of 2 lb of aluminum and 3 lb of calcium silicon per ton of steel. This deoxidizer was used as a ladle addition. However, because of variations in the melting operation (caused by the quality of the charge, that is the size, shape, and analysis of purchased scrap) heats required extra processing to make castings of satisfactory quality.

Many castings required extra heat treatments to meet minimum railroad physical specifications. Variations in ductility from heat to heat were evident from elongation and reduction of area tests. Consequently, it was apparent that a ladle deoxidizer was needed that would yield a more ductile steel; that was less critical in its effect for amounts used; and that would lend itself to better physical tests.

In 1945, it was decided to substitute Carbortam for aluminum as the deoxidizer to improve ductility. A number of heats of grade B steel for railroad castings were made, using 5 and 6 lb of Carbortam and 3 lb of calcium silicon per ton added slowly to the ladle through a 5x5 in. x 8 ft chute. Care was taken to add the deoxidizer at precisely the correct time to get the maximum effect.

This technique of deoxidizing in the ladle yielded a product that, after a normalizing heat treatment, had elongation and reduction of area values equal to or better than aluminum deoxidized heats that were normalized and tempered. Further, test bar fractures were noticeably more silky in appearance.

While these advantages were apparent, surface pinholes appeared in some castings varying in degree of severity, a condition that had to be corrected before Carbortam could be used in all electric furnace steel output. In addition, Carbortam was not as potent a deoxidizer as aluminum for eliminating gases in the metal and the molds.

A single slag practice was employed. Silicon and manganese finals were added to the bath after temperature and spiral tests were taken, then most of the slag was removed from the bath just before tapping. More complete removal of the slag resulted in practically eliminating the pinhole trouble, evidence that some of the Carbortam was lost by the slag action in the ladle.

Pinholes were more prevalent when using 5 lb of Carbortam and 3 lb of calcium silicon per ton of steel than when using 6 lb and 3 lb, respectively, per ton. Increasing Carbortam to 7 lb per ton resulted in little if any improvement in pinhole defect and physical properties decreased. Consequently, standard practice was set up for 6 lb of Carbortam and 3 lb of calcium silicon per ton of steel.

The bottleneck in plant output was heat treating. This was partly caused by the necessity of reheat-treatments and the need for a tempering treatment in addition to a normalize on practically all heats deoxidized with aluminum. Because of the improved results and almost complete elimination of surface pinholes from Carbortam deoxidized heats, in 1947 this deoxidizing practice was adopted for all electric furnace steel production, which consisted of grade B and C steels.

By 1948, sufficient data was accumulated in the quality control section of the Metallurgical Dept. to indicate something yet to be desired for better control in all phases of the melting procedure. Toward this end, the melting supervision concentrated on more uniform furnace charges, including such factors as weight, chemistry, size, and shape of purchased scrap. All incoming scrap was sampled and analyzed for undesirable elements such as sulphur, phosphorus,

---

W. O. Igelman is Metallurgist and D. A. Finch is Melting Supervisor at the Melrose Park, Ill., plant of National Malleable & Steel Castings Co. This paper will be presented at the Electric Furnace Steel Conference, Pittsburgh, Dec. 7 to 9, 1950.

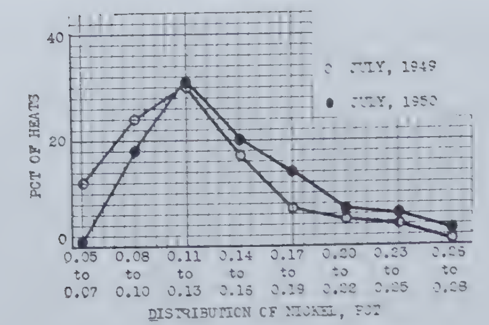

Fig. 2. Distribution of residual nickel in electric furnace heats.

Loading of dealers' bundles with bricks, wood and other worthless waste materials still occurs. In addition to the economic loss, such material may insulate and break an electrode, and the low yield resulting may lead to an off analysis heat.

In miscellaneous scrap, such items as pipe nipples poured with concrete, and not cleaned in preparation, lead to similar results.

Scale, excessive rust, and other oxidizing agents decrease the product yield and cause low carbon meltdown, sometimes leading to diverted heats or adverse effects upon quality. Scale is often found packed in bundles. Assemblies made up of ferrous combined with nonferrous metals, plastics, or ceramics may vitiate the slags, attack and damage the furnace refractories, or introduce residuals sufficient to cause rejection of the heat. Lead, zinc, and their alloys are especially destructive to the furnace. Plated and hot-dip coated steel must be more effectively stripped in preparation, for the same reasons.

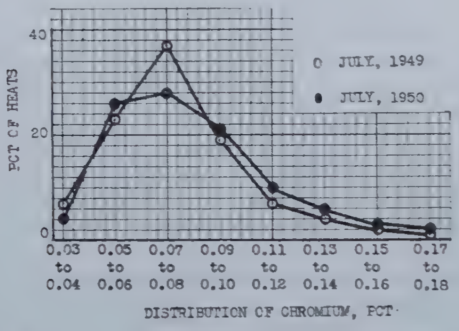

Fig. 3. Distribution of residual chromium in electric furnace heats.

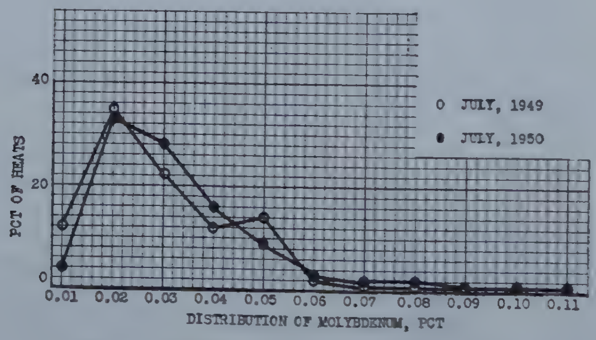

Fig. 4. Distribution of residual molybdenum in electric furnace heats.

Grease packed bearings and journal boxes, and containers not cleaned of their previous contents of paint, oil, or other organic liquids frequently are received. They particularly are to be guarded against, because of the danger to the furnace and equipment, and to the health and safety of the men. Finally, it need hardly be repeated that closed vessels and loaded shells are in a class by themselves, among the most vicious of contaminants.

This is not intended to be a complete list of scrap contaminants. There are others. Undoubtedly, the list of things that give trouble in one area is not the same as that in another area. The method of elimination of scrap contamination is nothing new; but begins with education and ends with enforcement.

Education has been a keynote in many of the papers read before this conference. It is the beginning and essence of any program to improve the scrap supply to the furnaces. It has two branches: Education of the workers in the supply industry, and education of the workers within the mill. The first may be conducted through the broker, by keeping him informed at all times what the requirements are and that they will be strictly enforced. The broker should be kept informed as to the troubles encountered through various defects, and why. He is in a position to pass this information along through the channels of scrap supply, and can enforce the buyer's requirements, especially when he is backed up by rejections when warranted on the part of the buyer.

Workers within the mill must be taught to maintain segregation all the way into the furnaces, to keep a sharp watch for contaminants, to load for maximum density and uniform cubage per charge, and to charge furnaces for maximum melting rate and safety to the equipment and personnel. Education is a never ending effort; more so today because its best results often have been lost by rapid turnover of labor. Be that as may, it remains the inescapable duty of every supervisor to teach—and teach—and teach.

In considering the various aspects of this problem, the close association of each factor with the problem of safety has been pointed out. This is, and must remain, the ultimate test for the suitability of scrap: "Is it safe for the men?" Safety, like education, is a never ending effort, and an effort which must be prosecuted by every means possible.

References

[1] Barker, George A., Jr.: Preparation of Scrap for Fast Melting. *Electric Furnace Steel Proc., AIME,* vol. 3, 1945, pp. 4 to 6.

[2] Gladding, Samuel D.: Preparation of Raw Materials for Fast Melting in an Electric-arc Furnace. *Electric Furnace Steel Proc., AIME,* vol. 4, 1946, pp. 81 to 87.

[3] Kaplan, Stanley M.: Problems in Supplying Scrap for Electric-furnace Requirements. *Electric Furnace Steel Proc., AIME,* vol. 5, 1947, pp. 94 to 97.

[4] Barringer, Edwin C.: The Outlook for Scrap. *Electric Furnace Steel Proc., AIME,* vol. 5, 1947, pp. 97 to 103.

[5] Staley, C. F.: Preparation of Scrap for Armco Electric Furnaces. *Electric Furnace Steel Proc., AIME,* vol. 7, 1949, pp. 18 to 23.

Deoxidizing in the Ladle With Carbortam

by W. O. Igelman
and D. A. Finch

WHEN operation of the acid electric furnaces for production of steel for castings started in 1943 at the Melrose Park plant of National Malleable & Steel Castings Co., previous experience at other company plants indicated that the best deoxidizer consisted of 2 lb of aluminum and 3 lb of calcium silicon per ton of steel. This deoxidizer was used as a ladle addition. However, because of variations in the melting operation (caused by the quality of the charge, that is the size, shape, and analysis of purchased scrap) heats required extra processing to make castings of satisfactory quality.

Many castings required extra heat treatments to meet minimum railroad physical specifications. Variations in ductility from heat to heat were evident from elongation and reduction of area tests. Consequently, it was apparent that a ladle deoxidizer was needed that would yield a more ductile steel; that was less critical in its effect for amounts used; and that would lend itself to better physical tests.

In 1945, it was decided to substitute Carbortam for aluminum as the deoxidizer to improve ductility. A number of heats of grade B steel for railroad castings were made, using 5 and 6 lb of Carbortam and 3 lb of calcium silicon per ton added slowly to the ladle through a 5x5 in. x 8 ft chute. Care was taken to add the deoxidizer at precisely the correct time to get the maximum effect.

This technique of deoxidizing in the ladle yielded a product that, after a normalizing heat treatment, had elongation and reduction of area values equal to or better than aluminum deoxidized heats that were normalized and tempered. Further, test bar fractures were noticeably more silky in appearance.

While these advantages were apparent, surface pinholes appeared in some castings varying in degree of severity, a condition that had to be corrected before Carbortam could be used in all electric furnace steel output. In addition, Carbortam was not as potent a deoxidizer as aluminum for eliminating gases in the metal and the molds.

A single slag practice was employed. Silicon and manganese finals were added to the bath after temperature and spiral tests were taken, then most of the slag was removed from the bath just before tapping. More complete removal of the slag resulted in practically eliminating the pinhole trouble, evidence that some of the Carbortam was lost by the slag action in the ladle.

Pinholes were more prevalent when using 5 lb of Carbortam and 3 lb of calcium silicon per ton of steel than when using 6 lb and 3 lb, respectively, per ton. Increasing Carbortam to 7 lb per ton resulted in little if any improvement in pinhole defect and physical properties decreased. Consequently, standard practice was set up for 6 lb of Carbortam and 3 lb of calcium silicon per ton of steel.

The bottleneck in plant output was heat treating. This was partly caused by the necessity of reheat-treatments and the need for a tempering treatment in addition to a normalize on practically all heats deoxidized with aluminum. Because of the improved results and almost complete elimination of surface pinholes from Carbortam deoxidized heats, in 1947 this deoxidizing practice was adopted for all electric furnace steel production, which consisted of grade B and C steels.

By 1948, sufficient data was accumulated in the quality control section of the Metallurgical Dept. to indicate something yet to be desired for better control in all phases of the melting procedure. Toward this end, the melting supervision concentrated on more uniform furnace charges, including such factors as weight, chemistry, size, and shape of purchased scrap. All incoming scrap was sampled and analyzed for undesirable elements such as sulphur, phosphorus,

W. O. Igelman is Metallurgist and D. A. Finch is Melting Supervisor at the Melrose Park, Ill., plant of National Malleable & Steel Castings Co. This paper will be presented at the Electric Furnace Steel Conference, Pittsburgh, Dec. 7 to 9, 1950.

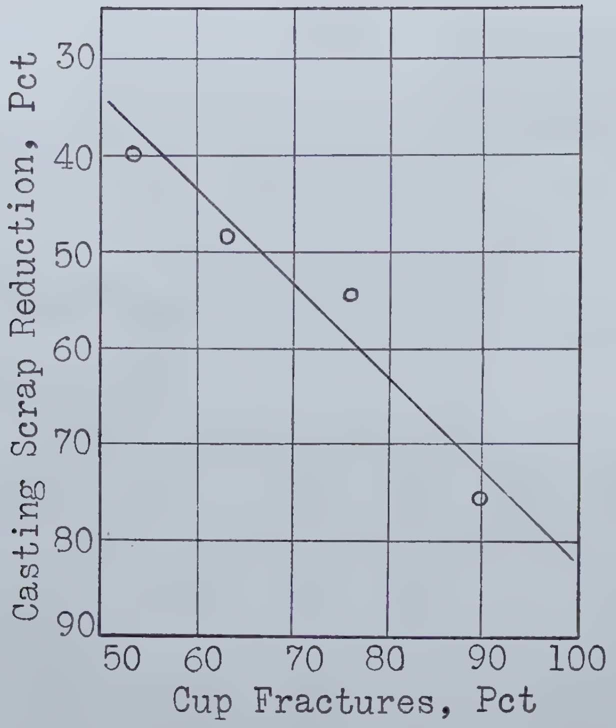

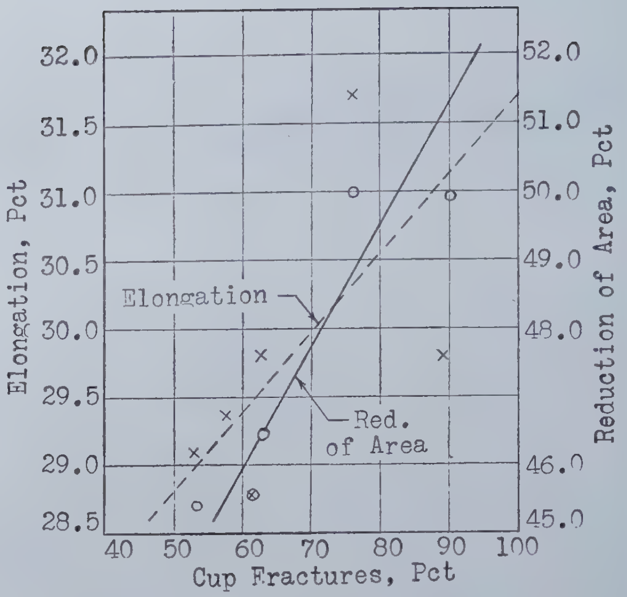

Fig. 1—(Left) Progress in scrap reduction.

Fig. 2—(Above) Quarterly averages of ductility figures correlated with the percentage of cup and cone type fractures.

Table I—Cost Reduction in Melting Dept.

Quarterly Periods	Reduction in Cost, Pct: Labor	Electric Power	Electrodes	Addition Agents
First, 1948	11.5*	10.6*	10.3*	—
Second				
Third	18.2	7.7	9.6	2.0
Fourth	26.8	18.2	11.5	3.9
First, 1949	23.7	15.1	11.2	1.8
Second**	10.0	—	4.5	3.3

*Base period, Jan. to Mar., 1948.
**Three shift operations ended, two shifts started.

Table II—Cost Reduction in Heat Treating Dept.

Quarterly Periods	Reduction in Cost, Pct: Labor	Fuel
First, 1948	15.1*	9.5*
Second		
Third	30.3	6.9
Fourth	33.3	20.7
First, 1949	36.4	31.9
Second	39.4	10.0**

*Base period, Jan. to Mar., 1948.
**Furnaces were used 16 hr and not fired during remaining 8 hr, thus requiring some additional fuel for heating up.

and copper. Records also showed too great a heat to heat spread in the manganese content. This resulted in a large measure from removing the slag too soon after alloy additions were made. Also, varying amounts of slag on the bath made it impossible to judge how much of the alloy addition was retained in the slag.

A change in slagging practice was instituted, whereby excess slag was removed from the bath before final alloy additions were made. There was an immediate improvement in casting quality and physical characteristics, and a decrease in rejections attributable to melting, such as surface pinholes, cracks, and misruns. The result was a reduction of costs in several departments, including the melting department.

Tables I and II illustrate savings obtained through improved melting practice and the use of Carbortam and calcium silicon as a ladle deoxidizing agent. Table III shows average physical data on railroad castings of grade B and grade C steel made between 1948 and July 1950.

Table III—Average Physical Data for Railroad Castings, Grade B and Grade C Steels

Quarterly Periods	Yield Strength, Psi	Ultimate Strength, Psi	Elongation, Pct	Reduction in Area, Pct	Cup Fractures, Pct	P Value	Reduction in Scrap Attributable to Metal, Pct	Reheat Treatment Pct
GRADE B STEEL								
First, 1948	44,011	74,826	28.8	45.6	62.2	69.7	—	14.5
Second	44,487	74,481	29.4	46.1	58.3	70.2	—	13.7
Third	45,862	75,640	29.1	45.4	53.3	69.6	38.9	12.2
Fourth	46,088	75,258	29.8	46.5	62.6	70.8	47.8	6.6
First, 1949	45,327	75,160	31.7	50.0	76.5	75.0	53.8	4.4
Second	45,415	75,458	29.8	49.9	89.6	74.9	75.1	1.1
Third	45,547	76,240	30.4	49.3	79.7	74.4	76.2	0.0
Fourth	45,966	75,943	31.5	50.9	93.9	76.3	73.9	1.1
First, 1950	44,847	75,700	31.0	50.9	96.9	76.2	73.6	0.3
Second	45,052	75,417	30.7	49.5	94.6	74.5	80.6	0.8
GRADE C STEEL*								
First and Second, 1948	64,219	95,045	25.47	47.63	—	76.2		
Third	65,784	95,730	26.47	49.27	78.0	78.4		
Fourth	67,942	96,274	26.27	51.58	91.7	81.4		
First, 1949	68,136	95,243	26.35	53.13	91.4	82.8		
Second	67,857	97,116	25.68	52.97	96.8	82.6		
Third and Fourth	67,647	97,270	26.50	53.00	96.5	83.0		
First, 1950	68,055	97,657	26.31	52.88	99.4	83.0		
Second	68,028	97,252	26.48	52.31	98.2	82.2		

*Grade C steel is medium manganese with 0.08 pct V, and accounts for 10 to 15 pct of total production. Heat treatment—normalize and temper.

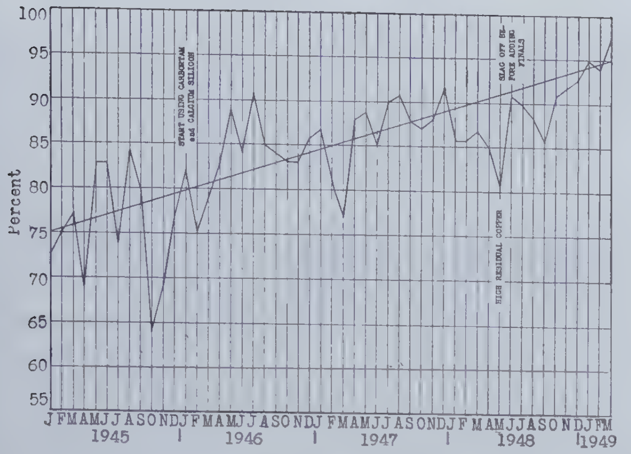

Fig. 3—Percentage of Grade B steel heats that passed the first test pulled.

The cup fracture column in Table III is a measure of continued improved performance and quality, accompanied by lower costs. A cup and cone type test bar fracture is indicative of a well-made heat of steel, and ductility is greater than when the test bar fracture is non-cupped. Reduction in scrap and reduction in reheat-treatments also are evident from this tabulation.

Fig. 1 shows the relation between the reduction in scrap and the cup fractures. Heats that gave cup and cone fractures reduced scrap consumption. Quarterly averages of ductility are shown in Fig. 2, correlated with the percentage of cup and cone fractures. As can be seen, reduction of area values improved more rapidly than elongation values as the percentage of cup fractures increased.

Fig. 3 shows the percentage of grade B steel heats that passed the first test pulled. Prior to January 1946, aluminum-calcium silicon was used as a deoxidizer, and subsequent to that time Carbortam-calcium silicon was used.

The percentage of non-cupped fractures in grade B steel that passed the first physical test is shown in Fig. 4. The monthly average values were plotted after the change in furnace slag removal time.

It was found that the following procedure in melting practice, when closely adhered to, yields a quality product, using Carbortam and calcium silicon as a ladle deoxidizer.

1—Charges should melt down as near to 0.30 pct C as possible. High or low carbon melt down is undesirable.

2—The faster the melt down, the more satisfactory the slag condition prior to the boil. A slow melt down with electrodes boring into the bottom causes a reduction of silica on the bottom and banks, often resulting in an excessive amount of viscous slag accompanied by a silicon pickup in the bath. This makes a good boil difficult to obtain.

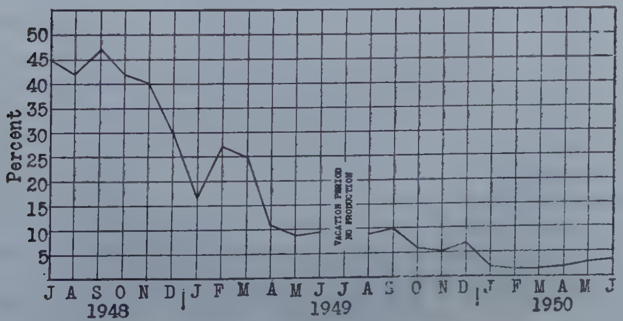

Fig. 4—Percentage of non-cupped fractures in Grade B steel that passed the first physical test.

3—A vigorous boil that lasts 3 or 4 min, tapering off to just a slight action in the furnace until the heat is tapped is desired.

4—Eight to twelve points of carbon should be removed from the melt at the rate of 4 to 6 points per min.

5—When carbon has been oxidized to the proper level and the slag has been shaped to the melter's specifications, the melt is then partially blocked with silicomanganese.

6—A preliminary carbon and manganese test is poured and analyzed. While waiting for the results of the test, the slag is raked from the bath, leaving only about ⅛-in. protective coating on the metal.

7—The final slag, just before the finals are added to the furnace, is judged as to its condition by the amount of green color in the slag sample.

8—The final ferroalloys are added as soon as the preliminary for carbon and manganese is returned from the laboratory.

9—A film test for temperature and a spiral test for fluidity are poured as soon as alloy additions are melted.

10—Sand is thrown on the bath in front of the tap hole to hold back the slag as the heat is tapped.

11—When 6-in. of metal is in the ladle, the Carbortam and calcium silicon addition is chuted into the ladle. It is desirable to have all of the deoxidizer in the ladle before the ladle is half full.

The FeO content of a few finishing slags range from 16 to 32 pct. Cup fractured test bars averaged the following analysis: Al, 0.015; Cu, 0.09; Ni, 0.06; Mo, 0.03; and Ti, 0.02 pct, with a trace of B. Test bar fractures that exhibit rock candy type fractures have been reported to contain equal or more boron than titanium, and when the residual titanium is two to three times the boron, satisfactory fractures result.

The chemical analysis of cup fractured test bars for inclusions indicate that the silicon and iron oxides are low and manganese oxides relatively high, yielding a low ratio of FeO to MnO. This is believed desirable. From additional work, it is assumed that a cup fracture can be expected when the FeO:MnO ratio is below 14:1. Two test bars breaking with a cup fracture and more than 55 pct reduction of area were reported to have 1.8:1 and 4.8:1 ratios, thus verifying such predictions.

There is one best method of melting that will produce high quality electric furnace steel castings when Carbortam is used as a ladle deoxidizer. Heats for castings requiring no higher pouring temperature than 2850°F can be sufficiently deoxidized with Carbortam. Ductility is increased when Carbortam instead of aluminum is used, and chain type inclusions are greatly reduced. Many tempering treatments are eliminated by the use of Carbortam, and the metal fluidity is increased, as reflected in a much lower percentage of cracked and misrun castings.

Control of Refractory Materials

by C. E. Sumpter

THE quality of the refractories used both in the construction and maintenance of an electric furnace, influences to a large degree the quality and cost of the steel produced. It is proposed to review the materials used in the various parts of a furnace, methods of checking and controlling the quality of the materials, and the results of trials completed recently at South Works, Carnegie-Illinois Steel Corp.

The primary materials generally employed for the construction and maintenance of the furnace bottom are dead-burned magnesite, commercially prepared ramming materials, and clinkered dolomite.

Commercially available dead-burned magnesite contains about 80 pct magnesia, but when slag or roll scale is added to promote a satisfactory rate of sintering, the M_gO content in the final bottom is decreased. The prepared ramming materials are essentially grain sized aggregates of 65 to 96 pct magnesia compounded with bonding chemicals which will air set after being tempered with water and dried. Two prime requisites of this material are proper grain sizing and rammed bulk density. The clinkered dolomites available on the market are prepared by dead-burning essentially pure dolomites with additions of iron oxide. The iron oxide content varies from 7 to 17 pct. The grain sizing of dolomite varies, some being as coarse as ¼ in., while others are on the order of 6-mesh, as determined by a standard Tyler screen.

Laboratory control tests conducted include screen analysis, chemical analysis, slaking, sintering characteristics, compressive strength at elevated temperatures, maximum dry rammed density, and fired properties of shrinkage, porosity, and density. Standard ASTM procedures are used wherever applicable.

There are no specifications for these materials; however, sufficient correlation of laboratory and service data has been obtained to permit the tabulation of desired properties in Tables I, II, and III. If any of the materials fail to meet these requirements, then further purchases of that product are curtailed until the deficiencies are corrected. For example, shipments of clinkered dolomites from one shipper were recently suspended because of poor sintering characteristics at fettling temperatures, which resulted in bank trouble.

Table I—Desired Properties of Magnesite

Chemical Analysis	M_gO—80 pct min, SiO_2—7.0 pct max, Al_2O_3—1.0 pct max
Screen Analysis	Plus 8 Mesh, 5 to 10 pct " 10 " 10 to 15 pct " 20 " 30 to 35 pct " 35 " 15 to 20 pct " 100 " 10 to 15 pct Thru 100 " 15 to 20 pct
Resistance to Hydration	Good
True Specific Gravity	3.40 min
Sintering Characteristics	10 pct max shrinkage and 175 lb per cu ft, min density with 15 pct max slag addition

Table II—Desired Properties of Basic Ramming Materials

Drying Ramming Density	150 lb per cu ft, min
Screen Analysis	Only as it affects dry ramming density
Compressive Strength at Elevated Temperatures	500 psi min, up to and including 2000°F
Shrinkage After Firing To 2910°F for Five Hr	10 pct max
Chemical Analysis	M_gO—65 pct min, SiO_2—10 pct max

Table III—Desired Properties of Clinkered Dolomites

Chemical Analysis	CaO—49 to 52 pct, M_gO—35 to 39 pct SiO_2—3 pct max, Al_2O_3—1 pct max Total Fe as Fe_2O_3—7 to 9 pct
Screen Analysis	Only as it affects sintering and angle of repose
Sintering Characteristics	After 30 min. at 2700°F, Fair to good After 30 min. at 2800°F, Excellent
Angle of Repose	Equal to or greater than angle of furnace banks on which material is applied
Apparent Specific Gravity	As received, 3.00 min After heating at 2800°F for ½ hr, 0.10 max increase
Slaking	None to slight after 72 hr
Oil	Grains Coated

C. E. Sumpter is General Supervisor of Ceramics at the South Works, Carnegie-Illinois Steel Corp., Chicago, Ill. This paper will be presented at the Electric Furnace Steel Conference, Pittsburgh, Dec. 7 to 9, 1950.

Basic furnace side walls are almost universally constructed of basic brick despite the relatively high initial cost. This condition has been brought about by the steady improvement in the quality of basic brick, the great need for all-out production, and the high temperatures required to produce certain grades of electric furnace quality steels. It is interesting to note that today, basic brick containing varying amounts of chrome ore are used successfully for this application, whereas a few years ago, chrome-free magnesite brick were considered essential to prevent chrome pickup in the steel.

There are two types of basic brick mainly used in the side walls. One type is the metal-encased, unfired, chemically bonded magnesite-chrome brick while the other type is the unplated, fired, magnesite-chrome brick. Chemically, these brick are 60 to 75 pct M_gO and 10 to 15 pct Cr_2O_3. The service performance of these brick has been superior to either the magnesite or chrome brick.

Laboratory tests are conducted for chemical analysis, apparent porosity, bulk density, temperature of failure under a load of 25 psi, permanent linear change after reheating for five hr at 2910° F, and resistance to bursting by iron oxide. Service information is being obtained to attempt to correlate service results with laboratory results, and this information will eventually be used to prepare specifications for basic brick. At the present time service trials are conducted with all promising new refractory materials to determine their merit compared with that of currently used refractories.

Silica brick are still the most commonly used refractory for furnace roofs. With their low initial cost, their performance, on a cost per ton basis, with few exceptions, is better than any other type of brick for this application. However, temperatures required to produce certain grades of steel are above the melting point of silica brick. Therefore it has become necessary in the past few years to seek a material which will withstand these high temperatures, and prolong roof life at no increase in cost per ton of steel.

An initial trial of a 13½-in. thick mullite-base brick roof on a furnace which produces only stainless steel has just been completed. Approximately ten pct of this production has been 0.03 pct max carbon steel which requires extremely high temperatures to obtain and maintain the low carbon content. The life obtained with this roof was better than three times that obtained with 18-in. thick silica roofs. The failure of the mullite-base brick roof was attributed to structural spalling rather than loss through melting in service. The chemical attack was limited to a zone of about ½ in. Further trials of roofs constructed with this type of brick are continuing.

Monthly samples of silica brick are obtained for laboratory testing for apparent specific gravity and $A1_2O_3$, TiO_2, and alkalis. These properties serve as an indication of the quality of brick being received with respect to refractoriness and firing treatment in manufacture.

Carnegie-Illinois has just completed an investigation to determine the spalling characteristics of silica brick. It was found that the method of forming, apparent specific gravity, raw material, and bulk density all influenced the spalling behavior. It is planned to continue this study, obtaining service information for correlation with laboratory results, to determine whether the quality of silica brick can be improved.

X-ray Examination of Small Parts

RESULTS of recent experiments in the metallurgical laboratory of Sam Tour & Co., Inc. have indicated that minute parts can be successfully examined by X-ray methods. Thin walled tubes, failures and problems involving instruments, tools, and fine mechanisms can be analyzed by using the proper techniques.

A fragment of a very thin stainless steel tube that had fractured in use was submitted for examination, and the problem was to determine the presence of any condition that could have contributed to failure. The tube was 0.025 in. OD, x 0.013 in. ID, and about ⅝ in. long. A preliminary visual examination revealed nothing, but an X-ray of the tube fragment indicated the possible presence of defects in the wall.

The X-ray was repeated using a sensitive technique and voids in the tube wall were clearly apparent. A positive print was made of the X-ray at a magnification of seven times, as a record of the defects for study. Microscopic examination of the mounted specimen confirmed the presence of voids in the tube wall at those points indicated by the X-ray. A cross section of the tube is shown in the accompanying photomicrograph.

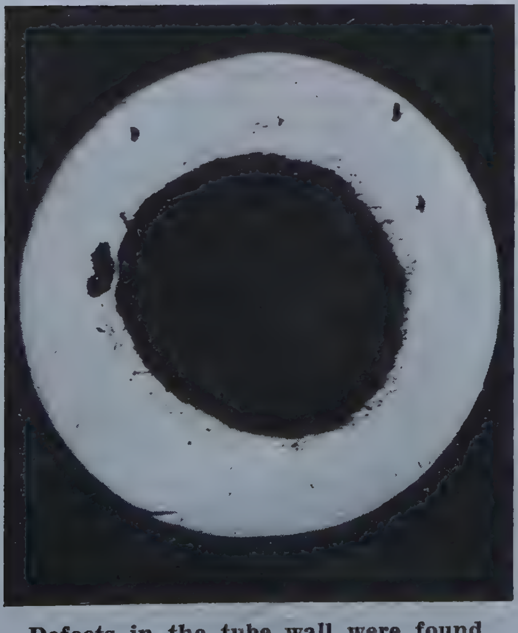

Defects in the tube wall were found by sensitive X-ray techniques (100X).

Measurement of Low Order Ductility

by Norman P. Pinto

IN the determination of the mechanical properties of metals, an evaluation of the ductility is essential for a complete description of engineering properties. Standard methods are entirely adequate for measuring the ductility of most metals, i.e., the relatively ductile metals. The low orders of ductility, however, are more difficult to measure and revisions of methods and techniques are required to obtain accuracy, which is usually more important for brittle metals. The measurement method described here has been used successfully for beryllium and tungsten specimens.

Ductility is evaluated by measuring the elongation of the outer fibers of a test specimen during tension and by computing the degree to which a specimen will contract before rupture. Compression tests, or upsetting tests, are usually applied only to very malleable metals. In the case of metals which deform only slightly, the reduction in cross-sectional area is particularly and restrictively difficult to measure, as is the calculation for elongation of metals which rupture without deforming plastically.

Measurements of the ductility of beryllium have been limited, since the metal in its present state of development is characterized by low ductility, which is less than 10 pct and often about 1 pct for elongation in 2 in. The use of a lever-type strain gauge during the development of metallurgical processes, such as powder metallurgy methods, is impractical due to the danger of breakage. It has been found, however, that specimens of brittle metals may be bent around radii of 1¾ to 6 in. It appears then, that a feasible method for ductility testing would be the bending of a bar over mandrels of successively smaller radii. A simplification of such a procedure would be the bending of a bar over a form, such as that in Fig. 1, in which the radius of curvature decreases progressively. Radii at each point are predetermined and elongation is read from a graph of radius of curvature at point of fracture versus known bar thickness, Fig. 2. In use, the test bar is bent by rolling it around the form with manual force normal to the curved surface; a flat metal bar is most useful for applying this force.

This test provides a value of elongation for the outer fibers of the test specimen at the point of fracture. Whereas a simple beam test gives a measure of deformation (a radius of curvature determined by three points) only within the elastic range, this bend test is valid through both elastic and plastic ranges. Only the fibers on one side of a specimen are in tension, and the problem of premature failure at a notch is less than with the axially loaded tensile test. The preparation of specimens is particularly simple, and round, square, or rectangular samples may be employed. Surface finish is not as critical as it is in the torsion test. Inasmuch as only a fraction of the surface of the specimen is tested at the fracture radius, the test should be checked on a second specimen. As with all other mechanical tests, the condition of the bend test, e.g., rate of load application, test temperature, must be defined.

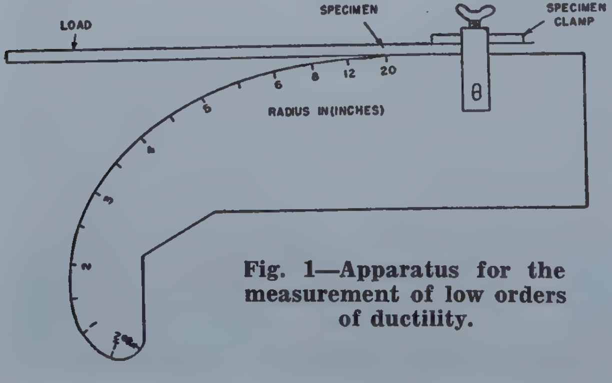

Fig. 1—Apparatus for the measurement of low orders of ductility.

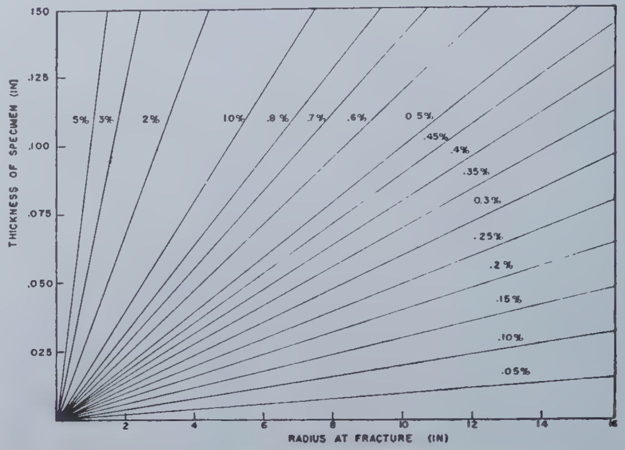

Fig 2—Graph for determining elongation from known specimen thickness and radius at fracture.

The simplicity of the design and ease of construction are definite advantages for this method of testing low orders of ductility; the specimen clamp may be eliminated by securing the form and specimen between the smooth jaws of a vise. The scale and proportions are, of course, arbitrary and should be selected to accommodate a particular range. The range illustrated has proven useful in the testing of beryllium and tungsten.

It should be noted that this test does not yield precise values of elongation but approximations useful particularly in comparing similar materials. The complex changes within a specimen during plastic deformation are functions of the mechanical properties of the particular metal, and although minimized by the small geometrical changes in this test, are significant in arriving at a definite value for elongation.

Norman P. Pinto is Metallurgist at the Metallurgical Labs of Sylvania Electric Products Inc., Bayside, N. Y.

Production of Malleable Zirconium on a Pilot-Plant Scale

by W. J. Kroll, W. W. Stephens, and H. P. Holmes

A pilot plant producing 600 lb of zirconium sponge a week is described. It comprises an arc furnace to make zirconium carbide, a chlorinator producing raw chloride, a purification vessel to eliminate zirconium oxide and iron from this chloride, two reduction vessels, two vacuum retorts for salt separation, and a graphite resistor vacuum furnace to melt ingots. A layout of the plant, power consumption, operation schedules, and production costs are given.

THE only two methods for producing commercial quantities of malleable zirconium, up to now, have been using magnesium reduction of the anhydrous chloride under a neutral gas, and using purification of raw zirconium by the iodide dissociation method on a hot filament. The purity of the metal obtained by the latter process is about the same as that resulting from the chloride reduction, with the exception of the oxygen content, which may be about 0.05 pct lower in the iodide metal. Even traces of oxygen have a strong hardening effect on zirconium. Since, in the iodide process, the impurities, Si, Al, Fe, Ni, and Mg in the raw zirconium used, are carried over, it would appear uneconomical to use this method of refining solely to eliminate the traces of oxygen, unless very soft metal is desired. One important step to improve the iodide method, namely, dissociating pure iodide made from carbide and recycling the iodine, which would change this refining process into a method for extracting zirconium from the ore, has not yet been made. The Bureau of Mines, by using the chloride reduction, wanted to produce quantities of a reasonably pure and malleable metal at low cost for large-scale industrial use. This aim has been achieved, and a pilot plant permitting production of 600 lb of malleable zirconium per week will be described (fig. 1).

Fig. 1—View of pilot plant.

Briefly, the Bureau of Mines process consists of reducing purified gaseous anhydrous zirconium chloride with fused magnesium under a noble-gas atmosphere. The reaction product, magnesium chloride, and any excess magnesium metal present are removed from the sponge zirconium in the next step by fusion and evaporation in a good vacuum at about 925°C. In this process, care is taken to keep air out of contact with the hot metal, which otherwise would contaminate the product with oxygen and nitrogen. Both these impurities embrittle zirconium even when present in an amount as low as 0.1 pct.

A number of previous reports[1-3] describe the method and the various improvements that finally led to a workable process. The major steps made were the production of large quantities of carbide, which is the raw material for producing the chloride, its chlorination with reasonable efficiencies, and the elimination of iron trichloride contained in the raw chloride, as well as that of the zirconium oxide which is always present in this product. The physical nature of the anhydrous chloride, which sublimes at 331°C at atmospheric pressure and melts at 420°C under a pressure of 25 atm, made it necessary to provide a special safety device on the purification and reduction vessels in the form of a lead-alloy seal, permitting escape of excess gases if pressure tended to build up. The main difficulties encountered in the reduction and in the following step, salt separation in a vacuum at elevated temperature, were caused by the material from which the reaction pot was constructed—iron. This metal reacts with zirconium at about 940°C with formation of a eutectic. The last step, salt separation by evaporation of the magnesium and magnesium chloride in a vacuum, is quite unconventional and has not been used before on such a scale. It is only due to the improved construction of high-vacuum pumps, especially oil-diffusion pumps, that such a method could be used.

The various steps of the Bureau of Mines process, as described in the general outline above, may be summarized as follows: (1) production of the carbide, (2) chlorination of the carbide, (3) purification of the raw chloride, (4) reduction of the pure chloride with fused magnesium, (5) separation of excess magnesium and magnesium chloride in vacuum at elevated temperature, and (6) melting of the sponge obtained.

Production of Carbide

The arc furnace, described in a previous report,[2] was improved both to reduce the graphite consumption caused by the burning of the bottom plates and to concentrate the heat in order to obtain better power efficiency. This was achieved by providing the bottom with graphite plates entirely embedded in refractory bricks, the contact with the current being made with three water-cooled copper plugs. Figs. 2 and 3 show the arrangement. The crucible, made

---

W. J. KROLL, Member AIME, is Consulting Metallurgist, W. W. STEPHENS, Junior Member AIME, and H. P. HOLMES are Metallurgists, Northwest Electrodevelopment Laboratory, U. S. Bureau of Mines, Albany, Ore.

AIME New York Meeting, February 1950.

TP 2980 D. Discussion (2 copies) may be sent to Transactions *AIME before Jan. 15, 1951. Manuscript received Jan. 16, 1950.*

Papers by authors on the U. S. Bureau of Mines staff are not subject to copyright.

This page of Transactions AIME is a continuation from p. 1396.
The missing pages appeared in Journal of Metals.

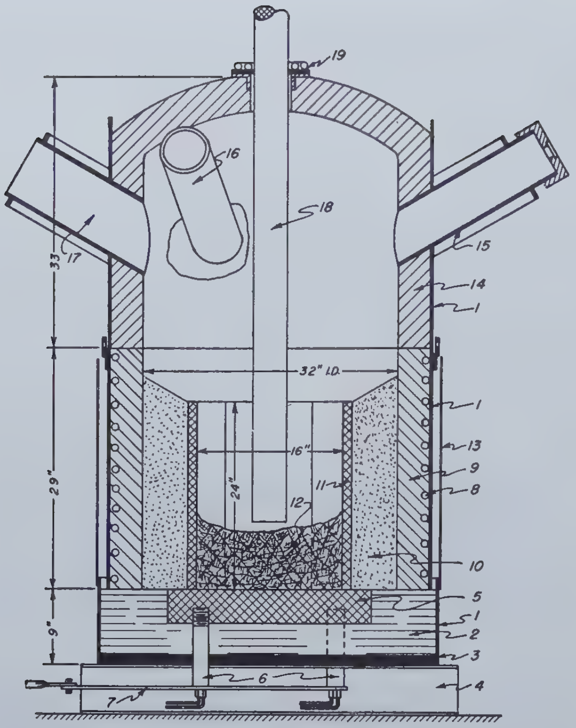

Fig. 2—Arc furnace.

1. Furnace shell. 2. Refractory lining. 3. Steel base plate. 4. I-beam support. 5. Graphite plates. 6. Water-cooled copper plugs. 7. Bus bars. 8. Water cooling. 9. Refractory lining. 10. Charcoal. 11. Graphite plate crucible. 12. Carbide 13. Lifting straps. 14. Refractory lining. 15. Observation tower, water-cooled. 16. Water-cooled charging hole. 17. Water-cooled gas outlet. 18. Graphite electrode. 19. Water-cooled electrode inlet.

of graphite plates, remains unchanged. It is embedded in charcoal within a refractory shell, which is water-cooled through pipes, welded inside the outer iron shell. A domelike upper section contains the water-cooled inlets to feed the reaction mixture into the crucible, to let the reaction gases out, and to observe the melting process. The lining for both shells is rammed super-duty fireclay. With a power input above 250 kva, this lining starts melting in spite of the water cooling. This is also the limit given by the section of the busbars.

The power consumption, which previously was about 8 to 10 kwh per lb of carbide produced from zircon sand, was lowered to about 6 to 8 kwh. The recoveries of zirconium in the carbide were 90 pct when —65-mesh Oregon beach sand was used, but some zirkite, which had been ground to great fineness for air separation, gave recoveries of only 70 pct, the fine particles being readily blown out by the blast of the arc. Therefore, such material is pelleted with addition of 2 pct dextrine, tumbled in a concrete mixer to form nodules that are dried in an electrically heated muffle furnace. This permits recoveries of 75 to 80 pct in the arc-fusion phase when fine materials are used.

Because of its small size, operation of the arc furnace is rather irregular. If too much reducing agent (graphite powder) is added to the batch, the carbide does not fuse, and its amenability to chlorination is poor. An addition to the batch of 18 to 20 pct carbon is satisfactory. Too little graphite results in production of a bluish carbide containing about 3 pct carbon and some quantities of oxide. This carbide sometimes does not give better recoveries than 50 pct in the chlorination. It is rather difficult to obtain the right carbon addition because the fine graphite is easily blown out by the arc when the powder mixture is charged, since it is lighter than the rest of the batch; also, when feeding, air is drawn into the crucible and the reducing agent is partly burned. Therefore, the care of the operator in charging influences the quality of the carbide obtained. With a larger power input, the batch would melt more evenly. With the present furnace, melting takes place only directly under the arc and the electrode therefore has to be moved around over the surface of the batch. Nevertheless, this arrangement gives satisfaction as to the quantity of carbide produced per week, which amounts to about 800 lb made in four working days. The composition of a normal batch is approximately 80 lb of zircon sand and 20 lb of powder graphite. The carbide obtained analyzes approximately 75 to 80 pct Zr, 3 to 4 pct Si, 3 to 5 pct C, up to 2 pct N_2, 1 to 2 pct Fe, about 2 pct Ti, traces of rare earths and uranium, chromium in small quantities, oxygen by difference 1 to 10 pct. Electrode consumption is approximately 0.19 lb per lb carbide produced.

The rather high electrode consumption is caused by burning when the furnace is fed. No carbon monoxide is formed by reduction of the sand at that moment, the arc being interrupted, air can rush into the furnace.

The fumes given off contain large quantities of very fine silica which is scrubbed in a tower with water sprays. Due to the colloidal nature of the particles, this scrubbing is rather inefficient. Bag-house or Cottrell precipitation would be needed for operation on a larger scale.

Chlorination of Carbide

The chlorinator previously described[2, 3] was replaced by a larger one, the inner dimensions of which are 12 in. ID x 55 in. high. This size shaft readily takes up to 750 lb of carbide. The heated condenser used before remained unchanged. A scrubbing device was added to take care of escaping chlorides by water spraying. The setup is shown in figs. 4 and 5. Chlorine, if present in appreciable quantities, of course, is not eliminated by water, which dissolves only a little of this gas. The chlorine is supplied alternately by either of two 1-ton tanks arranged on a scale to check the quantities used. The flow of chlorine is checked with a flowmeter, and a porcelain filter is installed in the line. The arrangement gives satisfaction, and no attempt was made to improve it.

Larger scale operation would call for mechanization in feeding and emptying the chlorinator, and arrangements would have to be made for discharging the condenser. While such improvements might

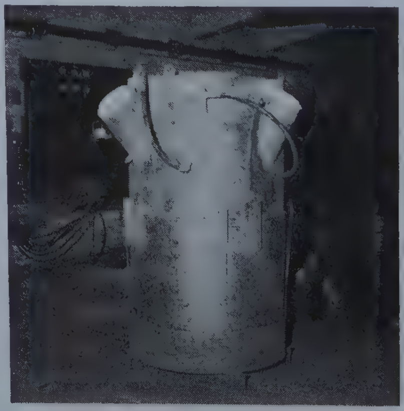

Fig. 3—Arc-furnace assembly.

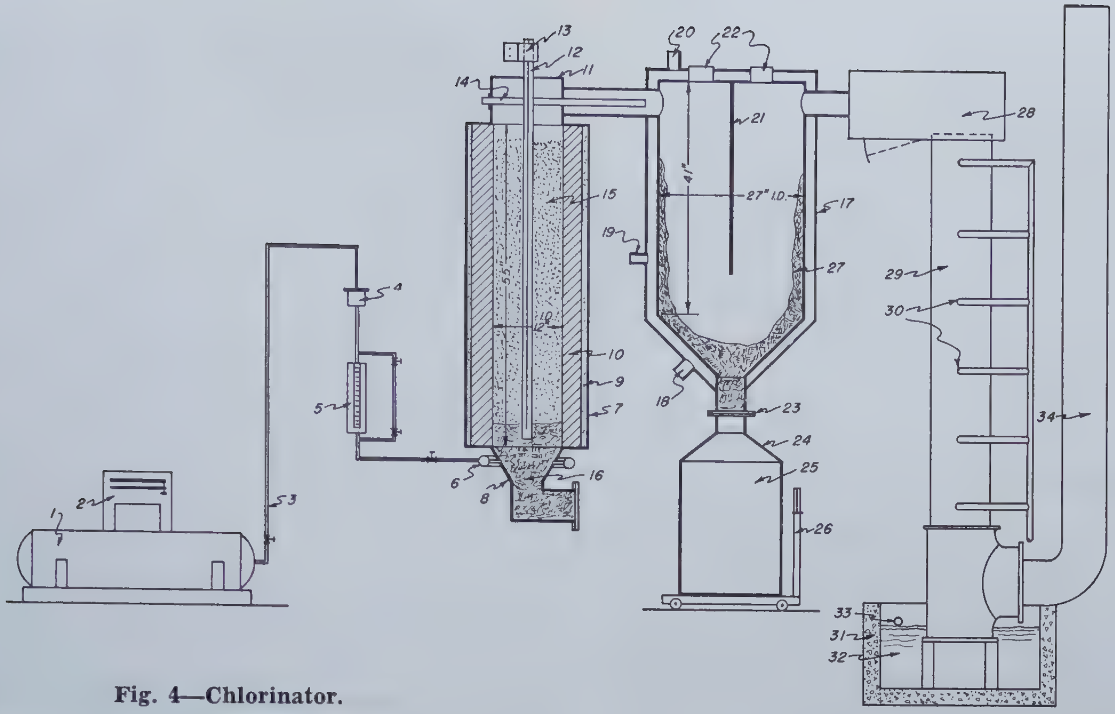

Fig. 4—Chlorinator.

1. Chlorine tank. 2. Scales. 3. Chlorine line. 4. Porcelain filter. 5. Flow gauge. 6. Tuyeres and manifold. 7. Nickel shell. 8. Iron discharge elbow. 9. Silica sand. 10. Silica brick. 11. Nickel manifold. 12 Split-graphite electrode. 13. Water-cooled clamp. 14. Bayonet heater. 15. Batch. 16. Coke bed. 17. Double-wall nickel condenser. 18. Hot air intake. 19. Air discharge. 20. Cold air intake. 21. Baffle. 22. Cleanout openings. 23. Sliding flange door. 24. Conical cover. 25. Drum. 26. Scales. 27. Condensate. 28. Nickel elbow and cleanout box. 29. Cast iron scrubber. 30. Water sprays. 31. Concrete water tank. 32. Water. 33. Overflow. 34. Discharge pipe.

permit obtaining a more uniform chloride and better recoveries, it would be difficult to develop such devices. Feeding the chlorinator mechanically while running would be troublesome, since the temperature of the top must be kept above 331°C to prevent chloride condensation, and free chlorine may sometimes be present. Condensation of zirconium chloride in the feeder would block the mechanism. Accretions within the shaft, which are observed frequently, would choke the feeder with piled-up carbide. The discharging mechanism of the chlorinator would have to run under chlorine, therefore tight stuffing boxes, operating in abrasive material at medium temperatures in chlorine, would have to be built. Automatic discharging of the condenser presents another problem because the chloride deposits partly in the form of heavy, dense layers on the wall of the apparatus and can be removed only by the use of iron scrapers. With all these difficulties in mind, it was thought that batch operation would be preferable for the present scale of operation, the more so since emptying and refilling the chlorinator does not take more than three man-hours.

Fig. 5—Chlorinator.

As mentioned above, the recoveries of chloride vary, depending on the quality of the carbide. Oxide-bearing, bluish carbide does not chlorinate well, even if it contains free carbon. Channeling always takes place to some extent, and chlorine may escape through the voids produced in those sections of the batch which chlorinate through. This difficulty can be overcome to a certain extent by poking the charge with an iron rod. Caking of the batch, caused by an accumulation of fine oxide around unreacted material, results in poor chlorination. The residues sometimes are so fine that they run like dry sand. They may entrap unreacted carbide particles and seal them off from the chlorine. As a result of these conditions, the recovery of zirconium as chloride usually does not exceed 80 pct, while 15 pct remains in the residue and 5 pct is lost through the exhaust. The residues are returned to the carbide furnace. The exhaust loss could be cut down by adding another condenser.

The chloride obtained is white in the beginning of the run and yellow to red toward the end. High-iron concentrations are found in the last-formed chloride. Iron trichloride gas formed in the lower parts of the chlorinator with excess chlorine is reduced to dichloride or to metal by the carbide in the upper sections of the batch, but once chlorine reaches this area, the iron is volatilized again as trichloride. Similar conditions are observed with silicon and titanium chloride. Both are reduced in the beginning of the operation in the upper regions of the shaft, and heavy fumes of both chlorides are observed when the chlorination is nearly finished. Continuous operation would overcome this trouble.

The product obtained contains about 1 to 2 pct iron as trichloride. The aluminum, titanium, and silicon chloride content is low, the exit gases being

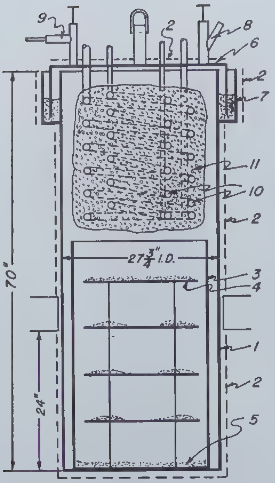

Fig. 6—Purification furnace.

1. Heat-resisting steel shell. 2. Four heating zones. 3. Nickel container. 4. Nickel trays. 5. Residue. 6. Floating top, iron. 7. Lead alloy seal. 8. Bleeding valve. 9. Helium needle valve. 10. Water-cooled coils. 11. Condensate.

held above the condensation point of the chlorides of these elements.

The production capacity of the chlorinator described exceeds 3000 lb a week.

Internal heat is supplied with a graphite hairpin heater element which absorbs up to 12.6 kw at maximum 14 v. The power consumption amounts to 0.56 kwh per lb of zirconium chloride produced.

Purification of Raw Chloride

As described in previous publications[2, 3] the main impurities of the raw chloride are eliminated by subliming under hydrogen. Zirconium oxide remains in the residue with iron dichloride or metallic iron, both of which result from the reduction of iron trichloride with hydrogen. Simultaneously, the powdery raw chloride is condensed as a hard, dense product, which occludes little gas.

This operation is performed in the vessel shown in fig. 6. It consists of a shell constructed of ¼-in. thick 25/20 chromium-nickel stainless steel (type 310) which is placed in a pit-type resistance furnace with three separately controlled heating zones. The furnace top is constructed of ¼-in. mild-steel plate with a flange that fits into an annular trough at the top of the stainless steel shell. This trough is partly filled with lead-antimony eutectic alloy (melting point 247°C) that may be melted or allowed to freeze by controlling the upper zone heating element. The top is heated with nichrome heating elements, and the pipe coils suspended from the top may be cooled with compressed air or water as required. The substitution of lead-antimony alloy for the lead-bismuth alloy previously used for the top seal results in a considerable saving in initial cost and upkeep, but with some slight inconvenience in operation due to the higher melting point of the lead-antimony alloy and its shrinkage on freezing.

The operation is performed as follows: The partly powdery raw chloride is placed on trays in a nickel can, which is deposited in the purification vessel. The floating top is lowered into the fused-alloy seal, which is frozen quickly by circulating water through a ring of ¼-in. iron pipe submerged in the alloy. The vessel is evacuated with a water-jet exhauster (Schutte & Koerting, size 1, 1-in. suction inlet) to about 15 mm Hg, the water pressure being boosted to 90 to 100 psi by a booster pump.

Hydrogen is filled in, and heat is applied to the lower zone until the temperature has reached about 200°C. The hydrochloric gas formed is pumped off with the ejector after a soaking period of a few hours. This operation is repeated. Solid iron trichloride is reduced to dichloride at this temperature, the hydrogen penetrating even compact zirconium chloride chunks to accomplish reduction of the iron. After the lead-alloy seal is melted, the temperature of the lower zone is brought up progressively to a maximum of 600°C, while a hydrogen atmosphere is maintained in the vessel. The coils are first cooled with compressed air, later with water. Any excess pressure caused by formation of hydrochloric gas is bled off through a heated valve. The lead-alloy seal acts as a safety device only. Excessive bleeding through the fused alloy would cause formation of scum. The purification operation takes less than 24 hr for an input of 420 lb of raw chloride. The residue contains mostly zirconium oxide, in addition to iron dichloride and free iron. Uranium and thorium, if present in the zircon sand, are found in this residue in concentrated form; the boiling point of the tetrachlorides of these metals is 618° and 720°C, respectively.

The purified chloride, which is condensed on the coils of the floating top as shown in fig. 7, is a white salt with a slight grayish tint. The recovery in the purification is usually about 96 pct, providing the raw chloride does not contain too many impurities. A small amount of chloride is lost when the hydrochloric gas formed is bled. The residues could be treated for their content of zirconium and rare earths.

Reduction of the Purified Chloride

A vessel of the same kind and size as described for the purification of raw chloride is used also for the reduction. The setup is shown in fig. 8. The crucible, constructed of ¼-in. mild-steel plate and containing buffed magnesium ingots of commercial grade, is lowered into the reduction vessel and covered with a vertically perforated baffle that permits movement of the gases between the inner part of the crucible and the atmosphere of the reaction vessel. This arrangement prevents contamination of the sponge with the lead-seal material, if by accident the seal was sucked back. A shallow pan on top of the perforated baffle permits collecting any particles that might drop off the dense chloride of the coils. The floating top with the chloride is inserted in the fused-lead seal, which is frozen by water cooling. The vessel is evacuated to about 1 mm Hg with a mechanical pump protected with soda lime mixture from any hydrochloric gas that might be present in the atmosphere of the vessel. If the frozen lead-alloy seal leaks, the holes may be plugged with fused paraffin poured on its surface. The vessel is filled with helium 99.8 pct. The evacuation is repeated, and after filling with helium for

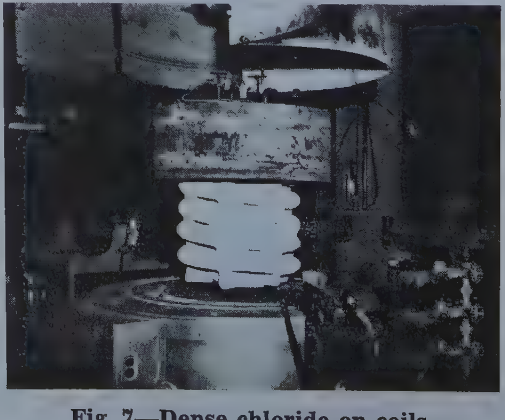

Fig. 7—Dense chloride on coils.

the second time, the seal is fused. The magnesium is raised to its melting point by heating the lower zone of the furnace. After this, the middle-zone temperature is raised to evaporate some zirconium chloride, and the lower zone temperature is raised to about 825°C. Excess gas pressure is taken care of by repeated bleeding through a heated valve. The reaction may start at once and the floating top may drop rapidly, making it necessary to fill in some helium to prevent lead alloy being sucked back. After this flash, the reduction goes on quietly.

It depends on the skill of the operator whether the run will be short or whether it will last over an extended period, the residual helium interfering with the reaction. The zirconium chloride, which is diluted with helium, is continuously eliminated from this gas mixture in the crucible area by the reaction with magnesium, while its concentration in the top zone is built up again by evaporation of solid chloride from the coils. In total absence of helium, zirconium chloride would have to be supplied at such a high rate to prevent formation of a vacuum that overheating would take place and the crucible would alloy with the sponge. It was found that, when the temperature of the controller is set at 825°C, the eventual run-away will not lead to excessive temperatures, if enough helium is present to dampen the reaction. The time needed for one reduction varies between 24 and 36 hr. The end of the operation is marked by a continuous drop in pressure when the middle zone has reached the maximum temperature of about 650°C. Also, the floating top rides high on the lead seal and feels light when moved. After shutting down, the crucible is cooled under dried helium, which is bled in with a heated needle valve from a series of automobile inner tubes used as a gasometer. When opening, after the crucible has cooled to about room temperature, the floating top is removed.

After this, the baffle and pan are removed from the top of the crucible. Both are covered with a black pyrophoric powder, the gas-phase reaction material mentioned in previous reports[2, 3] which may catch fire. Since it contains about 50 pct magnesium chloride, the burning is more like a glow, but much smoke is developed. The sponge in the crucible, being protected by the compact magnesium chloride in which it is entrapped, cannot catch fire. The burning of the vapor-phase material and the bleeding of the reduction and purification vessels make it necessary to provide for hoods with a good draft to take care of fumes.

The efficiency of the reduction can be checked by weighing the crucible with its magnesium content before and after the run. The transfer of purified chloride from the coils to the crucible was 93 pct on an average of 40 runs.

Separation of Excess Mg and $MgCl_2$ from Sponge

It has been shown that zirconium cannot be comminuted by pounding under water, since it reacts explosively under this condition. Titanium powder, however, is made readily by wet-grinding the chips in a ball mill.[6] The separation of the magnesium chloride in vacuum at elevated temperature as previously described[1, 2, 3] permits obtaining a zirconium sponge that is purer than any titanium powder produced by aqueous extraction. The total content of chlorine plus magnesium may be less than 0.1 pct. Simultaneously, the otherwise pyrophoric sponge is sintered, and its activity is greatly reduced.

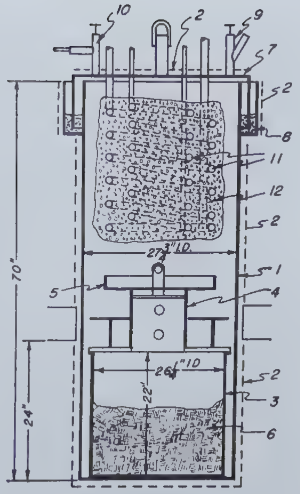

Fig. 8—Reduction furnace.

1. Heat-resisting steel vessel. 2. Four heating zones. 3. Heavy wall iron crucible. 4. Perforated baffle. 5. Pan. 6. Batch. 7. Floating top. 8. Lead alloy seal. 9. Bleeding valve. 10. Helium needle valve. 11. Water-cooled coils. 12. Condensate of dense chloride.

In this process, there are two phenomena that are directly opposed. Raising the temperature would result in a higher vapor pressure of the residual salts and should permit a more rapid and more complete elimination. However, sintering of the sponge, which is also a function of temperature, takes place, and, once the voids are closed, considerable gas pressure would have to be built up inside to permit escape of the salts. High temperature might, therefore, not be advisable for salt removal. However, it would help in eliminating the magnesium, which alloys with zirconium and, after diffusion from the inside, boils off its surface. A compromise temperature of about 825°C inside the crucible and 925°C measured on the retort wall was found suitable for good removal of the salts within 10 hr. There is, in addition, a strict limitation of the maximum temperature with iron as a material of construction for the crucible. At 940°C, iron reacts with the sponge forming a eutectic at this melting point that has an iron content of about 16 pct. Eutectic "tears" form and build up in stalagmites on the stool or on the funnel, on which the crucible rests.

The equipment used in the salt removal is detailed in fig. 9. The crucible containing the products of the reduction is placed upside down on a perforated funnel-shaped base of heat-resisting steel, which rests on a central support column attached to the bottom plate of the retort. A stool (not shown in the drawing) rests on the funnel and extends up into the crucible to hold the sponge in the hot zone after the chloride is melted out.

A can constructed of light-weight, heat-resisting steel is supported on the central column underneath the crucible holder to collect the fused chloride. The major portion of the chloride melts out of the crucible so that only the chloride and magnesium actually entrapped in the sponge must be eliminated by evaporation. Removable condenser shields of 24-gauge stainless steel are provided in the lower portion of the retort to collect the distilled chloride and magnesium.

The condenser portion of the retort is cooled with fuel oil circulated through the cooling jacket at the rate of about 15 gpm. The oil is in turn cooled with water in either one or two tube-type heat exchangers. Oil cooling was preferred to water cooling, since an oil leak would not harm zirconium appreciably. However, with reliable welds, there would be no objection to direct water cooling.

The vacuum system is made up of a mechanical pump, a phosphorus pentoxide drying tower, an oil-

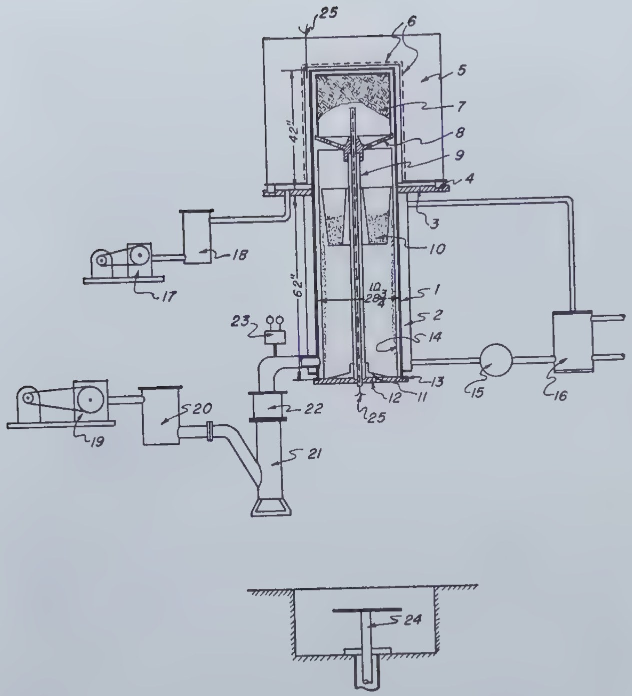

Fig. 9—Distillation retort.

1. Retort shell. 2. Oil cooling jacket. 3. Flange. 4. Water-cooled rubber gasket. 5. Vacuum nichrome resistor furnace. 6. Heating elements. 7. Crucible with batch. 8. Stainless steel funnel. 9. Stainless steel column. 10. Salt can, stainless steel. 11. Support for column, stainless steel. 12. Water-cooled base plate. 13. Water-cooled rubber gasket. 14. Condenser shields of stainless steel. 15. Oil circulating pump. 16. Heat exchanger. 17. Mechanical vacuum pump for vacuum furnace. 18. Drying tower. 19. Mechanical vacuum pump for inner retort. 20. Drying tower. 21. Oil diffusion pump. 22. High vacuum valve. 23. Box with vacuum gauges. 24. Hydraulic ram. 25. Thermocouples.

diffusion pump, and a vacuum valve. The diffusion pump can be bypassed with an auxiliary mechanical pump for pre-evacuation of the retort. Also, a separate vacuum line and valve permit bypassing the diffusion pump if pressure builds up. A thermocouple and RCA gas-discharge gauge are inserted in a separate chamber in the high-vacuum line. A filling system for admitting helium is connected with the high-vacuum line ahead of the vacuum valve. All thermocouples and vacuum gauges are wired to recorders on a panel board.

The retort is heated at its upper end by a separate vacuum furnace (fig. 10), which can be lifted off and moved to a second retort, as described later. The vacuum in this furnace is maintained with a small mechanical pump protected against moisture by a drying tower.

The bottom plate seals the retort against the atmosphere with a rubber gasket. The temperature is raised to the melting point of the magnesium chloride, about 714°C, at which point hydrogen is liberated. The quantities of hydrogen vary. There are three different sources for this gas, the magnesium used, the reaction of magnesium with hydrochloric gas and with moisture. The last two reactions originate from the moisture of the air, either when the chloride is handled or when the apparatus is opened.

It appears that with the 20 pct excess magnesium used in the reduction, some of the zirconium sponge, which is reduced first with a large magnesium excess, is obtained in a pasty, perhaps alloyed, form, the magnesium being a binder for the zirconium crystals. This sponge is dense and aggregates in the corners of the crucible. In the distillation, it sometimes melts off and runs down onto the funnel. It produces somewhat harder ingots than the light sponge, since it contains more iron and oxygen. This can be explained by the fact that the fused magnesium as a getter collects the atmosphere of the reaction vessel, and the first zirconium reduced by this magnesium alloys with the impurities. The light sponge, which is produced at the end of the reduction, is not fused but dendritic in appearance. It usually contains more magnesium and magnesium chloride after distillation than the dense sponge, because, in the distillation, it is located in the colder part of the retort and frequently drops onto the stool, as mentioned above.

The retort can be rapidly cooled by blowing air through the U-shaped inconel tubes built into the refractory of the heating furnace with a Roots-type blower mounted on the top of the furnace (not shown in drawing). With use of this forced cooling, the temperature at the outside wall of the retort is reduced from 920° to 400°C in 12 hr, as against 24 hr required without forced cooling. After cooling to 400°C, air is admitted to the outside vacuum chamber and the furnace is lifted off and transferred to the second retort. Cooling of the first retort is continued with a fan, about 24 hr being required to lower the temperature from 400° to 35°C. The whole cycle, including 10 hr at the maximum temperature, is about 60 hr.

Before the retort is opened, the sponge is conditioned with air, which is admitted in small increments for about 3 hr. For reasons of safety, the retort is once more evacuated and filled with helium. This prevents fires from spreading upward to the sponge when opening the retort, if the magnesium powder, sometimes found on the bottom plate, ignites. The inner retort parts, with the column and bottom plate, are lowered with a hydraulic hoist. Once the crucible is within reach, it is clamped into a special carriage and tilting device that permits turning it in the vertical position. In general, about two-thirds of the sponge is obtained in dense form, stuck to the bottom and in the corners of the crucible. The remaining third is light material from the center that is frequently found resting on the stool. The latter, which is evidently reduced last, must be handled with care, as it is more pyrophoric than the dense material.

There are small mechanical losses in the retort operation in the form of fine material adhering to the stool and funnel. The recovery may be as high as 99.5 pct in this phase of the process. A little zir-

Fig. 10—Vacuum retort and furnace.

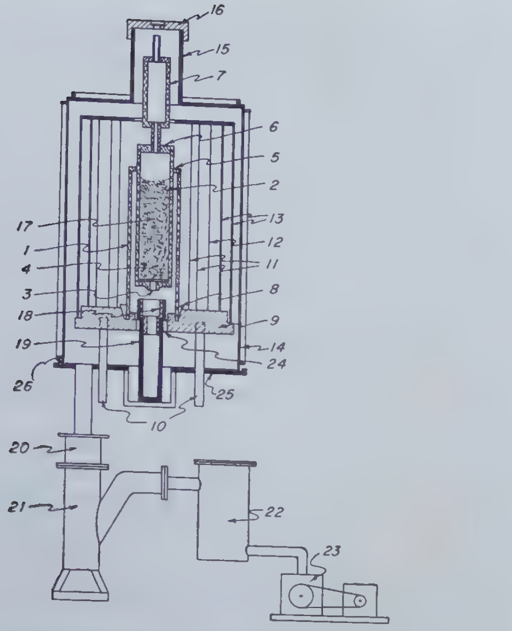

Fig. 11—Graphite-resistor split-tube vacuum furnace.
1. Split-tube graphite resistor. 2. Graphite crucible. 3. Tap holes. 4. Graphite spider. 5. Threaded support ring of graphite. 6. Graphite cover. 7. Graphite condenser. 8. Copper wedges. 9. Water-cooled copper clamp. 10. Water-cooled bus leads. 11. Double graphite radiation screen. 12. Molybdenum radiation screen. 13. Quartz shields. 14. Water-cooled iron shell. 15. Observation tower. 16. Cover with window. 17. Batch. 18. Expendable graphite hot top. 19. Graphite mold. 20. High vacuum valve. 21. Oil diffusion pump. 22. P_2O_5 drying tower. 23. Mechanical pump. 24. Quartz insulation ring. 25. Water-cooled brass base plate. 26. Water-cooled rubber gasket.

conium chloride remains dissolved in the salts after the reduction, since mixing is not possible. Also, some lower zirconium chloride is entrapped in the sponge and may break up to metal and zirconium tetrachloride during the salt separation. This residual tetrachloride and that contained in the magnesium chloride are reduced with gaseous magnesium in the retort, and a metallic deposit of zirconium may cover the funnel as a thin and rather pyrophoric sheet of zirconium.

The loose sponge in the center of the crucible can readily be removed, while the dense material sometimes sticks strongly to the walls. It is broken up with a heavy iron chisel that is operated with a 30-ton Arbor press. Both kinds of sponge are cut up with a strong knife in a hydraulic press, the chips being about 1 to 2 in. in size. These chunks are briquetted in a die made of nitrided nitralloy at about 100 tons pressure. The diameter of the briquets is 4 in.

Sponge Melting

The split-tube, graphite, resistor-type furnace, described before,[2-5] is used for this purpose. A larger, two-phase furnace was set up, as shown in figs. 11 and 12. The bottom plate is provided with an extension that permits inserting long graphite molds. A quartz ring centers this mold at the level of the clamp and also insulates it. The crucible is provided with a graphite condenser that fits tightly in the graphite cover. In this way, most of the magnesium and magnesium chloride driven off during melting is collected, and the furnace is not contaminated. The bottom of the crucible is provided with a protruding button that is perforated with six ⅛-in. diam holes, and a graphite cross is inserted over these tap holes. This cross was found necessary to eliminate rotation of the metal jet, once pouring starts. The two-phase current causes rotation of the bath; the metal jet, without these devices, would hit the wall of the mold by centrifugal force and cause cold shuts. The power input is 60 kw, which is supplied only during the last 2 min. The maximum voltage is 17 v. With this energy, up to 25 lb of compact metal are melted in 20 min. The power consumption is in the range of 1.4 kwh per lb. Briquets take more space, and the maximum output with this material is about 15 lb. Turnings and sheet clippings can be remelted with no appreciable increase in hardness. The former must be briquetted.

The carbon pickup is about 0.15 pct for the first melt. Remelts go up to 0.25 pct carbon. This content is not considered to be harmful for most uses to which zirconium is put. It was not possible to increase the carbon content above 0.37 pct, even by repeated remelting under graphite powder. This seems to be the limit of solubility of carbon in zirconium at its melting point. The wear on the graphite crucibles is only slight, and as many as 30 runs have been made with one.

The main difficulty in sponge melting is the splashing. Gas is evolved during fusion, and liquid metal is driven up to the cold top of the crucible, where it freezes and forms a gas-tight seal with unmelted briquets. Pressure now builds up beneath, and the liquid metal is pushed sometimes so violently into the mold that it runs over the rim and short-circuits the resistor slots. This difficulty can be overcome by draining the liquid metal as it forms. The briquets may be put on a graphite plate arranged in the middle of the crucible and provided with holes of 1-in. diam, or briquets of smaller diameter may be used. Loose sponge on top helps also, but this too reduces the capacity of the crucible. The causes of the gas evolution have not been reliably ascertained. It is probable that magnesium, magnesium chloride, zirconium chlorides, and helium escape during melting. The individual briquets glaze over with fused metal, pressure from the impurities builds up internally, and once it is released downward against the fused and extremely fluid metal, the metal is driven upward in the cold zone.

Castings can readily be made in a graphite mold. Because the metal is extremely fluid, the finest details of the mold are filled with metal, as shown in fig. 13.

Plant Layout and Furnace Description

A short report about this plant has already been published.[7] The viewpoints for increasing the production, from about 60 lb a week produced in the large laboratory-scale unit to 600, have been de-

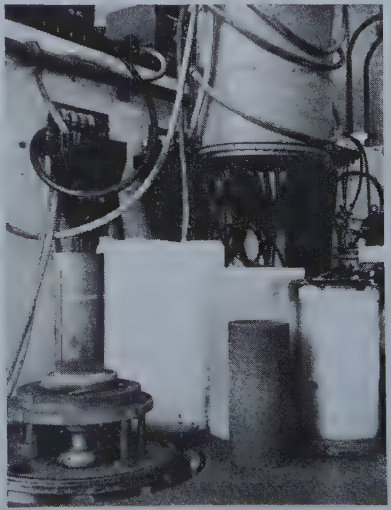

Fig. 12—Two-phase, split-graphite tube, vacuum resistor furnace.

scribed before.[3] As the purification cycle is only about 24 hr, one purification furnace could supply material for at least two reduction furnaces. Two distillation retorts are provided, but only one furnace is used to heat both of them. This furnace is taken off the first retort when the temperature has dropped below 400°C and slipped over the second retort for another run, as shown in fig. 14.

The purification and reduction furnaces have three heating zones; the bottom, middle, and lead seal zone are heated separately. Besides this, the floating tops are provided with separate heating elements. The power requirements for all furnaces are given in table I.

Table I. Power Requirements

Purification Furnace		
Floating top	220 v	7.6 amp max
Lead seal zone	115 v	16 kva
Middle zone	115 v	23 kva
Bottom zone	230 and 44 v	combined 46 kva
Reduction Furnace		
Floating top	220 v	7.6 amp max
Lead seal zone	230 v	13 kva
Middle zone	235 v	46 kva
Bottom zone	235 v	46 kva
Vacuum Retort Furnace		
	110 and 95 v	70 kva

Typical heating charts for the purification, reduction, and salt separation are shown in fig. 15. It may be observed that the present setup permits making up to three runs a week, corresponding to an output of 450 lb, providing sufficient personnel was available. A view of the operation floor is given in fig. 16.

The manpower requirements are:

Carbide furnace	2 semiskilled men	1 supervisor
Chlorination	2 semiskilled men	
Purification, reduction, and vacuum distillation	2 semiskilled men per shift, 3 shifts, 5 days 1 supervisor	
Melting	1 semiskilled man per shift, 2 shifts 1 supervisor	
Briquetting and sponge removal	1 semiskilled man	

Results

Sampling of the sponge is difficult, and its composition varies within the crucible. The sponge produced has the approximate composition given in table II.

Sponge taken directly from the wall of the crucible may have a few tenths of a percent iron. The determination of trace elements in zirconium by chemical methods, especially aluminum and silicon, is not reliable.

Ingots produced show only traces of chlorine and magnesium, but if melted in graphite, the metal from sponge picks up a small amount of carbon.

Fig. 13—Vacuum-cast zirconium diffuser.

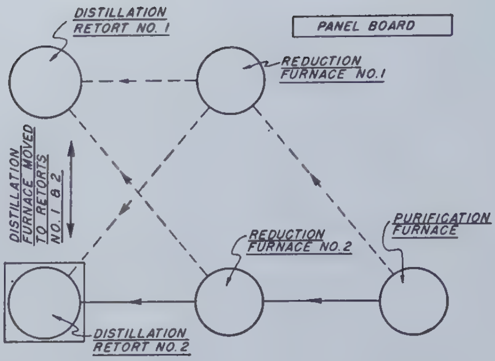
DISTILLATION RETORT NO. 1
PANEL BOARD
REDUCTION FURNACE NO. 1
DISTILLATION FURNACE MOVED TO RETORTS NO. 1 & 2
REDUCTION FURNACE NO. 2
PURIFICATION FURNACE
DISTILLATION RETORT NO. 2

Fig. 14—Diagram layout of zirconium pilot plant.

The oxygen content, determined by the dissolution of ingot material in iron (vacuum-fusion method) with carbon as a reducing agent, for a Rockwell B hardness of 75, is about 0.07 pct. Iodide zirconium rods analyzed by the same method indicated the presence of only 0.014 pct oxygen. The ratio of oxygen to nitrogen (0.07 : 0.02) in Bureau of Mines zirconium clearly shows that the oxygen does not originate from the air, since otherwise its content would be below 0.004 pct to maintain the ratio $O_2 : N_2$ that exists in the air. Part of the oxygen can be traced to the oxide skin on the magnesium, which buffing does not remove. Improvements can be expected by remelting the magnesium in a helium atmosphere to remove deeply entrapped oxide, before using it. Another source of oxide is moisture that is introduced in the reduction and salt separation, but this can only be a very small amount, since zirconium chloride and magnesium chloride eliminate any moisture before it can come in contact with zirconium. Very small amounts of oxygen may originate from the helium used. One certain source of oxygen is the oxide skin formed on the zirconium sponge when exposed to air. This is unavoidable. Only by reducing the surface could this contamination be minimized. Sintering in salt separation may, therefore, contribute to a reduction of the oxide content.

The recoveries recorded from 40 batches are, on an average, as follows: purification, 96.2 pct; reduction, 93.0 pct; salt separation, 96.8 pct; total recovery from the raw chloride to the sponge, 86.6 pct.

A loss of about 6 pct occurs when the sponge is removed from the crucible, the iron-rich parts found in contact with the wall being discarded at present, or recycled through the chlorination step.

Production Costs

Zirconium now sells, in its chloride, at about $0.95 per lb of metal contained, which is lower than the $1.03 paid today for titanium in its anhydrous chloride.[6] Zirconium in sand costs about $0.06 per lb, which is little more than titanium in ilmenite. Considering that titanium requires about twice as much magnesium for its reduction as does zirconium, this

Table II. Sponge Composition, Percent

Light Sponge					
Cl_2	0.02—0.80	C	0.02	Mn	0.02
Mg	0.06—0.80	Si	0.01	Al	0.02
Fe	0.05	Ti	0.01	N_2	0.02
Heavy Sponge					
Cl_2	0.01—0.20			Ti	trace
Mg	0.05—0.40			Mn	0.02
Fe	0.05—0.1			Al	0.02
Si	trace			N_2	0.02

more than compensates for the slightly higher price of the latter in its ores, the extraction methods for both metals being practically the same. It can, therefore, be expected that both metals will sell at virtually the same price, providing they are produced on the same scale.

In the cost estimate made in table III, the sales price of $0.37 per lb of raw zirconium chloride will be taken as a base. It was not possible to produce the raw chloride in the pilot plant described above at this low cost because of too small a scale of operation of the carbide furnace. The costs given are direct operating expenses only and do not include general overhead, interest, depreciation, insurance, or taxes.

Table III. Cost Estimate

A. Production of sponge, including purification, reduction, and salt separation:		
Chloride	2.96 lb @ $0.37	$1.10
Operating supplies including magnesium		0.31
Power	24 kwh @ $0.0025	0.06
Labor and supervision		2.15
Total per pound of sponge		$3.62
B. Cleaning, cutting and briquetting of the sponge:		
Raw sponge	1.175 lb	$4.25
Labor and supervision		0.22
Total per pound of briquets		$4.47
C. Melting and finishing the ingots:		
Briquetted sponge	1.035 lb	$4.63
Operating supplies and power		0.32
Analysis		0.49
Labor and supervision including machining ingots		1.38
Total per pound of finished, machined ingot		$6.82

In these costs the raw materials, chloride and magnesium, account for only 22.8 pct, labor and supervision 69.3 pct of the total. The cost of production of zirconium chloride seems to be much too high, considering that the metal in the ore can be bought for only $0.06 per lb, while it costs $0.95 in the raw chloride. Small savings could be made by passing the byproduct, magnesium chloride, through a fusion electrolysis to reclaim chlorine and magnesium, but the outlay for magnesium is only 4.5 pct of the total cost. The actual costs are a result of small-scale operation, as can be seen from the high percentage of the salaries and supervision. Improvements in that regard will result from the tapping of the salts and continuation of the reduction with liquid magnesium to make better use of the crucible and furnace capacity. Such methods have already been found successful on a small scale. The final development of this process will probably lead to continuous reduction, once the many problems concerning temperature control and materials of construction have been solved.

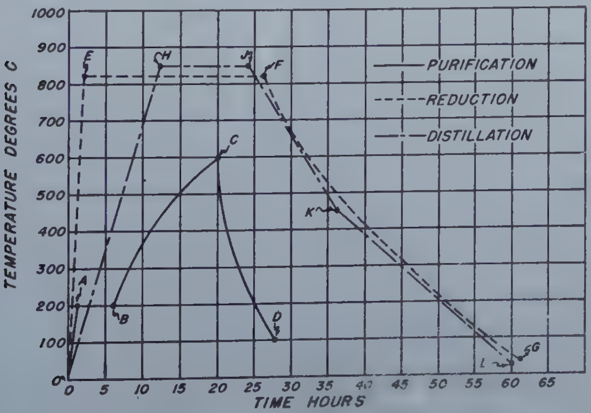

Fig. 15—Time-temperature schedules (inside temperature).

Fig. 16—Operation floor.

Conclusions

It has been shown that zirconium can be produced in units yielding 150 lb per batch at a reasonably low cost. The plant is described. The size of the present equipment can certainly be increased considerably before difficulties with heat dissipation will appear. Zirconium is favored in that regard in comparison with titanium, since the heat of formation of its chloride is much higher, the heat evolved in reducing, therefore, is much lower. Titanium reactors of 200 lb are in use now.

In the present pilot plant, zirconium ingots can be produced for $6.82 per lb. The future price of the metal will probably be the same as that of titanium, the methods of production are practically identical, and the higher cost of the one in its ore is more than compensated by the higher consumption of reducing agent for the second.

Acknowledgments

This investigation is part of a plan of the U. S. Bureau of Mines to develop the natural resources of the country. It is directed by O. C. Ralston, Chief Metallurgist, Bureau of Mines, and S. M. Shelton, Chief of the Albany station. The authors had in their work the valuable assistance of J. P. Walsted, who is in charge of carbide and chloride production, and of H. L. Gilbert, who operates the melting-furnace department. The important contributions of these investigators as well as those of the many other members of the staff are herewith gratefully acknowledged.

References

[1] W. J. Kroll, A. W. Schlechten, and L. A. Yerkes: Ductile Zirconium from Zircon Sand. *Trans.* Electrochem. Soc. (1946) **89**, 263-276.

[2] W. J. Kroll, A. W. Schlechten, W. R. Carmody, L. A. Yerkes, H. P. Holmes, and H. L. Gilbert: Recent Progress in the Metallurgy of Malleable Zirconium. *Trans.* Electrochem. Soc. (1947) **92**, 99-113.

[3] W. J. Kroll, C. T. Anderson, H. P. Holmes, L. A. Yerkes, and H. L. Gilbert: Large Scale Laboratory Production of Ductile Zirconium. *Journal* Electrochem. Soc. (1948) **94**, No. 1, 1-20.

[4] W. J. Kroll, C. T. Anderson, and H. L. Gilbert: A New Graphite Resistor Vacuum Furnace and Its Application in Melting Zirconium: *Transactions* AIME (1948) **175**, 766-773; *Metals Technology* (Jan. 1948) TP 2310E.

[5] W. J. Kroll and H. L. Gilbert: Melting and Casting Zirconium Metal. *Journal* Electrochem. Soc. (Sept. 1949) **96**, No. 3, 158-169.

[6] F. S. Wartman, J. P. Walker, H. C. Fuller, M. A. Cook, and E. L. Anderson: Production of Ductile Titanium at Boulder City, Nevada. Bureau of Mines. *Report of Investigations* No. 4519, Aug. 1949.

[7] W. J. Kroll and W. W. Stephens: Pilot Plant for the Production of Malleable Zirconium. *Industrial and Engineering Chemistry* (1950) **42**, 395-398.

The Torsion Texture of Copper

by W. A. Backofen

Pole figures are presented which describe the texture of OFHC copper and electrolytic, tough-pitch copper subjected to various amounts of torsional strain. The development of the torsion texture does not appear to be influenced by the principal normal strain history since all pole figures are symmetrical about directions parallel and perpendicular to the longitudinal axis of the torsion specimen. An explanation of the mode of plastic flow in pure torsion has been suggested.

THE preferred orientations, or textures, resulting from many of the various methods for testing and forming metals have been the subject of numerous investigations.[1, 2]* Despite this large amount of work, however, only a few limited studies have been made of the texture that is developed by torsional deformation.

Ono[3] found that in severely twisted wires of copper and aluminum a [111] direction lies parallel and a [110] direction perpendicular to the longitudinal axis of the wire. Sachs and Schiebold[4] have reported that a double-fiber texture exists in a twisted aluminum wire with both the [111] and [100] directions parallel to the axis of the wire. Twisted iron wires have also been examined by Ono.[3] Both the [110] and [112] directions were reported as parallel to the axis of the wire. Goss[5] concluded from a study of twisted rods of a low-carbon steel that the preferred orientation existing at fracture is quite complex, but that many grains have a [110] direction parallel to the axis of the wire.

In addition to the earlier experimental work, some suggestions have been made about the possible nature of the torsion texture. These suggestions are based on the results of many experiments which indicate that the cold-working texture of a particular metal is largely determined by the geometrical change in shape that the metal undergoes during plastic deformation.[1, 6] Hibbard and Yen[7] have considered the problem of deformation textures and have presented an analysis which is able to explain why equivalent changes in shape should yield similar textures.

Therefore, a knowledge of the principal strains associated with torsional deformation would seem helpful in the interpretation of the torsion texture. The necessary analysis has been made of the state of strain in an element of metal lying in the surface of a cylindrical rod or tube that has been subjected to pure torsion.[8, 9] This analysis shows that the directions of the principal normal strains rotate continuously within a torsion specimen while it is being twisted. After the first infinitesimal amount of twisting, these directions make angles of 45° with the longitudinal axis of the bar. They rotate from this position as twisting proceeds, and after an infinite amount of twisting, the direction of the principal tensile strain is perpendicular, and the direction

---

* References 1 and 2 contain excellent summaries of the results of these investigations.

W. A. BACKOFEN, Student Associate AIME, is Assistant Professor of Metallurgy, Massachusetts Institute of Technology, Cambridge, Mass.

AIME St. Louis Meeting, February 1951.

TP 2976 E. Discussion (2 copies) may be sent to Transactions *AIME before April 1, 1951. Manuscript received July 24, 1950; revision received Oct. 20, 1950.*

of the principal compressive strain is parallel, to the longitudinal axis. The amount of twisting, which is most conveniently expressed as a shear strain, determines the orientation of the principal normal strain directions. Following this analysis, Hill[8] has proposed that the torsion texture is symmetrical about the principal directions of normal strain, and therefore the symmetry axes of the texture must rotate within the above-mentioned limits as twisting progresses.

Barrett[1] has been even more specific and has suggested that the torsion texture and the cold-rolling texture are related in the following way. There are no appreciable changes in the diameter of a cylindrical rod or tube deformed in plastic torsion. Consequently, the radial direction in the torsion specimen may be considered equivalent to the transverse direction of a rolled sheet which similarly does not undergo any marked change during cold-rolling. The direction of the principal tensile strain associated with torsional deformation is then comparable to the rolling direction of the sheet. Therefore, it is likely that the torsion texture consists of a cold-rolling texture inclined with respect to the axes of the torsion specimen. The "rolling direction" and the normal to the "rolling plane," both of which are considered to be symmetry axes of the texture, are expected to lie in the surface of the specimen.

Experimental Procedures

Materials and Testing: Pole figures were obtained from five specimens of OFHC copper and one specimen of electrolytic tough-pitch copper. Two sizes of OFHC copper specimens were used. Their dimensions are shown in fig. 1. Only one specimen of size *B* was twisted. The OFHC copper bars were machined from cold-swaged stock. Size *A* was annealed in a salt-bath for ½ hr at 450°C and size *B* in air for 1 hr at 500°C. The resulting structures were both fine-grained and randomly oriented. The bar of electrolytic copper was a 16-in. length of a ¾-in. diam cold-finished round. No reduced section was machined into this specimen. It was annealed in air at 650°C for 1 hr before twisting.

The four bars of OFHC copper of size *A* were twisted in a torsion testing machine which has been described elsewhere.[10] Three of these bars were twisted to shear strains of 0.70, 1.90, and 3.95. The fourth bar was twisted first to a shear strain of 5.25 and then untwisted by exactly the same amount. The maximum shear strain, γ, at the surface of a test specimen is defined as:

$$\gamma = \frac{r\,\theta}{l}$$

where r is the radius of the bar; θ the total number of radians through which the bar is twisted; and l the length over which twisting takes place. l is considered equal to the distance between the bottom of the radius at each end of the gauge length. Examination of the twisted bars showed that the deformation was largely confined to this length. All twisting of size *A* specimens was done at a constant rate of 120° per min. Unfortunately, the provision incorporated in this machine for accomodating the small amount of axial extension of a bar subjected to plastic torsion did not appear to operate consistently and satisfactorily. Therefore, a slight deviation from deformation in pure torsion undoubtedly resulted due to the presence of a low compressive stress directed along the axis of the specimen. This was found, however, to have negligible effect upon the texture.

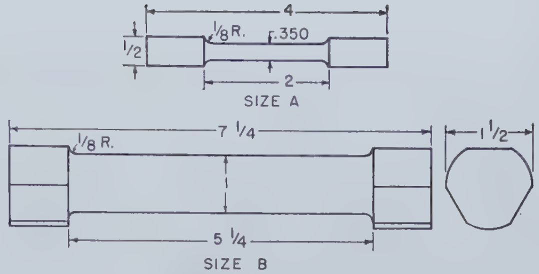

Fig. 1—OFHC copper torsion specimens.

The remaining specimens were twisted in a Riehle torsion testing machine of 60,000 in-lb capacity. The fixed jaw gripping one end of the bar is in the weighing head which is supported by chains and thus perfectly free to move when any lengthening occurs in the bar being twisted. The OFHC copper specimen of size *B* was twisted to a maximum shear-strain of 7.7. The distance, l, over which twisting occurred, was again defined as the distance between the bottom of each radius. The electrolytic copper specimen was twisted to a maximum shear-strain of 5.25. The length, l, in this case, was the distance between the jaws of the machine. Twisting of these specimens was done at a constant rate of 215° per min.

Construction of Pole Figures: After twisting, a 1-in. length cut from the middle of each bar (except the one of OFHC copper of size *B*) was carefully bored out to form a tube with a 1/32-in. wall. A small rectangular specimen was removed from the wall of each tube with a jeweler's saw. The larger dimension of the specimen was parallel to the longitudinal direction (L.D.) of the tube. The smaller dimension, perpendicular to the longitudinal direction, is described below as the transverse direction (T.D.). Each specimen was etched to a thickness of about 0.0025 in. in a 50 pct solution of nitric acid. All specimens possess a uniform amount of shear strain which is approximately equal to the maximum amount introduced into the surface of the bar by the twisting.

Methods Employing a G-M Counter Tube for Intensity Measurements: The method of constructing pole figures developed by Decker, Asp, and Harker[11] was used for the (111) pole figures of the specimens obtained from the bars of OFHC copper of size *A* and the bar of electrolytic copper. This method requires the use of an X-ray unit, such as a Norelco recording X-ray spectrometer, fitted with a Geiger-Mueller (G-M) counter tube. A specimen is mounted in a special sample holder in the path of the X-ray beam and is rotated about two mutually perpendicular axes. For each setting of the sample holder, the counter is used to determine the intensity of the diffracted beam and therefore the pole density for a particular point within the pole figure. A correction factor must be applied to the measured intensities to provide for the change in the angular position of the sample with respect to the incident beam. The magnitude of this factor is presented graphically in the appendix for various sample thicknesses and inclinations to the incident beam. All pole figures constructed by this method are found in figs. 2 through 4. Only one quadrant of each pole figure is presented, since X-ray photograms showed that the pole figures are symmetrical about the longitudinal and transverse axes.

The pole figures for electrolytic copper and for OFHC copper twisted to a shear strain of 3.95 were constructed from two complete quadrants. The intensity maxima lying on the basic circle of all pole figures were accurately determined in four quadrants. Within the areas of low pole density, intensity measurements were made after every 10° interval of rotation. Rotation intervals of 5° were used when regions of greater pole density were encountered. All intensity maxima were located with rotations of 2½°.

Six intensity ranges could be conveniently established. These were used in plotting all figures. Since the thicknesses of all specimens were not exactly the same, it is not possible to make a rigorous comparison of the pole figures. Nevertheless, the development of the texture as twisting proceeds is readily observed.

Information about the central area is absent in all pole figures constructed in this way. However, the technique that Norton[12] has developed for making pole figures of rolled sheet can be used to obtain this information. This method also employs an X-ray unit equipped with a G-M counter for measuring intensities.

Many small rod-specimens are required by this procedure and these were extracted from a twisted bar in the manner illustrated in fig. 5. The OFHC copper bar of size *B*, twisted to a maximum shear strain of 7.7, was bored out to form a tube with a ⅛-in. wall. Square blanks of 1/16 in. were then cut out with a jeweler's saw and carefully turned to a diameter of 0.045 in. Each rod was then slowly revolved in a 50 pct solution of nitric acid until its diameter was 0.030 in. Since the shear-strain gradient in plastic torsion is linear, it can be readily computed that the material from which these rods were made was subjected to a shear strain of approximately 6.75.

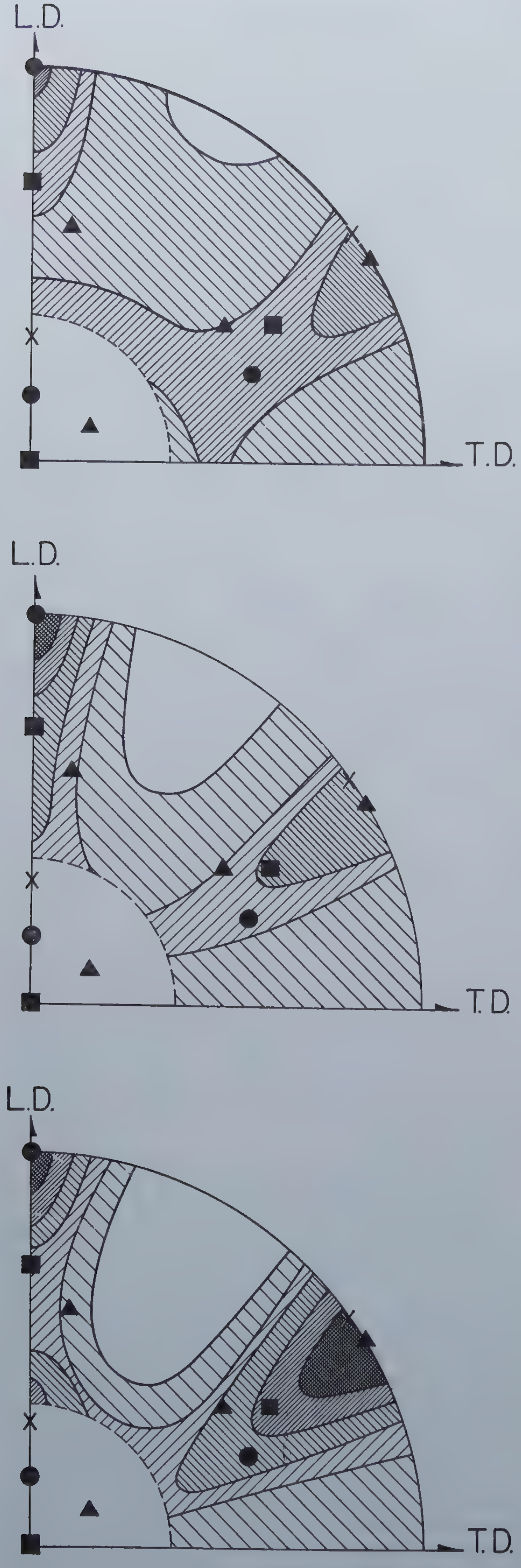

Fig. 2—(111) pole figures of twisted OFHC copper.

a. Top — Shear strain of 0.70
b. Center — Shear strain of 1.90
c. Bottom — Shear strain of 3.95

Ideal orientations indicated as follows:
● (112) [11$\bar{1}$], ■ (11$\bar{1}$) [112], x (110) [001], ▲ (112) [1$\bar{3}$1]

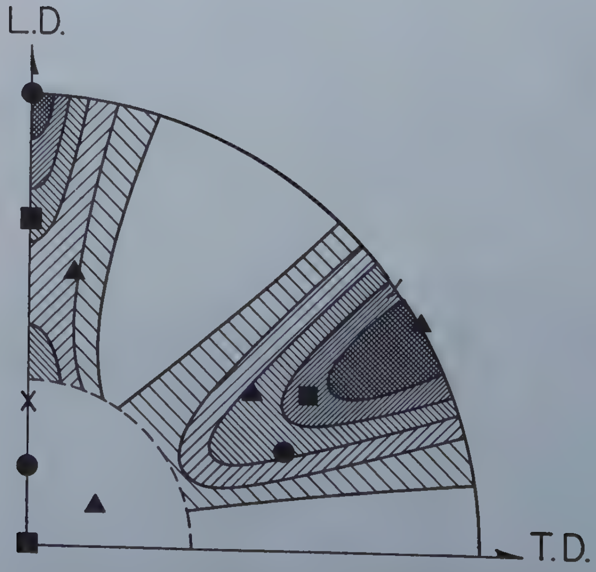

Fig. 3—(111) pole figure of OFHC copper twisted to a shear strain of 5.25 and then completely untwisted.

Ideal orientations indicated as follows:
● (112) [11$\bar{1}$], ■ (11$\bar{1}$) [112], x (110) [001], ▲ (112) [1$\bar{3}$1]

Each rod in turn was held in a special mount, placed in a beam of CuK$_\alpha$ radiation, and slowly rotated about its axis through 360°. The G-M counter tube was set to receive the diffracted radiation from the {111} planes. The intensity measured by the counter tube was autographically recorded, and a curve was obtained of intensity vs. angular position. The curve for each rod describes the intensity variation in arbitrary units along a particular diameter of the pole figure. No absorption correction is necessary since all rods are cylindrical and of the same diameter. Contours drawn through points of equal intensity on all diameters describe the pole density in the figure. One quadrant of such a pole figure is shown in fig. 6. Each plotted point in this figure is the average of intensities measured in four quadrants.

The pole figures constructed by the methods described above have made possible a reasonably detailed study of the texture of copper that has been strained various amounts in torsion. The stresses accompanying torsional deformation are known. Therefore, from the interpretation of these figures and a knowledge of the stresses, it should now be possible to obtain some understanding of the mode of plastic flow in pure torsion.

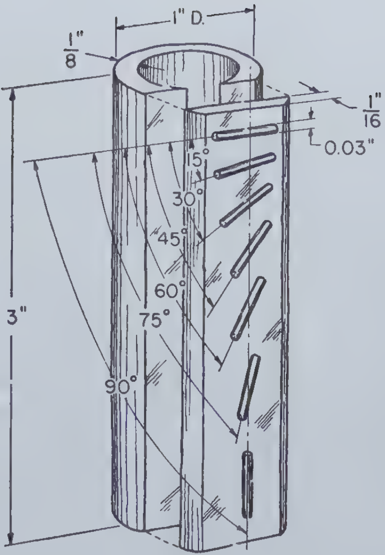

Fig. 5—Method of obtaining the specimens used in the construction of the pole figure in fig. 6.

Discussion of Results

The combination of the four ideal orientations or textures, (112) [11$\bar{1}$], (11$\bar{1}$) [112], (110) [001], and (112) [1$\bar{3}$1], which have been included in each of the preceding pole figures, may be used to describe the torsion texture observed in copper. In these orientations, the crystallographic planes are tangential to the surface and the directions are parallel to the longitudinal axis of the torsion specimen. An analogous scheme is used to describe the texture of drawn tubing which undergoes only a reduction in wall thickness. Although four ideal orientations have been chosen, it is difficult to emphasize any one more than the others, since all are necessary for an adequate description of the pole distribution within the figures.

This description of the torsion texture applies after various amounts of unidirectional twisting as well as equal amounts of forward and reverse twisting. But the direction of the principal normal strains are different for each value of shear strain and the rotation of the principal normal strain directions may be reversed by untwisting. Therefore, contrary to what might be expected, the principal normal strain history does not appear to influence the development of the torsion texture.

The ideal orientation (112) [1$\bar{3}$1] is but one of the four, (112) [1$\bar{3}$1], (112) [$\bar{3}$11], ($\bar{1}\bar{1}$2) [1$\bar{3}\bar{1}$] and ($\bar{1}\bar{1}$2) [$\bar{3}$1$\bar{1}$], derived from {112} planes and <113> directions that can be selected to account

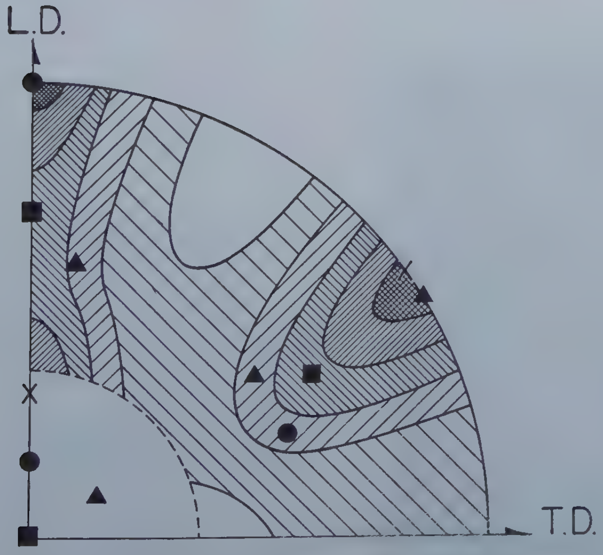

Fig. 4—(111) pole figure of electrolytic, tough-pitch copper twisted to a shear strain of 5.25.

Ideal orientations indicated as follows:
● (112) [11$\bar{1}$], ■ (11$\bar{1}$) [112], x (110) [001], ▲ (112) [1$\bar{3}$1]

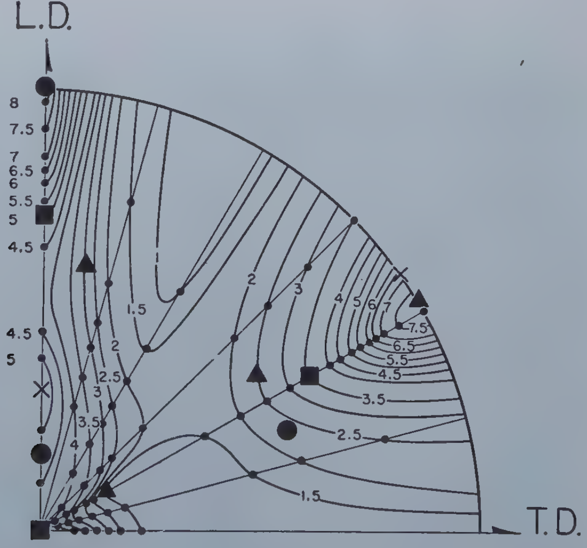

Fig. 6—(111) pole figure of OFHC copper twisted to a shear strain of 6.75.

Ideal orientations indicated as follows:
● (112) [11$\bar{1}$], ■ (11$\bar{1}$) [112], x (110) [001], ▲ (112) [1$\bar{3}$1]

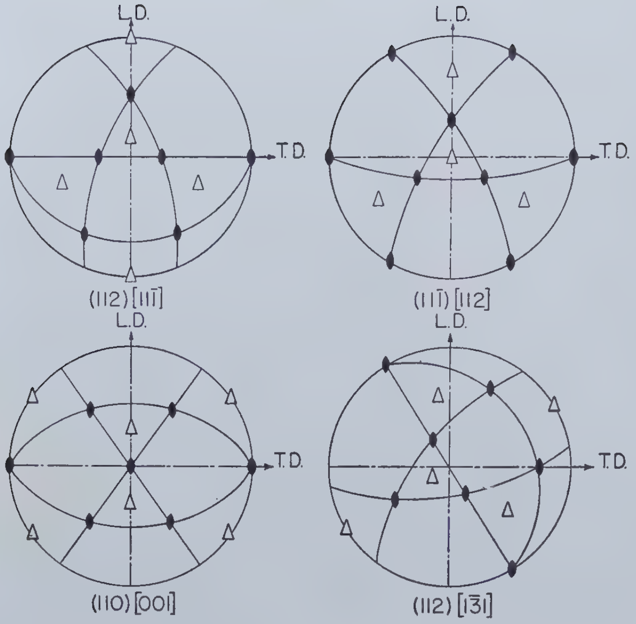

Fig. 7—Stereographic projection of all ideal orientations and slip directions.

Pole of {111} plane
<110> slip direction

for the intensity maxima lying on the basic circle of all pole figures between 58° and 60° from the ends of the longitudinal axis. These represent an ideal texture composed of four parts which can be generated by the reflection of each part across the transverse and longitudinal axes of the pole figure. The ideal orientations (112) [11$\bar{1}$] and (11$\bar{1}$) [112] must be qualified in a similar manner. Each describes but one-half of a composite ideal texture. Stereographic projections of the ideal orientations together with all possible slip directions are plotted in fig. 7.

The stress system associated with torsional deformation may be considered to lie in a plane which is tangential to the surface of the torsion specimen. This plane has been chosen as the plane of the pole figures and of the projections presented in fig. 7. Therefore, shear stresses theoretically can be resolved only along directions which are diameters of the basic circle of a pole figure or one of the projections in fig. 7. Maximum shear stresses act along both the longitudinal and transverse axes regardless of the amount of twisting.

The three ideal orientations, (112) [11$\bar{1}$], (11$\bar{1}$) [112] and (110) [001] provide possible slip directions along the transverse axis (a direction of maximum shear stress). In addition, there are possible slip directions associated with the two ideal orientations, (11$\bar{1}$) [112] and (112) [1$\bar{3}$1], which are also diameters of a basic circle but inclined approximately 30° from the longitudinal axis. It can be shown, however, that the shear stress resolved along a slip direction in the latter position is only one-half the maximum value. Therefore, it seems reasonable to suggest that plastic flow in pure torsion occurs primarily by slip along directions tangential to the surface and perpendicular to the longitudinal axis of the bar, when the texture is sufficiently developed so that it can be described by these ideal orientations. This possibility receives considerable support from the pole figure presented in fig. 3 which was constructed from a torsion specimen subjected to equal amounts of forward and reverse twisting. It is apparent from this pole figure that reverse torsion does not alter the texture established by the initial twisting. This observation can perhaps be most readily explained if it is considered that the direction of slip during the initial twisting is merely reversed when the bar is untwisted. Such a reversal in slip along the transverse direction of

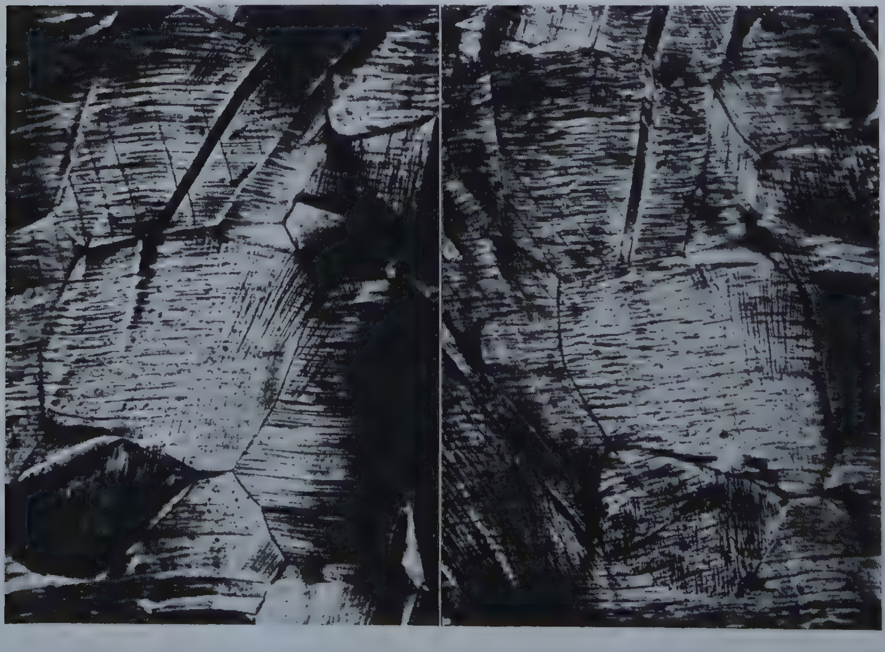

Fig. 8—Microstructure of OFHC copper after torsional strain.

Left — After twisting to a shear strain of ½.
Right — After twisting and untwisting through a shear strain of ½.

The longitudinal axis of the specimen is in the vertical position. Magnification X100; electropolished in 35 pct orthophosphoric acid; chromic acid etch.

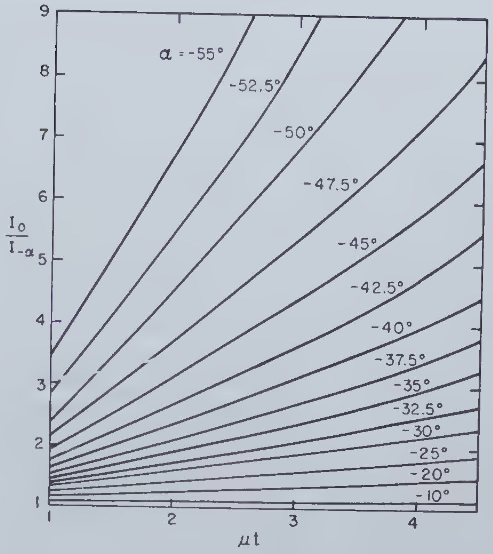

Fig. 9—Solution of the correction formula from Decker, Asp, and Harker[11] applicable to CuKα radiation reflecting from {111} planes of copper: valid for values of —α.

maximum shear stress would not be expected to effect any change in the texture.

The results of microstructural studies made in conjunction with the reverse-torsion experiments are also in agreement with this proposed mode of flow. The micrographs of fig. 8 were obtained from the surface of a coarse-grained specimen after it had been twisted to a shear strain of ½ and again after it had been untwisted by this amount. The same group of grains is included in both micrographs. Traces of slip planes which appear predominantly as horizontal lines are perpendicular to the longitudinal axis of the specimen and coincide with a direction of maximum shear stress. Although untwisting restores the grains to their original shape, it does not markedly alter the pattern made by the traces of the slip planes. Evidently, slip systems of the same orientation are operative during both twisting and untwisting, an observation consistent with the suggestion that torsional plastic flow occurs primarily by slip in directions which are tangential to the surface of the bar and perpendicular to its longitudinal axis.

The ideal orientation (112) [$1\bar{3}1$] furnishes a slip direction in the plane of the equator but inclined 17° to the plane of the projection. Theoretically, no shear stress exists in this direction and since no slip should occur, this orientation does not appear to be one that could persist under the proposed, but undoubtedly oversimplified, conditions of flow. However, it is difficult to reconcile this observation with the presence of an intense maximum on the basic circle of all pole figures at the position occupied by a (111) pole resulting from this orientation.

Summary

The present work may be summarized as follows:

1. The torsion texture of oxygen-free, high conductivity (OFHC) copper and electrolytic, tough-pitch copper, may be described by a composite of the four ideal orientations, (112) [$11\bar{1}$], ($11\bar{1}$) [112], (110) [001], and (112) [$1\bar{3}1$]. The crystallographic planes of these various orientations are tangential to the surface and the directions are parallel to the longitudinal axis of the torsion specimen.

2. From a consideration of the possible slip directions associated with the ideal orientations (112) [$11\bar{1}$], ($11\bar{1}$) [112], and (110) [001], it has been suggested that torsional plastic flow occurs primarily by slip along the direction of maximum shear stress which is tangential to the surface of the specimen and perpendicular to its longitudinal axis. The results of microstructural studies also agree with this mode of flow. The mechanism of torsional plastic flow outlined in the paper is consistent with the details of the pole figures, and also with current plasticity theory, but indicates that the relationship between strain and the development of textures is by no means a simple one.

Acknowledgments

The author is indebted to Sidney Rolle of the Scomet Engineering Co. for supplying the OFHC copper, to the Office of Naval Research for partial support of this work, and to John Wulff and A. J. Shaler for their helpful criticisms during the preparation of this paper.

Appendix

Fig. 9 is a solution of the correction formula derived by Decker, Asp and Harker[11] to be used with their method of constructing pole figures.

References

[1] C. S. Barrett: Structure of Metals. p. 381-419. (1943) New York. McGraw-Hill Book Co.

[2] C. F. Elam: Distortion of Metal Crystals. p. 50-67. (1935) London. Oxford University Press.

[3] A. Ono: Mem. Coll. Eng. Kyushu Imp. Univ. (1922) **2**, 241, 261, also (1925) **3**, 195.

[4] G. Sachs and E. Schiebold: *Naturwissenschaften.* (1925) **13**, 964.

[5] N. P. Goss: The Working of Metals. A.S.M. Symposium (1937) p. 1009.

[6] B. Chalmers: Progress in Metal Physics. Vol. I. Chapter by T. Richards, Ll., p. 281. (1949) New York. Interscience Publishers.

[7] W. R. Hibbard, Jr. and M. Yen: *Transactions* AIME (1948) **175**, 126; *Metals Technology* (Feb. 1948) TP 2334.

[8] A. L. Nadai: *Applied Mechanics Proceedings,* Inst. Mech. Eng. (1948) **157**, 121.

[9] R. Hill: *Proceedings* Roy. Soc. (1948) **193A**, 281.

[10] G. S. Burr, W. J. Gailus, J. O. Silvey, S. Yurenka, and A. G. H. Dietz: ASTM *Bulletin,* No. 149 (Dec. 1947) p. 51.

[11] B. F. Decker, E. T. Asp, and D. Harker: *Journal of Applied Physics.* (1948) **19**, 388.

[12] J. T. Norton: *Journal of Applied Physics.* (1948) **19**, 1176.

Lattice Parameters of Magnesium Alloys

by Robert S. Busk

The effect of solute additions on the lattice parameters of magnesium alloys is reported. Empirical equations are derived from the data which have allowed the calculation of the lattice parameters of ternary solid solutions from binary data. The data are taken both from the literature and from additional experimental work.

TWO groups of binary alloys were prepared. The first group consisted of those elements relatively soluble in magnesium: Li, Al, Zn, Ga, Ag, Cd, In, Sn, Hg, Tl, Pb, and Bi. These are predominately Group B elements. The second group consisted of most of the remaining metallic elements, all of which are relatively insoluble in magnesium: As, Au, Ba, Ca, Ce, Cu, Ir, La, Mn, Ni, Pd, Pt, Rh, Sb, Si, Te, Ti, W, and Zr. These are all Group A, transition, or rare earth elements.

Alloys of the first group were prepared by melting sublimed magnesium and elements as pure as obtainable in a graphite crucible, using a standard flux[1] for protection. The melts were poured into a small graphite mold to produce 3x¾ in. diam slugs. Spectroscopic analyses were made of each slug. In all cases, the total impurity content was less than 0.05 pct. The slugs were then heat treated 5°C below the eutectic temperature until complete solution, as judged metallographically, was obtained. Filings from the center of the slugs were compacted at room temperature into ½ in. long x ¼ in. diam cylinders, sealed in pyrex under ½ atm of purified argon, annealed at the heat-treating temperature for 1 hr, and quenched in water. After the X-ray diffraction patterns were made, each compact was analyzed chemically for the solute.

It was found that the Mg-Li alloys reacted during filing to reduce the Li in solid solution. For this series of alloys, the slug was cold worked, annealed in purified argon, the surface dissolved in dilute HCl to a depth of about 0.005 in., and the X-ray exposure made on the fresh surface. This procedure resulted in sharp, continuous lines and in true values for the lattice parameters.

The alloys in the second group were prepared in the same way except that about 1 wt pct of each solute was added. Since the solubility limit was exceeded, not all the solute dissolved. These alloys were analyzed spectroscopically only to confirm the presence of the solute.

The diffraction patterns were of the back-reflection type using the characteristic copper radiation* and a flat cassette. Both the film and the specimen were rotated. The specimen temperature was maintained at 25° ± 1°C. The films had sharp lines; their diameters were measured directly to 0.01 cm.

The parameters were calculated from the line diameters using a modified version of Cohen's extrapolation method.[2] This method effectively eliminates systematic errors such as film shrinkage, inaccurate alignment, and non-precise film-to-specimen distance. The random errors were minimized

---

ROBERT S. BUSK, Member AIME, is Director, Laboratory Development Division, Magnesium Laboratories, Dow Chemical Co., Midland, Mich.

AIME St. Louis Meeting, February 1951.

TP 2985 E. Discussion (2 copies) may be sent to Transactions *AIME before April 1, 1951. Manuscript received April 19, 1950; revision received Sept. 25, 1950.*

* $K\alpha_1 = 1.537{,}395$ kX; $K\alpha_2 = 1.541{,}232$ kX; $K\beta_1 = 1.389{,}35$ kX.

Table I. Lattice Parameters of Binary Magnesium Alloys

(All values in kX units corrected to 25°C)

Element	Reference	Atomic Pct	a_0	c_0	c/a
Silver	3	0.455	3.2000_9	5.1953_9	1.6235_1
		0.903	3.1970_7	5.188_5	1.622_9
		1.367	3.1948_3	5.1855_5	1.6231_1
		1.868	3.1929_2	5.179_9	1.622_3
		2.049	3.1906_3	5.173_4	1.621_4
		2.199	3.1897_3	5.1730_8	1.6218_0
		2.630	3.1868_6	5.164_9	1.620_7
		3.029	3.1871_4	5.1665_4	1.6210_8
		3.225	3.1841_4	5.1597_1	1.6204_4
	4	0.74	3.1984_3	5.1936_4	1.6238_1
		1.67	3.1920_8	5.1785_4	1.6223_1
		2.31	3.1897_6	5.1728_1	1.6217_1
		3.38	3.1846_9	5.1624_2	1.6210_1
Aluminum	3	0.91	3.1992_6	5.195_6	1.624_0
		1.807	3.1955_9	5.1895_5	1.6239_7
		1.680	3.1960_1	5.1913_0	1.6243_1
		1.956	3.1952_3	5.1898_4	1.6242_5
		2.378	3.1930_2	5.1868_8	1.6244_4
		3.594	3.1886_0	5.180_3	1.6246_3
		3.508	3.1887_3	5.1812_1	1.6248_5
		3.612	3.1887_5	5.1812_2	1.6248_1
		3.930	3.1868_3	5.1791_0	1.6251_8
		4.33	3.1851_7	5.1750_6	1.6247_4
		5.224	3.1819_2	5.1727_9	1.6256_3
		5.365_0	3.1814_0	5.1716_5	1.6256_0
		5.420	3.1808_3	5.1702_9	1.6254_5
		5.799	3.1808_9	5.1711_0	1.6256_8
		6.31	3.1772_4	5.1651_4	1.6256_7
		7.230	3.1733_7	5.1598_3	1.6259_8
		7.482	3.1738_3	5.161_4	1.6262_4
		8.138	3.1699_9	5.155_8	1.6264_6
		9.217	3.1659_6	5.1503_3	1.6267_8
		9.35	3.1645_6	5.148_3	1.6268_6
		10.028	3.1628_1	5.1477_3	1.6275_8
	5	0.496	3.2005_8	5.1964_9	1.6236_1
		1.997	3.1950_2	5.1884_2	1.6239_1
		3.785	3.1877_3	5.1791_3	1.6247_1
		6.31	3.1785_2	5.1660_8	1.6253_1
	6	0.50	3.2008_8	5.1969_8	1.6236
		2.00	3.1952_7	5.1885_1	1.6238
		3.79	3.1879_8	5.1795_4	1.6247
		6.31	3.1788_5	5.1666_2	1.6253
		8.45	3.1707_2	5.1562_6	1.6262
		10.43	3.1632_5	5.1479_0	1.6274
Bismuth	3	0.284	3.20303	5.20266	1.62429
		0.500	3.20419	5.20504	1.6244_5
		0.863	3.20405	5.20411	1.6242_8
		1.037	3.20422	5.20588	1.6246_9
	7	0.24	3.20320	5.20187	1.62396
		0.46	3.20366	5.20358	1.62426
		0.57	3.20355	5.20452	1.62461
		0.58	3.20342	5.20473	1.62474
		0.80	3.20412	5.20592	1.62476
		0.81	3.20428	5.20585	1.62466
		1.00	3.20428	5.20735	1.62512
		1.01	3.20526	5.20749	1.62567
Cadmium	3	1.071	3.1999_0	5.196_2	1.6238_6
		1.220	3.2001_8	5.1963_0	1.6237_5
		2.302	3.1966_6	5.1899_1	1.6235_4
		2.347	3.1969_5	5.192_1	1.624_1
		3.605	3.1948_5	5.1893_7	1.6242_9
		3.619	3.1947_0	5.1888_4	1.624_2
		4.261	3.1930_9	5.183_2	1.6232_6
		4.628	3.1918_9	5.183_6	1.624_0
		7.96	3.1836_9	5.171_6	1.6244_0
	4	1.98	3.19771	5.19279	1.6239
		4.16	3.19315	5.18602	1.6241
		6.04	3.18851	5.17913	1.6243
		8.20	3.18340	5.17146	1.6245
		9.50	3.18058	5.16720	1.6246
		11.78	3.17548	5.15860	1.6245
		13.90	3.17085	5.15044	1.6243
		16.20	3.16603	5.14071	1.6237
Gallium	3	0.549	3.2008_3	5.1974_0	1.6237_7
		1.312	3.1972_9	5.1920_3	1.6238_8
	6	0.17	3.2024_4	5.1995_1	1.6236
		0.37	3.2018_7	5.1982_6	1.6235
		0.37	3.2019_0	5.1983_1	1.6235
		0.75	3.2004_1	5.1955_8	1.6234
		1.04	3.1990_1	5.1942_7	1.6237
		1.76	3.1963_1	5.1902_0	1.6238
		2.50	3.1943_9	5.1870_9	1.6238
Mercury	3	0.193	3.2021	5.1996	1.6238_1
		0.370	3.2012_8	5.1980	1.6237_3
		0.368	3.2000_1	5.1977	1.6242_8
		0.936	3.1983_3	5.1928_5	1.6236_1
		1.165	3.1977_4	5.1918	1.6235_8
Indium	3	0.518	3.2019_6	5.199_7	1.6239_1
		1.077	3.2008_0	5.198_9	1.6242_5
		2.158	3.1995_8	5.198_3	1.6246_8
		3.182	3.1987_6	5.1991_0	1.6253_5
	5	0.63	3.20193	5.19900	1.62371
		2.16	3.19998	5.19901	1.62471
		4.01	3.19780	5.19965	1.62601
		7 98	3.19288	5.20027	1.62871
		11.65	3.18797	5.20210	1.63179
	6	0.63	3.20208	5.1989_3	1.6236_1
		2.16	3.2003_3	5.1996_1	1.6247_1
		4.01	3.1979_9	5.1999_6	1.6260_1
		7.98	3.1933_0	5.2009_6	1.6287_1
		11.65	3.1878_8	5.2042_4	1.6325_1
Lead	3	0.243	3.2034_2	5.2019_8	1.6238_8
		0.611	3.2034_0	5.202_4	1.6240_2
		1.289	3.2035_1	5.2064_3	1.6252_3
		1.998	3.2044_9	5.2078_9	1.6251_9
		4.305	3.2077_5	5.223_9	1.628_5
	6	0.10	3.20316	5.20068	1.6236_1
		0.30	3.20331	5.20060	1.6235_1
		0.49	3.20352	5.20254	1.6240_1
		1.48	3.20463	5.20691	1.6248_1
		2.86	3.20618	5.21520	1.6266_1
		3.45	3.20663	5.21881	1.6275_1
		4.04	3.20701	5.22104	1.6280_1
		4.43	3.20719	5.22358	1.6287_1
		4.97	3.20748	5.22630	1.6294_1
		6.73	3.20829	5.23371	1.6313_1
	7	0.51	3.20330	5.20199	1.62395
		0.53	3.20338	5.20236	1.62402
		1.00	3.20360	5.20439	1.62454
		1.21	3.20440	5.20536	1.62444
		1.21	3.20401	5.20523	1.62460
		1.93	3.20462	5.20827	1.62524
		2.00	3.20475	5.20852	1.62525
		2.32	3.20527	5.21001	1.62545
		2.73	3.20600	5.21257	1.62588
		2.84	3.20552	5.21279	1.62619
		3.59	3.20562	5.21685	1.62741
		3.73	3.20664	5.21720	1.62703
		4.37	3.20689	5.22069	1.62796
		5.07	3.20698	5.22479	1.62919
		6.20	3.20744	5.23163	1.63109
Lithium	3	0.70	3.2029	5.2001	1.6236
		2.80	3.2003	5.1883	1.6212
		4.15	3.1988	5.1845	1.6208
		5.80	3.1978	5.1783	1.6193
		7.40	3.1961	5.1698	1.6175
		11.07	3.1932	5.1585	1.6155
		12.25	3.1922	5.1523	1.6140
		18.40	3.1904	5.1320	1.6086
	8	17			1.6074
Tin	3	0.474	3.2019_9	5.2002_0	1.6240_5
		1.131	3.2022_8	5.2018_0	1.6244_1
		2.248	3.2009_5	5.204_9	1.626_1
		2.352	3.2015_5	5.206_0	1.626_1
	6	0	3.2030_2	5.2004_0	1.6236
		0.18	3.2029_0	5.1999_4	1.6235
		0.40	3.2026_5	5.2011_3	1.6240
		0.92	3.2023_8	5.2026_2	1.6246
		2.00	3.2015_7	5.2051_4	1.6258
		2.47	3.2011_5	5.2063_8	1.6264
Thallium	3	0.266	3.2023_8	5.2000_4	1.6238_0
		0.580	3.2022_3	5.1999_5	1.6238_5
		1.222	3.2017_8	5.1991_6	1.6238_3
		1.800	3.2012_6	5.200_2	1.6244_2
		4.486	3.19926	5.201_7	1.6259
	6	0.25	3.2028_7	5.2002_1	1.6236
		0.75	3.20236	5.19938	1.6236
		1.31	3.2019_3	5.1999_7	1.6240
		2.23	3.2011_8	5.2003_5	1.6245
		4.29	3.1995_6	5.2012_4	1.6256
		6.29	3.1976_9	5.2033_1	1.6272
		9.13	3.1949_9	5.2059_4	1.6294
Zinc	3	0.742	3.1994_5	5.1946_9	1.6236_2
		0.753	3.1989_5	5.1940_8	1.6236_8
		1.460	3.1954_1	5.1873_9	1.6233_9
		1.534	3.1955_3	5.1876_6	1.6234_1
		2.311	3.1920_0	5.1817_5	1.6233_6
		2.408	3.1916_6	5.1811_5	1.6233_4
		2.379	3.1915_8	5.1810_1	1.6233_4
		2.850	3.1888_6	5.1766_5	1.6233_5

by a least-squares solution of the 7-12 lines measured. This treatment also allowed an estimate of the accuracy of each determination. In almost all cases, individual measurements of line diameter varied from the mean by 0.01 cm or less.

Binary Alloys Results

The lattice parameters of the binary alloys of magnesium with the relatively soluble solutes, as determined both in this laboratory and as reported in the literature, are given in table I. Only those literature sources which report work based upon precision techniques are given.

When the parameters were plotted against the atomic percent solute, linear functions were obtained. A least squares solution was made for each solute based upon the equations:

$$a_o = a_{Mg} + S_a\, x$$
$$c_o = c_{Mg} + S_c\, X$$
$$c/a = c/a_{Mg} + S_{c/a}\, x$$

Where x is the atomic percent.

The standard deviations for each equation were calculated and these were used to estimate the standard error of the mean for each equation:

$$\delta_m = \frac{\delta}{\sqrt{N}}$$

Where δ = Standard deviation of the parameter
δ_m = Standard error of the mean of the parameter
N = Number of data points.

The summary of the data as calculated in this manner is given in table II. This table also includes data for pure magnesium, based on twenty determinations, using five different samples of sublimed magnesium.

The data for the relatively insoluble group are given in table III. The standard error for each determination was compared with that for pure magnesium to determine the probability that a given result is different from that for pure magnesium:

$$T = \frac{a_o - a_{Mg}}{[\delta_a^2 + \delta_{Mg}^2]^{1/2}}$$

Since the data were determined on a small number of samples, the observed standard deviations were corrected to give a better approximation to the true standard deviations.[9]

A value of $T = 1.65$ means that there is a 10/1 chance that the difference is real. Higher values of T represent still higher probabilities that the difference is real. The value of $T = 1.65$ was arbitrarily selected as a division point for determining elements that have a significant effect on the lattice parameters of magnesium.

When the data for c/a in table I are plotted against electron concentration,

$$E = 2 + (\text{Valence} - 2)x$$

a series of straight lines are obtained for each element (fig. 1). In those cases in which the solute results in an increase in E, there is first a horizontal line representing no change in c/a with addition of solute, and then a straight line representing an increase in c/a with increasing E. In those cases in which the solute addition results in a decrease in E, there is again a short horizontal line, and then a straight line representing a decrease in c/a with decreasing E.

Raynor[4,6] and Hume-Rothery and Raynor[5] have pointed out the dependence of c_o on electron concentration. They have advanced an explanation based upon the energy levels occupied by the conduction electrons and the occurrence of an overlap of occupied energy levels beyond the first Brillouin Zone.

When c/a is plotted against E, the lines for all elements are close together. Assuming that the small differences observed are due solely to differences in ionization of the solute atoms, it is possible to calculate a relative effective valence,

$$V' = 2 + \frac{S_{c/a}}{S^\circ_{c/a}}$$

where $S^\circ_{c/a}$ is an arbitrarily selected slope of c/a against electron concentration. Since indium has the largest slope, its effective valence was set at 3.00 and $S^\circ_{c/a}$ made equal to $S_{c/a}$ for indium, or 0.77. The relative effective valences of the remaining

Table II. Summary of Data for Lattice Parameters of Binary Alloys

	Constants		In kX Units						Standard Error of the Mean of the Parameter, A		
			a_o		c_o		c/a				
Elements	Effective Radius, (kX Units)	Effective* Valence	a_{Mg}	S_ax10^3	c_{Mg}	S_cx10^3	c/a_{Mg}	$S_{c/a}$x10^3	a_o	c_o	c/a
Silver	1.33	0.66	3.20206	—5.36	5.20069	—12.18	1.62401	—1.028	0.0019	0.00018	0.00012
Aluminum	1.40	2.49	3.20269	—3.93	5.19937	—5.22	1.62335	0.38	0.00015	0.00020	0.00003
Bismuth	1.69	3.50	3.20272	1.78	5.20124	5.40	1.62383	1.16	0.00003	0.00018	0.00012
Cadmium	1.49	2.00	3.20240	—2.27	5.20043	—3.60	?	?	0.00011	0.00031	
Gallium	1.42	2.00	3.20296	—3.65	5.20010	—5.48	1.62365	0	0.00012	0.00010	0.00005
Mercury	1.39	2.00	3.20245	—4.23	5.20093	—8.16	1.62380	0	0.00021	0.00007	0.00011
Indium	1.54	3.00	3.20267	—1.24	5.19799	0.41	1.62293	0.77	0.00004	0.00016	0.00008
Lithium	1.55	0.84	3.2030	—0.90	5.2010	—3.97	1.6243	—0.89	0.00009	0.00048	0.00042
Lead	1.64	3.55	3.20313	0.84	5.19902	5.24	1.62312	1.20	0.00007	0.00003	0.00005
Tin	1.57	3.50	3.20282	—0.66	5.19951	2.67	1.62344	1.16	0.00009	0.00018	0.00004
Thallium	1.56	2.87	3.20290	—0.84	5.19865	0.75	1.62303	0.67	0.00004	0.00012	0.00006
Zinc	1.37	2.00	3.20267	—4.71	5.20021	—8.13	1.62343	0	0.00006	0.00021	0.00005
Magnesium	1.60	2.00	3.20233		5.19942		1.62364		0.00009	0.00015	0.00006
Avg.			3.20270		5.20041†		1.62362†				

* Relative for In = 3.00.

† Averaged for elements of Valence = 2.00.

elements are then as given in table II. It is possible to set up a general equation which will describe the relation between c/a and electron concentration for all the binary magnesium alloys studied using relative effective valence. The resulting three-part equation is:

$$c/a = 1.47298 + 0.07554E' \quad E' \leqq 1.994$$

$$c/a = 1.62364 \quad 1.994 \leqq E' \leqq 2.005$$

$$c/a = 1.47567 + 0.0738E' \quad E' \geqq 2.005$$

where E' is the electron concentration based upon the relative effective valence as given in table II.

The a_o vs. atomic percent relation for each element can be used to determine an "effective radius" for each solute in the magnesium lattice:

$$R = \frac{a_{Mg} + 100\ S_a}{2}$$

The values for R for each element are given in table II. The atomic radii determined in this way differ by only a small amount from the radii determined from the lattice of the pure metals. Hume-Rothery and Raynor[5] have discussed possible causes of this difference. These figures allow a general equation to describe the relation between a_o and atomic percent for all the binary magnesium alloys studied. The resulting equation is:

$$a_o = 3.20268 + (-0.032044 + 0.020014R)\ x$$

where x is atomic percent, and a_o is in kX units.

It is apparent, then, that the unit cell size of magnesium is affected by both the size of the solute element and its effective valence. The relation is such that the spacing of the atoms in the basal plane is dependent only upon the solute radius. The spacing between the basal planes is also affected by the solute radius but is further adjusted so as to allow the c/a ratio to conform with the electron concentration.

To be useful, the general equations should give the parameters of polynary alloys from composition. A series of ternary Mg-Al alloys were prepared and the parameters measured. The results are shown in table IV. Two of the alloys were such that the additional solute contributed no additional electrons, one added electrons, and one subtracted electrons. With one exception, the agreement between the values calculated from the equations and those measured is within the experimental error.

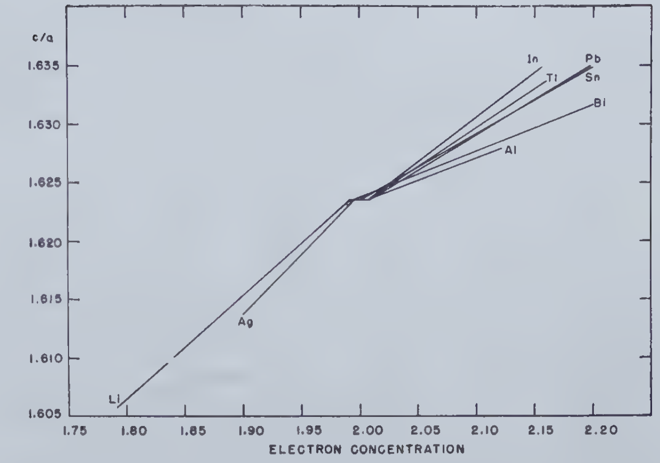

Fig. 1—Data for c/a plotted against electron concentration.

The data for the relatively insoluble elements (table III) show some significant differences from the values for pure magnesium. The effect of a_o can be summarized: Elements decreasing a_o—Au, Mn, Rh, and Zr; and elements increasing a_o—As, Ba, Ce, La, Ni, and Pd.

All the elements causing a decrease in a_o have atomic radii (½ distance of closest approach in the room temperature structure) less than that of magnesium. Each of these must, therefore, dissolve in sufficient quantity to affect the parameter values. There is no way from the data in this paper to estimate the amount dissolved. Ba, Ce, and La all have atomic radii larger than Mg and the effect of these elements is straightforward. As, Ni, and Pd, however, have atomic radii less than that of Mg, and the reason that these elements cause an increase in the a_o value is not known.

The effect of these solutes on the c/a ratio can be summarized: Elements decreasing c/a—Au, Ce,

Table III. Lattice Parameters of Some Binary Magnesium Alloys as Compared to Those for Pure Magnesium

	a_o			c_o			c/a		
Element	kX	δ_M	T	kX	δ_M	T	c/a	δ_M	T
Arsenic	3.20327	0.00051	1.81	5.20114	0.00079	2.10	1.62369	0.00014	0.03
Gold	3.20147	0.00037	2.26	5 19731	0.00089	2.35	1.62341	0.00010	1.91
Barium	3.20333	0.00011	7.14	5.20170	0.00024	8.15	1.62384	0.00010	1.66
Calcium	3.20331	0.00092	1.07	5.20079	0.00174	0.79	1.62357	0.00020	0.33
Cerium	3.20461	0.00094	2.43	5.20092	0.00113	1.31	1.62295	0.00024	2.76
Copper	3.20200	0.00071	0.46	5.19874	0.00139	0.49	1.62360	0.00014	0.27
Iridium	3.20220	0.00102	1.12	5.20042	0.00145	0.69	1.62402	0.00020	1.81
Lanthanum	3.20396	0.00076	2.14	5.20116	0.00114	0.64	1.62335	0.00024	1.16
Manganese	3.19805	0.00224	1.91	5.19481	0.00204	2.26	1.62437	0.00087	0.84
Nickel	3.20366	0.00033	3.91	5.20148	0.00032	5.89	1.62360	0.00007	0.43
Palladium	3.20390	0.00056	2.75	5.20019	0.00060	1.24	1.62308	0.00020	2.94
Platinum	3.20147	0.00054	1.56	5.19982	0.00132	0.30	1.62419	0.00017	3.05
Rhodium	3.20067	0.00066	2.47	5.19761	0.00133	1.35	1.62391	0.00008	2.70
Antimony	3.20318	0.00094	0.91	5.19984	0.0022	0.19	1.62334	0.00039	0.75
Silicon	3.20260	0.0010	0.27	5.19981	0.0019	0.20	1.62362	0.00024	0.08
Tellurium	3.20416	0.0021	0.87	5.20175	0.0040	0.58	1.62344	0.00041	0.49
Titanium	3.20255	0.00061	0.35	5.20172	0.00126	1.81	1.62424	0.00013	4.28
Tungsten	3.20324	0.0013	0.70	5.19920	0.0026	0.08	1.62310	0.00033	1.58
Zirconium	3.19891	0.0019	1.80	5.19635	0.0030	1.02	1.62441	0.00037	2.08
Magnesium	3.20233	0.00009		5.19942	0.00015		1.62364	0.00006	

Table IV. Calculation of Lattice Parameters of Ternary Alloys

Atomic Pct		Average Values			a_o, kX			c/a		
		R, kX	$Sa \times 10^3$	E′	Calc.	Obs.	$\Delta \times 10^{-3}$	Calc.	Obs.	$\Delta \times 10^{-3}$
Al	Zn									
2.0	2.25	1.38	—4.42	2.0098	3.1839	3.1833	0.6	1.62399	1.62387	0.12
3.6	2.2	1.39	—4.22	2.0176	3.1782	3.1780	0.2	1.62457	1.62433	0.24
5.6	1.6	1.39	—4.22	2.0274	3.1723	3.1732	0.9	1.62529	1.62515	0.14
1.8	0.35	1.39	—4.22	2.0088	3.1936	3.1944	0.8	1.62392	1.62442	0.50
5.1	0.4	1.40	—4.02	2.0250	3.1806	3.1815	0.9	1.62512	1.62550	0.38
7.7	0.5	1.40	—4.02	2.0377	3.1697	3.1716	1.9	1.62605	1.62600	0.05
9.5	0.4	1.40	—4.02	2.0466	3.1629	3.1648	1.9	1.62671	1.62551	1.20
Al	Cd									
2.2	0.9	1.43	—3.42	2.0108	3.1921	3.1912	0.9	1.62407	1.62436	0.29
3.8	1.0	1.42	—3.62	2.0186	3.1853	3.1861	0.8	1.62464	1.62520	0.56
6.2	1.1	1.41	—3.82	2.0304	3.1748	3.1768	2.0	1.62551	1.62550	0.01
8.4	1.3	1.41	—3.82	2.0412	3.1656	3.1680	1.8	1.62631	1.62623	0.08
10.4	1.1	1.41	—3.82	2.0510	3.1588	3.1610	2.2	1.62703	1.62674	0.29
Al	Sn									
1.3	0.42	1.44	—3.22	2.0127	3.1971	3.2030	5.9	1.62421	1.62383	0.38
2.9	0.32	1.42	—3.62	2.0190	3.1914	3.2028	11.4	1.62467	1.62366	1.01
5.4	0.40	1.41	—3.82	2.0325	3.1805	3.1799	0.6	1.62567	1.62652	0.85
7.2	0.35	1.41	—3.82	2.0408	3.1738	3.1719	1.9	1.62628	1.62669	0.41
3.55	0.40	1.42	—3.62	2.0233	3.1884	3.1875	0.9	1.62499	1.62527	0.28
9.75	0.38	1.41	—3.82	2.0532	3.1640	3.1672	3.2	1.62720	1.62735	0.15
Al	Ag									
3.3	0.8	1.39	—4.22	2.0053	3.1854	3.1876	2.2	1.62366	1.62406	0.40
5.3	0.8	1.39	—4.22	2.0152	3.1769	3.1775	0.6	1.62439	1.62504	0.65
8.4	0.85	1.39	—4.22	2.0296	3.1636	3.1654	1.8	1.62545	1.62586	0.41
0.4	1.5	1.34	—5.23	1.9818	3.1927	3.1947	2.0	1.62269	1.62283	0.14
2.7	1.5	1.37	—4.62	1.9929	3.1833	3.1834	0.1	1.62352	1.62341	0.11
5.4	1.5	1.38	—4.42	2.0062	3.1722	3.1712	1.0	1.62373	1.62391	0.18

and Pd; and elements increasing c/a—Ba, Ir, Pt, Rh, Ti, and Zr.

The fact that Au lowers the c/a ratio is in accord with its known valence of 1. The lowering of the c/a ratio by Ce is interesting. Normally, this element has a valence of two or more. However, it does have an incomplete f shell and may be acting as an electron receiver in the magnesium lattice.[10–12] It is interesting that La, having a lower solubility than Ce in Mg, shows the same effect on c/a but to a lesser extent than does Ce. The lowering of the c/a ratio by Pd is puzzling, especially since Ir, Pt, and Rh all raise it. It is also difficult to believe that Ba increases the c/a ratio. The significance of the result by the arbitrary standard selected is borderline, and it may be that there is no real effect. The fact that enough Ti goes into solid solution to raise the c/a ratio is interesting, and in view of its extremely low liquid solubility,[13] probably means that the Mg-Ti, like the Mg-Zr, system is a peritectic.

There remain the elements Ca, Cu, Sb, Si, Te, and W which show no change in either a_o or c/a. Of these, Ca and Cu do have some solid solubility in Mg, but the change in parameter is apparently too small to be found. The other elements seem to have vanishingly small solid solubility in Mg.

Summary

1. The change in a_o with addition of solute is proportional to the radius of the solute alone.

2. The effective radius shown by a solute in binary solid solution is retained in ternary alloys.

3. The change in c_o with addition of solute is proportional to both the radius and the valence of the solute, the relative effect of each being such that the c/a ratio is proportional to the electron concentration alone.

4. Few, if any, solutes in magnesium are fully ionized.

5. The relative effective valence shown by a solute in binary solid solution is retained in ternary alloys.

6. The rare-earth elements Ce and La may act as electron receivers in magnesium solid solutions.

7. The Mg-rich, Mg-Ti binary alloys probably constitute a peritectic system.

Acknowledgment

The experimental procedures were established and some of the parameter results on the binary solid solution alloys determined by J. B. Hess while he was at the Dow Chemical Co. Mr. Hess is now with the Institute for the Study of Metals, University of Chicago.

References

[1] C. E. Nelson: *Transactions* AIME (1944) **159**, 392.

[2] J. B. Hess: *Acta Crystall.* Not yet published.

[3] The Dow Chemical Co. Laboratories.

[4] G. V. Raynor: *Proceedings* Roy. Soc. (1940) **174A**, 457.

[5] W. Hume-Rothery and G. V. Raynor: *Proceedings* Roy. Soc. (1940) **177A**, 27.

[6] G. V. Raynor: *Proceedings* Roy. Soc. (1942) **180A**, 107.

[7] F. Foote and E. R. Jette: *Transactions* AIME (1941) **143**, 124.

[8] H. Jones: *Phil. Mag.* (1950) **41**, 663.

[9] F. C. Mills: Statistical Methods. (1938) p. 598. Henry Holt & Co.

[10] G. V. Raynor: *Phil. Mag.* (1945) **36**, 770.

[11] G. V. Raynor: *Journal* Inst. Met. (1945) **71**, 493.

[12] G. V. Raynor: *Journal* Inst. Met. (1947) **73**, 397.

[13] K. T. Aust and L. M. Pidgeon: *Transactions* AIME, **185**, 585; *Journal of Metals* (Sept. 1949) TP 2680E.

[14] H. Jones: *Proceedings* Roy. Soc. (1934) **147A**, 396.

Effect of Ferrite Grain Structure Upon Impact Properties of 0.80 Pct Carbon Spheroidite

by M. Baeyertz, W. F. Craig, Jr., and E. S. Bumps

SOME time ago during a study of impact properties of tempered martensite,[1] it was postulated that the consistently good ductility of tempered martensite might be caused by its relatively small and peculiarly shaped ferrite grains. The ferrite grains of tempered martensite have approximately the same size and shape as the martensite "needles." Thus they form an interlocking mass of needle-shaped grains quite different from equiaxed or lamellar ferrite grain structures.

When the common mechanical test methods are applied to steel, variations are often observed in the ductility of specimens that have closely similar hardness and tensile strength values. The ductility so measured appears to be structure dependent. When steel from the same heat has been heat treated to produce different structures with the same hardness, the elongation and reduction of area values from the tensile test and the transition temperature determined by the notched-bar impact test vary according to whether pearlite, tempered martensite, or other structural constituents were produced by the heat treatment. It has been widely recognized that tempered martensite gives a consistently good performance, when tempered to the same hardness as many other structures with which it has been compared. In recent years the isothermal transformation of austenite to specific structural products and the quantitative evaluation of the character of these products with respect to their nature and response to deformation has received considerable attention.

The objective of the present study was to pursue somewhat further the dependence of ductility upon structure; specifically, it was desired to ascertain whether ferrite grain structure, including both shape and size of the grains, can account for the consistently good performance of tempered martensite in the notched-bar impact test.

It was thought that a simple experiment would indicate whether the ferrite grain structure plays any part in the good ductility exhibited by tempered martensite in contrast to other steel structures with different types of ferrite grains. By determining the impact transition temperature, it was proposed to compare spheroidites having similar carbide particle size and spacing but obtained in such a manner that their ferrite grain structures would be very different. Spheroidite obtained by tempering martensite, with its small, needle-shaped grains, was to be compared with spheroidite from pearlite. If the latter is produced by sub-critical annealing, the ferrite grains correspond to the pearlite colonies. Thus, if the pearlite was not too coarse, the ferrite grains of spheroidite from pearlite are equiaxed in contrast to the needle-shaped grains of spheroidite from martensite.

It was thought that the ferrite grain structure of spheroidite from martensite might depend to some extent upon the grain size of the prior austenite. The austenite grain boundaries limit the maximum attainable size of the martensite needles and thus of the ferrite grains in the derived spheroidite. In order to evaluate any possible influence of prior austenite grain size, spheroidites were to be prepared from martensites that had been formed from fine-grain austenite and also from coarsened austenite.

As the carbide particle size and distribution were to be essentially alike in the various spheroidites, the difference would be in the ferrite grain size and shape. Thus any marked difference in transition temperature could be attributable to the character of the ferrite grain structure.

There are certain considerations in assuming that these spheroidites would be equivalent in all respects except ferrite grain structure, and an attempt was made to take them into account. One of the considerations was the choice of the carbon content of the steel. An approximately eutectoid steel was selected for two reasons. First, the pearlitic structure would contain no proeutectoid ferrite which might complicate the picture by producing a nonuniform ferrite grain structure in the resulting spheroidite. Then, too, the high-carbon content would inhibit ferrite grain growth during the subcritical treatment.

Another factor to be taken into account was the choice of an alloying element to assure a martensitic structure throughout on quenching the impact specimens. Nickel was chosen, because it is a common alloying element and resides in the ferrite both upon its formation from austenite and throughout tempering. The formation of alloy carbides, or even a large solubility of the alloying element in cementite, would have complicated the interpretation by changing the composition of the ferrite during spheroidization.

The possibility of temper brittleness was minimized insofar as possible by using a tempering temperature as high as consistent with the 1 pct of nickel in the steel, namely, 1150°F.

While it certainly is not claimed that no difference other than ferrite grain structure could exist between the spheroidites, nevertheless, reasonable precaution has been exercised within the limits of steel metallurgy. It is believed that any large difference in transition temperatures would reflect the difference in ferrite grain structure and that relatively good ductility in the spheroidites from mar-

---

M. BAEYERTZ, Member AIME, is Senior Metallurgist, Armour Research Foundation of Illinois Institute of Technology, Chicago, Ill.; W. F. CRAIG, JR., formerly Supervisor, Ferrous Metals Research, Armour Research Foundation, now Metallurgical Engineer, Climax Molybdenum Co., Chicago, Ill., and E. S. BUMPS, Junior Member AIME, is Associate Metallurgist, Armour Research Foundation.

AIME St. Louis Meeting, February 1951.

TP 2983 E. Discussion (2 copies) may be sent to Transactions *AIME before April 1, 1951. Manuscript received May 15, 1950; revision received Oct. 5, 1950.*

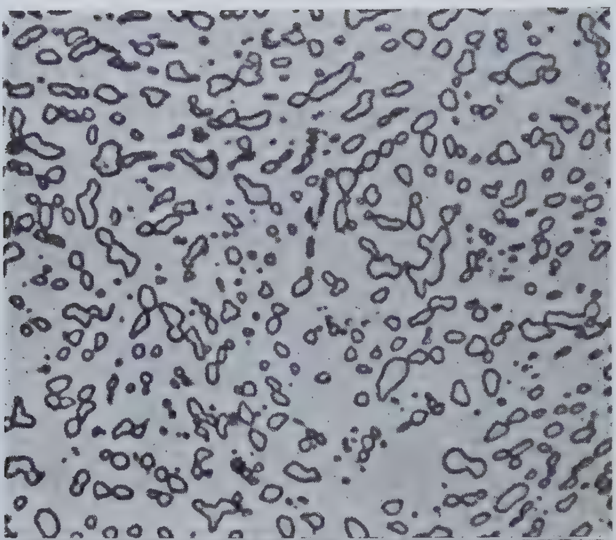

Fig. 1—Spheroidite from martensite, etched with picral, X2000. Austenitization was at 1550°F to ASTM grain size No. 6 to 7.

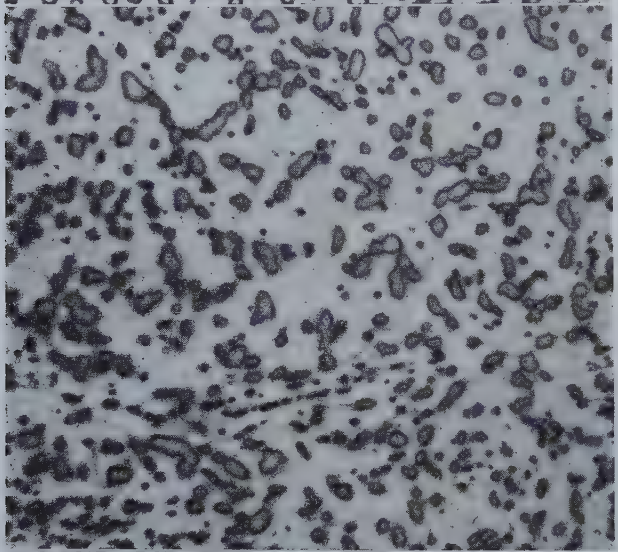

Fig. 2—Spheroidite from martensite, etched with picral, X2000. Austenitization was at 1900°F to ASTM grain size No. 2 to 5.

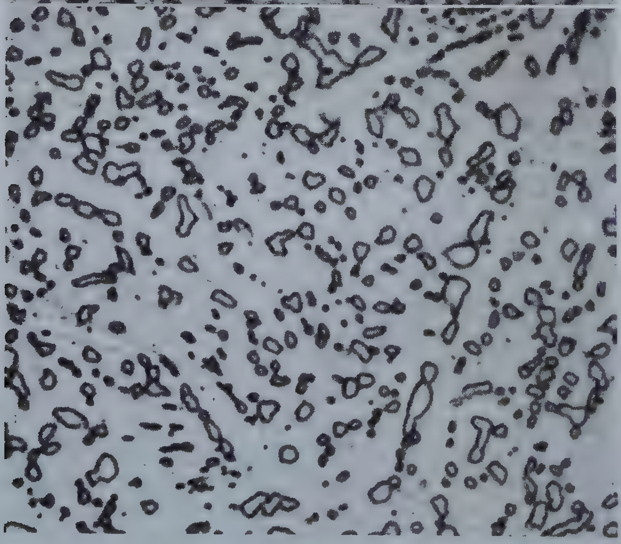

Fig. 3—Spheroidite from martensite, etched with picral, X2000. Austenitization was at 2050°F to ASTM grain size No. —1 to 3.

tensite would be caused by the same factor as the consistently good ductility observed in tempered martensite, at least when the martensite is tempered at relatively high temperatures and does not exhibit temper brittleness.

Experimental Data

The steel was from a 65-lb ingot from a laboratory induction furnace heat (No. 2440) of the following analysis: C, 0.77 pct; Mn, 0.36; P, 0.007; S, 0.011; Si, 0.32; Ni, 1.03; Al, none added.

The ingot was forged to ½x2½-in. bars. These were normalized from 1550°F and then tempered for 1 hr at 1200°F. Longitudinal Charpy impact blanks, four abreast, were machined from the bars. The blanks were 0.16-in. oversize before heat treatment, after which they were ground to size and notched with a 45°, 0.010-in. radius V-notch.

The heat treatment consisted of austenitizing, and then either quenching in oil directly, or giving an arrested quench in salt at 900°F for 3 min and then in oil. The former treatment resulted in martensite; the latter, pearlite. Both pearlite and martensite were produced after austenitization at 1550°F; also, martensites were obtained from austenite that had been coarsened by heating at 1900° and 2050°F. Before quenching from the two, high austenitizing temperatures, a 5 or 7 min equalization at 1550°F was employed in order to avoid quench cracking. After quenching, the specimens were tempered at 1150°F for the period required to produce a hardness of about 93 Rockwell B. Details of the heat treatments, of the as-austenitized grain size, and of the hardness of the spheroidized specimens are given in table I.

Table I. Heat Treatment, Austenite Grain Size, and Hardness of Spheroidites

Austenitization			Quenching			Spheroidization at 1150°F	
°F	Hr*	ASTM Grain Size	Equalization	Arrest	Final Quench	Hr	RB Hardness
1,550	1	6 to 7	none	none	oil	54	94
1,900	1	2 to 5	5 min, 1550°F	none	oil	46	93
2,050	2	—1 to 3	7 min, 1550°F	none	oil	46	93
1,550	1	6 to 7	none	salt; 3 min, 900°F	oil	100	92

* Austenitized in a protective atmosphere.

The structures of the three spheroidites obtained from martensite are illustrated by figs. 1, 2, and 3; the spheroidite produced from pearlite, by fig. 4. The specimens were etched in picral to show only the outlines of the carbide particles. Figs. 5, 6, 7, and 8, respectively, illustrate the appearance of the same specimens after etching with nital to reveal the ferrite grain size and shape as well as the cementite particles.

Both the "average distance between carbide particles" and the "average uninterrupted ferrite path" were determined. The average distance between carbide particles is the mean, free-ferrite path as defined by Gensamer and his coworkers,[2] which by their experimental procedure amounts to the average, straight-line distance between carbide particles or lamellae. This definition takes no account of ferrite grain boundaries. We are indebted to Professor Cohen[3] for the suggestion that the mean free path should include ferrite grain boundaries as well as phase boundaries between the carbide particles or inclusions and the ferrite. "Average uninterrupted ferrite path" has been used to indicate the latter definition of mean, free-ferrite path.

The determinations of mean free-ferrite path were made with a Hurlbut counter, set up to drive a filar micrometer eyepiece. A magnification of 2000 diam was used, attained with an oil immersion objective. The respective distances along the horizontal cross-hair were measured on twenty-five representative fields for each specimen and etchant. The average, straight-line distance between carbides was determined after etching in picral. The average, uninterrupted ferrite path was measured after etching with nital. The ferrite grain size was determined by similar measurements after the specimens had been etched in nital. The data are given in table II.

The spheroidite prepared from pearlite contained relatively few ferrite grain boundaries; therefore the average distance between carbides and the average, uninterrupted ferrite path were essentially alike. While the difference was not very large in the spheroidites prepared from martensite, the average, uninterrupted ferrite path was a little shorter than the average distance between carbides, because of the number of ferrite grain boundaries that had to be taken into account in the determination of the average, uninterrupted ferrite path.

The average, ferrite grain diameter of the spheroidite obtained from pearlite was about four times that of the spheroidites obtained from martensite, as shown in table II. In terms of ASTM grain size number, the ferrite grain sizes were No. 15 for the spheroidites from martensite and No. 12 for the spheroidite from pearlite.

Table II. Microscopic Observations

	Spheroidite from Martensite			Spheroidite from Pearlite
	1550°F Aust.	1900°F Aust.	2050°F Aust.	1550°F Aust.
Average distance between carbides, mm	0.0021	0.0018	0.0018	0.0018
Average uninterrupted ferrite path, mm (all phase and ferrite grain boundaries)	0.0016	0.0015	0.0016	0.0017
Average distance between ferrite grain boundaries, mm	0.0023	0.0022	0.0022	0.0091
Average carbide particle diameter, mm	0.0007	0.0007	0.0007	0.0006
Prior austenite grain size, ASTM No.	6 to 7	2 to 5	—1 to 3	6 to 7

It is significant that the average, ferrite grain diameters of the spheroidites from martensite are essentially alike in spite of the large difference in the as-austenitized grain size. The import of this will become apparent when the data from the impact tests are discussed. However, there was one difference in the structures of these spheroidites that should be noted. As the as-austenitized grain was coarsened, the length of occasional martensite needles increased. These were the needles that were oriented preferentially with their long axes in the prior austenite grain boundaries. This is illustrated by fig. 9, a micrograph of the spheroidite of a specimen that was austenitized at 2050°F. These preferentially oriented grains are smaller and thus not

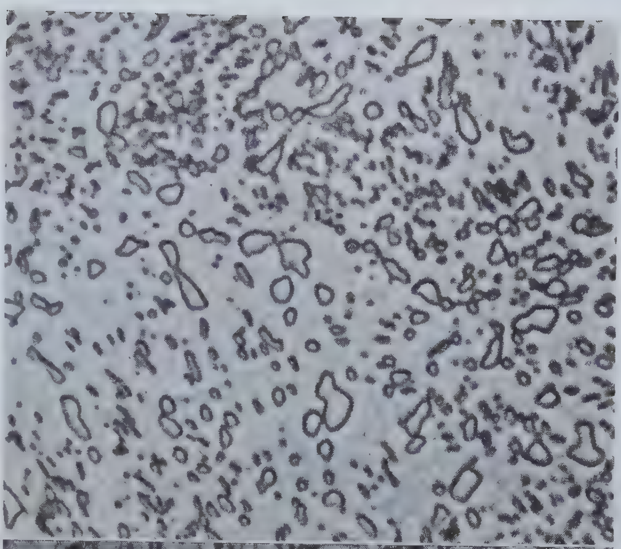

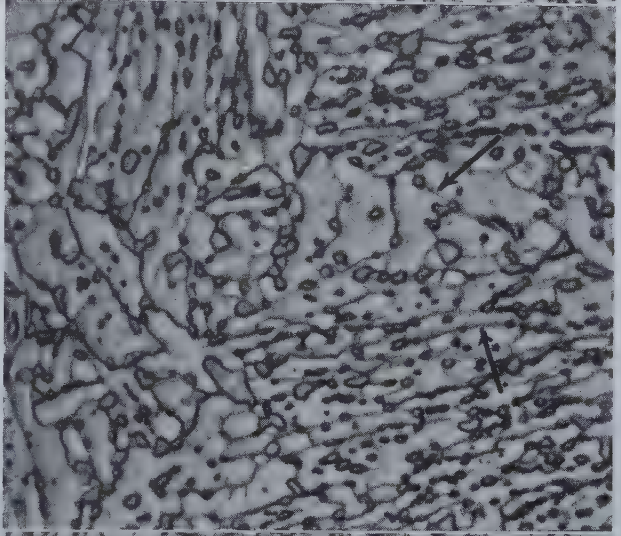

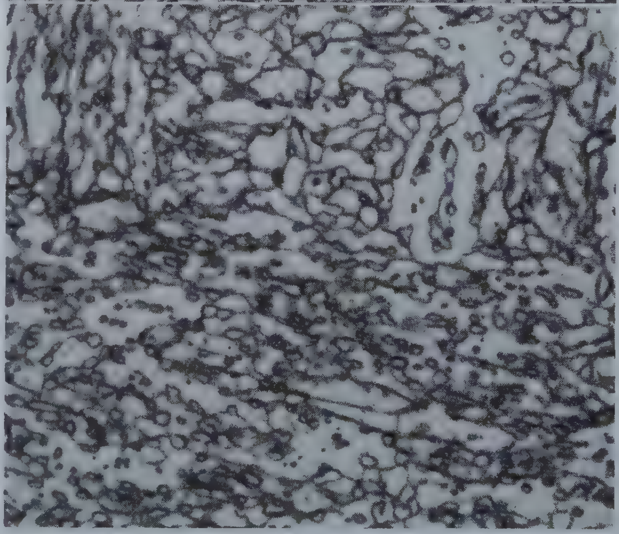

Fig. 4—Spheroidite from pearlite, etched with picral, X2000. Austenitization was at 1550°F to ASTM grain size No. 6 to 7.

Fig. 5—Spheroidite from martensite, etched with nital, X2000. Ferrite grain boundaries are indicated by arrows. Austenitization was at 1550°F to ASTM grain size No. 6 to 7.

Fig. 6—Spheroidite from martensite, etched with nital, X2000. Austenitization was at 1900°F to ASTM grain size No. 2 to 5.

so evident in the structure obtained by austenitization at 1900°F, as shown in fig. 10. While a representative proportion of the long ferrite grains derived from these needles was included in the fields used for the microscopic observations, it was not sufficient to influence the values given in table II.

The energy values obtained in notched-bar impact tests are plotted against testing temperature in the conventional way in fig. 11. Also, macroscopic evaluations of the percentage of brittle fracture are given in the figure. Except for some scatter in the energy values above the transition range, both energy and fracture curves for the three spheroidites from martensite are superimposed. Also, while there has been considerable difference of opinion concerning the definition of transition temperature, it will be evident that by any of the usual criteria the notched-bar transition of the spheroidite from pearlite was much higher than that of the spheroidites from martensite. Using the lowest testing temperature that gave a zero percent brittle fracture as the criterion, the transition temperature was 150°F for the spheroidites from martensite and 350°F for the spheroidite from pearlite. Thus the difference in transition temperature amounted to 200°F. The differential in transition temperature would be about the same if the criterion of transition were to be taken as a 90 pct brittle fracture.

Results

The microscopic evidence showed that the spheroidites from martensite were essentially equivalent in microstructure regardless of the as-austenitized grain size. The only difference noted was an occasional long ferrite grain, in the prior austenite grain boundaries of the specimens that had been coarsened in the austenitization. With the exception of slight irregularities above the energy transition, both the energy and fracture curves of the three spheroidites from martensite were superimposed. The prior austenite grain sizes of these spheroidites were, respectively, ASTM No. 6 to 7, 2 to 5 and —1 to 3. These observations would suggest that austenite grain size has but slight influence upon the subsequent ferrite structure obtained upon quenching to martensite and spheroidizing, and thus has little effect on the energy values and transition range obtained by the notched-bar impact test, at least in the absence of temper embrittlement and other reactions that involve the prior austenite grain boundaries. An attempt was made to avoid such effects in this evaluation, which as nearly as possible was limited to the influences of ferrite grain size and shape in the absence of embrittling reactions.

Rather close coincidence of the average distances between carbide particles and the average uninterrupted ferrite paths was attained in the spheroidites from both martensite and pearlite, as shown in table II. The average distance between carbide particles, of course, depended entirely upon carbide-ferrite interfaces. The average, uninterrupted ferrite path depended to a large extent on these interfaces. There were few ferrite grain boundaries in the spheroidite from pearlite compared to the number of carbide-ferrite interfaces, and even in the spheroidites from martensite a major percentage of the interruptions were caused by carbide-ferrite phase boundaries. In view of this it does not seem reasonable to assume that the observed difference of 200°F in transition temperature, between the spheroidites from martensite and the spheroidite from pearlite, was caused by the distribution of the carbide particles. That is to say, the V-notch Charpy transition appears to depend profoundly upon some factor other than the mean, free-ferrite path.

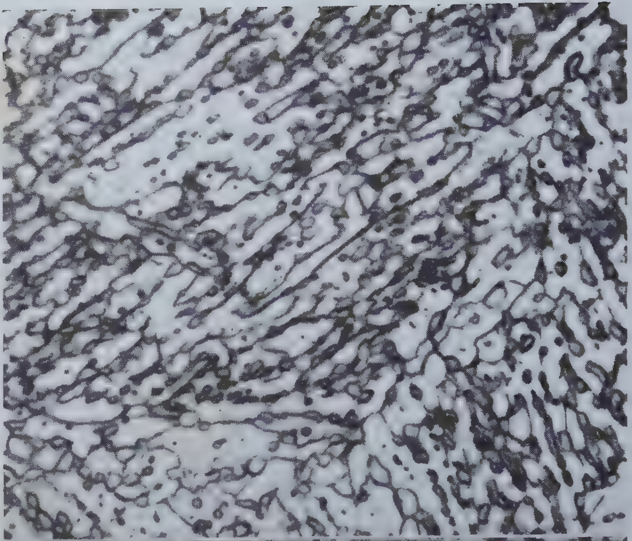

Fig. 7—Same as fig. 3, etched with nital, X2000.

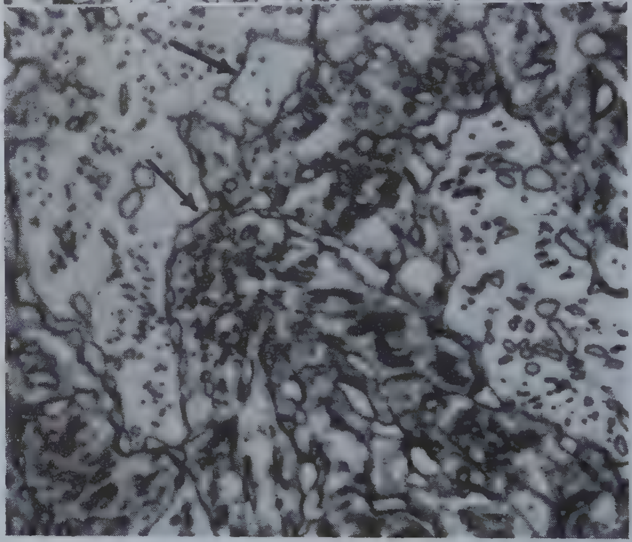

Fig. 8—Same as fig. 4, etched with nital, X2000. Ferrite grain boundaries are indicated by arrows.

On the other hand, if the carbide particles are disregarded and consideration is given only to ferrite grain structure, it would seem that sufficient difference exists so that the better ductility of the spheroidites from martensite might be ascribed to their ferrite grain structure. This includes both size and shape of the ferrite grains, for it is not possible at the present writing to separate the two effects.

The ferrite grain diameter of the spheroidite from pearlite was about four times that of the spheroidite from martensite. It is unfortunate that this work using V-notch Charpy bars is not directly comparable with study of ferrite grain size by Hodge, Manning and Reichhold[4] which was done on practically carbon-free steel with keyhold-notch Charpy bars. Notwithstanding it may be presumed, in harmony with their work, that a decrease in the ferrite grain size would lower the transition temperature with the V-notch as well as the keyhold-notch bar, so that all of the observed superiority of the spheroidite from martensite over the spheroidite from pearlite cannot be ascribed to the elongated shape of the

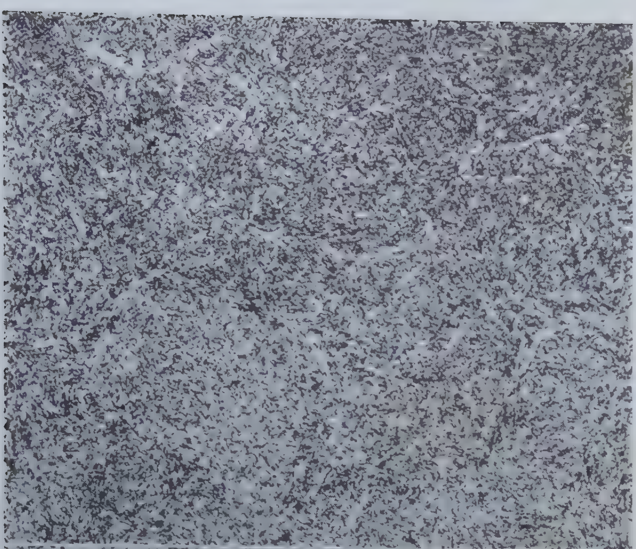

Fig. 9—Same as fig. 3, etched with nital, X150.

Fig. 10—Same as fig. 2, etched with nital, X150.

ferrite grains in the spheroidites from martensite.

Assuming that the straight-line relation between ASTM grain size number and transition temperature found by these investigators can be extrapolated to ferrite grain sizes of this work, the difference in transition temperature with a keyhole-notch Charpy would amount to 90°F for the change from a ferrite grain size of ASTM No. 12 to No. 15. The difference observed using the V-notch Charpy was about 200°F. The greater differential in the present work might be due to one or more of several causes. For one thing, notch conditions are less severe with the keyhole than the V-notch. Again, the 30°F differential per ASTM grain size number observed with practically carbon-free steel may become larger, for spheroidites having the same carbide particle size, as the carbon content of the steel is increased. Another reason for the 200°F differential in transition temperature has already been mentioned, namely, the difference in the ferrite grain shape between spheroidite from martensite and spheroidite from pearlite.

Observation of Fractures

The extent to which the difference in ferrite grain structures influenced the transition temperatures of the spheroidites described above made it seem of interest to examine broken impact specimens. The object was to see what structural features were involved in the brittle failures that persisted to such high testing temperatures in the spheroidite from pearlite.

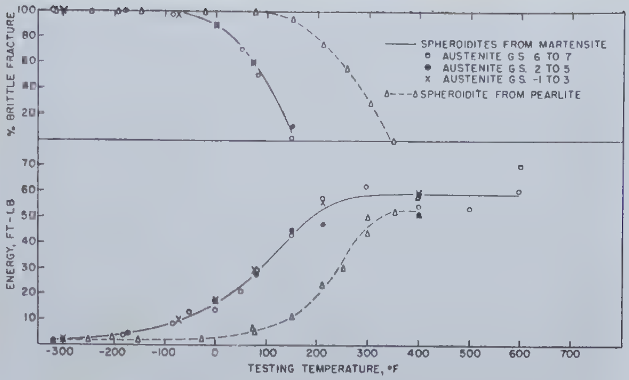

Fig. 11—V-notch Charpy impact data for spheroidites from martensite and pearlite as indicated in legend. Hardness Rockwell B 92-94.

The specimens were plated with nickel and sectioned normal to the fractured surface. In both types of spheroidites, subsidiary cleavages that had not become a part of the final path of rupture were observed in the metal immediately adjacent to the brittle portion of the fractures. The illustrations to follow are drawn from micrographs of specimens broken at —320°F; however, enough specimens from within the transition range were examined to conclude that the features of the brittle fracture at —320°F also represented features of the brittle portions of fractures obtained within the transition range.

Figs. 12, 13, and 14 illustrate cleavages under the brittle portion of fractures in spheroidite derived from pearlite. The cleavages are reasonably straight within a single ferrite grain, or have zig-zag paths with roughly parallel zigs or zags. An instance of this may be seen in fig. 14. Cleavage may involve a number of rather similarly oriented adjacent grains, as illustrated by figs. 13 and 14. The zig-zag crack in fig. 14 passes through at least three ferrite grains. The zigs or zags in each grain are roughly parallel to those in the other grains.

As indicated by the arrows in figs. 13 and 14, the cracks may cut through the carbide particles. They may go around also, as indicated at No. 1 in fig. 14. When passing through the carbide particles the crack may change direction, as in fig. 13, presumably

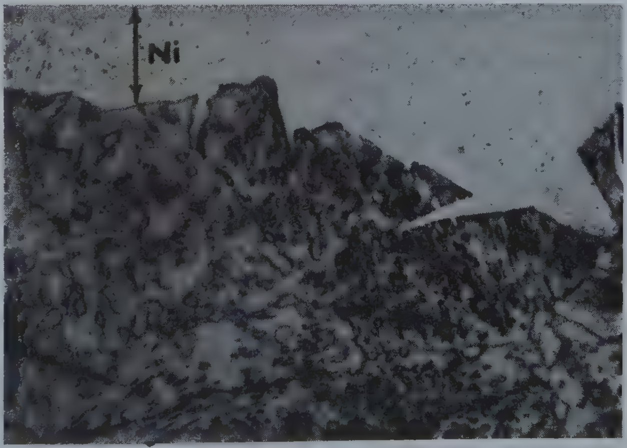

Fig. 12—Final path of rupture and subsidiary cracks in spheroidite from pearlite, etched with nital, X1500. Brittle fracture at —320°F.

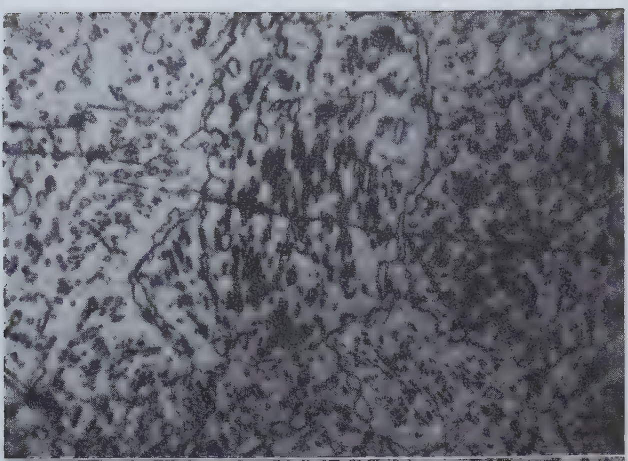

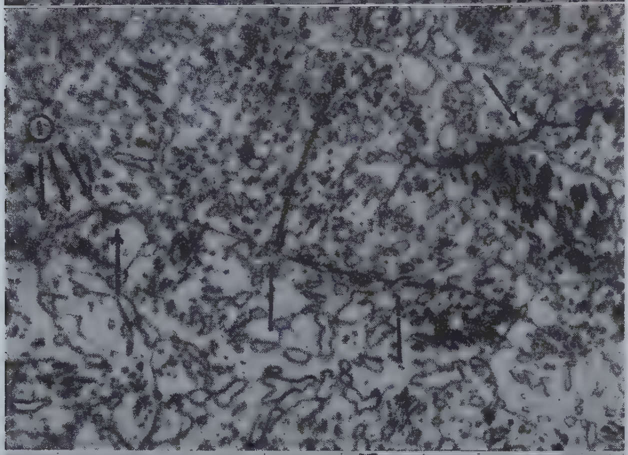

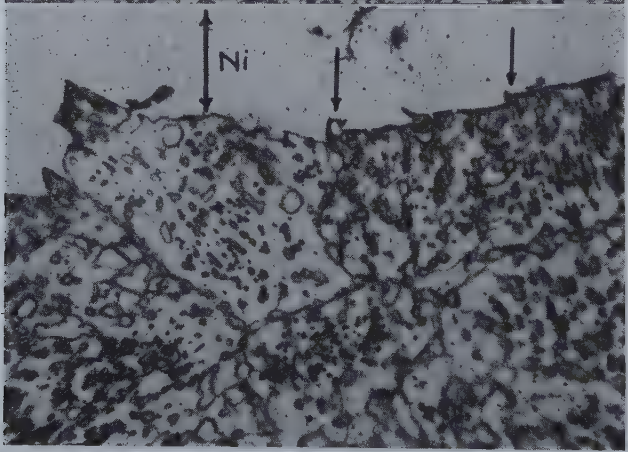

Fig. 13—Same specimen as shown in fig. 12, but another area, X1500.

Fig. 14—Same specimen as shown in fig. 12, but another area, X1500.

Fig. 15—Same specimen as shown in fig. 12, but another area, X1500. Tearing between cleavages indicated by small tongues of deformed metal at arrows.

to accommodate the characteristic cleavage direction of the cementite.

The features of the subsidiary cleavages in the spheroidized pearlite were similar to those described by Tipper[5] in the case of brittle fractures of mild steel. Tearing between cleavages in the formation of the final path of rupture was observed. This is illustrated by fig. 15, as indicated by the arrows. Deformation after cleavage but before final rupture is illustrated by fig. 16. The upper side of the cleavage, indicated by the arrow, had been bent upward and then torn away in the final rupture of the specimen.

Figs. 17, 18, and 19 illustrate the final path of brittle rupture and subsidiary cracking observed in the spheroidite from martensite. The same sort of deformation after cleavage may be seen as was observed in the spheroidite from pearlite. This is illustrated at the double arrows in figs. 17 and 18. The ferrite cleavages may propagate through one or more contiguous ferrite grains, as in the case of the cleavages indicated by the single arrow in fig. 17. The ferrite grains are smaller and the cracks that are made up of multiple cleavages in adjacent grains are shorter than in the spheroidite from pearlite. The arrows in fig. 19 indicate about the maximum length of multiple cleavage path observed in the spheroidites from martensite. Another difference from the subsidiary cleavages observed in the spheroidite from pearlite was noted, namely, the tendency for subsidiary cracks to follow the ferrite grain boundaries. This is illustrated at Nos. 1 and 2 in fig. 17 and at No. 1 in fig. 18. Just as in the case of spheroidite from pearlite, the subsidiary cracks were often observed to pass through carbide particles. An instance of this is indicated by the arrow in fig. 20.

The foregoing microscopic evidence of the nature of the brittle fractures in the impact specimens suggests that the grain structure is an active agent in limiting the propagation of cleavage from one ferrite grain to the next. It is presumed that disorientation of adjacent ferrite grains would act in this way, and that a decrease in ferrite grain size would increase the probability of disorientation within any given unit volume of the specimen. On the other hand, even though the effect might be small in rapid deformation such as impact loading, it is possible that deformation at the grain boundaries in preference to slip within the grains may use energy that in the absence of sufficient grain boundary surface might be expended in initiating ferrite cleavage. As the grain boundary area is greater in the case of nonequiaxed than in equiaxed grain structures of the same average grain diameter, this might form the basis for an effect of grain shape. More data are needed before further discussion would be warranted.

Conclusions

The following conclusions apply to 0.80 pct carbon, 1 pct nickel spheroidites of essentially the same carbide particle size and distribution, with hardness of Rockwell B 93. These spheroidites are believed

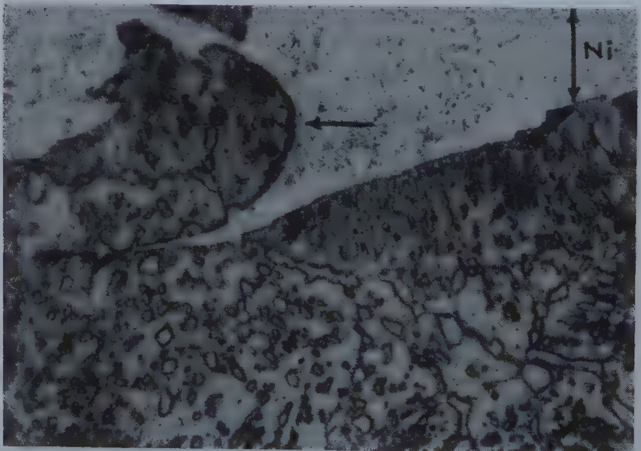

Fig. 16—Same specimen as in fig. 12, X1500. Deformation after cleavage indicated by arrow.

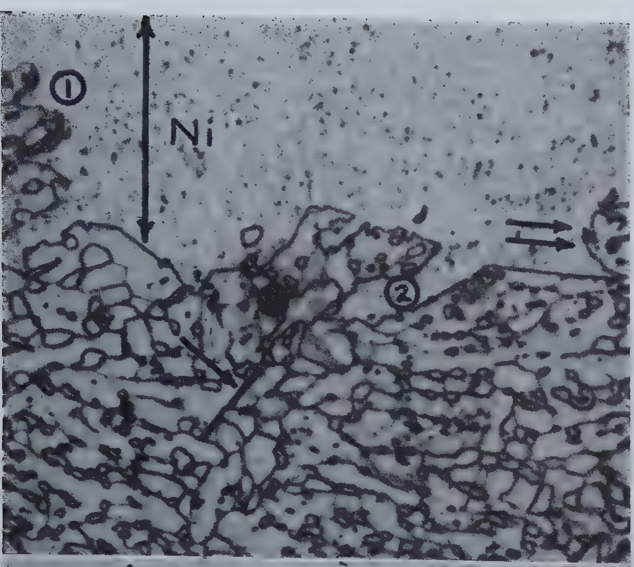

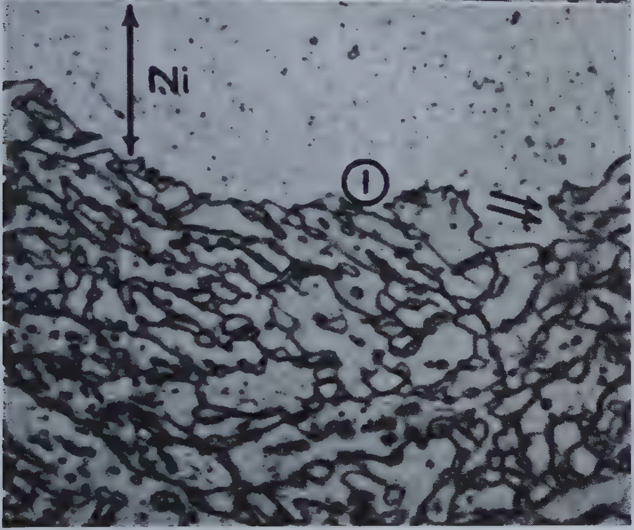

Fig. 17—Final path of rupture and subsidiary cracks in spheroidite from martensite, etched in nital, X2000. Brittle fracture at —320°F. Single arrow indicates ferrite cleavage, double arrow indicates deformation after cleavage, numerals 1 and 2 indicate failure along ferrite grain boundaries.

Fig. 18—Same specimen as shown in fig. 17, X2000. Double arrow indicates deformation after cleavage, numeral 1 indicates failure along ferrite grain boundary.

to have been practically free from temper embrittlement.

In spheroidites produced by sub-critical treatment of martensite, the austenite grain size at the moment of quenching to martensite exerted little influence on the ferrite grain size and shape of the spheroidite. A range of as-austenitized grain size of ASTM No. 6.5 to 1 was examined. The V-notch Charpy energy and fracture testing temperature curves for these spheroidites were practically identical.

A change in ferrite grain structure influenced the notched-bar impact transition temperature of the spheroidite. The small, nonequiaxed ferrite grain structure of the spheroidites from martensite gave a considerably lower transition temperature than the larger, equiaxed ferrite grain structure of a spheroidite obtained by sub-critical annealing of pearlite.

It is believed that the uniform structure of small, nonequiaxed ferrite grains in spheroidites derived from martensite offers an explanation of the consistently good performance of unembrittled tempered martensite, when compared with other steel structures by the notched-bar impact test.

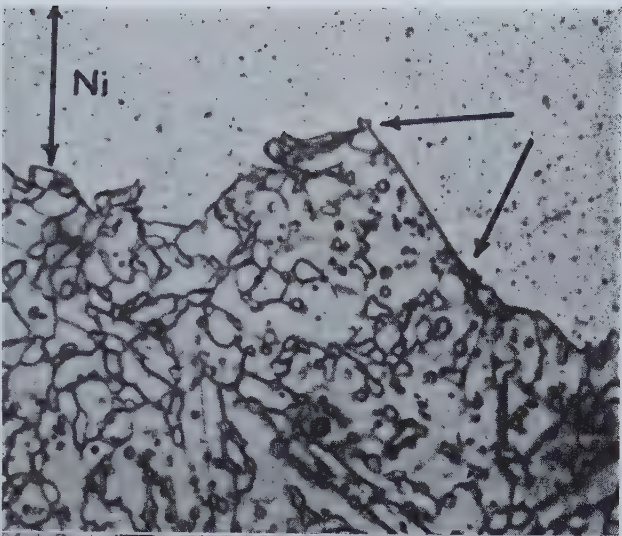

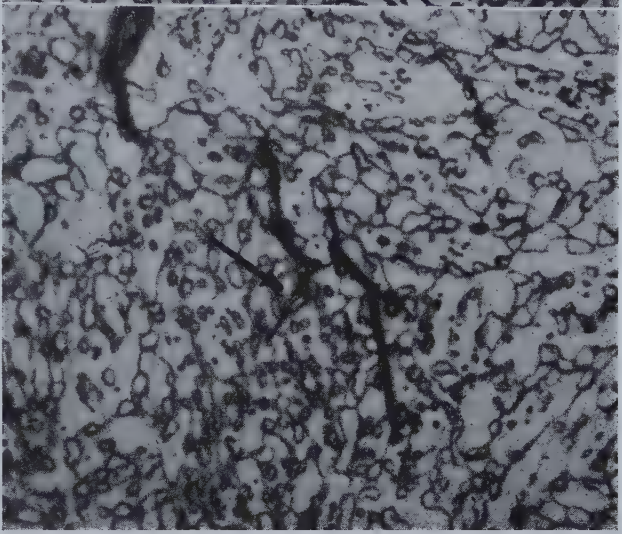

Fig. 19—Same specimen as shown in fig. 17, X2000. Multiple cleavage through adjacent ferrite grains at arrow forming part of final path of rupture.

Fig. 20—Same specimen as shown in fig. 17, X2000. Arrow indicates cracked carbide particle.

Acknowledgment

This work was sponsored by the Office of Naval Research. The authors take pleasure in acknowledging the cooperation of several members of that organization, in particular the interest and helpful criticism of I. R. Kramer.

References

[1] Office of Naval Research, Contract N6 onr 274 T.O.I. Project NR 031-115.

[2] M. Gensamer, E. B. Pearsall and G. V. Smith: *Transactions* A.S.M. (1940) **28**, 380-395.

M. Gensamer, E. B. Pearsall, W. S. Pellini and J. R. Low, Jr.: *Transactions* A.S.M. (1942) **39**, 983-1019.

M. Gensamer: *Transactions* A.S.M. (1946) **36**, 30-60.

[3] Prof. Morris Cohen, Massachusetts Institute of Technology. Private communication.

[4] J. M. Hodge, R. D. Manning and H. M. Reichhold: *Transactions* AIME, **185**, 233-240; *Journal of Metals* (March 1949) TP 2553E.

[5] C. F. Elam Tipper: The Fracture of Mild Steel Plate. Report No. R.3. The Admiralty Ship Welding Committee. 1948.

Crystal Structures and Transformations in Indium-Thallium Solid Solutions

by Lester Guttman

X-ray diffraction and metallographic studies of the indium-thallium system have shown the existence of a transformation from face-centered tetragonal to face-centered cubic in the indium-rich solutions. The equilibrium diagram has been revised to conform with these measurements and published thermal data.

THE equilibrium diagram of the indium-thallium system was of interest to us in connection with a study of the superconducting properties of metallic solid solutions in progress at this Institute. For this purpose, a series of alloys was prepared covering the range from pure indium to 75 atomic pct Tl, and X-ray diffraction patterns were obtained. Roughly speaking, the results indicated a region of continuous decrease in the axial ratio of the face-centered tetragonal structure from the value *ca.* 1.08 in pure indium to unity at about 23 atomic pct Tl. From this concentration to the solubility limit, the structure was face-centered cubic, a form not reported by Hansen.[1] At this point we became aware of the work of Valentiner,[2] who had found the same structures at room temperature but had not investigated further the relationship between them. To study the transformation f.c.c.⇄f.c.t., and to clarify the phase diagram, we undertook the work reported in this paper and that which follows.[3]

Preparation of Alloys

Pure indium and thallium* (both about 99.9 pct, as estimated from spectroscopic analyses) were weighed out in quantities sufficient to prepare 10 to 25 g of alloy of the desired concentration. (Occasionally indium was mixed with a previously prepared solution.) The metals were melted over a flame, in an open graphite crucible, stirred with a graphite rod, and poured into a graphite trough. The rough slug was hammered and swaged into a rod of 2 to 3 mm diam, and annealed in a drying oven at about 125°C for 1 to 2 days. Samples were taken from the rod for analysis, as well as for diffraction and other measurements. The thallium was determined by electrometric titration, using a modification of the method of Beale and co-workers.[4] The precision of analysis was generally about ± 0.2 pct of the thallium content. The rods were sometimes found to vary in thallium content as much as 1.5 pct from end to end, but since analyses were also made close to the segments used in the various studies, the composition was usually known as accurately as the analyses could be made. Where one less significant figure is given, the error is estimated to be ±0.4 pct of the thallium content.

X-Ray Diffraction Measurements

Three different cameras were used: (1) A 7 cm Debye camera, with oscillating specimen (manufactured by the Picker X-ray Corp., Cleveland, Ohio); (2) a 9 cm diam Debye camera of the type designed by Bradley;[5] (3) a 10 cm diam symmetrical focusing back-reflection camera (manufactured by Geo. C. Wyland, Ramsay, N. J.). Samples were prepared from the homogenized rods, either by filing under liquid nitrogen, or more often, in the form of wires or foils made by working at room temperature or liquid nitrogen temperature. Sharp patterns were obtained from specimens annealed at room temperature, although higher annealing temperatures were also used (cf. below). Generally, copper radiation was used; a few patterns were obtained with

---

* The indium and thallium were supplied by the American Smelting and Refining Co., New York, N. Y.

L. GUTTMAN is associated with the Institute for the Study of Metals, University of Chicago, Chicago, Ill.

AIME St. Louis Meeting, February 1951.

TP 2973 E. Discussion (2 copies) may be sent to Transactions *AIME before April 1, 1951. Manuscript received Aug. 2, 1950; revision received Oct. 2, 1950.*

chromium radiation. Lattice parameters were evaluated by the well-known analytic method of Cohen,[6] as modified by Hess.[7] The wavelengths used, expressed in units of 10^{-8} cm, are as follows:

Cu	$K\alpha_1$	1.54050
	$K\alpha_2$	1.54434
	$K\beta$	1.39217
Cr	$K\alpha_1$	2.28962
	$K\alpha_2$	2.29352
	$K\beta$	2.08479

The results of these measurements are collected in table I, which gives, at each concentration, the dimensions of the tetragonal unit cell, *a* and *c*, the standard error, σ, of each, and the axial ratio. (In the case of cubic structures, of course, only one dimension is needed.) The temperature of cold working and the annealing time and temperature are included; if the last is omitted, room temperature is to be understood. The seventh column gives the *deviation* of the unit cell volume, a^2c (or a^3), from a linear function of the atomic fraction of thallium, fitted to the values for the pure metals. The value for thallium is that given by Sekito[10] for the *metastable* f.c.c. form which he obtained by quenching liquid thallium in ice water; (the volume of stable hexagonal thallium is only 0.16 pct greater). The standard error of the volume deviation, given in the eighth column, includes a contribution from the estimated uncertainty in the composition, as well as that due to the errors in the lattice parameters from which it was computed. The same data are presented graphically in figs. 1, 2, and 3.

It can be seen that *a* increases and *c* decreases as the Tl concentration rises, the smallest value of the ratio observed being 1.023 at 22.24 atomic pct Tl. The sample containing 22.73 pct Tl had an axial ratio of over 1.03 before annealing, and the f.c.c. structure afterwards. Material containing about 23.7 pct Tl, rolled at room temperature in an attempt to produce a structure with still smaller *c/a*, gave diffuse back-reflection patterns. This evident lack of equilibrium makes it impossible to fix the boundary between the two phases more closely, or to state more precisely the dependence of lattice parameters on concentration in the vicinity of the boundary.

The fact that the volume of the terminal solid solution is so nearly the sum of the volumes of its components over the entire concentration range suggests that the deviation from additivity may be used as a sensitive test of approach to equilibrium. Inspection of fig. 3 shows, in fact, that data from specimens annealed for more than a few minutes above 100°C (solid circles) lie on a markedly smoother curve than those from specimens annealed for shorter times or at lower temperatures (open circles). Indeed, one might conclude from fig. 3 that at equilibrium there is no discontinuity in volume exceeding 0.1 pct (and probably none greater than 0.03 pct) across the boundary between the f.c.t. region and the f.c.c. region, although some caution must be exercised in the face of the evidence for irreversibility.

Table I. Results of X-Ray Diffraction Measurements on In-Tl Solid Solutions at Room Temperature (24 ± 1°C)

Atomic Pct Tl	a*	$10^5\sigma(a)$*	c*	$10^5\sigma(c)$*	c/a	ΔV**	$\sigma(\Delta V)$**	Heat Treatment
Face-centered tetragonal								
0	4.59929	26	4.94778	37	1.07577	(0)		(1) (3)
12.5	4.64362	34	4.90928	79	1.05721	0.011	0.023	(1) ; annealed 130°C, 30 min
18.06	4.66135	33	4.88902	85	1.04884	—0.152	0.022	(1)
18.06	4.67019	23	4.87829	59	1.04456	0.022	0.016	(1) ; annealed 125°-135°C, 10 min
19.64	4.66766	54	4.88052	78	1.04560	—0.195	0.022	(2)
19.64	4.67294	65	4.87092	98	1.04237	—0.164	0.031	(2) ; annealed 100°C, 1 min
19.64	4.67950	19	4.86779	43	1.04024	0.066	0.012	(2) ; annealed 105°C, 10 min
19.75	4.68678	26	4.85960	50	1.03687	0.209	0.016	(1) ; annealed 100°C, approx. 3 min
20.75	4.68792	35	4.85475	61	1.03559	0.059	0.017	(1) ; annealed 110°C, 2 min
22.2	4.70566	18	4.82598	38	1.02557	0.093	0.014	(1)
22.24	4.70930	45	4.81751	72	1.02298	0.066	0.022	(2)
22.73	4.69193	38	4.84943	63	1.03357	—0.064	0.018	(1)
22.73	4.69193	57	4.84506	100	1.03264	—0.160	0.031	(1) ; annealed room temp, 3 days
Face-centered cubic								
22.73	4.7445	110				—0.02	0.044	filed nitrogen temp; annealed 110°C, 20 min
25.16	4.74942	21				0.082	0.010	(1) ; annealed 125°C, 30 min
30.4	4.75719	22				0.112	0.014	(1) ; annealed 125°C, 90 min
34.7	4.76417	9				0.175	0.018	(1) ; annealed 125°C, 60 min
39.9	4.77163	41				0.193	0.019	(1) ; annealed 125°C, 30 min
50.7	4.78368	27				—0.009	0.022	(1) ; annealed 110°C, 20 min
55.33	4.78982	40				—0.024	0.019	(1) ; annealed room temp, 24 hr
55.33	4.79014	35				—0.002	0.017	(1) ; annealed 100°C, 20 min
66	4.79543	24				(0)	(0)	(1) ; annealed room temp, 28 days
100	4.851					(0)	(0)	quenched from liquid (Sekito)
Body-centered cubic								
74.9	3.82796	16				0.203		(1) ; annealed 120°C, 15 min
66	3.82799	16						(1) ; annealed room temp, 28 days

Notes:

* In units of 10^{-8} cm

** In units of 10^{-24} cm^3

(1) Heavily cold worked at room temperature.

(2) Heavily cold worked at liquid nitrogen temperature.

(3) For purposes of comparison, we give the values for pure In obtained by other workers:
$a = 4.5986 \times 10^{-8}$ cm $c = 4.9471 \times 10^{-8}$ cm $c/a = 1.07578$. Error—"3-8 parts in 10^5". Ref. 8.
$a = (4.5981 \times 10^{-8}$ cm $\pm 0.001)$ $c = (4.9457 \times 10^{-8}$ cm $\pm 0.001)$ $c/a = 1.0756 \pm 0.001$ Ref. 9.

$\Delta V = a^2c$ (obs) — [104.663 x (atom-fraction In) + 114.153 x (atom-fraction Tl)]

σ = standard error

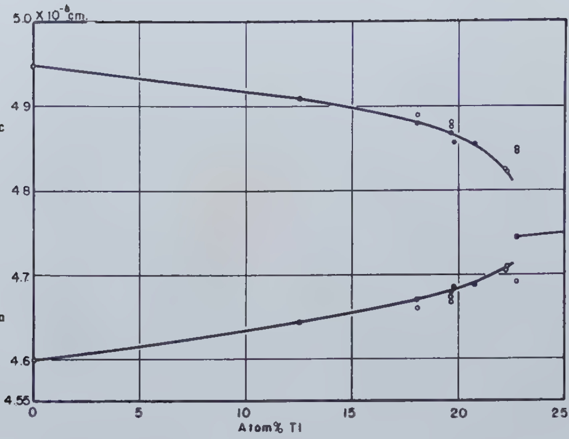

Fig. 1—Unit cell dimensions of indium-thallium solid solutions at room temperature (24 ± 1°C).
● More thoroughly annealed specimens. (Cf. table I.)

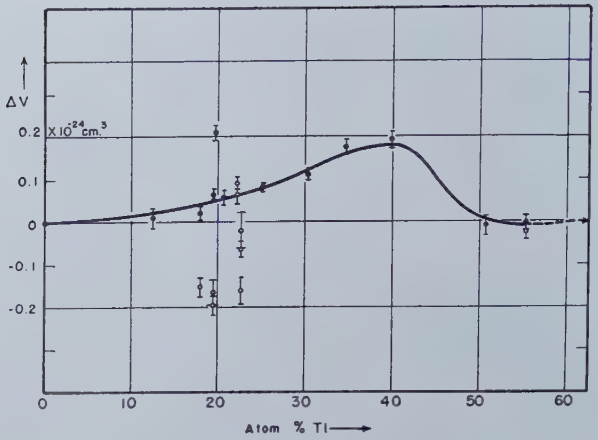

Fig. 3—Deviation of unit-cell volume from additivity in indium-thallium solid solutions at room temperature (24 ± 1°C).
● More thoroughly annealed specimens. (Cf. table I.)

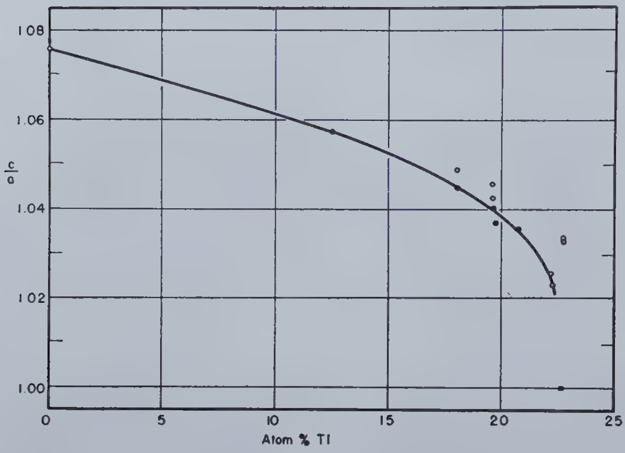

Fig. 2—Axial ratio of indium-thallium solid solutions at room temperature (24 ± 1° C).
● More thoroughly annealed specimens. (Cf. table I.)

No lines have been observed, at any composition, that would correspond to ordered structures.

Microstructure of the Tetragonal Phase

Since the cubic and tetragonal structures lie in adjacent composition regions at room temperature, it was anticipated that a given composition could be converted into one form or the other by change of temperature. By analogy with the system Cu-Mn,[11] which seems to exhibit a similar transformation, it was also expected that the tetragonal phase after transformation would show a lamellar microstructure. This expectation has been confirmed, as shown, for example, in fig. 4, which is a micrograph of a sample containing 20.75 pct Tl. This sample had been pressed at about 100°C between polished steel blocks lightly coated with mineral oil, and photographed under oblique illumination when cool. The surface, which had been flat when hot, was now distorted, and every grain was seen to be traversed by one or more sets of alternately dark and light bands. For each of three concentrations of Tl, a sample prepared in this way was observed at moderate magnification on an electrically heated stage, while its temperature was measured with a copper-constantan thermocouple pressed into the face. The markings disappeared on heating and reappeared on cooling. The temperature of disappearance (or appearance) was different at different places in a given sample, and at a given place was also somewhat different for each reheating (or recooling). In table II are shown the lowest and highest temperatures at which appearance or disappearance was seen in several cycles of heating and cooling.

Table II. Temperatures of Appearance and Disappearance of Surface Markings in In-Tl Solid Solutions

Atomic Pct Tl	Extreme Temperatures at which Changes Occurred, °C: Heating Min	Heating Max	Cooling Min	Cooling Max
18.06*	104.4	111.6	103.9	106.7
19.64	78.1	80.0	75.8	81.0
20.75**	61.3	63.7	57.3	59.9

* Two different samples. ** Two different fields.

These results show that the temperatures of appearance and disappearance vary several degrees, and that the former usually lie 1° to 5°C lower than the latter. No other systematic effects, as of heating or cooling rate (in the range 0.1° to 5°C per min) or of thermal history, were noticed. However, any such effects would necessarily be small, in view of the small hysteresis, and could easily have escaped detection by the rather crude method used here. The changes in the surface markings occurred

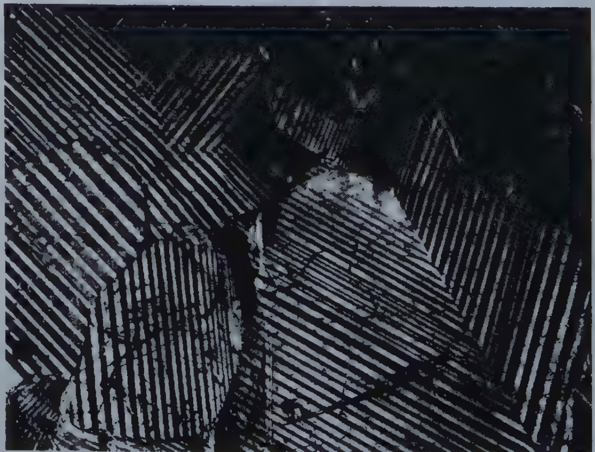

Fig. 4—Surface distortion after transformation to tetragonal structure in 20.75 atomic pct Tl.
Oblique illumination, X75. Area reduced approximately 50 pct for reproduction.

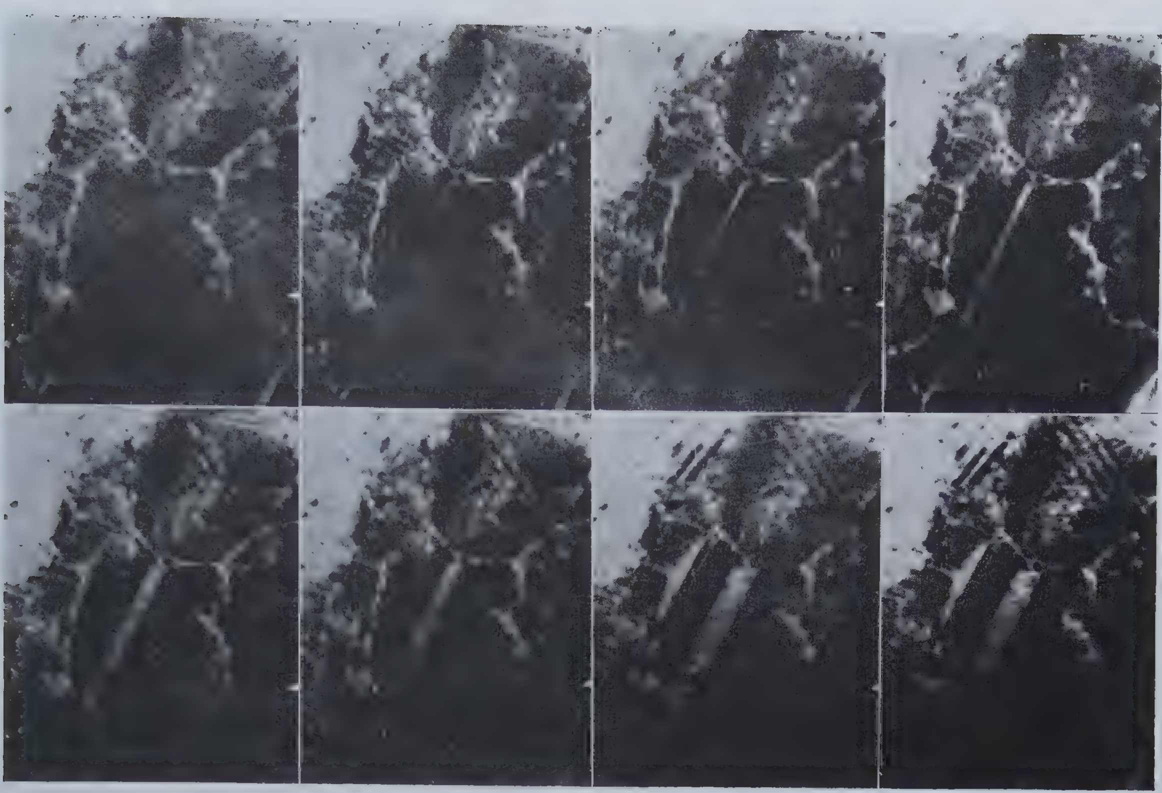

Fig. 5—Frames selected from motion pictures of 20.75 pct Tl on cooling.

Oblique illumination, about X50. Frames (1,2,3,4), (5,6), and (7,8) are consecutive, at about 15 frames per sec. Frames are numbered consecutively starting with the top left frame and reading from left to right. Area reduced approximately 50 pct for reproduction.

slowly enough under the conditions described that motion pictures of the process could be made. A series of frames, illustrating the development of the markings, is shown in fig. 5. The process on cooling is characterized by the following features:

1. The first bands appear suddenly in a given grain, extending from one boundary to the opposite (frame 2).
2. The bands then fill the grain, by more or less rapid broadening of existing bands (frames 3, 4, 5, 7), by production of new bands parallel and adjacent to those already existing (frames 6, 8), by the production of new bands at a distance from existing bands (frame 7, top grain), or by a combination of these steps.
3. The surfaces of two adjacent bands contrast not only with each other, but with the unbanded surface.
4. Bands on either side of a grain boundary, although not parallel, frequently grow at the boundary simultaneously, i.e., the unaided eye can detect no time interval between events on either side.

On heating, the process takes place very much in the reverse way as on cooling, with the additional feature that the contrast between bands decreases, and the boundaries become less distinct before the final abrupt vanishing.

The finer details of the microstructure are only revealed on polished and etched surfaces. The following procedure has been found satisfactory for concentrations between zero and about 25 pct Tl:

When a flat surface has been produced by careful mechanical polishing, the unmounted specimen is annealed and electropolished in a solution containing 75 ml "Carbitol," 5 ml concentrated HNO_3, and 2 ml concentrated HCl, at 40 to 60 v, 0.3 to 0.6 amp per cm^2, with constant stirring, at room temperature (1 cm or less from an Al cathode). An anodic film soon forms which prevents further polishing, and must be removed occasionally with 10 pct HF. The electroetching is carried out in the polishing solution at about 3 v.

The etched surfaces show the presence of bands in every grain, particularly in polarized light, where, if the anodic film has not been removed, the coloration is striking. The most noteworthy feature, however, is the presence of *fine markings within the main bands* (fig. 6). To show the markings best, the etching conditions must be rather critically adjusted, and the sample must be properly oriented with respect to the plane of polarization of the incident light. Under the right conditions, the fine markings can be seen in nearly every grain, and it seems safe to assume that when they cannot be seen, it is only because of unfavorable orientation of the grain with respect to the exposed surface. Photographs of the fine markings at very high magnification appear as in fig. 7.

The microstructure is interpreted in terms of a mechanism of transformation in ref. 3. For the present, it will be assumed that the appearance of the surface markings coincides with the formation of the tetragonal structure, and *vice versa*.

X-Ray Measurements at Higher Temperatures

To confirm the qualitative relationships between the various phases suggested by the X-ray results at room temperature, observations were made of the diffraction patterns of various compositions at higher temperatures. The technique, which is described in more detail in ref. 3, was to mount a foil of alloy on an electrically heated Dural block in the focusing position of a Geiger counter X-ray spectrometer (General Electric XRD-3). The tempera-

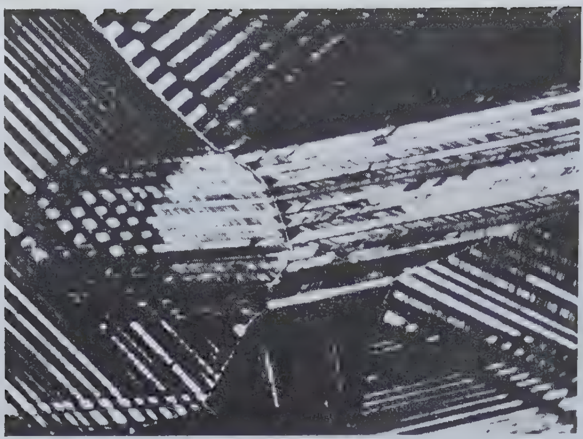

Fig. 6—Fine lamellae in 20.75 pct Tl, electropolished and electroetched.

X250, polarized light. Area reduced approximately 66 pct for reproduction.

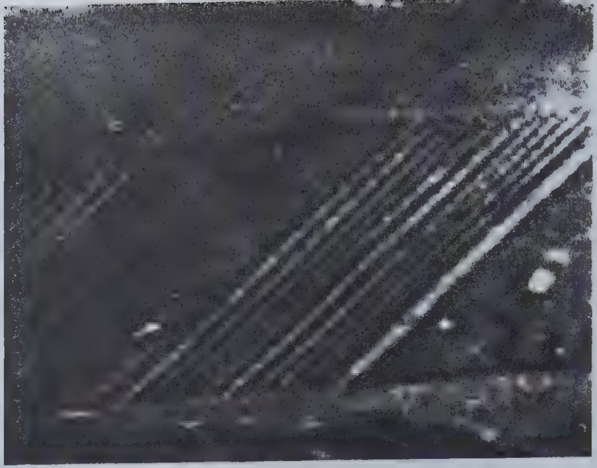

Fig. 7—Fine lamellae in 20.75 pct Tl, electropolished and electroetched.

X2000. Area reduced approximately 50 pct for reproduction.

ture was controlled automatically, and was measured by a copper-constantan thermocouple pressed into the face of the sample.

From observations of any tetragonal doublet, such as (220) (202), it is possible to calculate the unit cell dimensions. A set of such results, from a specimen containing 20.75 pct Tl, is plotted in fig. 8. Because of inaccurate sample alignment, the observed diffraction angles had to be corrected by a small amount (0.06° at $2\theta = 27°$) to bring them into agreement with the precision room-temperature values. For the same reason, the ratio c/a is probably more accurate than the individual dimensions. These data, which were actually taken on cooling, show that the cubic lattice is distorted, in a temperature interval of less than 0.2°C, to a tetragonal lattice of the same volume, which then undergoes a further gradual increase in axial ratio as it cools. The temperature of transformation lies close to the range in which surface effects were observed in other specimens of the same composition (table II). This point is discussed further in ref. 3.

Other results obtained by this method are reported at the relevant places in the next section.

Discussion of Results

The equilibrium diagram of the indium-thallium system shown in fig. 9 is derived from the results of Valentiner[2] and the present work and is presented as a basis for further discussion.

1. The body-centered cubic form found at room temperature is undoubtedly a terminal solid solution derived from the high-temperature form of Tl, as determined by Lipson and Stokes.[12] The boundary (b.c.c.+h.c.p.)/(h.c.p.) is that determined by Valentiner from thermal measurements. The boundary (b.c.c.)/(b.c.c.+h.c.p.) has been located at two points only: (*a*) The transformation temperature in pure Tl; (*b*) at room temperature at about 77 pct Tl, from Valentiner's diffraction results, combined with the observation in this study that a sample containing nominally 75 pct Tl consisted of b.c.c. along with a small amount of h.c.p. Since another portion of the same material contained only one phase (table I), the difference must be ascribed to a small variation in composition within the sample; at any rate, the boundary cannot lie at much more than 77 pct Tl. The boundary (f.c.c.+b.c.c.)/(b.c.c.) is determined at three points: (*a*) It terminates at the peritectic temperature and the composition found by Valentiner; (*b*) at room temperature, the lattice parameter of the b.c.c. in the two-phase region is identical with that of the single-phase material (74.9 pct Tl, table I); hence the boundary must lie close to 75 pct Tl; (*c*) diffraction measurements, made as described in the previous section, on a sample containing 66 pct Tl, showed it to become homogeneous on heating to 88°C, whereas two phases were present at 84°C and below.

2. The boundary (f.c.c.)/(f.c.c.+b.c.c.) is determined at three points: (*a*) At its upper end, it is fixed by Valentiner's peritectic temperature and composition; (*b*) at room temperature, the evidence from fig. 3 is that deviations from volume additivity approach zero in the region 50 to 55 pct Tl; hence, from the lattice parameter of the f.c.c. phase in the two-phase region (66 pct Tl, table I), a simple computation gives $59._{15}$ pct Tl as the solubility limit; (*c*) from observations on the Geiger counter spectrometer, a sample of 50 pct Tl contained less than

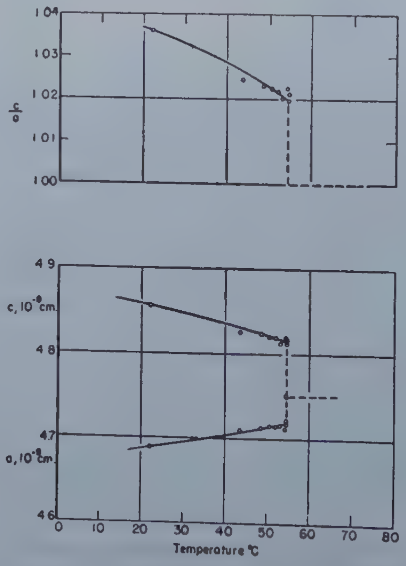

Fig. 8—Unit cell dimensions and axial ratio of 20.75 pct Tl at higher temperatures.

1 pct of the b.c.c. phase on cooling to 121°C, and certainly consisted of two phases at 122°C and above.

3. The boundary (f.c.t.)/(f.c.c.) has been drawn through the average of the temperatures of appearance and disappearance of surface markings, and at room temperature passes through 22.7 pct Tl, the only composition obtained in both forms. The 25 pct material was tetragonal at liquid nitrogen temperatures, while 30 pct was still cubic. *No two-phase region* has been drawn separating these solutions, since all diffraction patterns at room temperature contain only lines from one structure or the other, never from both. This behavior is typical of a transformation of the *second order* (or higher). In a one-component system such a transformation is characterized by equality of the entropy and volume of the phases in equilibrium at the transformation temperature; in two-component solutions, as has been shown by Stout,[13] the composition is also the same in the two phases, and the system consists entirely of one or the other phase, according to whether it is above or below the transformation temperature.† Additional support for this possibility is provided by the observed continuity of volume (fig. 3). However, it should be mentioned that transformation of a f.c.c. solution containing 75 pct Tl to the b.c.c. form at the same composition would involve an increase in volume of only 0.4 pct (if the extrapolation of volume additivity is valid), yet this transformation is clearly of *first order*, with an unambiguous two-phase region.

At higher temperatures, both forms have been simultaneously observed visually (fig. 5), and in diffraction patterns (in the case of 18 pct material, tetragonal lines have been recorded as much as 25°C above the temperature at which the bulk of the transformation takes place). Nevertheless, it is felt that these were nonequilibrium situations, produced perhaps by local stresses or fluctuations in composition or temperature, and that the results at room temperature, indicating no two-phase region wider than about 0.5 pct Tl, represent a closer approach to equilibrium through recrystallization after cold working.

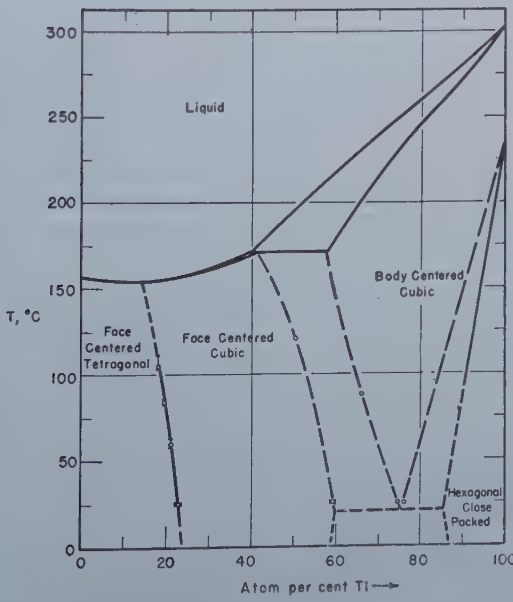

Fig. 9—Equilibrium diagram of indium-thallium system.

Summary

X-ray diffraction and metallographic studies have been made on the In-Tl system.

1. A transformation f.c.t.⇄f.c.c. has been found to occur at a temperature of about 105°C at 18 atomic pct Tl and 25°C at about 23 pct Tl. The tetragonal form is the stable one at low temperatures.

2. The transformation produces a distinctive lamellar microstructure, and the progress of the interface between the phases can be followed by the surface distortions produced.

3. Precision X-ray diffraction measurements at room temperature from 0 to 75 pct Tl have been combined with observations at higher temperatures and published thermal data to construct an equilibrium diagram for the system.

Acknowledgment

The work reported here has been discussed with nearly every member of the Institute staff. Thanks are due particularly to the following: C. S. Barrett and J. S. Bowles, for permission to use the data in fig. 8, and for many stimulating discussions; K. K. Ikeuye, for much of the metallographic and photographic work; C. S. Smith, for pointing out the parallelism with the Cu-Mn system and predicting a similar microstructure; L. J. Howell, for the spectrographic analyses, and N. H. Nachtrieb and R. E. Fryxell for the chemical analyses. The superconductivity work was initiated by J. W. Stout, and has been continued in collaboration with him.

References

[1] M. Hansen: Aufbau der Zweistofflegierungen. Pp. 827-828.

[2] S. Valentiner: *Ztsch. für Metallkunde.* (1940) **32,** 244-248.

[3] J. S. Bowles, C. S. Barrett, and L. Guttman: The Crystallography of the Cubic-Tetragonal Transformation in the Indium-Thallium System. *Transactions* AIME, **188,** 1478; *Journal of Metals* (Dec. 1950) TP 2972E.

[4] R. S. Beale, A. W. Hutchison, and G. C. Chandlee: *Industrial Engineering Chemistry.* Anal. Edition (1941) **13,** 240.

[5] A. J. Bradley, W. L. Bragg, and C. Sykes: *Journal* Iron and Steel Inst. (1940) **141,** 63; and A. J. Bradley, H. Lipson, and N. J. Petch: *Journal Scientific Instruments* (1941) **18,** 216.

[6] M. U. Cohen: *Review Scientific Instruments* (1935) **6,** 68; (1936) **7,** 135.

[7] J. B. Hess: *Acta Cryst.* (1950). In press.

[8] C. J. Fink, E. R. Jette, S. Katz, and F. J. Schnettler: *Transactions* Electrochem. Soc. (1945) **88,** 229.

[9] W. Betteridge: *Proceedings* Phys. Soc. (1938) **50,** 519-524.

[10] S. Sekito: *Ztsch. für Krist.* (1930) **74,** 189-201.

[11] F. T. Worrell: *Journal of Applied Physics* (1948) 19. 929.

[12] H. Lipson and A. R. Stokes: *Nature* (1941) **148,** 437.

[13] J. W. Stout: *Physical Review* (1948) **74,** 605.

---

† Since the results of Stout's treatment are not in accord with the usual concepts of phase relationships, it is perhaps worth emphasizing that they have been deduced strictly thermodynamically. Therefore, no violation of the Phase Rule is involved in not showing any two-phase region when experiment indicates that no latent heat accompanies the transformation. In fact, there are commonly accepted diagrams showing just such transformations, *e.g.,* the magnetic transformations in iron and nickel alloys, and the order-disorder transformation in β-brass. It should also be mentioned that highly precise measurements of the heat capacity in the vicinity of the transformation temperature are needed to distinguish a first from a second-order transformation (even in the unlikely event that equilibrium is rapidly established), because there is no isothermal absorption of heat in either case when two components are present.

Crystallography of Cubic-Tetragonal Transformation In The Indium-Thallium System

by J. S. Bowles, C. S. Barrett, and L. Guttman

The diffusionless transformation from cubic to tetragonal in In-Tl alloys on cooling is analyzed by metallographic and X-ray measurements. Theories of atom movements are tested by precision pole figures, and it is concluded that the transformation occurs by a double shear process, $(101)\ [\bar{1}01]$ followed by $(011)\ [0\bar{1}1]$.

THE transformation from the face-centered cubic (A1) to the face-centered tetragonal (A6) structure in certain alloys of the indium-thallium system reported in the preceding paper[1] exhibits many interesting crystallographic and metallographic features, most of which presumably are similar to those of other cubic to tetragonal transformation such as, for example, the one which occurs in the chromium-manganese system,[2] the one which, judging by microstructures and X-ray patterns,[3] probably occurs in the copper-manganese system, the ones accompanying ordering in FePt,[4] CoPt,[4] and AuCu,[5] and the transformation near 115°C in barium titanate.[6, 7, 8] If, as mentioned in ref. 1, the transformation is second order, the phases in equilibrium do not differ in composition, and it is both possible and likely that the mechanism is a diffusionless one. The present paper reports the results of a detailed study of the indium-thallium transformation and presents a theory for the atomic movements of the transformation which accounts for the observations.

Experimental

Crystallography of Transformation Markings

The transformation from cubic to tetragonal in the indium-thallium alloys produces microstructures of the type illustrated in fig. 1. These structures are observable either as relief effects produced on a smooth surface by the transformation, or after polishing and etching. These microstructures are markedly similar to those found in copper-manganese alloys,[3] iron-platinum alloys,[4] and barium titanate,[7, 8] where it has been demonstrated that the lamellae are parallel to the {101} planes of the original cubic crystal. That the observed lamellae in indium-thallium alloys are also parallel to the {101} planes was proved by the following analyses performed on single grains in polycrystalline samples containing 20.75 atomic pct Tl.

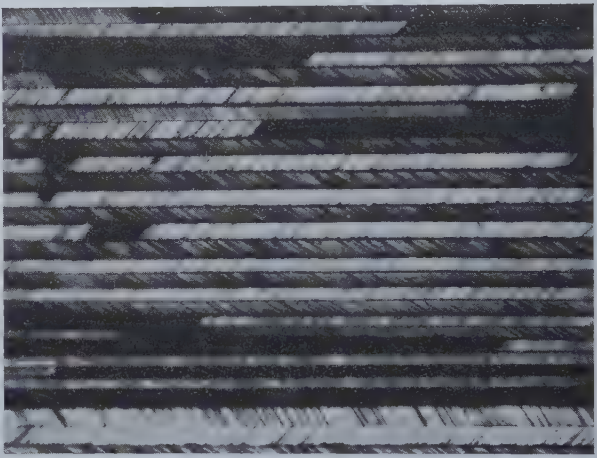

Fig. 1—Typical micrograph of the lamellar structure in a 20.75 pct Tl alloy after etching. X250. Polarized light.

A study of the microstructures of a number of specimens revealed the fact that in many specimens the transformation markings continued unchanged in direction across the {111} interfaces of annealing twins. This at once demonstrates that the lamellae are parallel to a plane that is common to both parent and twin orientations, i.e., a plane in the zone <112>. This conclusion is compatible with the lamellae being parallel to {101} planes. To make a more complete determination of the habit plane of the lamellae, two grains were selected in which annealing twins ({111} twins) had been present in the high-temperature modification (cubic). The traces of the annealing twins, and of the transformation markings in both parent and twin crystals, were plotted together in stereographic projection, and a parent-twin pair of orientations was found that accounted for all lamellae as {101} planes. The projection of one of these twinned grains is reproduced in fig. 2.

In view of these results the probability of there being another solution for the habit plane remote from {101} is very small, but to explore the possibility that the habit plane deviates slightly from {101}, a more precise analysis was undertaken. In this, the orientation of a grain in the cubic modification was determined from a Laue back-reflection photograph taken with the sample at 90°C. The traces of the lamellae that formed in this grain on cooling were plotted in the stereographic projection

---

J. S. BOWLES, formerly associated with the Institute for the Study of Metals is now with the Division of Tribophysics, Commonwealth Scientific and Industrial Research Organization, University of Melbourne, Carlton, Vic., Australia, and C. S. BARRETT, Member AIME, and L. GUTTMAN are associated with the Institute for the Study of Metals, University of Chicago, Chicago, Ill.

AIME St. Louis Meeting, February 1951.

TP 2972 E. Discussion (2 copies) may be sent to Transactions *AIME before April 1, 1951. Manuscript received Aug. 2, 1950.*

of the parent orientation, fig. 3, and the poles of {101} planes were found to lie accurately on the trace normals as predicted for the {101} habit.

By these and several other analyses of the traces in grains free from {111} twins, it was established that the transformation markings, both the main (long) lamellae and the sub-bands within them, are accurately parallel to the {101} planes of the parent cubic crystal. These analyses also showed that the sub-bands were always parallel to those {101} planes that lie at 60° (never 90°) to the plane of the main bands. Furthermore, in a given main band, e.g., the light set in fig. 1, more than two different sets of sub-bands were never observed. The different sets of sub-bands within a single main band were invariably parallel to {101} planes at 90° to each other.

Transformation Mechanism

Two fundamentally different mechanisms can be visualized for this transformation, and experiments were conducted to test each of these hypotheses. The first of these assumes that the original cubic crystal becomes tetragonal, by simple expansion along one cube axis and contraction along the other two, without change of orientation. Such a transformation would lead, at least in polycrystalline specimens, to high internal stresses which could be relieved by twinning the tetragonal grains on {101} planes. Alternatively, the transformation could be of the martensitic type, with the change in structure from cubic to tetragonal being achieved by means of shears on the {101} planes. It can be shown (Appendix 1) that a cubic lattice can be distorted into a tetragonal lattice by means of consecutive shears on two {101} planes at 60° to each other.

Transformations occurring by these two mechanisms might differ with respect to the relative temperatures at which the tetragonality and the lamellar structure appear. The double shear mechanism would predict that the tetragonality and the relief effects would appear at the same instant, whereas from the twinning mechanism it might be expected that twinning would not occur until the tetragonality reached some critical value. Experiments were accordingly carried out to elucidate this point. Coarse-grained polycrystalline samples containing 20.75 atomic pct Tl were mounted in a small furnace supported by a goniometer head, and this in turn was centered on an automatically recording Geiger counter X-ray spectrometer. The goniometer was adjusted so that a cubic (220) reflection from a selected and identified grain on the specimen, as well as the (220) and the (202) reflections from the tetragonal lamellae that formed within the grain during cooling, entered the counter when the latter was set at the appropriate diffraction angle for each reflection, respectively. Thus as a small range of angles was scanned repeatedly during very slow cooling, the appearance of tetragonality was evident on the chart record. Simultaneously, the grain under investigation and its neighbors were kept under observation in a low-power metallurgical microscope, so that the appearance of the lamellar structure could be detected. The smooth surface was prepared by pressing against a polished block at 90°C. The temperature was read continuously by means of a thermocouple embedded in the specimen not far from the grain being studied.

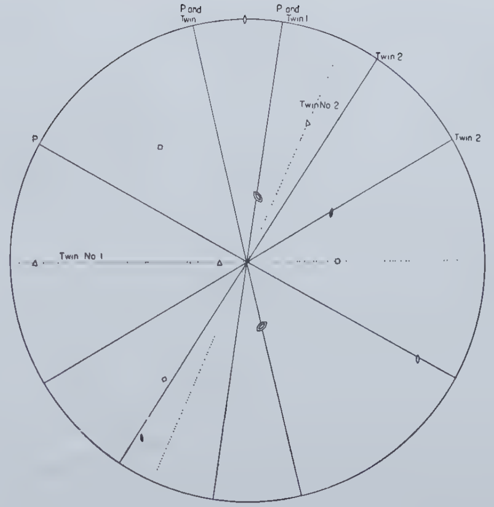

Fig. 2—Stereographic analysis of a transformed twinned grain.

Open squares, triangles, ellipses are poles of {100}, {111}, {110} in parent crystal. The two filled symbols are {110} poles of twin No. 2 and the double ellipses are {110} poles of twin No. 1 (as well as the parent "P"); these superimpose on the appropriate trace normals of the lamellae (diameters). Dotted diameters are trace normals of {111} twin boundaries, which superimpose on {111} poles.

The results of these experiments can be summarized as follows:

1. To within the accuracy of the method used (0.2°C), the lamellar structures and the tetragonality appear at the same temperature.
2. The first plates to form possess a finite degree of tetragonality, the axial ratio being 1.020. As the temperature is lowered to room temperature the degree of tetragonality increases.
3. The lamellar structures are formed by the propagation of an interface parallel to the main bands. The interface moves at a rapid but observable rate. Each nucleus develops into a large number of main bands tilted in opposite senses.
4. The transformation occurs only during cooling and ceases if cooling is interrupted.
5. The range of temperatures over which transformation occurs, and the hysteresis gap between

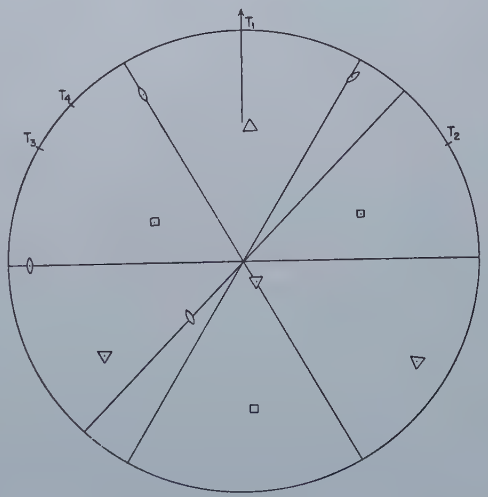

Fig. 3—Stereographic analysis of traces of a transformed grain.

X-ray orientation indicated by squares, ellipses, and triangles for poles of (100), (110), and (111) planes; trace directions are T_1, T_2, T_3, T_4; trace normals are diameters.

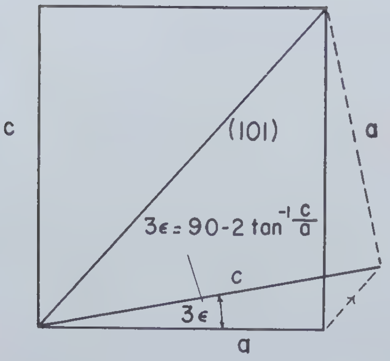

Fig. 4—{101} twinning in a tetragonal crystal. The angle "3ε" is 2°0′ for $c/a = 1.0356$.

the direct and inverse transformations, are quite small, ¾°C and 4½°C, respectively.

6. The tetragonal to cubic transformation apparently proceeds by a mechanism that is just the reverse of the direct transformation, since except for occasional residual markings, the relief effects produced on cooling disappear on heating.

The simultaneous appearance of the tetragonality and the lamellar structures, and the observation that the first plates possess a finite tetragonality are not contradictory to the double shear theory. However, they excluded a twinning theory based on a gradual appearance of tetragonality on cooling.*

Orientation Relationships

Opportunity for more definitive tests of shear and twinning hypotheses is provided by the orientation relationships in the transformation products of an individual grain.

The orientations predicted by the twinning hypothesis are merely first and second generation twins of the original orientation. A grain showing main bands parallel to a single {101} plane would be regarded in the twinning hypothesis as divided into alternate bands of the original orientation and its twin on the indicated {101} plane. The sub-bands would be regarded as further subdividing these main bands into other first-generation and second-generation twins, respectively. Since the axial ratio is nearly unity ($c/a = 1.0356$ for 20.75 pct Tl), these twin orientations would differ from each other by nearly 90°. For a first order twin, the (100) plane is at 2° from the (001) plane of the original (fig. 4). The axes of all orientations produced by twinning are therefore clustered within a few degrees of the original axes. Fig. 5 shows the region of the pole figure around the original tetragonal axis, if all first and second generation twins are formed.

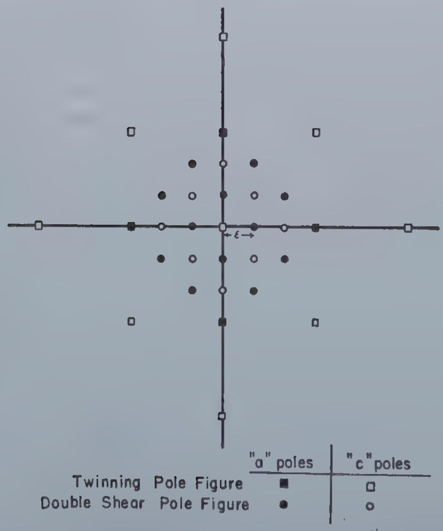

Fig. 5—Pole figure of all possible orientations for the double shear and the twinning mechanisms.

Only the region around one of the original axes is shown, and for the twinning mechanism the axis in question is the c axis.

Somewhat different orientations would result from the double shear mechanism. As is shown in Appendix 1, the required first shear amounts to one-third that required for twinning the final tetragonal crystal and occurs on the same system, i.e., (110) [$1\bar{1}0$]. In a cubic crystal this shear may occur equivalently in either of the opposite senses. Thus the interpretation given to the main bands by this mechanism is that they represent regions in which the first shear has occurred in opposite senses.† This shear produces a structure one-third of the way between two tetragonal twins. Two twin tetragonal orientations can therefore be produced by a second shear on the appropriate {101} plane. Occurring in one sense this second shear would be equal in magnitude to the first; in the opposite sense it would be double the magnitude of the first. The shears involved in the production of one set of main bands, with each main band of the set containing one set of sub-bands, are shown schematically in table I, together with the approximate changes in length of unit vectors along [100], [010] and [001].

The orientations produced by this double shear mechanism can be determined very simply by carrying out the proposed shears in stereographic pro-

Table I. Schematic Representation of Double Shear Mechanism

[100] = 1
[010] = 1 **Face-centered cubic**
[001] = 1

First shear (101)

(101) [$\bar{1}01$], 2ε | **(101) [$10\bar{1}$], 2ε**

[100] = 1—ε [010] = 1 [001] = 1+ε		[100] = 1+ε [010] = 1 [001] = 1—ε	
Second shear (011)		**Second shear (110)**	
(011) [$0\bar{1}1$], 2ε	**(011) [$01\bar{1}$], 4ε**	**(110) [$1\bar{1}0$], 2ε**	**(110) [$\bar{1}10$], 4ε**
[100] = 1—ε [010] = 1—ε [001] = 1+2ε	[100] = 1—ε [010] = 1+2ε [001] = 1—ε	[100] = 1+2ε [010] = 1—ε [001] = 1—ε	[100] = 1—ε [010] = 1+2ε [001] = 1—ε
Tetragonal	**Tetragonal**	**Tetragonal**	**Tetragonal**

Four more tetragonal orientations could be produced by using ($0\bar{1}1$) and ($1\bar{1}0$) as second shear planes.

---

* These data are not adequate to test a twinning theory in which tetragonality appears abruptly with an axial ratio sufficient to cause twinning, but this possibility is excluded by data described in the next section.

† The double shear mechanism predicts that the surface in neighboring main bands would be tilted in opposite senses. The twinning mechanism discussed above predicts that only alternate bands would be tilted, and these all in the same sense. Motion picture studies[1] show that neither main band reflects light in the same direction as the untransformed surface. This is as demanded by the double shear theory and contrary to the simple twinning theory. To account for this by a twinning mechanism it would be necessary to assume that none of the main bands retained the original orientation; this modified theory fails to account for the orientations observed (see later).

jection, as was done for a similar case by Greninger and Troiano.[9] Fig. 5 shows the region of the pole figure around one of the original cubic axes, when all possible tetragonal orientations are present. It is immediately apparent that these orientations are different from those predicted by the twinning mechanism. There are more possible orientations and only a few of the various pairs of orientations are twin pairs.

To test these orientation predictions, precision determinations were made of the relative orientations of the tetragonal regions produced in a single grain of the original cubic material. For this purpose a two circle goniometer constructed from a surveyor's transit was used in conjunction with a General Electric XRD3 Geiger counter X-ray spectrometer. The goniometer was mounted with its optical center in the X-ray beam, and at the center of rotation of the Geiger counter. The collimating slit was replaced by a pinhole system 0.76 mm in diam, and the counter slit by an aperture 3 mm wide horizontally by 0.5 mm vertically. Absorption in the specimen precluded the possibility of determining the complete pole figure from a single grain, but investigation of different grains allowed a complete picture to be obtained. Polycrystalline specimens of the 20.75 pct Tl alloy were used in which the grains were about 1 mm in diam.

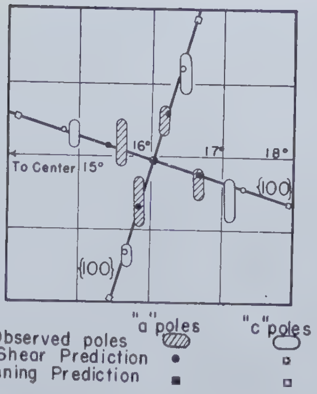

Fig. 7—Comparison of observed pole cluster with those predicted by the double shear and the twinning mechanisms for the case where the cluster was generated from that cube axis lying in the plane of the main band.

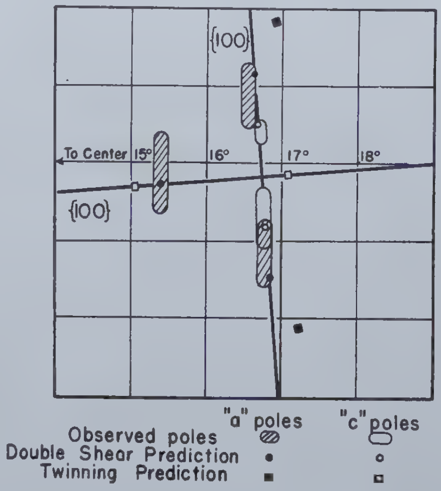

Fig. 8—Comparison of observed pole cluster with those predicted by the double shear and the twinning mechanisms for the case where the cluster was generated from a cube axis not lying in the plane of the main band.

In the interests of simplicity a single set of main bands was always selected for investigation. To eliminate reflections from neighboring grains, or other sets of main bands in the grain being studied, the region around the selected area was painted out with a paste of litharge and glycerin. The mean orientation was first determined approximately from the traces of the single set of main bands and the sub-bands within them. The goniometer was then adjusted so as to bring one group of {100} planes into a reflecting position. The relative positions of reflecting planes, both (400) and (004), were then determined and the results plotted in stereographic projection on a large scale. The radius of the projection was adjusted to make a scale of 1 in. = 1° in the vicinity of the cluster. This is equivalent to a projection radius of approximately 112 in. The centers of other groups of poles, e.g., (113), (311), were also determined in order to obtain a more accurate mean orientation than that determined from the traces.

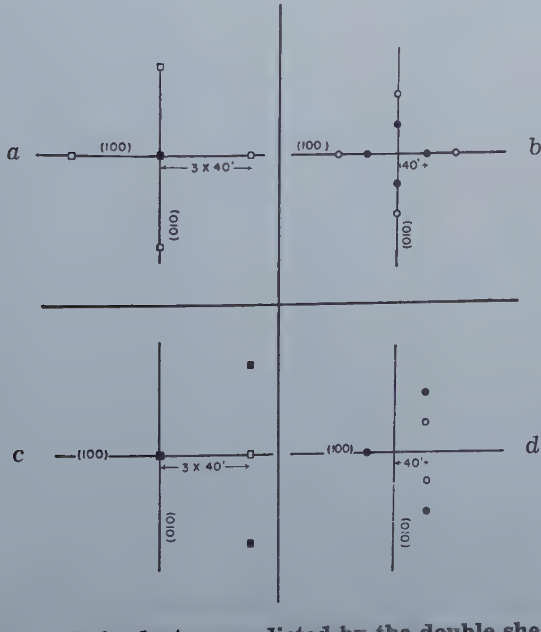

Fig. 6—Pole clusters predicted by the double shear and twinning mechanisms (see text).

Filled symbols are *a* poles; open symbols, *c* poles.

With the restriction of studying only a single set of main bands, the group of poles may be of two types depending on whether or not the group originated from a cube axis parallel to the plane of the main band. If the cluster of poles investigated was generated from the cube axis lying in the {101} plane parallel to the main band, then the final cluster predicted by the simple twinning mechanism and the modifications of it that have been mentioned would be as shown in fig. 6*a*. This cluster consists of four *c* poles and one *a* pole, arranged in the form of a cross on intersecting <100> zones. The cluster predicted from the double shear mechanism is shown in fig. 6*b*. Here again the poles are arranged in the form of a cross on intersecting <100> zones, but in this case there are four *c* poles and four *a* poles. Five clusters originating from the cube axis contained in the main band were examined experi-

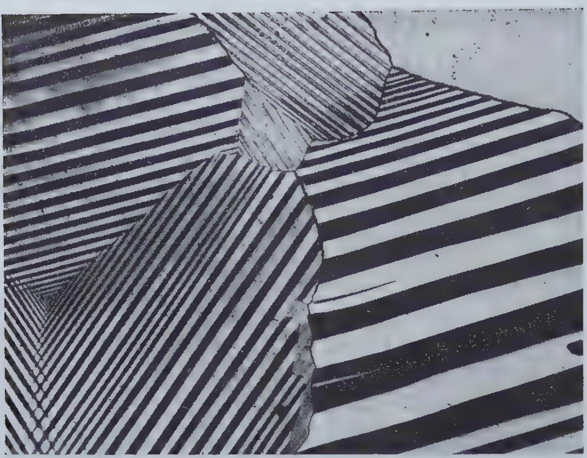

Fig. 9—Micrograph of a 20.75 pct Tl alloy illustrating the variation in width of the main bands as the colony propagates. X75.

mentally. The experimentally observed cluster shown in fig. 7 is typical of the results. As can be seen there are four *c* poles and four *a* poles and their relative positions are in excellent agreement with those predicted by the double shear mechanism.

The clusters of poles predicted by the two mechanisms for the case where the cluster has been generated from a cube axis *not* lying in the main band, are shown in figs. 6*c* and *d*. In this case the twinning mechanism predicts three *a* poles and one *c* pole, while the double shear mechanism predicts three *a* poles and two *c* poles. In both cases the poles are arranged in the form of a "T" at the intersection of two $<100>$ zones. Two clusters of this second type were examined and both were found to contain three *a* poles and two *c* poles. The arrangement of these poles was again in excellent agreement with that predicted by the double shear mechanism. The projection of one of these clusters is shown in fig. 8.

It should be noted that, whereas the clusters predicted from the double shear mechanism are the only possible arrangements, those predicted from the twinning mechanism have been derived to comply with the observed $\{101\}$ traces. The double shear mechanism is consistent with the observation described earlier, that the sub-bands are always parallel to $\{101\}$ planes at 60° to the main bands. It also follows from the double shear mechanism that a single main band can contain only *two* different sets of sub-bands, these being parallel to $\{101\}$ planes at 90° to each other. This is the observed behavior. In the case of the twinning mechanism however, there would be other possibilities, for the parent orientation may form four first-generation twins and any one of these may form three new second-generation twins. Thus a single set of main bands, consisting initially of alternate bands of the parent orientation and one of its twins, could further subdivide into *three* sets of sub-bands in each main band.

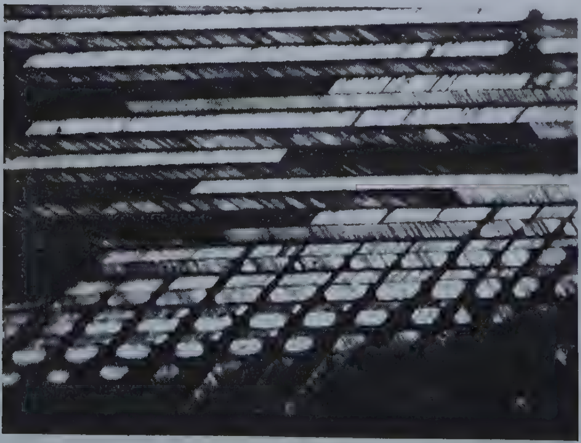

Fig. 10—Micrograph showing interpenetration of two sets of main bands. X250. Polarized light.

Discussion of Results

In view of the results that have been described there can be little doubt that this transformation occurs by the double shear mechanism that has been proposed. This mechanism is consistent with the observed tetragonal orientations and the observed microstructures, and predicts relief effects of the observed type. The transformation is therefore to be regarded as a diffusionless or martensitic transformation.

Transformation mechanisms involving two distortions of the parent lattice have also been proposed for the martensite transformations in steel.[9, 10] It is important that the significance of these shears be made clear. Briefly, they describe the correspondence in position between atoms before and after transformation. If both shears occurred homogeneously, the total distortion of the lattice could be described by a single homogeneous distortion which would not be a simple shear. However, in order to explain the observed relief effects, it is necessary to propose that the second shear is a heterogeneous shear. Thus the total distortion of the lattice cannot be described by a single homogeneous distortion, and it is necessary to describe it as two shears, one homogeneous and the other heterogeneous.

That the shears in the indium-thallium transformation are not instantaneous shears of discrete regions of the parent lattice is evident from the observed mode of development of the tetragonal crystals, for it is observed that the transformation proceeds by the propagation of an interface parallel to the main bands.

This mode of transformation is closely analogous to that proposed by Bowles for the martensite transformation in Fe-C alloys.[10] In both transformations the "habit plane" is a plane of zero macroscopic distortion, for it is not distorted at all by the first "shear" and suffers no macroscopic distortion during the second shear. If one imagines the first shear to occur by the propagation of an interface parallel to the main bands, it is evident that by continuously displacing the matrix in the shear direction ahead of the developing plate, perfect coherence can be maintained. For a shear occurring in this fashion, every atom moves identically when the interface passes it. The macroscopic displacements of atoms remote from the origin of the shear take place while the atoms are still in the unsheared matrix. Direct evidence that this displacement of the matrix does actually occur is provided by the fact that scratches that have been distorted by the transformation remain continuous across the interface.

With the realization that part of the total displacement of every atom occurs simply as a translation of the matrix prior to the arrival of the interface, the double shear mechanism takes on added significance. Not only does it describe the correspondence between atom positions before and after the transformation, but it also describes the path taken by every atom during the transformation in the sense that it describes a set of intermediate positions for each atom.

The second shear results in displacement of atoms in a <110> direction at 60° to the first shear direction. The displacements of atoms in the first shear plane resulting from this second shear are not all identical, and thus after the second shear the interface plane is not common to both the cubic matrix and the final tetragonal crystal. However, since it can occur in opposite senses, this second shear need not cause macroscopic rotations of rows of atoms in the interface. If the sense of the second shear reverses after every 42 ($= 1/\tan 2\epsilon$) atomic radii in one sense and after 21 in the opposite sense, no atom would be moved through a distance greater than one atomic radius. This would produce a very fine set of twins in the main band.‡ Whether the scale of this effect is consistent with observation is difficult to judge. The sub-bands are certainly on a very fine scale, for no sign of them can be detected in the relief structures; they are only visible after etching and then only under critical conditions of illumination. It would of course be possible to produce thicker sub-bands if the second shears occurred heterogeneously, i.e., if slip occurred at intervals on the second shear plane. For no atom to be displaced more than one atom radius, the period of this heterogeneity would again have to be 42 and 21 atomic radii for the shears in opposite senses.

The difference in symmetry of the transformation distortions in the indium-thallium and iron-carbon transformations is probably of importance in explaining some of the differences between these two transformations. In the iron-carbon transformation the first distortion cannot occur in opposite senses. As a martensite plate broadens, opposing stresses are built up in the matrix, and Fisher, Hollomon and Turnbull[11] have proposed that these stresses ultimately prevent any further broadening. In the indium-thallium transformation, the first shear can occur in opposite senses so that when stresses in the matrix inhibit shear in one sense they aid it in the opposite sense. Thus extensive growth of a single nucleus as alternate bands sheared in opposite senses can occur. This effect would be expected to lead to a decrease in the width of the main bands as more and more of the original grain is consumed, for there is then a smaller volume in which the shear strains can be accommodated. Such an effect is indeed frequently observed, fig. 9.

Another consequence of the symmetry of the transformation distortions is that they permit the phase change to occur with essentially no overall distortion of the grain. Consideration of table I shows that even with a single set of main bands there can be sub-bands in which the c axis (of length $1+2\epsilon$) is nearly parallel to each of the original cube axes. Thus the relative volumes of the various sub-bands could be chosen to balance expansion and contraction along all cube axes.

The small magnitude of the shears involved in this transformation, and the effect of the symmetry in reducing the shear strain energy, are probably responsible for the narrow range of temperatures over which the transformation occurs, and the small hysteresis gap between the direct and inverse transformations.

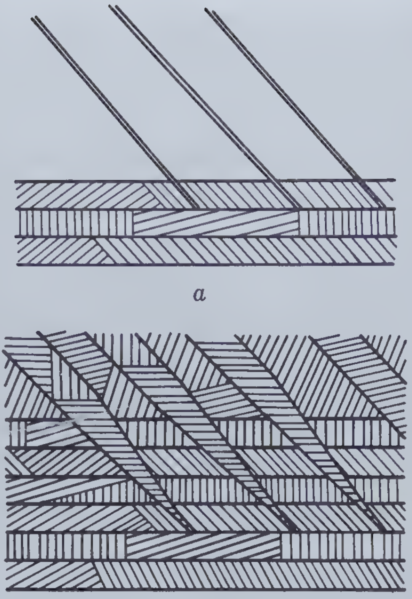

Fig. 11—Schematic representation of the origin of interpenetration.

Another interesting feature of the microstructures of the In-Tl alloys, which also seems to have its origin in the symmetry of the transformation distortions, is the observed interpenetration of different sets of main bands, fig. 10. This effect apparently arises from the possibility of generating the same orientation by carrying out the shears in reverse order. Two different situations can be distinguished: the two sets of main bands may either be parallel to {101} planes at 60°, or at 90°; to each other. In the former case interpenetration is frequently observed and apparently originates as follows. It can be shown quite simply that of the sixteen orientations contained in two sets of main bands, at 60° to each other, (8 in each set), two, and only two, are identical. This can be seen from the fact that since the two main bands are at 60°, each may be parallel to one of the sub-bands in the other. If, in one set of main bands, the second shear required for the production of this particular orientation is propagated beyond the region in which the first shear has occurred, one member of the new set of main bands would be produced, fig. 11*a*. The second shear in the original set of main bands would become a first shear in the new set. Only alternate bands of the new set of main bands could be produced in this way for the two sets have only one orientation in common. The transformation of the material between the new main bands that have been thus nucleated could take place by lateral propagation of either the original or the new bands. These processes are apparently competitive and this leads to the observed "interpenetration," fig. 11*b*. "Interpenetration" would not be expected when two sets of main bands originating from widely separated nuclei grow together. Interpenetration should be impossible when the two sets of main bands are at 90° to each other. In this case no two of the sixteen orientations are identical so the effect described above is not possible and the two colonies of main bands simply join along a surface, fig. 12. Many examples of these junctions have been seen.

---

‡ Precisely the same effect is geometrically possible in Fe-C martensite. However, martensite crystals do not seem to be highly twinned. Apparently a heterogeneous second shear can occur more readily than a reversed second shear in this case.

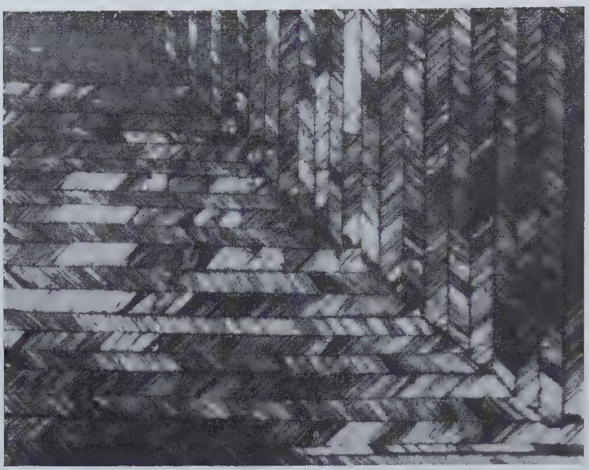

Fig. 12—Boundary between two colonies in which the main bands are parallel to {101} planes at 90° to each other. X100. Polarized light.

The In-Tl transformation differs from other martensite transformations in that the structure of the transformation product is variable. In the 20.75 pct Tl alloy, the axial ratio of the tetragonal phase varies from 1.020 at M_s to 1.0356 at room temperature. The double shear mechanism is flexible enough to accommodate this change for the tetragonality can be increased simply by further shear on the same systems. That this additional shear does occur is demonstrated by the agreement between the observed pole clusters, and those predicted from the *room temperature* tetragonality. The clusters predicted from the tetragonality at M_s would be significantly different, for the angle ϵ in fig. 5 would then be 23′ instead of 40′.

The gradual change in axial ratio with composition, to $c/a = 1$, of many solid solutions in tetragonal metals, e.g., Cu-Mn,[3] Cr-Mn,[2] In-Cd,[12, 13] etc., demonstrates that cubic to tetragonal transformations also occur in these systems, since an identical composition dependence of axial ratio at different temperatures would only be coincidental. There is every reason to believe that these transformations also will occur by the proposed double shear mechanism. The lamellar structures observed in the indium-thallium alloys have also been found in the copper-manganese and chromium-manganese alloys. Although Worrell did not report sub-bands in the copper-manganese microstructures, a subsequent study of the micrographs has shown that they are indeed occasionally visible.

In view of the close similarity between the {101} lamellar structures produced by the indium-thallium transformation, and those produced by the cubic to tetragonal transformations that accompany ordering in many systems, it is of interest to speculate upon the mechanisms of these transformations. It is obvious that these transformations cannot occur by a diffusionless mechanism since ordering of necessity involves diffusion. However, there seems to be no reason why they should not be otherwise analogous to the indium-thallium transformation; the ordering diffusion and the shear displacements could occur together at an advancing interface. In this connection the recent results of Newkirk, Geisler, Martin and Smoluchowski,[14] are of interest. These investigators have shown that on tempering quenched disordered specimens of CoPt, coherent platelets of the ordered solution are formed parallel to the original {101} planes. They have also concluded that these tetragonal platelets have the same orientation as the original cubic crystal. This, however, is only a qualitative observation and precision determinations of the tetragonal orientations in these alloy systems will be needed to determine whether or not these tetragonal structures are formed by a shearing mechanism.

Summary

The diffusionless transformation from cubic to tetragonal in indium-thallium alloys produces lamellae on {101} planes with sub-lamellae also on selected {101} planes. It progresses only with falling temperature, by the movement of an interface parallel to the main lamellae, and ceases when cooling stops. An axial ratio of $c/a = 1.020$ is found at the transformation temperature in 20.75 atomic pct Tl, increasing to 1.0356 at room temperature.

It is proposed that the transformation occurs by a shear on the (101) plane in the $[\bar{1}01]$ direction followed by a second shear on (011) $[0\bar{1}1]$. The main lamellae result from oppositely directed shears of the first type, the sub-lamellae from oppositely directed shears of the second type. A precision, single-crystal X-ray goniometer has been used to determine the orientation changes produced by the transformation; these are in good agreement with the double shear mechanism but not with the frequently postulated twinning mechanism.

Acknowledgments

One of the authors (J. S. Bowles) is indebted to the Commonwealth Scientific and Industrial Research Organization, Australia and to the University of Chicago for research studentships.

The authors wish to acknowledge gratefully the assistance of K. K. Ikeuye, who carried out the metallographic work connected with this investigation.

References

[1] L. Guttman: Crystal Structures and Transformations in Indium-Thallium Solid Solutions. *Transactions* AIME, **188**, 1472; *Journal of Metals* (Dec. 1950) TP 2973E.

[2] S. J. Carlile, J. W. Christian and W. Hume-Rothery: *Journal* Inst. Metals (1949) **77**, 169.

[3] F. T. Worrell: *Journal Applied Physics* (1948) **19**, 929; and C. Zener: Elasticity and Anelasticity of Metals. University of Chicago Press.

[4] H. Lipson, D. Shoenberg and G. V. Stupart: *Journal* Inst. Met. (1941) **67**, 333.

[5] D. Harker: *Transactions* A.S.M. (1944) **32**, 210.

[6] H. D. Megaw: *Proceedings* Roy. Soc. (London) (1947) **189A**, 261.

[7] B. Matthias and A. von Hippel: *Physical Review* (1948) **73**, 1378.

[8] P. W. Forsbergh: *Physical Review* (1949) **76**, 15.

[9] A. B. Greninger and A. R. Troiano: *Transactions* AIME **185**, 590; *Journal of Metals* (Sept. 1949) TP 2652E.

[10] J. S. Bowles: The Crystallographic Mechanism of the Martensite Reaction in Iron-Carbon Alloys. *Acta Cryst.* (1950).

[11] J. C. Fisher, J. H. Hollomon and D. Turnbull: *Transactions* AIME, **185**, 691; *Journal of Metals* (Oct. 1949) TP 2674E.

[12] W. Betteridge: *Proceedings* Phys. Soc. (1938) **50**, 519.

[13] C. L. Wilson and O. I. Wick: *Industrial and Engineering Chemistry* (1937) **29**, 1164.

[14] J. B. Newkirk, A. H. Geisler, D. L. Martin and R. Smoluchowski: *Transactions* AIME, **188**, 1249; *Journal of Metals* (Oct. 1950) TP 2947E.

Appendix

Proof That the Transformation Cubic → Tetragonal Can Be Accomplished by Two Shears

Let the points of a primitive cubic lattice lie at

$$\mathbf{r} = n_1\mathbf{e}_1 + n_2\mathbf{e}_2 + n_3\mathbf{e}_3$$

where the n_i are integers, and the $\mathbf{e}_i$ are unit orthogonal vectors:

$$\begin{aligned} \mathbf{e}_i \cdot \mathbf{e}_k &= 0 & i &\neq k \\ \mathbf{e}_i \cdot \mathbf{e}_k &= 1 & i &= k = 1,\ 2,\ 3. \end{aligned}$$

The distance of the point (x, y, z) from a (101) plane through the origin is $\frac{1}{\sqrt{2}}(x+z) = \frac{1}{\sqrt{2}}(n_1+n_3)$.

Also, a unit vector in the direction $[10\bar{1}]$ is $\frac{1}{\sqrt{2}}(\mathbf{e}_1-\mathbf{e}_3)$.

Hence the vector

$$\bar{\rho} = \varepsilon(n_1+n_3)\ (\mathbf{e}_1-\mathbf{e}_3) \qquad \varepsilon<<1$$

gives the displacement of the lattice point (n_1, n_2, n_3) by a homogeneous shear on the (101) plane in the direction $[10\bar{1}]$ by an angle 2ε. The new lattice points lie at

$$\mathbf{r}' = \mathbf{r}+\bar{\rho} = n_1\mathbf{e}_1' + n_2\mathbf{e}_2' + n_3\mathbf{e}_3'$$

where the $\mathbf{e}_i'$ are new primitive vectors:

$$\begin{aligned} \mathbf{e}_1' &= \mathbf{e}_1(1+\varepsilon) && -\mathbf{e}_3\varepsilon \\ \mathbf{e}_2' &= && \mathbf{e}_2 \\ \mathbf{e}_3' &= \mathbf{e}_1\varepsilon && +\mathbf{e}_3(1-\varepsilon) \end{aligned}$$

The new lattice is monoclinic, since

$$\mathbf{e}_1' \cdot \mathbf{e}_2' = \mathbf{e}_2' \cdot \mathbf{e}_3' = 0;\ \mathbf{e}_1' \cdot \mathbf{e}_3' = 2\varepsilon^2$$

and

$$\begin{aligned} e_1' &= |\,\mathbf{e}_1'\,| = (1+2\varepsilon+2\varepsilon^2)^{1/2} \\ e_2' &= 1 \\ e_3' &= (1-2\varepsilon+2\varepsilon^2)^{1/2} \end{aligned}$$

The distance of the point (n_1, n_2, n_3) from a (110) plane through the origin (fig. 13) is now

$$s = x' \sin\varphi + y' \cos\varphi$$

where

$$\tan\varphi = \frac{e_2'}{e_1'} = (1+2\varepsilon+2\varepsilon^2)^{-1/2}.$$

Since

$$\begin{aligned} x' &= n_1e_1' = n_1(1+2\varepsilon+2\varepsilon^2)^{1/2} \\ y' &= n_2e_2' = n_2 \end{aligned}$$

a second displacement

$$\bar{\sigma} = \varepsilon\ (1+2\varepsilon+2\varepsilon^2)^{1/2}\ (n_1+n_2)\ (\mathbf{e}_1'-\mathbf{e}_2')$$

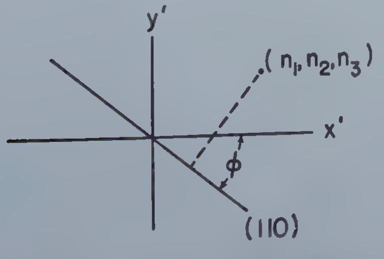

Fig. 13—Coordinate system after first shear. Distance between point (n_1, n_2, n_3) and the (110) plane through the origin is indicated by the dashed line.

represents a homogeneous shear of angle 2ε (approximately) on the plane (110) and in the direction $[1\bar{1}0]$. The lattice points now lie at

$$\mathbf{r}'' = \mathbf{r}' + \bar{\sigma} = n_1\mathbf{e}_1''+n_2\mathbf{e}_2''+n_3\mathbf{e}_3''$$

where

$$\begin{aligned} \mathbf{e}_1'' &= \mathbf{e}_1' + \varepsilon(1+2\varepsilon+2\varepsilon^2)^{1/2}\ [(1+\varepsilon)\mathbf{e}_1-\mathbf{e}_2-\varepsilon\mathbf{e}_3] \\ &= \mathbf{e}_1\ [1+\varepsilon+\varepsilon(1+\varepsilon)(1+2\varepsilon+2\varepsilon^2)^{1/2}] \\ &+ \mathbf{e}_2\ [-\varepsilon(1+2\varepsilon+2\varepsilon^2)^{1/2}] \\ &+ \mathbf{e}_3\ [-\varepsilon-\varepsilon^2(1+2\varepsilon+2\varepsilon^2)^{1/2}] \end{aligned}$$

$$\begin{aligned} \mathbf{e}_2'' &= \mathbf{e}_2 + \varepsilon(1+2\varepsilon+2\varepsilon^2)^{1/2}\ [(1+\varepsilon)\mathbf{e}_1-\mathbf{e}_2-\varepsilon\mathbf{e}_3] \\ &= \mathbf{e}_1\ [\varepsilon(1+\varepsilon)(1+2\varepsilon+2\varepsilon^2)^{1/2}] \\ &+ \mathbf{e}_2\ [1-\varepsilon(1+2\varepsilon+2\varepsilon^2)^{1/2}] \\ &+ \mathbf{e}_3\ [-\varepsilon^2(1+2\varepsilon+2\varepsilon^2)^{1/2}] \end{aligned}$$

$$\begin{aligned} \mathbf{e}_3'' &= \mathbf{e}_3' \\ &= \mathbf{e}_1\varepsilon + (1-\varepsilon)\mathbf{e}_3 \end{aligned}$$

The final lattice is, strictly speaking, triclinic, but as ε is small, the lattice is nearly tetragonal. We can replace the radical by $1+\varepsilon$, and neglecting higher powers of ε than the second, we have, approximately,

$$\begin{aligned} \mathbf{e}_1'' &= \mathbf{e}_1(1+2\varepsilon+2\varepsilon^2)-\mathbf{e}_2\varepsilon(1+\varepsilon)-\mathbf{e}_3\varepsilon(1+\varepsilon) \\ \mathbf{e}_2'' &= \mathbf{e}_1\varepsilon(1+2\varepsilon) + \mathbf{e}_2\ [1-\varepsilon(1+\varepsilon)]-\mathbf{e}_3\varepsilon^2 \\ \mathbf{e}_3'' &= \mathbf{e}_1\varepsilon \qquad\qquad +\mathbf{e}_3(1-\varepsilon) \end{aligned}$$

and the magnitudes of the primitive vectors are

$$\begin{aligned} e_1'' &= 1+2\varepsilon+ 3\varepsilon^2 + O(\varepsilon^3) \\ e_2'' &= 1- \varepsilon-\tfrac{1}{2}\varepsilon^2 + O(\varepsilon^3) \\ e_3'' &= 1- \varepsilon+\tfrac{1}{2}\varepsilon^2 + O(\varepsilon^3) \end{aligned}$$

with "O" denoting "terms of the order of."

The direction cosines of the various axes with respect to one another are

$$\mathbf{e}_1'' \cdot \mathbf{e}_2'' = O(\varepsilon^3) \quad \mathbf{e}_2'' \cdot \mathbf{e}_3'' = O(\varepsilon^3) \quad \mathbf{e}_3'' \cdot \mathbf{e}_1' = 2\varepsilon^2+O(\varepsilon^3)$$

while the axial ratio is

$$c/a \cong e_1''/e_2'' \cong e_1''/e_3'' = 1+3\varepsilon+O(\varepsilon^2)$$

For $c/a = 1.03$, $\varepsilon = 0.01$; thus e_2'' and e_3'' differ in length by one part in 10^4, the angle between $\mathbf{e}_2''$ and $\mathbf{e}_3''$ differs from 90° by $O(\varepsilon^3) = 10^{-6}$ radian $= 0.2''$, and the angle between $\mathbf{e}_1''$ and $\mathbf{e}_3''$ differs from 90° by $2\varepsilon^2 = 2\text{x}10^{-4}$ radian $= 0.7'$.

Essentially the same results are obtained if the sense of the second shear is reversed, and its magnitude is doubled. That is, let the second displacement be

$$\bar{\tau} = -2\varepsilon\ (n_1+n_2)\ (\mathbf{e}_1'-\mathbf{e}_2')$$

Then, to the same degree of approximation as before,

$$\begin{aligned} \mathbf{e}_1'' &= \mathbf{e}_1\ [1-\varepsilon-2\varepsilon^2] + 2\varepsilon\,\mathbf{e}_2+\mathbf{e}_3\,[-\varepsilon(1+2\varepsilon)] \\ \mathbf{e}_2'' &= \mathbf{e}_1\ [-2\varepsilon(1+\varepsilon)] + \mathbf{e}_2\ [1-2\varepsilon] + 2\varepsilon^2\mathbf{e}_3 \\ \mathbf{e}_3'' &= \mathbf{e}_1\varepsilon \qquad\qquad + (1-\varepsilon)\mathbf{e}_3, \end{aligned}$$

the lengths of the vectors are

$$\begin{aligned} e_1'' &= 1- \varepsilon +\tfrac{1}{2}\varepsilon^2+O(\varepsilon^3) \\ e_2'' &= 1+2\varepsilon + 2\varepsilon^2+O(\varepsilon^3) \\ e_3'' &= 1- \varepsilon +\tfrac{1}{2}\varepsilon^2+O(\varepsilon^3) \end{aligned}$$

and the direction cosines are

$$\mathbf{e}_1'' \cdot \mathbf{e}_2'' = 4\varepsilon^2 + O(\varepsilon^3) \qquad \begin{aligned} \mathbf{e}_2'' \cdot \mathbf{e}_3'' &= O(\varepsilon^3) \\ \mathbf{e}_3'' \cdot \mathbf{e}_1'' &= -2\varepsilon^2+O(\varepsilon^3) \end{aligned}$$

That is, the final lattice has again two nearly equal axes and one longer axis, all at very nearly right angles to each other.

Alloys of Copper and Iron

by Cyril Stanley Smith and Earl W. Palmer

Studies were made of the mechanical and other properties of alloys over the entire composition range from pure copper to pure iron. Though the two-phase alloys have poor corrosion resistance unless protected, the composition in the vicinity of 65 pct Cu possesses an excellent combination of strength and electrical conductivity in the form of cold drawn wire. The alloys about 5 to 10 pct Cu have the highest strengths and are the most susceptible to improvement by age hardening treatment.

IN 1934, when Gregg and Daniloff[1] wrote their excellent monograph on the alloys of iron and copper, the most recent literature on the constitution of the alloys indicated a narrow single-liquid area for 20° above the liquidus with a closed liquid miscibility gap above this. Since that time, however, a number of investigators have confirmed the much earlier studies of Mushet[2] and Stead[3] who, among others in the nineteenth century, had described the true state of affairs. Liquid copper and iron are completely miscible in the absence of carbon, but small amounts of carbon cause liquid segregation. In 1934, one of the writers[4] mentioned evidence for the absence of liquid separation in carbon-free alloys at temperatures up to 1700°C. Two years later, Maddocks and Claussen[5] unequivocally established the absence of liquid segregation and published a revised diagram, reproduced in fig. 1. They also studied the limits of the two-liquid area in ternary alloys of iron, copper, and carbon as a function of carbon and iron content. In the same year Simpson and Bannister[6] and Schumacher and Souden[7] described in some detail the properties of alloys containing 50 to 75 pct Cu. More recently Hodges et al.[16] have developed the copper-rich alloys for use as high-strength conductors. In 1937, Iwase, Okamoto, and Ameniya[8] published data on the miscibility gap in ternary alloys of iron, copper, and carbon that supported the conclusions of Maddocks and Claussen, and definitely located the two-liquid area at temperatures of 1450° and 1540°C. They also reported that additions of 1 pct Al, Ni, Pb, Sn, or Zn caused no segregation in 50 pct Cu alloys at 1540°C.

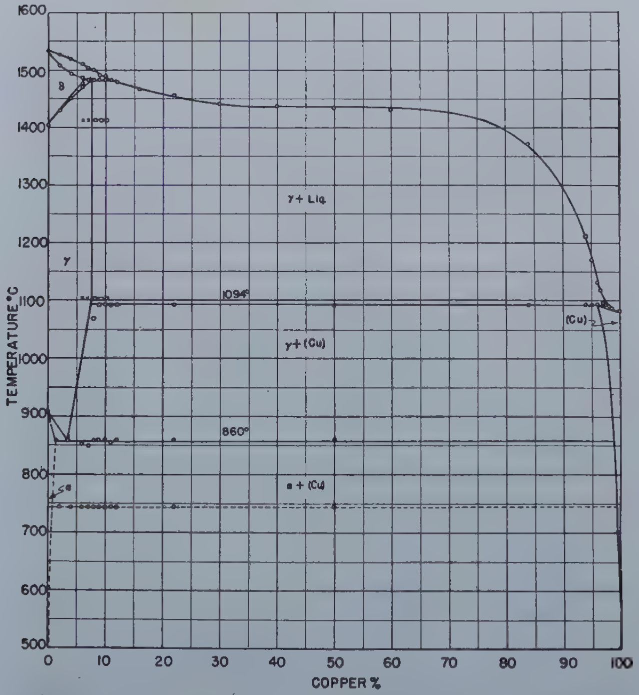

Fig. 1—Constitution of copper-iron alloys (Maddocks and Claussen[1]).

The use of copper in amounts approximating 1 pct has found industrial employment to an increasing degree in both wrought and cast steels, for such steels are capable of being precipitation-hardened following normalizing, and have high yield strengths. This is summarized by Gregg and Daniloff,[1] Sallitt,[9] and Lorig and Adams,[10] while Alexander[11] gives additional information on the heat treatment of copper-steel castings. Lippert[12] has described Digby's two-phase steels containing copper and chromium.

The work described in the present paper was done in the years 1932 to 1934, at which time much of the information was new. The excellent work subsequently done in other laboratories but more promptly published makes the present paper in part only a confirmation of what is now well known. There has not, however, been published any unified study of

---

CYRIL STANLEY SMITH, Member AIME, now Director, Institute for the Study of Metals, University of Chicago, Chicago, Ill., formerly was Research Metallurgist, American Brass Co., Waterbury, Conn., and EARL W. PALMER, Member AIME, is Research Metallurgist, American Brass Co.

AIME St. Louis Meeting, February 1951.

TP 2599 E. Discussion (2 copies) may be sent to Transactions *AIME before April 1, 1951. Manuscript received Jan. 22, 1949.*

so many properties of the alloys over the whole range of composition from copper to iron.

Fabrication and Structure of Alloys

Casting: The alloys for the following investigation were made by melting 12 or 30 lb heats in a laboratory induction furnace, in silica or magnesia crucibles. Armco iron punchings and cathode copper were used. The normal practice was to melt the desired amount of iron with about 20 pct of its weight of copper before diluting with additional copper to the desired composition. Deoxidation practice was important. To most of the alloys a standard addition of 0.5 pct Mn and 0.1 pct Si was made. Generally the silicon addition was made to the first pool of molten metal and the manganese added not long before pouring. Experiments were made with zirconium, titanium, aluminum, magnesium, calcium, boron, and lithium as deoxidizers, both with and without the manganese-silicon additions. Of these elements, magnesium (0.2 pct, added in the form of 10 pct Mg-Cu) proved to be the most satisfactory deoxidizer and desulphurizer and gave castings that could be hot-worked. It is the preferred deoxidizer where high electrical conductivity is desired.[13]

The alloys were cast at a temperature 50° to 100°C above the liquidus into square cast iron molds fitted with refractory hot tops. The large difference in temperature between the solidus and liquidus, about 350°C for the 50 pct alloy, renders the alloys difficult to cast and liable to segregation. At 1300°C the 50 pct alloy is already approximately half solid and consists of a spongy mass of iron dendrites, with the interstices filled with liquid copper. There is little change during further cooling until the copper-rich liquid solidifies at 1094°C. Many ingots were found in which surface defects and occasional blowholes were filled with copper, and a partial shell of copper often was found where the partly solid ingot had shrunk away from the mold during solidification. The alloys are extremely hot-short and it is necessary to see that the molds are in perfect condition; a hung ingot is sure to be cracked and the crack may or may not be filled with molten copper before solidification. Alloys in the range 70 to 90 pct Cu burned into the mold wall (which was lightly coated with a dry carbonaceous dressing) and would be expected to give considerable trouble in commercial casting.

Segregation and Microstructure of Castings: The microstructures of some of the cast alloys are shown in figs. 2 to 7, inclusive, which need little comment. The cast alloys consist of iron dendrites whose interstices are filled with copper-rich material. No evidence of coring or other solid state reaction is visible. Heat treatment had little effect on the microstructure, except at the extreme ends of the systems.

To investigate the extent of segregation, a number of 12-lb ingots of various carbon contents were cast at temperatures 50°C above the liquidus, sectioned, and analyzed. The carbon was added in the form of wash metal containing 3.83 pct C, balance Fe, after the major constituents had formed a uniform melt. Deoxidation was with 0.1 pct Si and 0.5 pct Mn. If the alloy in the crucible had separated into two liquid layers, the lower density iron-rich alloy flowed into the mold first, forming a layer which rose in the mold and formed a shell as the remainder of the alloy was poured in. Etched cross-sections of some of the ingots are shown in figs. 8 and 9. From the analyses of the ingots given in table I, it will be seen that, though the 50 pct Cu alloy containing 0.11 to 0.12 pct C (ingot 1407) did not segregate significantly, ingot 1408, with very little more carbon, shows signs of partial segregation in the ingot, although there is no evidence that the molten alloy had separated in the crucible. The mottled structure shown in fig. 10 is very similar to that observed by Maddocks and Claussen in an alloy with 0.18 pct C solidified in a small crucible. The addition of 0.20 pct C produces unmistakable and sharp separation into two liquids, one iron-rich with high carbon and

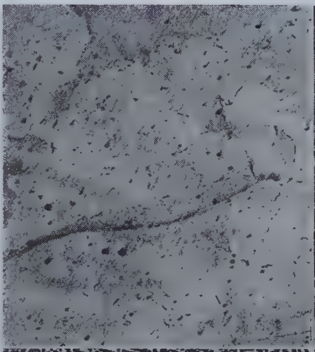

Fig. 2 (top left)—5 pct Cu alloy. As-cast. X75.

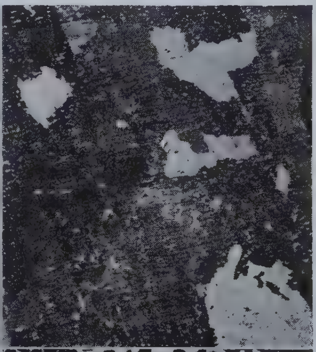

Fig. 3 (top right)—15 pct Cu alloy. As-cast. X75.

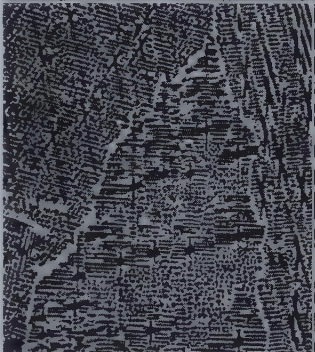

Fig. 4 (center left)—Structure of columnar outer section of 30 lb ingot of 50 pct Cu-Fe alloy. X75.

Fig. 5 (center right)—Structure of equiaxed center section of same ingot as fig. 4. X75.

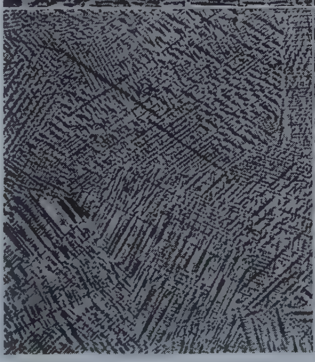

Fig. 6 (bottom left)—70 pct Cu alloy. As-cast. X75.

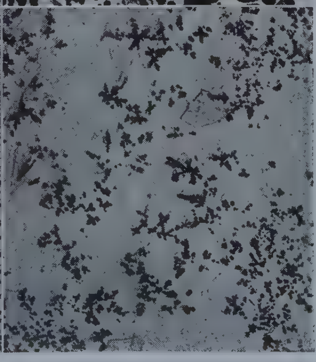

Fig. 7 (bottom right)—89 pct Cu alloy. As-cast. X75.

Figs. 2 to 7 reduced approximately 33 pct for reproduction. All microspecimens etched, unless otherwise noted, with 4 pct nital.

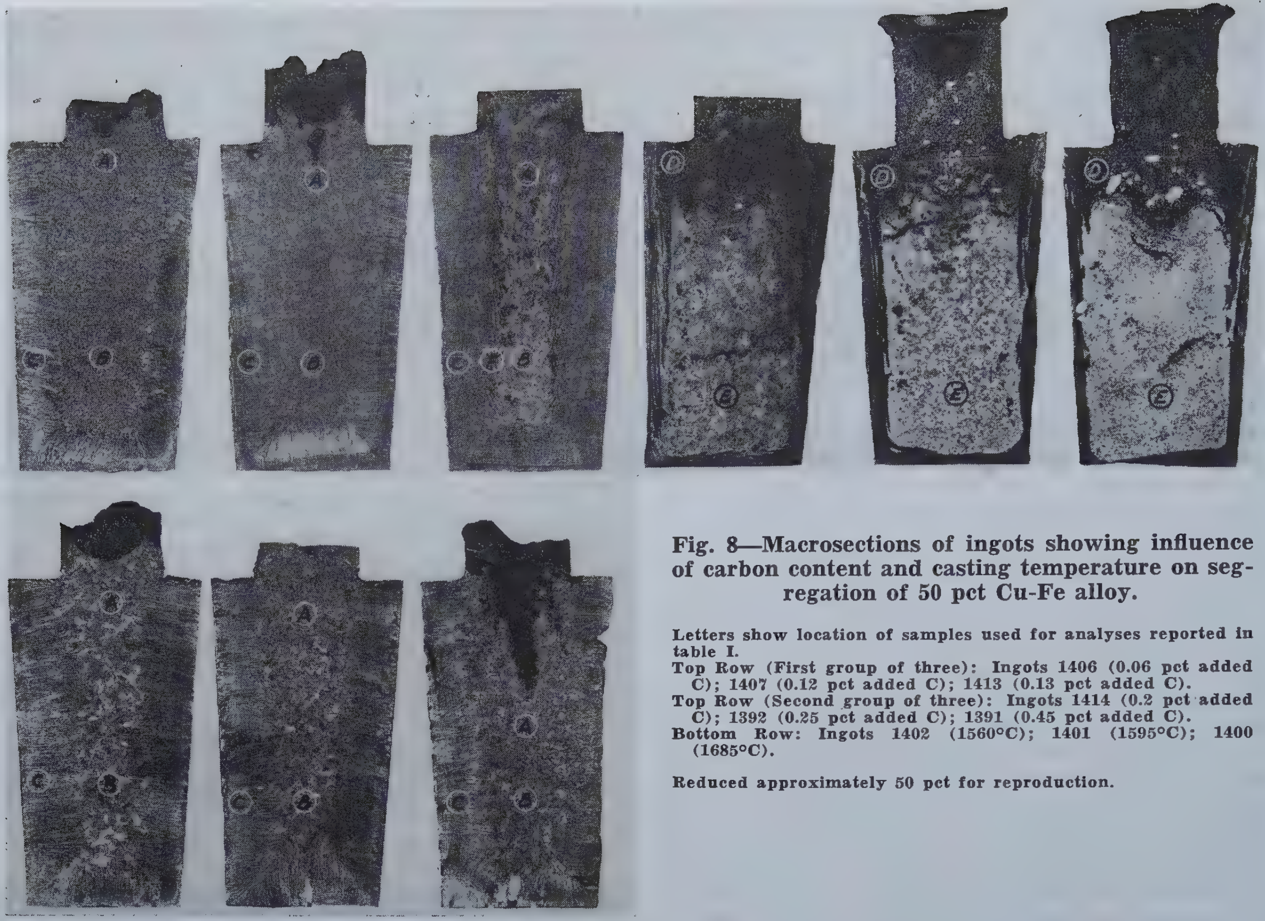

Fig. 8—Macrosections of ingots showing influence of carbon content and casting temperature on segregation of 50 pct Cu-Fe alloy.

Letters show location of samples used for analyses reported in table I.
Top Row (First group of three): Ingots 1406 (0.06 pct added C); 1407 (0.12 pct added C); 1413 (0.13 pct added C).
Top Row (Second group of three): Ingots 1414 (0.2 pct added C); 1392 (0.25 pct added C); 1391 (0.45 pct added C).
Bottom Row: Ingots 1402 (1560°C); 1401 (1595°C); 1400 (1685°C).

Reduced approximately 50 pct for reproduction.

the other copper-rich with low carbon. The interface between the two zones is shown in the micrograph, fig. 11. It was noted that all of the ingots that had iron-rich shells were cracked badly in the copper-rich cores, obviously a result of restrained shrinkage.

Müller[14] suggested that liquid iron and copper are completely miscible just above the liquidus, but that two immiscible liquids appeared above about 1520°C. That this is not the case with the alloys used in the present investigation was shown by pouring ingots at 1560°, 1595°, and 1685°C. There was a deep shrinkage cavity in the ingot cast at the highest temperature, but there is no excessive segregation visible or detectable by analysis in any of the three ingots (fig. 8 and table I).

Table I. Analyses of 12 Lb Ingots of Copper-Iron Alloys, To Show Segregation

Alloy No.		Intended Composition		Composition by Analysis											
				Position A		Position B		Position C		Position D		Position E		Position F	
		Pct Cu	Pct C	Pct Cu	Pct C	Pct Cu	Pct C	Pct Cu	Pct C	Pct Cu	Pct C	Pct Cu	Pct C	Pct Cu	Pct C
1406		50	0.10	47.1	0.060	47.6	0.065	51.1	0.056						
1407		50	0.15	48.2	0.125	47.4	0.114	50.1	0.110						
1413		50	0.16	49.9	0.123	56.4	0.098	48.9	0.135					51.5	0.122
1414		50	0.20							31.0	0.296	71.5	0.068		
1392		50	0.25							26.2	0.366	73.7	0.061		
1391		50	0.45							28.9	0.579	77.1	0.095		
1408		35	0.11	32.5	0.090	33.5	0.106	34.4	0.102						
1409		35	0.15	34.7	0.130	34.4	0.127	35.5	0.136						
1410		35	0.25							30.4	0.292	69.7	0.070		
1415		70	0.05	68.1	0.036	68.9	0.028	71.7	0.029						
1416		70	0.075	68.1	0.044	68.8	0.065	70.8	0.055						
1411		70	0.10	71.7	0.074							75.7	0.061		
1412		70	0.20	24.0	0.868							81.8	0.071		
1441*		45	0.03	42.5	0.023	43.3	0.024	46.0	0.021	45.3	0.028	44.8	0.022	44.0	0.015
1418†		50	0.08	49.8	0.069	48.1	0.054	46.4	0.076	45.0	0.066	54.6	0.073	55.3	0.061
	Pouring Temp, °C														
1402	1560	50		47.5	0.039	48.8	0.016	50.9	0.017						
1401	1595	50		48.0	0.019	48.6	0.013	51.9	0.021						
1400	1685	50		49.3	0.012	49.9	0.025	53.8	0.017						

For location of Samples A, B, C, D, E, and F, see figs. 8 and 9.
* No. 1441 was 30 lb ingot.
† No. 1418 was 30 lb block allowed to solidify slowly in furnace.
All melts except 1400 to 1402 were poured at a temperature 50°C above the liquidus.

The amount of carbon necessary to cause liquid separation increases with the iron content of the alloy. Fig. 16 shows the composition of the two segregated areas in the various ingots, connected by tie-lines and forming a very approximate constitution diagram. They are in fair agreement with the results of both Iwase and Maddocks and Claussen, which are shown as dotted lines in fig. 16.

Even in alloys where there is no separation into two liquids, some segregation occurs on solidification. This is greater the larger the ingot and the slower the solidification, and may cause local differences of composition of as much as 4 pct Cu on the laboratory ingots used. It is a simple form of inverse segregation and probably results from the first parts to solidify being "fed" by the withdrawal of molten copper-rich material from the interstices of the iron-rich dendrites in the last parts to solidify.

Hot-working: The ingots deoxidized and cast as described above proved to be quite easily forgeable in the ranges 0 to 7 pct and 30 to 100 pct Cu, but between approximately 7 and 30 pct hot-forging was extremely difficult. All alloys could be cold-rolled after suitable annealing at 800°C, or at higher temperatures followed by slow cooling. After many failures it was found that alloys in the difficult range could be hot-forged if the castings had previously been annealed for about 16 hr at 800°C, that is, just below the eutectoid temperature, and if they were also forged at temperatures not exceeding this. Evidently copper-saturated gamma iron is harder than copper-saturated alpha iron and is so much stiffer than the copper-rich phase that a two-phase alloy containing only a little copper deforms entirely in the soft network and soon fails. Once the alloys have been extensively worked by forging between 750° and 825°C, they become less sensitive and may be hot-rolled with heavy reductions. Alloys containing from 0 to 5 pct and 40 to 100 pct Cu could be hot-rolled directly as-cast without particular precautions, but those of intermediate composition could be rolled only at temperatures below 840° and then after the preliminary annealing and forging treatment.

Two lots of material were used for the tests described below. Alloys in the first series were made in 12-lb heats and cast into ingots tapering from 2½ to 3 in. sq in a height of 5¼ in. Each ingot was forged at 950° to rod ¾ in. in diam, to ½ in. sq rod, and to a 3x⅝-in. section. The round and square rods were machined into tensile test pieces and into impact specimens, respectively, and the flat section was milled and then cold-rolled to strip 0.04 in. thick with intermittent anneals of 30 min at 800°C (followed by air-cooling) at each of the gauges 0.320, 0.160, and 0.080 in. The final material was therefore cold-rolled 50 pct reduction. The second series was prepared after the forging treatment outlined above had been developed. The alloys containing between 8 and 25 pct Cu inclusive were cast in 12 or 30-lb ingots and annealed at 800°C for 14 hr and forged carefully at 800°C to a section about 3x¾ in., before being hot-rolled at 950°C to ¼x3 in. in a commercial copper strip mill. Other castings in the same series (i.e., containing 0 to 5 pct and 35 to 90 pct Cu) were all 30-lb castings and were hot-rolled at 950°C directly to a ¼-in. sheet. All the ¼-in. slabs were milled to remove surface defects, then reheated and hot-rolled to 0.08 in. gauge. They were annealed for 1 hr at 800°C, pickled, and cold-rolled to the final gauge, 0.04 in.

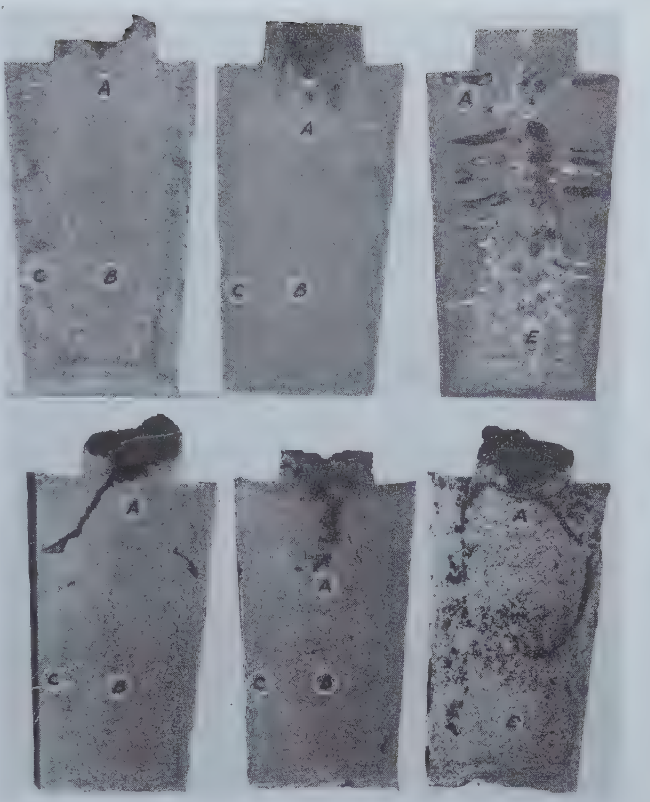

Fig. 9—Macrosections of ingots showing influence of carbon content on segregation of copper-iron alloys containing 35 and 70 pct Cu.

Letters refer to table I.
Top Row: 35 pct Cu: Ingots 1408 (0.11 pct C); 1409 (0.13 pct C); 1410 (0.25 pct C).
Bottom Row: 70 pct Cu: Ingots 1415 (0.03 pct C); 1416 (0.06 pct C); 1411 (0.10 pct C).

Reduced approximately 50 pct for reproduction.

A small quantity of each alloy was hot-rolled directly to 0.04 in. The hot-rolling was performed at the Ansonia plant of the American Brass Co., using passes that were designed for rolling copper bus bar. The alloys stood this severe treatment without failure, except those with copper in the range 10 to 35 pct, which cracked, although not enough to warrant complete discard.

Microstructure of Worked Alloys: The dendrites of iron in the castings become elongated as the castings are hot-forged or rolled, and the structure of the rod or sheet consists of extended fibers of iron in a copper matrix. It is probable that prolonged annealing at high temperatures would partially spheroidize these fibers. Typical structures are shown in figs. 12 to 15, 17 to 24, and 27.

Annealing and Pickling: When the alloys are annealed in air, a complex scale is formed that is peculiarly difficult to remove by pickling. An outer black scale of normal type seems to contain both iron and copper oxides. Below this there is a "subscale" zone wherein iron is oxidized *in situ* but copper is not visibly affected (figs. 25 and 26). The depth of penetration is greater in a longitudinal than in a transverse direction, obviously because of the elongated shapes of the iron particles.

If the annealed alloys are pickled in the usual acid solutions used for either iron or copper, the oxide can be removed; but when this is done there is left a subscale layer containing metallic copper. If pickling is continued, the acid will preferentially attack

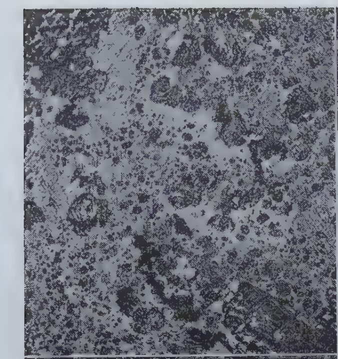

Fig. 10 (top left)—Alloy with 50 pct Cu, 0.16 pct C. As-cast, showing partial separation of two liquids. X15.

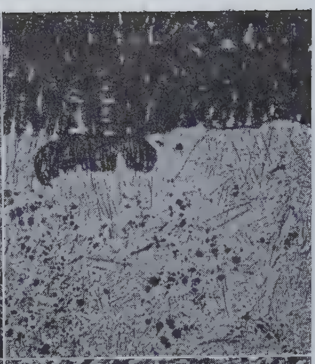

Fig. 11 (top right)—Alloy with 50 pct Cu, 0.25 pct C. As-cast, showing junction of two liquid layers. X15.

Fig. 12 (center left)—Alloy with 29.9 pct Cu. Forged rod, ¾ in. diam. Longitudinal section. X75.

Fig. 13 (center right)—Alloy with 49.9 pct Cu. Forged rod, ¾ in. diam. Longitudinal section. X75.

Fig. 14 (bottom left)—Alloy with 88.6 pct Cu. Forged rod, ¾ in. diam. Longitudinal section. X75.

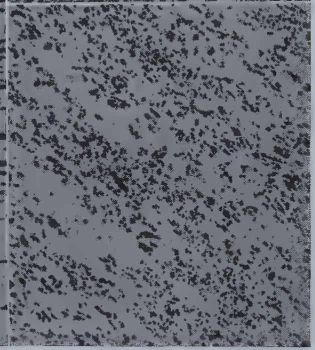

Fig. 15 (bottom right)—Alloy with 88.6 pct Cu. Forged rod, ¾ in. diam. Transverse section. X75.

Figs. 10 to 15 reduced approximately 33 pct for reproduction.

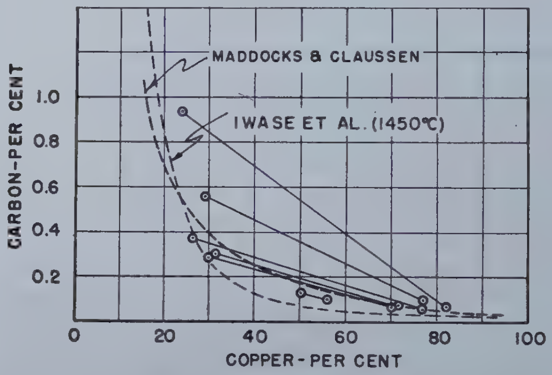

Fig. 16—Composition of related segregated areas in Fe-Cu-C alloy ingots, based on analyses of table I.

Table II. Tensile Tests on Sand Cast Bars of Copper-Iron Alloys

Alloy No.	Composition Percent Cu	C	Mn	Si	Tested as Cast: Yield Strength Lb per sq in. (0.5 pct on 2 in.)	Tensile Strength Lb per sq in.	Elongation on 2 in., Pct	Reduction of Area, Pct	Brinell Hardness (3000 kg)	Normalized 930° + 800°C: Yield Strength Lb per sq in. (0.5 pct on 2 in.)	Tensile Strength Lb per sq in.	Elongation on 2 in., Pct	Reduction of Area, Pct	Brinell Hardness (3000 kg)
1473	0.08	0.005	0.374	0.070	25,250	46,900	45.5	78.5	92	34,750	48,650	45.3	80.9	92
1472	1.29	0.030	0.447	0.215	41,250	57,700	36.3	70.3	122	48,450	58,800	41.3	78.3	120
1474	4.62		0.312	0.068	72,750	84,550	11.5	39.0	191	57,050	58,900	33.0	73.7	132
1465	10.19		0.356	0.063	81,300	82,550	1.0	1.5	216	57,200	64,450	10.3	27.1	144
1466	20.32		0.159	0.016	76,400	90,950	2.5	5.7	213	48,850	61,000	21.5	33.7	132
1467	31.31		0.485	0.054	59,450	81,150	13.0	21.0	173	44,700	60,400	27.8	54.0	128
1468	38.55		0.411	0.056	53,900	77,750	15.8	28.3	164	41,200	58,400	30.0	56.6	122
1475	50.28	0.011	0.552	0.056	45,550	71,950	20.0	35.8	150	36,900	54,400	32.8	66.8	110
1362	50.				43,050	70,750	17.7	27.7						
1469	66.14		0.451	0.014						29,850	49,950	35.0	63.7	100
1470	84.96		0.495	0.005	22,600	53,000	11.5		99	25,000	45,450	24.8	49.5	86
										Normalized 850°C, Reheated 500°C				
1472	1.29	0.03								75,350	89,100	27.5	66.0	192
										Normalized at 850°C				
1471	1.24	0.305			59,500	85,200	5.8	9.3		65,550	85,850	9.8	17.8	184
										Normalized 800°C, Reheated 500°C				
1471	1.24	0.305								86,650	105,950	5.8	7.6	229

All above figures are an average of two tests, except 1470 in cast condition, which is one test only, and 1362 which represents three castings. All bars of 1471 were porous and of low ductility. Test pieces were cast ⅝ in. in diam, machined to 0.505 in. diam.

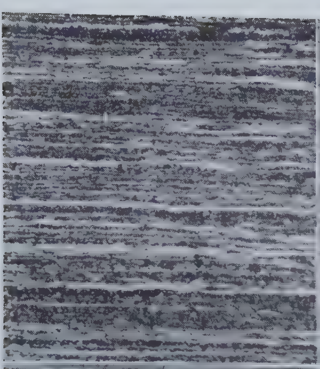

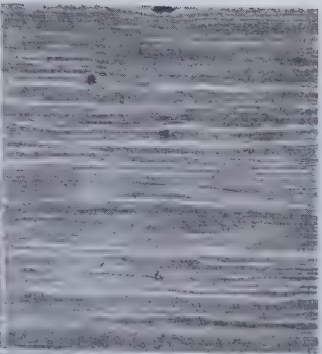

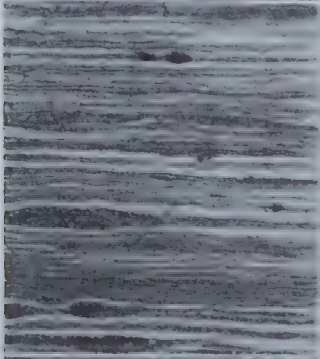

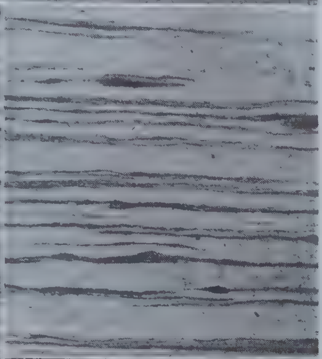

Fig. 17 (top left)—Alloy with 29.9 pct Cu. Cold-rolled sheet, 0.04 in. thick. Longitudinal section. X500.

Fig. 18 (top right)—Alloy with 49.9 pct Cu. Cold-rolled sheet. Longitudinal section. X500.

Fig. 19 (center left)—Alloy with 69.6 pct Cu. Cold-rolled sheet. Longitudinal section. X500.

Fig. 20 (center right)—Alloy with 88.6 pct Cu. Cold-rolled sheet. Longitudinal section. X500.

Fig. 21 (bottom left)—Alloy with 29.9 pct Cu. Cold-rolled sheet annealed 1 hr at 800°C and quenched. Longitudinal section. X500.

Fig. 22 (bottom right)—Alloy with 29.9 pct Cu. Rolled sheet annealed 1 hr at 1050°C and quenched. Longitudinal section. X500.

Figs. 17 to 27 reduced approximately 33 pct for reproduction.

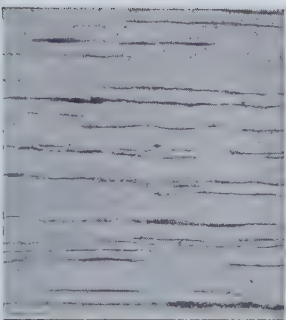

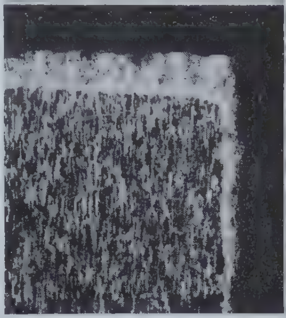

Fig. 23 (top left)—Alloy with 88.6 pct Cu. Rolled sheet annealed 1 hr at 1050°C and quenched. Longitudinal section. X500.

Fig. 24 (top right)—Alloy with 49.9 pct Cu. Sheet annealed 1 hr at 1050°C and quenched. Longitudinal section. X500.

Fig. 25 (bottom left)—Subscale formed by annealing 50 pct Cu alloy in air for 1 hr at 950°C. X75.

Fig. 26 (bottom right)—Same specimen as fig. 25; junction of subscale and unoxidized metal. X500.

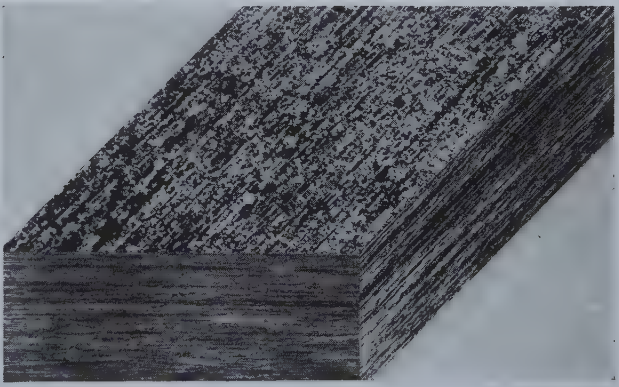

Fig. 27—Composite micrograph showing structure of cold-rolled 0.040-in. sheet of 50 pct Cu alloy. X75.

the iron in the alloy underneath, leaving a copper skeleton. Since the oxide scale spalls off irregularly, attack is uneven and results in considerable pitting.

A satisfactory pickle for these alloys consisted of a 15 pct solution of sodium cyanide in water, used at a temperature near the boiling point. The addition of 15 pct sodium hydroxide considerably accelerated the action. With alloys containing below 30 pct Cu the formation of subscale is not significant and with the copper-rich alloys an acid pickle alone seems to be satisfactory, but the cyanide pickle was essential in alloys in intermediate compositions if truly clean metal was desired. For many purposes, however, the shell of copper remaining after an acid pickle is not undesirable, for it provides an excellent lubricant in rolling or drawing. It is not sufficiently continuous to provide any protection against corrosion.

Mechanical Properties

Sand Castings: Table II shows the tensile properties of a number of alloys of iron and copper cast in dry sand molds. Standard 0.505 in. diam tensile test pieces were machined from castings made from patterns ⅝ in. diam x 2 in. on the gauge length, with ends 1 in. diam. Four bars were cast simultaneously. The alloys with 66 and 85 pct Cu failed to fill the mold completely, but all others ran satis-

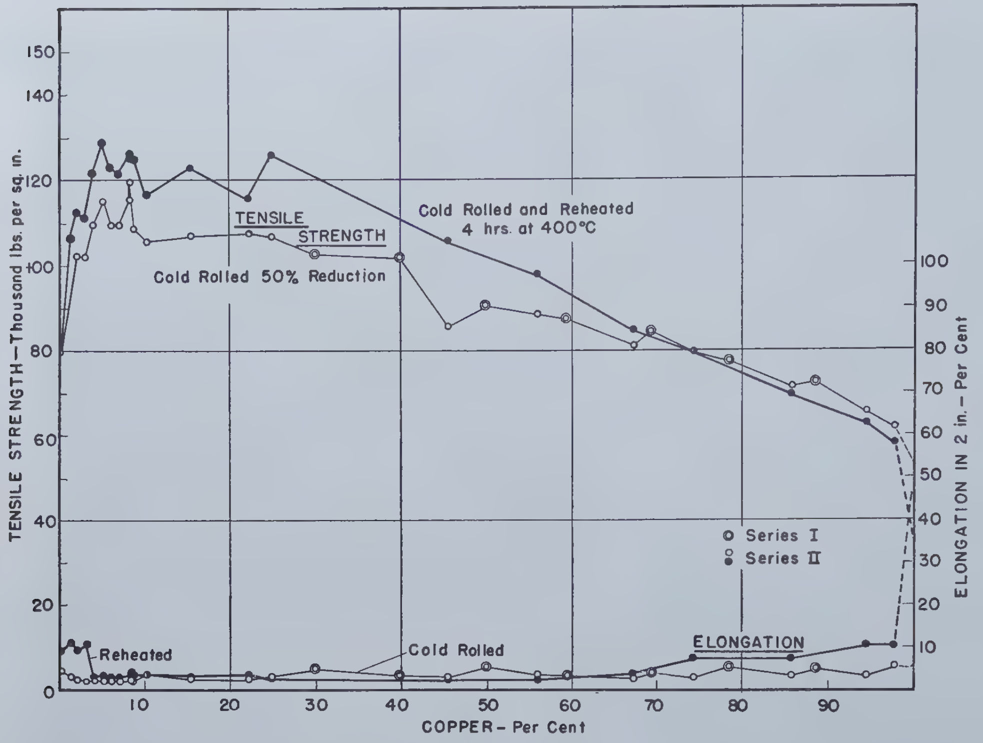

Fig. 28—Tensile properties of Cu-Fe alloys; 0.040-in. sheet cold-rolled 50 pct reduction after annealing at 800°C; and the same material after reheating 4 hr at 400°C.

factorily and gave castings of good surface quality, except for some slight "sweating" of copper. Two bars were tested as-cast, and two (whenever available) after a double normalizing treatment. The 1¼ pct Cu steel was subjected to a precipitation hardening treatment at 500°C after both 850° and 800°C normalizing. None of the alloys showed more attractive combinations of strength and ductility than the ordinary cast steel of today.

Forgings: Ingots 2½ in. sq were forged at 950°C to ¾-in. round rods. Standard 0.505-in. test pieces were machined from these rods as-forged and after heat treatments, consisting of air cooling after 1 hr at 800°C, or quenching from 950°C, and tested with the results shown in table III. The high yield ratio of the alloys containing 30 to 50 pct Cu and the very high reduction of area figures should be noted. The 40 pct Cu alloy as normalized actually withstood a higher stress before yielding than it was able to withstand during subsequent elongation, i.e., the load dropped suddenly when it had reached a value sufficient to produce the first plastic extension by local yielding and did not thereafter rise to a higher value. This effect was more marked in the rolled alloys. The alloys quenched from 950°C have higher strength and lower ductility than those annealed at 800°C, clearly a result of the higher copper content retained by the iron-rich phase on cooling.

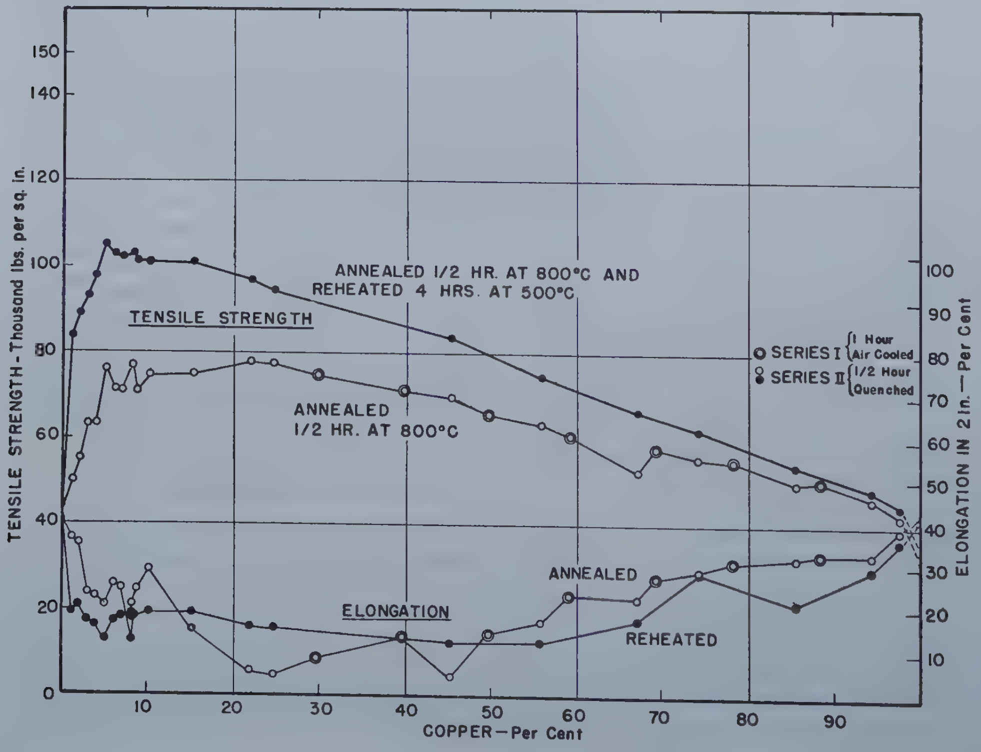

Fig. 29—Tensile properties of Cu-Fe alloys; 0.040-in. sheet annealed ½ hr at 800°C and air cooled; and the same material after reheating 4 hr at 450°C.

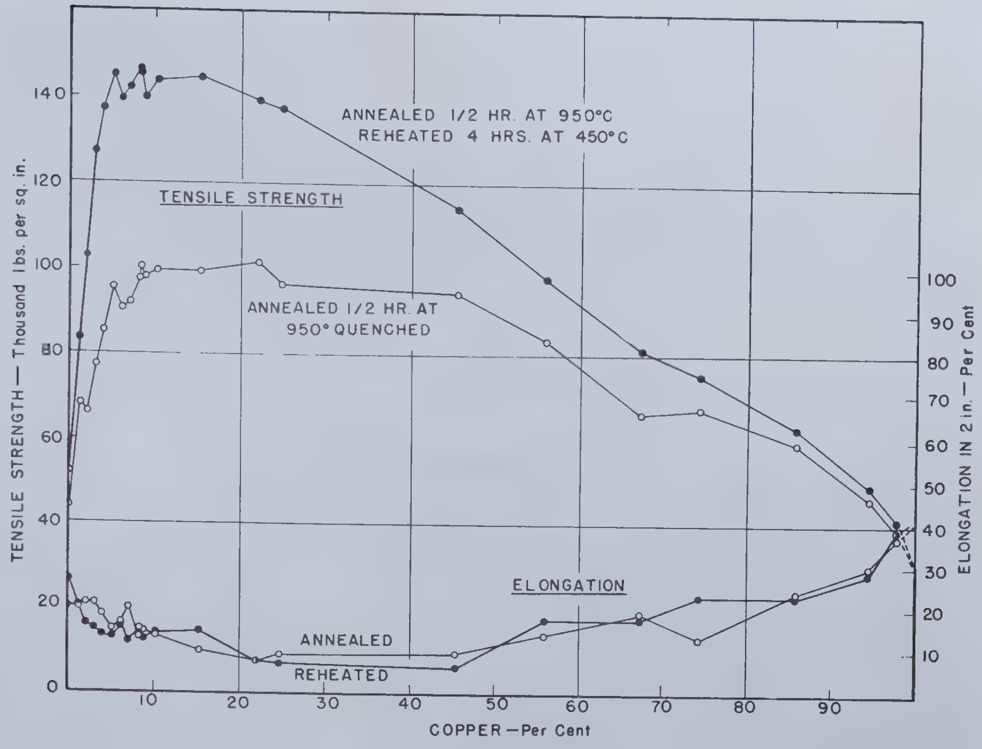

Fig. 30—Tensile properties of Cu-Fe alloys; 0.040-in. sheet annealed ½ hr at 950°C and quenched; and the same material after reheating 4 hr at 450°C.

Impact tests, using the standard 1 cm sq U-notched Charpy specimen machined from ½ in. sq forged rods, gave values increasing from 43 to 55 ft-lb for alloys with 50 to 90 pct Cu. None of the specimens fractured but pulled through the supports without breaking.

It was expected that the mechanical properties of these fibrous alloys would be highly dependent on orientation. Small specimens, ⅜ in. diam x 1 in. gauge length, were cut longitudinally and transversely from a 3x⅝ in. slab of a 50 pct alloy and tested with surprisingly little difference in the two directions (table IV).

Properties of Rolled Sheet: A complete series of alloys from 0 to 100 pct Cu was fabricated in the form of strip by forging if necessary, hot-rolling in two stages to 0.080 in., annealing for 1 hr at 800°C, pickling, and cold-rolling to 0.040 in. The tensile properties of ½ in. wide specimens cut from this strip as-rolled and after various single and double heat treatments are shown in figs. 28 to 30. The data marked "I" were obtained on alloys cold-rolled from 0.25 to 0.080 in., instead of hot-rolling, but the properties are substantially the same. The detailed effect of heat treatment on initially cold-rolled alloys of selected composition is shown in figs. 31 and 32; the effect of reheating on the hardness of alloys previously quenched from 800°C and from 950°C is shown in figs. 33 and 34.

It will be noticed from figs. 28 to 30 that the strength of the alloys after any treatment reaches a flat maximum in the vicinity of 5 to 10 pct Cu and thereafter slowly declines with increasing copper content. This would be expected from the constitution of the alloys, for beyond this point there is progressive dilution of the iron-rich solid solution with softer copper.

The iron-rich alloys containing 1.25 pct Cu and over show considerable precipitation hardening at temperatures in the range of 300° to 500°C. Beyond this temperature and until 800°C the hardness progressively decreases due to overaging, recrystallization, and grain growth. On passing the copper-iron eutectoid temperature (*ca.*860°C), copper progressively goes into solution, resulting in greater hardness on quenching from increasing temperatures, at least up to 1000°C.

A curious effect of local yielding was frequently observed in testing these alloys. The specimen behaved in nearly elastic fashion up to a certain stress, where it yielded with sudden considerable decrease in load and large local extension. Thereafter the stress slowly increased with subsequent elongation,

Table III. Tensile Properties of Forged Rods of Iron-Copper Alloys

Alloy No.	Copper, Pct	Yield Strength, Lb per sq in. (0.5 Pct Extn.)	Tensile Strength, Lb per sq in.	Elongation, Pct on 2 in.	Reduction of Area, Pct
Tested in Forged Condition					
1353	50.1	65,450	68,000	25.0	66.0
1387	59.4	67,700	68,200*	28.0	69.9
1388	69.5	55,450	63,150	33.5	68.8
1389	78.5	43,350	56,150	30.3	74.3
1390	88.6	33,250	52,050	36.3	76.2
Annealed 1 hr at 800°C, Air Cooled					
1384	29.9	61,300	63,250	38.3	77.4
1385	39.8	70,700	63,700*	39.5	80.7
1399	49.9	55,250	58,400	37.0	77.2
1353	50.1	55,950	60,800	33.3	70.9
1387	59.4	57,100	57,200*	38.0	76.8
1388	69.5	50,450	53,750	35.8	75.1
1389	78.5	38,100	49,500	38.8	79.3
1390	88.6	30,350	47,000	38.5	83.3
Annealed 1 hr at 950°C, Quenched					
1384	29.9	103,000	112,600	23.0	58.4
1399	49.9	74,250	87,750	33.0	62.6
1353	50.1	67,100†	80,350†	27.3†	63.4†
1387	59.4	61,200	75,150	29.5	64.2
1388	69.5	46,950	66,250	29.5	64.3
1389	78.5	35,350	59,300	33.8	70.3
1390	88.6	28,450	50,750	38.0	77.0

Tensile test specimens 0.505 in. in diam, machined from forged rod ¾ in. diam.

* One test only. All other figures are average of two tests.

† Specimen air cooled from 950°C, not quenched.

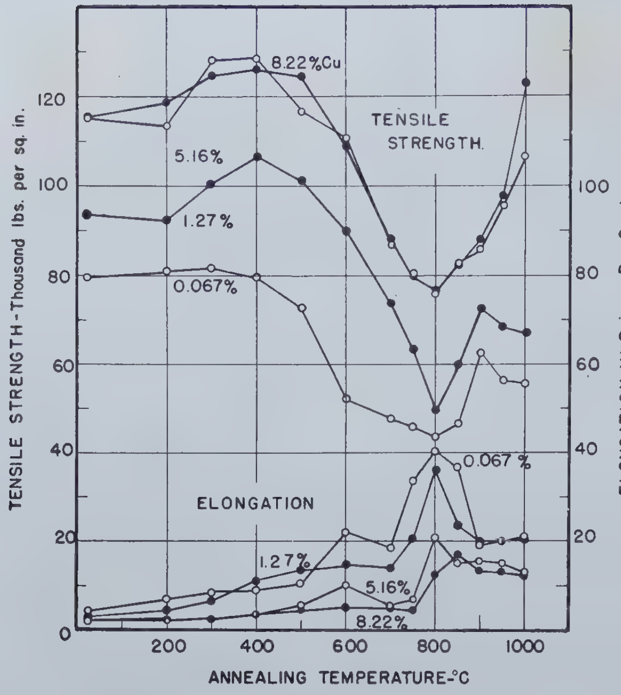

Fig. 31—Effect of annealing on tensile properties of cold-rolled Cu-Fe alloys. 0.040-in. sheet (6 B&S Nos. hard), annealed ½ hr at temperatures plotted, and quenched.

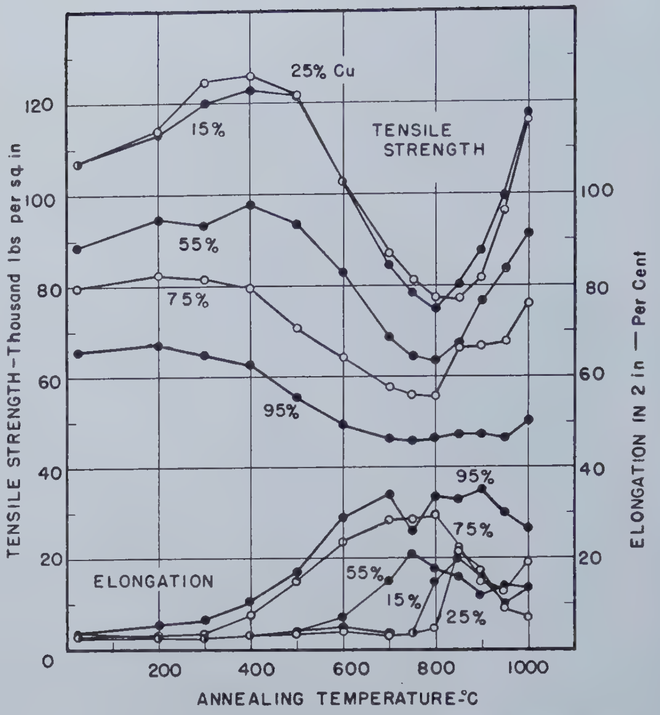

Fig. 32—Effect of annealing on tensile properties of cold-rolled Cu-Fe alloys. 0.040-in. sheet (6 B&S Nos. hard), annealed ½ hr at temperatures plotted, and quenched.

but frequently failed to reach or exceed the stress that originally caused yield. The yield strength (i.e., the stress needed to produce 0.5 pct total extension) was actually greater than the maximum stress obtained during subsequent elongation. This phenomenon was observed in alloys containing between 5 and 56 pct Cu. It occurred rarely in the cold-rolled alloys, where the yield ratio was about 0.9, but was very evident in alloys annealed at temperatures between 300° and 700°C. In this range, the yield strength usually exceeded the subsequent maximum stress by about 2000 psi and in some cases was 7000 psi higher.

Miscellaneous Properties: Fig. 35 shows the ap-

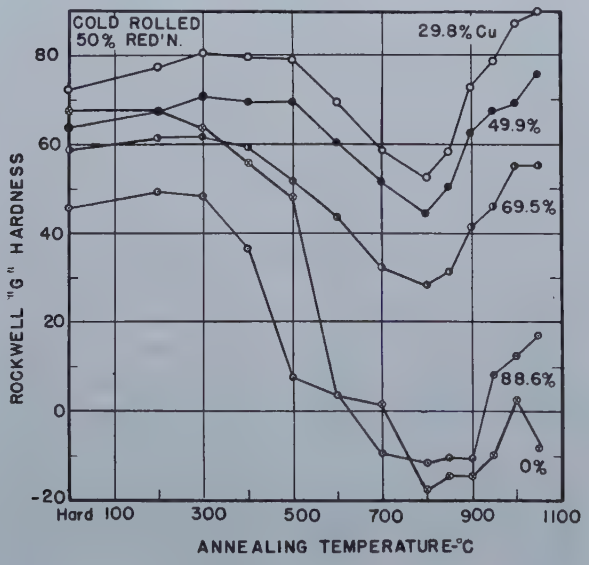

Fig. 33 (above)—Effect of annealing on the hardness of cold-rolled Cu-Fe alloy strip (6 B&S Nos. hard following 800°C anneal).

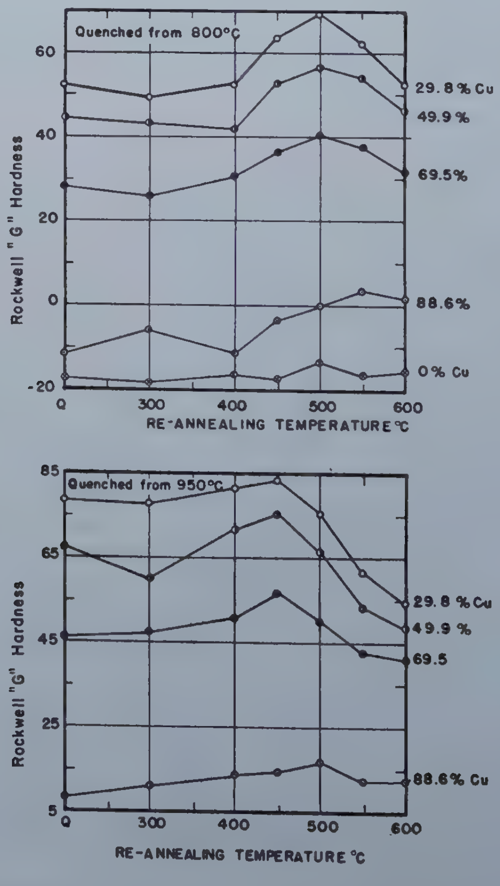

Fig. 34 (right)—Effect of re-annealing on the hardness of some quenched Cu-Fe alloys.

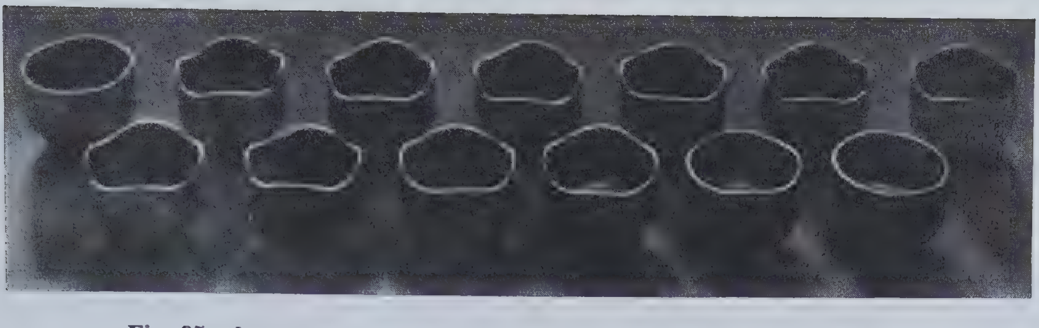

Fig. 35—Appearance of ears on cups drawn from Cu-Fe alloy strips.
Top Row (left to right): 1.2 pct Cu, 5 pct Cu, 8 pct Cu, 10 pct Cu, 15 pct Cu, 20 pct Cu, 25 pct Cu.
Second Row (left to right): 45 pct Cu, 65 pct Cu, 75 pct Cu, 85 pct Cu, 95 pct Cu, 98 pct Cu.

pearance of some cups made in a single cut-and-draw operation from strip 0.04 in. thick, that had been annealed at 800°C and air cooled. The blank was 1.94 in. in diam and was formed into a cup using a ball punch 1.030 in. in diam and a die 1.110 in. in diam with a mouth radius of 0.2 in. In all cases the metal withstood the operation perfectly. With the exception of the 1 pct Cu alloy which had minute "ears" at 0° and 90° to the direction of rolling, all the others had "ears" at 45° to the direction of rolling, the height of ear being greatest in the 25 pct Cu alloys, where it was 0.09 in. It seems unlikely that an alloy with the duplex structure of these could ever be produced in a condition that would be plastically isotropic.

Table IV. Influence of Direction of Test on Properties of 50 Pct Copper-Iron Alloys

	Transverse	Longitudinal
Yield strength, 0.5 pct exten.	46,700	45,250 psi
Yield strength, drop of beam	51,200	49,900 psi
Tensile strength	59,100	57,450 psi
Elongation in 2 in.	36.5	39.3 pct
Reduction of area	62.6	73.4 pct
Charpy impact (Std. U-Notch)	37.5	39.2 ft-lb

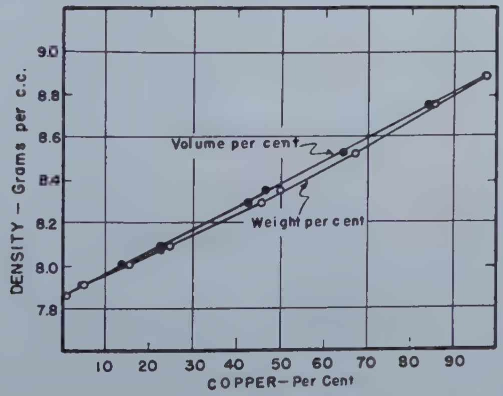

Fig. 36 (above)—Density of Cu-Fe alloys.

Alloys with 20 to 50 pct Cu were welded by both oxyacetylene and resistance methods, but the latter is much to be preferred. The long interval between solidus and liquidus gives great difficulty, and successful welds were produced only by melting the copper and suitably deforming the unmelted iron phase.

Fig. 36 shows the density of some alloys, all of which contain about 0.4 to 0.5 pct Mn and 0.04 to 0.06 pct Si in addition to the copper content shown. In fig. 37 are plotted some electrical conductivity data obtained on cold-rolled and annealed strip. It would be expected that the conductivity in the two-phase region would be a linear function of the volume percentage of the two phases, for the two constituents are essentially arranged as parallel conductors. Actually, the alloys of curves 1 and 2 follow much more closely a linear *resistance* relation, corresponding to the resistances being connected in series. These alloys contained manganese and silicon as stated above, and the discrepancy is probably due to the increasing manganese content of the copper-rich phase as the iron content increases. The alloys deoxidized with magnesium (curves 3 and 4 in fig. 37) are more nearly in accord with the expected linear variation of conductivity with composition.

No quantitative study was made of the magnetic properties of the alloys. They seem to have quite high remanence and made fairly good permanent magnets. It was noticed that the alloys on cold-

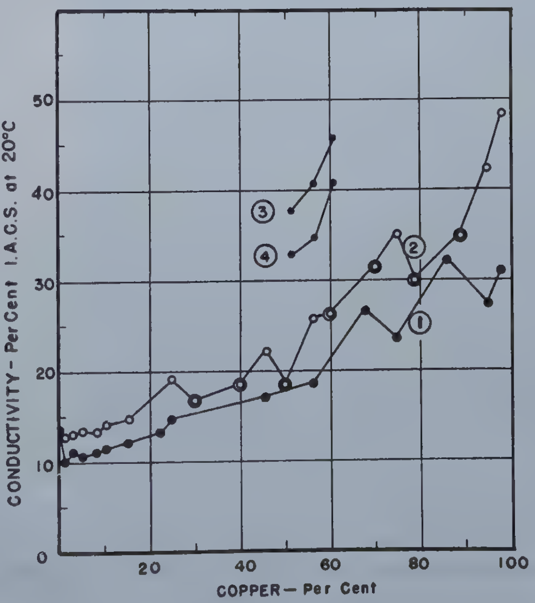

Fig. 37—Electrical conductivity of Cu-Fe alloys.
Curve 1. Strip 0.04 in. thick, annealed 1 hr at 800°C and air cooled. Alloys contain about 0.4 pct Mn and 0.05 pct Si residual deoxidants.
Curve 2. Same as 1, reheated at 600°C for 24 hr, furnace cooled to and held 50 hr at 500°C; furnace cooled to and held 20 hr at 400°C; furnace cooled to room temperature.
Curve 3. Wire 0.045 in. diam. Annealed 800°C, air cooled, reheated to 600°C and cooled to 500°C in 2 hr. Contains 0.1 to 0.2 pct Mg residual deoxidant.
Curve 4. Wire heat treated same as Curve 3 at 0.182 in. diam, cold drawn to 0.045 in. (94 pct reduction of area).

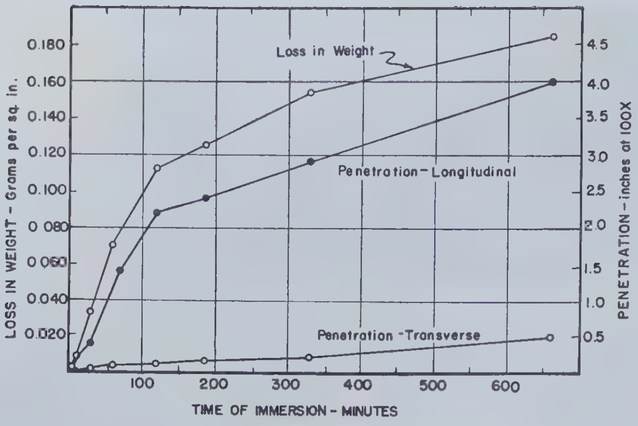

Fig. 38—Corrosion of 50 pct Cu-Fe alloy in 15 pct H_2SO_4 at 80°C.

drawing alone became permanently magnetized—indeed as strongly so as could be induced by external magnetization.

As little as 2 pct Cu added to pure iron increases the machinability considerably. The alloys with between 2 and 75 pct Cu are very readily machinable and finish to a beautiful surface. All alloys containing over 15 pct Cu have a copper-colored fracture, for the fracture passes through the weaker phase. Machined or polished sections show no visible coppery appearance until the copper content exceeds 20 pct. Even the 55 pct alloy is only faintly red, but beyond this point the color progressively deepens to that of pure copper.

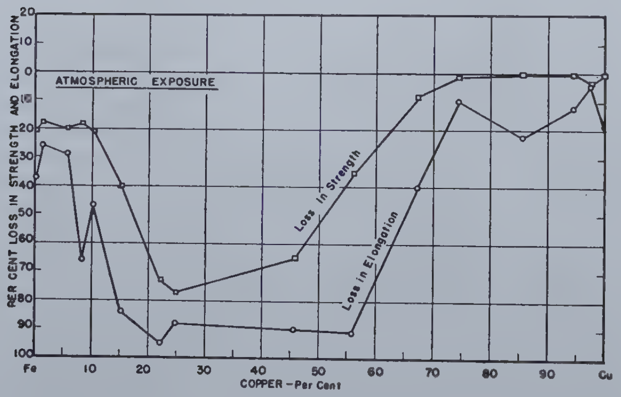

Fig. 39—Changes in tensile properties of Cu-Fe alloys caused by 23 month exposure to the atmosphere in Waterbury, Conn., with twice daily spraying with water.

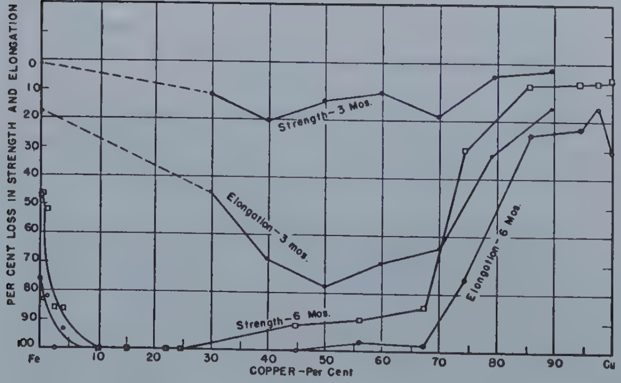

Fig. 40—Changes in tensile properties of Cu-Fe alloys caused by exposures of 3 and 14 months to 20 pct salt spray.

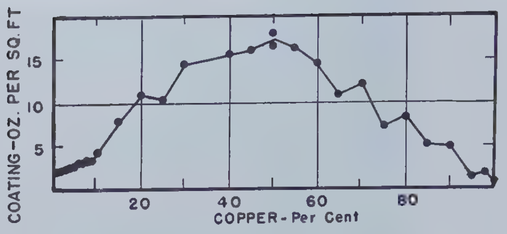

Fig. 41—Weight of coating formed on Cu-Fe alloys immersed for 60 sec in molten zinc at 440°C. Surface area 5 sq in.

X-ray pin hole patterns of a 50 pct Cu alloy cold-rolled 87 pct reduction to 0.01 in. thickness after annealing at 800°C showed strong preferred orientation of both phases. Separation of the two phases by selective solution (in acid to leave copper, and in cyanide to leave iron) permitted patterns to be obtained for each phase uncomplicated by lines from others. The texture was identical with that of cold-rolled pure metals (i.e., (110) $[\bar{1}12]$ for copper, (100) [011] for iron). Annealing at 800°C did *not* change textures, although both phases had recrystallized and would have been expected to take new orientations. Evidently the two phases influence the recrystallization and grain growth of each other. Müller[14] has observed that the face-centered cubic phase of the iron-copper-nickel system has a recrystallization texture identical with the rolling texture in all compositions approximately coincident with the two-phase area of the constitution diagram.

Corrosion Resistance

The existence of two phases in the alloy and the great difference of electrolytic solution potential leads one to anticipate that the alloys would be poorly resistant to corrosion. Some studies were nevertheless made. Fig. 38 shows the loss in weight

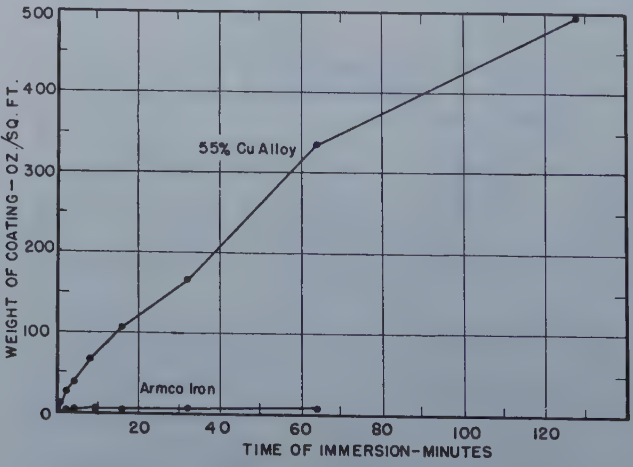

Fig. 42—Effect of time on weight of galvanized coatings formed on 55 pct Cu alloy at 440°C.

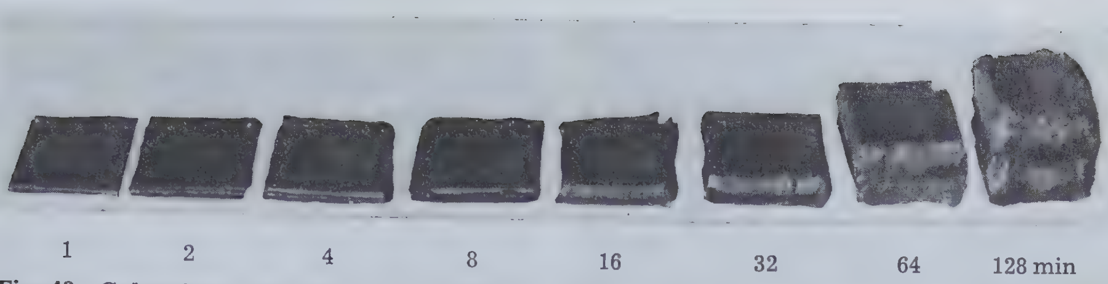

Fig. 43—Galvanized coatings formed on 55 pct Fe-Cu alloy strip after various times in zinc bath at 440°C. Specimens initially 1x1x0.04 in.

and depth of attack (i.e., depth of removal of iron, measured microscopically) when a rolled strip of the 50 pct Cu alloy was subjected to corrosion in 15 pct sulphuric acid at 80°C. The fibrous character of the alloy causes the rate of corrosion in a longitudinal direction to be much higher than that normal to the direction of fibers.

A number of specimens were exposed to a variety of corrosive environments, including 20 pct salt spray at room temperature,* industrial and marine atmospheres, and to sea water at a mid-tide point on Faulkner's Island (Long Island Sound). The samples exposed were tensile test pieces, cut from 0.04-in. rolled strip, ¾ in. wide and 8 in. long, with a reduced section 0.5 in. wide and 2.5 in. long. They were mounted on insulators to prevent one specimen electrolytically influencing another. After exposure the specimens were cleaned and broken in tensile test. In all environments the properties of the alloys of intermediate composition were inferior to the alloys at either end of the system. Curves typical of the change of tensile properties after exposure are shown in figs. 39 and 40. The alloys do not possess a corrosion resistance greater than that of ordinary copper-bearing mild steel until the copper content exceeds about 75 pct.

The iron-rich phase in the duplex alloys was always corroded to a much greater depth than was the copper, and there was always a layer in which the copper was relatively unaffected. In the marine exposure tests it was noticed that barnacles were occasionally found on alloys with a copper content as high as 80 pct.

It seems obvious that the alloys of intermediate composition cannot be used in even mildly corrosive environments without effective surface protection.

No improvement in corrosion resistance was observed in alloys with equal amounts of copper and iron and with added constituents of up to 5 pct Al, 5 pct Ni, or 8 pct Mn. With 10 and 15 pct of Ni some improvement was observed, but the alloys were still not to be classed as corrosion resistant.

Protection Against Corrosion: Protection against corrosion can be provided by the usual surface treatments. Tin coating by hot-dipping was found to be simple and effective, although the coating would not withstand severe deformation. The best protection for the alloy in service would probably be electrogalvanizing. Hot-dip galvanizing produces some remarkable results.

The thickness of coating formed on mild steel after short but constant immersion in molten zinc is increased by the presence of copper, and the coating remains normal up to about 10 pct Cu. Beyond this the alloy layer is evidently continually permeable to liquid zinc and does not retard further growth. The thickness of coating continues to increase with little slowing of rate and coatings of enormous thickness were obtained after prolonged sojourn in a zinc bath (figs. 41 and 42). Reaction

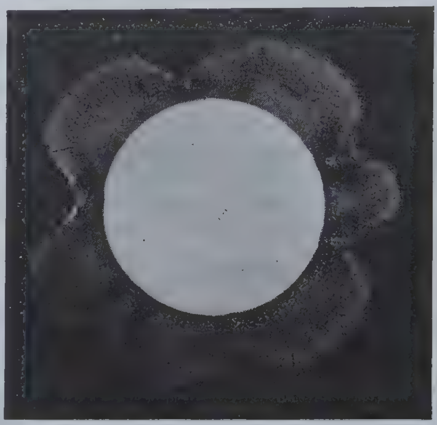

Fig. 44—Cross-section of rod (51.2 pct Cu) with heavy galvanized coating, formed in 15 min at 440°C. X4.

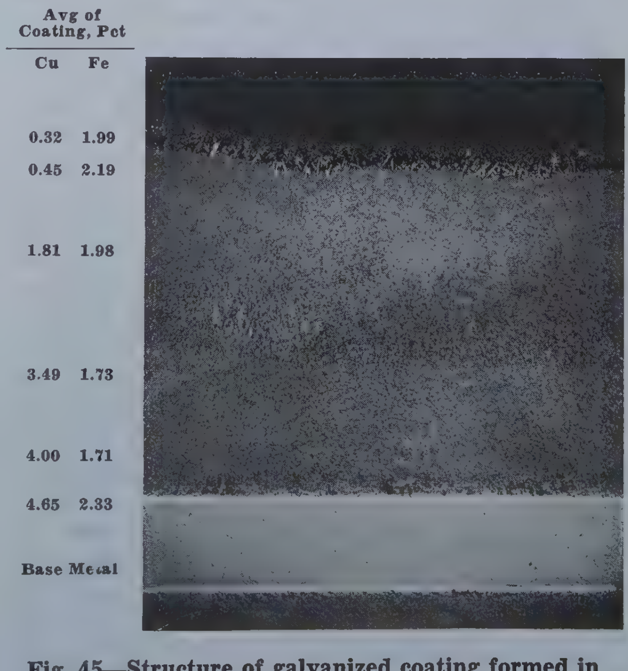

Fig. 45—Structure of galvanized coating formed in 32 min at 440°C on strip with 56 pct Cu. X15.

---

* The salt spray tanks and test method were essentially as described by A. N. Finn.[15]

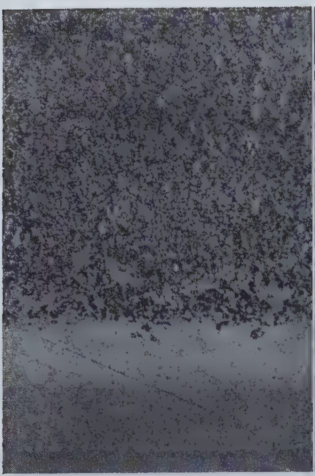

Fig. 46 (left)—Structure of inner part of coating shown in fig. 45. X150.

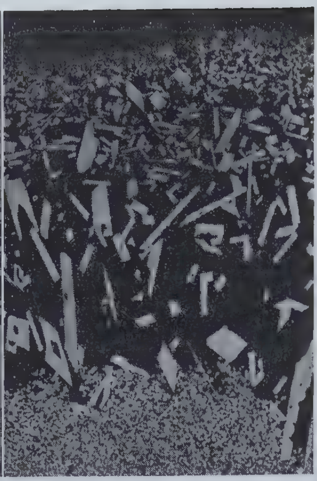

Fig. 47 (right)—Structure of outer part of coating shown in fig. 45. X150.

between the zinc and the alloy occurred at the surface of the solid sample, not at the interface between the partly solid area and liquid zinc. Curious shapes were produced, for growth was always parallel to the initial surface of the specimen (figs. 43 and 44). The microstructure of the coating is shown in figs. 46 and 47, and the composition at various points in the coating is shown in fig. 45.

High-Strength Conductor Alloys

The conductivity of both of the iron-rich and copper-rich constituents is greatly affected by impurities and the presence of 0.5 pct Mn and 0.1 pct Si had a great adverse effect on the conductivities of the alloys shown in curves 1 and 2 in fig. 37. A search was made for other deoxidizers that would have less effect on the conductivity but would give alloys capable of being hot- and cold-rolled commercially. After studying 50 pct Cu alloys deoxidized with Al, Zr, Ti, Mg, Ca, B, and Li, it was found that either calcium or magnesium additions provided an excellent combination of forgeability and conductivity but magnesium (added as 10 pct Mg-Cu) seemed to be the most reproducible in its effect. A residual content of between 0.1 pct and 0.2 pct Mg was preferred.

Ingots of 12 lb were cast of alloys in 50, 55, and 60 pct Cu after additions of 0.2 pct Mg. These were hot-rolled to 0.390-in. rod in the copper alloy mill of the American Brass Co., and drawn to wire 0.045 in. in diam following standard copper mill practice. Pickling was done in 10 pct sulphuric acid at 180°F, which left a copper surface as a useful lubricant in drawing. Wire was drawn 12 B&S numbers hard (from 0.182 to 0.045 in. in diam) with no difficulty whatever and even greater reductions are undoubtedly commercially feasible. Samples were taken at various intermediate gauges, annealed at 800°C for 1 hr and air-cooled, and then all drawn down to a final gauge of 0.045 in. for testing. The continued increasing strength on progressive drawing is shown in fig. 48, plotted against B&S numbers reduction, which provides a logarithmic scale of reduction of area. Unlike most copper alloys that quickly approach a limiting strength asymptotically and do not thereafter increase, this alloy increases progressively in tensile strength even to large reductions. It is therefore possible to obtain phenomenally high tensile strength associated with relatively good electrical conductivity.

The solubility of iron in copper is highly temperature-dependent and the maximum conductivity can be obtained only after heat-treatment which precipitates iron as completely as possible. Fig. 49 shows the effect on the conductivity of three typical alloys of successive treatments at 700°, 600°, and 500°C. Other tests are shown in fig. 50. Higher conductivity is obtained when the alloy is annealed at successively lower temperatures. Quenching from 800°C, prior to the lower temperature heat treatment, does not accelerate the rate of approach to equilibrium. Evidently the presence of many particles of iron throughout the structure changes the behavior from that normally shown by precipitation from a solid solution. Uniform cooling in 2 hr through the range 600° to 450°C gave a conductivity (42 pct I.A.C.S. for the 55 pct Cu alloy) very little below the maximum obtained by prolonged heat treatment at 500°C, and probably approximates the best commercial treatment. If maximum softness and ductility are required for subsequent cold-working, this treatment should be preceded by an 800°C anneal and air-cooling.

The combination of tensile strength and conductivity—over 160,000 psi and 35 pct I.A.C.S.—is not unattractive.

Summary

A study was made of the properties of binary alloys of iron and copper. Contrary to some statements in the literature, no difficulty was encountered in making homogeneous melts of all compositions, except in the presence of carbon, which caused segregation into two liquid layers. The alloys can be hot- and cold-worked over the entire range of composition, although the alloys between 8 and 30 pct Cu are difficult to work unless the castings are first

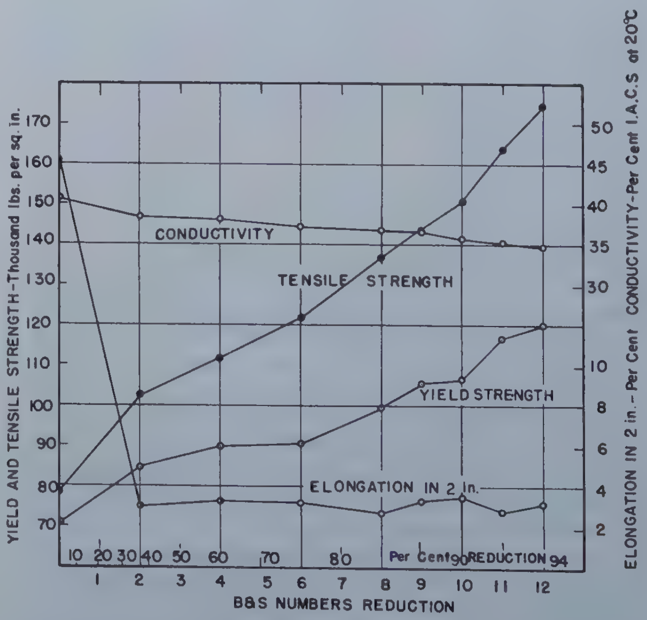

Fig. 48—Alloy wire containing 56.35 pct Cu. Material of various gauges was given heat treatment consisting of annealing at 800°C and air-cooling, reheating to 600°C, and very slowly cooling therefrom, prior to drawing to the final gauge of 0.045 in.

annealed and then forged just below the eutectoid temperature (*ca.* 860°C). The tensile strength of the alloys reaches a maximum in the range 5 to 10 pct Cu and thereafter declines uniformly as the copper content is increased. The greatest strength is obtained by quenching from 950°C and reheating at 450°C to cause precipitation hardening. Greatest ductility is obtained after annealing at 800°C, and alloys in this condition, if quenched or air-cooled, are also susceptible to some precipitation hardening. All alloys after initial forging can be drawn into wire or rolled into strip. The electrical conductivity of the alloys progressively increases with copper content and is greatly influenced by deoxidation practice (for which an addition of 0.2 pct Mg is preferred) and by heat-treatment. The highest conductivity for a given alloy is obtained by slowly cooling through the range 600° to 450°C, although extremely long annealing at 500°C will produce the same result. The corrosion resistance of the alloys is not good. The alloys progressively increase in strength on cold-working and wires drawn from magnesium-deoxidized material containing about 55 pct Cu show excellent combinations of strength and conductivity. A wire heat treated to give maximum conductivity and drawn 11 B&S numbers hard (92 pct reduction in area) to 0.045 in. diam had the following properties: tensile strength, 158,000 psi; elongation, 2.3 pct on 2 in.; conductivity, 35.5 pct I.A.C.S.

Acknowledgments

The authors are indebted to The American Brass Company and The Anaconda Copper Mining Company (at whose request this research was started) for permission to publish the results. The late W. H. Bassett had general supervision over the work and was a constant source of inspiration and encouragement. W. Earl Lindlief and Philip H. Kirby carried out a major part of the work on galvanizing and corrosion respectively, and E. T. Candee developed effective pickling procedures.

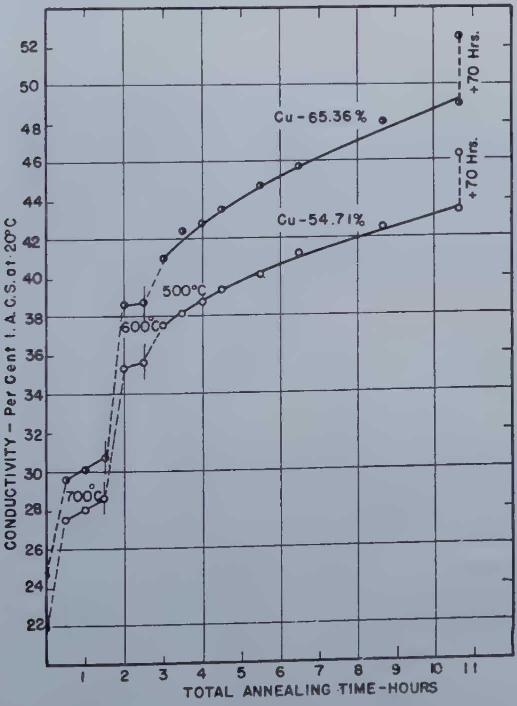

Fig. 49—Effect of heat treatment on electrical conductivity of Fe-Cu wires.

(Wire 0.142 in. diam, cold drawn 6 B&S Nos. hard from hot-rolled rod).

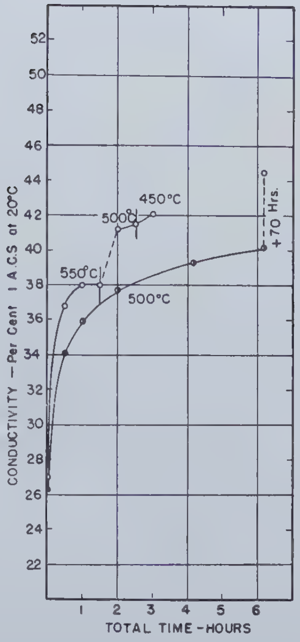

Fig. 50—Effect of heat treatment on electrical conductivity of Cu-Fe alloy wires (54.7 pct Cu) after prior heat treatment at 800°C.

References

[1] J. L. Gregg and B. N. Daniloff: The Alloys of Iron and Copper. 1934. New York.

[2] D. Mushet: On the Practicability of Alloying Iron and Copper. *Phil. Mag.* (1835) ser. 3, **6**, 81-85.

[3] J. E. Stead: Notes on Alloys of Copper and Iron. *Journal* Iron and Steel Inst. (1901) **60**, 104-121.

[4] C. S. Smith: Discussion on paper by D. Hanson and E. G. West on the Constitution of Copper-Iron-Silicon Alloys. *Journal* Inst. Metals (1934) **54**, 251.

[5] W. R. Maddocks and G. E. Claussen: Alloys of Iron-Copper-Carbon-Cobalt. Iron and Steel Inst. Special Report No. 14 (First Report of the Alloy Steels Research Committee) 1936.

[6] K. M. Simpson and R. J. Bannister: Alloys of Copper and Iron. *Metals and Alloys* (1936) **7**, 88-94.

[7] E. E. Schumacher and A. G. Souden: Some Alloys of Copper and Iron; the Tensile, Electrical, and Corrosion Properties. *Metals and Alloys* (1936) **7**, 95-101.

[8] K. Iwase, M. Okamoto, and T. Amemiya: On the Formation of Two Liquid Layers in Copper-Iron Alloys. *Sci. Rep.* Tohoku Imp. Univ. (1938) (i) **26**, 618-640.

[9] W. B. Sallitt: Copper in Cast Steel and Iron. (Copper Development Association, Pub. No. 29, 1937).

[10] C. H. Lorig and R. R. Adams: Copper as an Alloying Element in Steel and Cast Iron. 1948. New York.

[11] M. Alexander: Copper Steel Castings. Iron and Steel Inst. Special Report No. 23 (Third Report of the Steel Castings Research Committee) 1938, pp. 61-72.

[12] T. W. Lippert: Digby's Cypritic Alloy. *Iron Age* (Oct. 14, 1937) **140**, 54-63.

[13] U. S. Patent No. 1,999,850, 1935.

[14] H. G. Müller: Recrystallization Texture of Face-Centered Iron-Nickel-Copper Alloys. *Ztsch. Metallkunde* (1939) **31**, 322-325.

[15] A. N. Finn: Method of Making Salt Spray Test. *Proc.* A.S.T.M. (1918) **18**, 237-239.

[16] W. Hodge, R. I. Jaffee, J. G. Dunleavy, and H. R. Ogden: A Copper-base Alloy Containing Iron as a High-strength, High-conductivity Wire Material. *Transactions* AIME (1949) **180**, 32; *Metals Technology* (Aug. 1948) TP 2422E.

Kinetics of Solid Phase Reactions in Oxide Films on Iron — The Reversible Transformation At or Near 570°C

by Earl A. Gulbransen and Roswell Ruka

The forward and reverse reactions, $Fe_3O_4 + Fe \rightleftarrows 4FeO$, are studied by electron diffraction methods. In thin films the forward reaction occurs at temperatures 170°C below the equilibrium value. The mechanism of the forward reaction is shown to be governed by the diffusion of iron. Studies on the reverse reaction as a function of time, temperature, and oxide composition indicate a nucleation and a growth process is rate controlling.

ONE of the interesting questions in the understanding of the reaction of iron with oxygen is the kinetics and the mechanism of the crystal structure changes occurring in the formation and breakdown of the oxide film. In a recent work[1] the electron diffraction method was applied to the study of the solid phase reactions occurring internally in the oxide film on iron above 570°C and under vacuum conditions. The higher oxides which form under oxidizing conditions are reduced internally by the diffusion of iron into the oxide leaving the bulk of the oxide FeO (wüstite).

This paper will ask and consider three questions. These are: (1) What is the nature of the depressed transformation temperature for the $Fe_3O_4 + Fe \rightleftarrows 4FeO$ reaction in very thin oxide films?; (2) What is the mechanism of the forward transformation of Fe_3O_4 to FeO at or near 570°C?; and (3) What is the nature and mechanism of the slow reverse transformation of FeO to Fe_3O_4 and Fe below 570°C?.

The composition of the oxide as well as its electrical, magnetic, mechanical, and chemical properties depends upon the kinetics of these reactions.

Literature Survey

The composition of the oxide film on pure iron at temperatures up to 570°C has been studied extensively by the electron diffraction method. Nelson,[2] Jackson and Quarrell,[3] and Gulbransen and Hickman[4] have shown that Fe_3O_4 and α-Fe_2O_3 are formed in the temperature range of 225° to 570°C, while γ-Fe_2O_3 is most likely formed below 225°C for long oxidation times. In very thin films FeO (wüstite) is found to form at temperatures as low as 400°C, and its existence depends essentially upon the extent of initial oxidation. FeO is not found in the formation of thick films below 570°C.

On the other hand X-ray[5] and micrographic[6] studies show that Fe_3O_4 may exist as the main component in thick films up to 650°C, well above the equilibrium temperature for the reaction $Fe_3O_4 + Fe \rightleftarrows 4FeO$.

The kinetics of the forward and reverse transformations of the reaction $Fe_3O_4 + Fe \rightleftarrows 4FeO$ have not been studied in oxide films. However, analysis of the data of Gulbransen and Hickman[4] on the heating and cooling of iron oxide films of known thicknesses in high vacua shows that the forward reaction proceeds rapidly even for a 4000 Å film at temperatures of 575° to 600°C. The reverse reaction or decomposition of wüstite (FeO) occurs at temperatures below 450°C. Thus, there appears to be a slow process in the decomposition which is in marked contrast to the rapid forward reaction.

The decomposition of a bulk sample of FeO free from the metal has been studied extensively by Chaudron, Bénard and coworkers using the micrographic, X-ray diffraction, and thermomagnetic methods. Chaudron[7, 8] first observed that the decomposition of FeO (wüstite) below 570°C occurs by the reaction $4FeO \rightarrow Fe_3O_4 + Fe$. Later work by Chaudron and Forestier[9] showed that the rate of de-

---

EARL A. GULBRANSEN, Member AIME, and ROSWELL RUKA are associated with Westinghouse Research Laboratories, East Pittsburgh, Pa.

AIME St. Louis Meeting, February 1951.

TP 2986 E. Discussion (2 copies) may be sent to Transactions *AIME before April 1, 1951. Manuscript received Aug. 25, 1950.*

composition increases to a maximum at 480°C and then decreases as the temperature is further lowered. An X-ray diffraction study by Bénard and Chaudron[10] indicated that between 350° and 500°C the iron which is first liberated dissolves in the remaining FeO and increases its lattice parameter.

In a recent paper, Chaudron and Bénard[11] have shown from a thermomagnetic study that the stability of FeO depends upon the temperature of formation of the bulk oxide and upon the composition of the oxide. The oxides richest in iron are the most stable. The temperature for onset of the decomposition is found to vary between 350° and 450°C.

Thermal Data on the Fe_3O_4-FeO Equilibrium

Two reactions are of interest: (1) $Fe_3O_4 + Fe \rightleftarrows 4FeO$, and (2) $3FeO + \frac{1}{2}O_2 \rightleftarrows Fe_3O_4$. The data of Chipman[12] are used to calculate the free energy changes for these reactions. Other reactions in the iron-oxygen system have been previously calculated and discussed.[1] Fig. 1 shows a plot of the results expressed in terms of log *K*, where *K* is the equilibrium constant. The results show that the oxidation reaction (2) is favorable over the temperature range given, while the solid phase reaction (1) is only favorable above 570°C. In these calculations the free energies of the wüstite phase, FeO, and of the magnetite phase, Fe_3O_4, are assumed to be independent of the composition. Darken and Gurry[13, 14] have shown that there is an effect of composition on the free energy of FeO at temperatures of 1100°C and higher. However, data are not available for the evaluation of this effect at 570°C.

The variation of log *K* with temperature for reaction (1) in fig. 1 is small. Therefore, a wide variation in the equilibrium temperature is possible if free energy differences exist for the FeO or Fe_3O_4 films in contact with iron.

In this paper it should be noted that when we refer to FeO and Fe_3O_4 we are discussing wüstite and magnetite whose compositions are determined by the iron-oxygen diagram. The wüstite, or FeO, region of stability has been studied with great care although considerable disagreement exists between the recent diagrams of Bénard[15] and of Darken and Gurry.[13, 14] Little information exists on the region of homogeneity of magnetite at temperatures near 570°C.

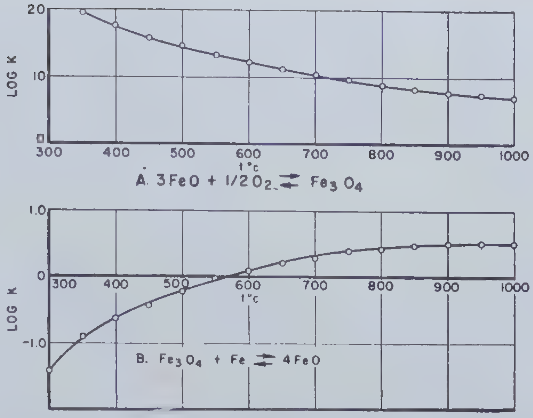

Fig. 1—Fe_3O_4-FeO equilibria. Log *K* vs. t°C.

The electron diffraction camera, furnace, and specimen manipulator are similar to those previously described.[1, 16, 17]

Specimens are prepared from Puron and Armco grades of iron. The analyses and preparation of these materials have been described.[1, 4]

Results and Discussion

Depressed Transformation Temperature in Thin Oxide Films: Although the existence of FeO on Fe at temperatures as low as 400°C has been noted,[4] this fact is not sufficient evidence that the equilibrium temperature for the reaction $Fe_3O_4 + Fe \rightleftarrows$

A. First Cycle

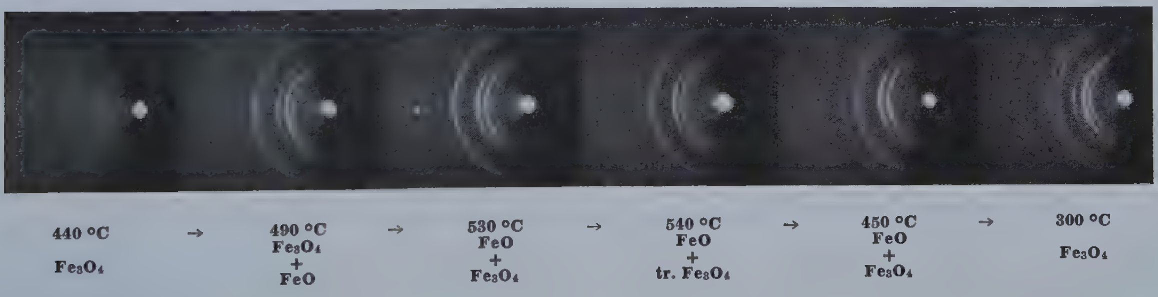

B. Second Cycle

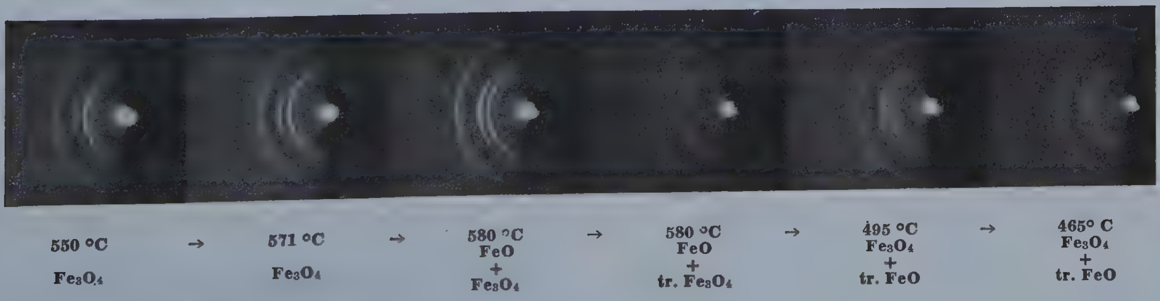

Fig. 2—Forward and reverse transformation, $Fe + Fe_3O_4 \leftrightarrows 4FeO$.
Vacuum formed film (2×10^{-5} mm Hg) on Puron.

Table I. Effect of Heat Treatment on the Forward and Reverse Transformation Temperatures

Vacuum Condition	Cycle	Temperature, °C Forward Reaction	Temperature, °C Reverse Reaction
1x10^{-5} mm of Hg Oxide	1	530	450
	2	570	465 to 490
3x10^{-6} mm of Hg Oxide	1	Too diffuse for study	
	2	500	412
	3	525	

$4FeO$ is different for thin films. Rather, it is necessary to show that the reaction actually proceeds in both directions below 570°C for thin films.

Experiments are made to show this effect for very thin oxide films on Puron and Armco iron. To add further information, studies are made on (1) the effect of vacuum heating and cooling, (2) the nature of the lattice parameter changes in the transformation, and (3) the nature of the orientation of the oxide crystallites before, during, and after the transformations.

Vacuum Formed Oxide Film on Puron

Fig. 2 shows the diffraction patterns obtained in a typical heating and cooling cycle. An abraded Puron sample is heated and oxidized in a vacuum of 2x10^{-5} mm of Hg. The diffraction patterns show, at 440°C, a pattern of Fe_3O_4 which on heating to 490° and 530°C changes to a mixture of FeO and Fe_3O_4. At 540°C the pattern is FeO with only a trace of Fe_3O_4. The reverse transformation starts to occur at 450°C.

A reheat of this sample shows the forward transformation occurring between 571° and 580°C while the reverse transformation starts to occur between 495° and 465°C.

The trend of these results has been checked many times with (1) different heats of Puron, (2) freshly abraded samples, and (3) samples which have been oxidized and abraded many times. The experiments show that the depressed transformation effect is not unique for one heat of Puron and is not affected greatly by any concentration of impurities in the oxide occurring in the vacuum oxidation of a new sample of Puron.

Table II. Orientation Relationships in Oxide Films and Effect of Heat Treatment

Vacuum Condition	Cycle	Temperature	Structure	Orientation
1x10^{-5} mm of Hg Oxide	1	Below 530	Fe_3O_4	Random
	1	530*	FeO	Nearly random
	1	Below 450†	Fe_3O_4	Nearly random
	2	450	Fe_3O_4	Some orientation
	2	500 to 570	Fe_3O_4	Highly oriented
	2	570*	FeO	Highly oriented (Same as Fe_3O_4)
	2	Below 465†	Fe_3O_4	Oriented (Same as in original Fe_3O_4)
3x10^{-6} mm of Hg Oxide	1	Below 570*	Very diffuse	Random
	1	Below 400†	Very diffuse	Random
	2	Below 500	Fe_3O_4	Random
	2	500*	FeO	Random
	2	Below 412†	Fe_3O_4	Random
	3	Below 525	Fe_3O_4	Some orientation
	3	525*	FeO	Some orientation

* Forward transformation occurring.
† Reverse transformation occurring.

This transformation was also studied by visual observations alone. For example, two specimens of Puron are heated and oxidized in a vacuum of 1x10^{-5} mm of Hg at a rate of 2° to 3°C per min. A diffuse and randomly oriented pattern of Fe_3O_4 is observed until a temperature of 500°C is reached at which point the transformation to FeO occurred.

Vacuum Formed Film on Armco Iron

The analysis of Armco iron is approximately C, 0.015; S, 0.050; Mn, 0.03; Si, 0.01; P, 0.007; and balance, Fe. A specimen is heated in a vacuum of 2x10^{-5} mm of Hg. The patterns at low temperatures are very diffuse and impossible to analyze. At 425°C a pattern of FeO can be distinguished. To obtain a thicker oxide film a second specimen is heated in a poor vacuum of 8x10^{-4} mm of Hg. A mixture of FeO and Fe_3O_4 is found at 470°C. The transformation to FeO occurred at 525°C. We concluded that the effect of the additional impurities in Armco iron has no effect on the phenomena.

Effect of Film Thickness

This effect has been previously studied.[4] We have confirmed this work by noting the transformation temperature in a thin film of oxide on Puron. A specimen is oxidized at 400°C for 1 min and 1 cm of O_2 pressure. Fe_3O_4 is observed until a temperature of 552°C is reached at which point the transformation to FeO occurred. This experiment, together with previous experiments,[4] shows that the transformation temperature is a function of the oxide thickness and has the normal value of 570°C for thick films. It should be noted that thick films may give higher transformation temperatures since finite heating rates are used. These higher temperatures are due to the fact that the rate of the reaction is limited by the diffusion rate.

Effect of Heat Treatment and Film Thickness

Table I shows the results of consecutively heating and cooling oxide films for two different vacuum conditions. In a vacuum of 1x10^{-5} mm of Hg the second heating cycle gives the normal value for the transformation temperature. However, the temperature for onset of the reverse transformation is not greatly affected. The second experiment is carried out in a vacuum of the order of 3x10^{-6} mm of Hg. The forward transformation temperature increases for each consecutive cycle, however, the normal value is not observed even after three cycles.

The trend of the results may be explained on the basis of vacuum oxidation, the extent of which is determined by the pressure, temperature, and time. The initial layers of oxide are in an unstable state on the iron. However, as the oxidation proceeds in the vacuum, the influence of this initial layer of oxide becomes less important and in a vacuum of 1x10^{-5} mm of Hg the second forward transformation occurs in the regular manner. The experiment carried out in a vacuum of 3x10^{-6} mm of Hg suggests that a number of cycles are necessary to give sufficient oxidation for the reaction to occur in the normal way.

Orientation Relationships in the Oxide Film

An analysis of a number of transformations of oxides of varying thickness shows that in some cases

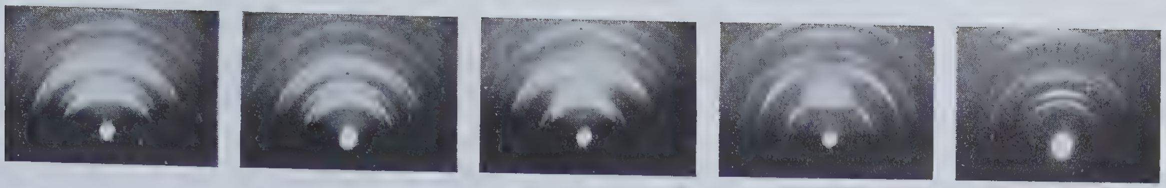

Fe_3O_4 390 °C → Fe_3O_4 412 °C → Fe_3O_4 440 °C → FeO + tr. Fe_3O_4 + tr. $\alpha - Fe_2O_3$ 562 °C → Fe_3O_4 300 °C

Fig. 3—Orientation effects. Forward and reverse transformations.
Second cycle vacuum is 10^{-5} mm Hg.

the patterns consist of a number of arcs, indicating certain crystallographic directions are favored in the growth of the film while other patterns consist of uniform half circles and indicate a random growth of the film. The presence of arcs in the diffraction pattern will be referred to as the presence of orientation effects in the oxide film. An analysis of the transformation where orientation effects are present leads to some interesting conclusions.

Table II shows the effect of heat treatment on the orientation effects observed for two vacuum-formed oxide films. The oxide film formed under a vacuum of $1x10^{-5}$ mm of Hg shows no appreciable orientation during the first heating cycle, where a depressed transformation temperature is noticed. However, a second heating cycle gives a highly oriented oxide and a normal transformation is observed. The second vacuum-formed oxide film ($3x10^{-6}$ mm of Hg) shows no orientation effects for the three heating cycles and depressed transformation temperatures are observed in each case. Thicker oxide films give no orientation effects.

The results shown in table II and evidence on thicker films may be summarized as follows: (1) The thin oxide films which are nearly random in orientation have depressed transformation temperatures, (2) as the oxide increased in thickness the Fe_3O_4 lattice takes on a highly oriented structure—these films giving more nearly normal transformation temperatures, and (3) above a certain film thickness the oxide need not be oriented to have the normal transformation temperature.

Fig. 3 shows a typical second cycle transformation. As the Fe_3O_4 is heated the orientation increases and is carried over into the FeO and Fe_3O_4 formed by transformation. Thus, the prominent orientation of the 2.54 and 2.10 Å lines in Fe_3O_4 corresponding to the 311 and 400 planes is carried over into the 2.47 and 2.14 Å lines in FeO corresponding to the 111 and 200 planes.

Lattice Parameters

It has been suggested that the Fe_3O_4 formed in the thin oxide films on Fe is in an unstable state due to the effect of the underlying Fe. This may be expected to occur in the first layers of oxide if we compare the reduced parameters as suggested by Goldschmidt[18] for Fe_3O_4 (2.803Å) with that for Fe (2.86Å) and that for FeO (2.86Å).

Unfortunately, it is very difficult to make precision measurements of these thin oxide films by electron diffraction and especially so if the lines are very diffuse. A comparison of the Fe_3O_4 parameters of a number of depressed transformations reveals consistently higher values. The magnitude of the effect, 1 to 3 pct, is within the range expected. However, the diffraction data give values for a_o which are a function of the radii of the diffraction ring. Further experimental work is necessary to show the effect conclusively.

Interpretation of Depressed Transformation Temperature

The fact that the transformation of Fe_3O_4 to FeO occurs at or near 570°C indicates that the reaction follows the equation $Fe_3O_4 + Fe \rightleftarrows 4FeO$ and the depression of the equilibrium temperature must result from a change in free energy of either FeO or Fe_3O_4 in thin films when present on iron as compared to their normal values. The extent of this free energy change can be evaluated from fig. 1. Table III shows the free energy change necessary to account for the depressed transformation temperature. At 400°C, for example, this value is 1940 cal per mol.

It is interesting to speculate on the sources of this amount of energy. The following reasons may be suggested: (1) Differences in the surface free energy associated with the transformation of small crystallites of Fe_3O_4 to FeO, (2) the greater degree of unmatching of the Fe_3O_4 lattice with the Fe lattice than for FeO, (3) the effect of composition of the FeO and Fe_3O_4 phases on the free energy and the effect of film thickness on the composition, and (4) the concentration of impurities in the surface films forming different oxides or solid solutions with FeO or Fe_3O_4.

Let us consider each of these reasons in turn. (1) Crystal size may explain not only the depressed transformation temperature, but also the effect of film thickness, since the crystallites are found to grow as the oxide thickens.[19] However, crystal size does not explain the increase in lattice parameters and the orientation effects. (2) Traces of impurities may concentrate in the surface layer if the oxide is formed under vacuum conditions. However, spectroscopic analysis does not reveal such a concentration. A comparison of the results of freshly abraded samples with those which have been oxidized and repolished many times shows no difference in behavior. In addition, the additional impurities pres-

Table III. Free Energy Associated with Lowered Transformation Temperatures

Transformation Temperature, °C	Free Energy Cal per Mol
400	1,940
450	1,422
500	778
550	150
570	0

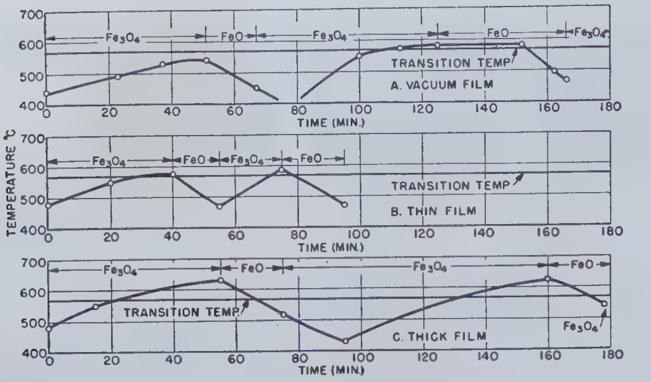

Fig. 4—Effect of film thickness on transformation temperature.

A. Vacuum formed film. B. Thin film (300°C 1 mm O_2 1 min). C. Thick film (550°C 1 cm O_2 30 min).

ent in Armco iron do not affect the results. (3) The effect of composition of the Fe_3O_4 on the transformation is impossible to predict because the essential thermodynamic data are lacking. (4) The most plausible explanation which fits the observed facts is that the Fe_3O_4 which forms in the first few layers is in a strained state due to the underlying iron lattice. Since the Fe_3O_4 cannot match the Fe as well as the FeO, an extra strain energy exists in the thin film of Fe_3O_4 relative to its value in the bulk state.

The strain energy is a positive free energy term and will act to give a lower equilibrium temperature for the transformation. As the oxide layer thickens the influence of the underlying iron lattice becomes less important and the strain energy approaches zero with a normal transformation occurring.

The lack of orientation or preferred growth of the Fe_3O_4 formed during the initial film formation is of interest. It should be realized that the abraded surfaces used consist of a highly broken down structure of Fe and it is not expected that the orientation relationships observed by Mehl and McCandless[20] for FeO on Fe single crystals would show up in our diffraction patterns.

Bénard[21] has suggested that two factors determine the orientation relationships of the oxide to the metal. These are: (1) The conservation of the planes of greatest atomic density, and (2) the conservation of close to identical repeat distances in the two lattices. Further studies are contemplated using single crystals of iron of known orientation.

Nature of Forward Transformation—Effect of Film Thickness: In a previous study[1] data were presented on the kinetics of the reduction of the higher oxides Fe_3O_4 and α-Fe_2O_3 when present in the outer layers of a thick oxide film consisting mainly of FeO. Iron atoms from the underlying metal were shown to diffuse through the FeO and react with the Fe_3O_4 forming additional FeO. A similar mechanism probably accounts for the forward transformation on heating a film of Fe_3O_4 through its transformation temperature of 570°C, except that initial FeO is not present. In this section the effect of film thickness on this forward transformation will be studied, and how such information explains the observed oxide structures in the temperature range of 570° to 650°C.

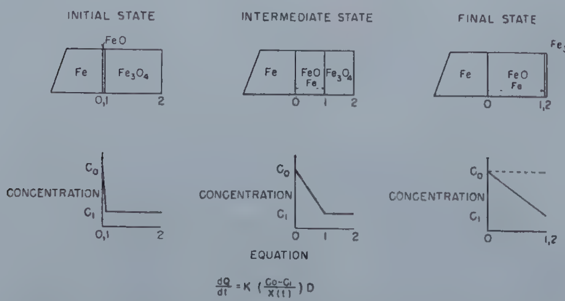

Fig. 5—Mechanism of $Fe + Fe_3O_4 \rightleftharpoons 4FeO$ reaction on pure iron in vacua.

Fig. 4 shows the observed structures of several oxide films when heated and cooled at a constant rate through the transformation temperature. The following oxide film thicknesses are used for the study on Puron: (1) A vacuum-formed film, (2) a thin film formed by oxidizing at 300°C and 1 mm of O_2 for 1 min, and (3) a moderately thick film formed by oxidizing at 550°C in 1 cm of O_2 for 30 min. The specimens are heated separately in the camera at a rate of 1° to 3°C per min with the diffraction patterns being observed visually on the fluorescent screen. Photographs of the patterns are taken at the points marked on the figure.

Part *A* of fig. 4 shows the forward transformation occurring at 540°C for the vacuum film on the first heating cycle and 570°C on the second heating cycle.

Part *B* shows that for thin films the transformation to FeO occurs at 575°C. A second heating cycle gave identical results.

Part *C* of fig. 4 shows that for a moderately thick film the transformation occurs at a temperature of 630°C for both the first and second heating cycles.

These experiments show that time and temperature are the important variables in the forward reaction. Thus, a thick film requires a longer time for transformation than a thin film at 570°C. A diffusion picture appears to be consistent with the facts.

Mechanism of the Forward Transformation

Fig. 5 shows one interpretation of the mechanism for the forward reaction. The conditions existing in the film at the start of the reaction are shown at the left in the figure. FeO is assumed to form at the Fe-Fe_3O_4 interface. This new interface of FeO-Fe_3O_4, shown at (1) in the figure, moves across the FeO film until reaction is complete. The kinetics of this phase transformation may be governed either by the diffusion of iron through the new phase to the old or by the nucleation and growth of the new phase. Since 8 unit cells of FeO[18] can be derived from the Fe_3O_4 unit cell by a rather simple process of shifting of some ions and electrons and the addition of 8 Fe ions to the original Fe_3O_4 unit cell, this process should occur readily and with a low energy of activation.

If we assume that the transformation is under diffusion control, then the quantity dQ of Fe_3O_4 transformed in a time interval dt is

$$\frac{dQ}{dt} = \frac{K(C_o - C_1)\,D}{X(t)}$$

Here $X(t)$ is the thickness at time, t; D is the diffusion constant; K is a dimensional constant; and C_o and C_1 are the concentrations of iron vacancies in FeO in equilibrium with Fe and Fe_3O_4, respectively.[15]

The rapid forward transformation is due to two facts, first, the quantity of Fe_3O_4 necessary to trans-form is small and second, the rate $\frac{dQ}{dt}$ is large since the expression $\frac{C_o - C_1}{X(t)}$ is large. For thick films the transformation is slower since $X(t)$ is large and therefore $\frac{C_o - C_1}{X(t)}$ is small and the quantity of Fe_3O_4 to be transformed is larger.

The concentrations C_o and C_1 vary with temperature and are given by the iron-oxygen diagram.[15] The influence of the term $(C_o - C_1)$ increases as the temperature is raised above the eutectoid. The increased velocity of transformation is due to the temperature effect on $(C_o - C_1)$ and on D.

The above mechanism adequately explains the fact that Fe_3O_4 is the main constituent of thick films at 650°C as observed by Tesche[5] and Bénard,[6] since for short oxidation times the solid phase reaction has not had time to occur, as well as the fact that electron diffraction studies on thin films show Fe_3O_4 transforming to FeO at 570°.

Nature and Mechanism of the Reverse Transformation: The reverse transformation or decomposition of FeO on Fe to form Fe_3O_4 and Fe is a complex reaction and occurs by the reaction $4FeO \rightleftarrows Fe_3O_4 + Fe$. We have noted in the "Literature Survey" that in both thick and thin films the reaction requires a definite undercooling ΔT before reaction. In this section we will study the products formed in the transformation for both thick and thin films and the kinetics of the transformation as a function of time, temperature, cooling rate, film thickness, composition of the oxide, and oxygen pressure.

Products Formed

Both Fe_3O_4 and Fe should be formed during the reverse transformation or decomposition of FeO. However, the diffraction patterns obtained for thin and moderately thick oxide films do not usually show the Fe structure. It was noted that a thick oxide film formed at 700°C by oxidation for 10 min with 1 cm of O_2 will give a pattern of Fe before Fe_3O_4 appears when cooled at a rate of 10°C per min for the first time. However, subsequent heating and cooling cycles show no evidence for the Fe structure.

Fig. 6 shows an example of this effect. Fe is first observed with FeO at 442°C and Fe_3O_4 finally appears at 402°C. Upon heating the Fe lines persist even after transformation to FeO has occurred. These lines disappear upon further heating. Vacuum oxidation probably plays a part in this disappearance.

Similar results are obtained for a film formed at 500°C for 1 min and 1 cm of O_2 when heated to 590°C and then cooled. Fe lines are observed upon slow cooling together with FeO and Fe_3O_4 at 488°C. A second heating and cooling cycle does not show this effect.

Kinetics

Chaudron and Bénard[11] have used two factors to characterize a decomposition reaction of this type. These are: (1) The undercooling, ΔT, at which temperature the reaction proceeds, and (2) the rate of decomposition. We feel that three factors should be used: (1) The temperature, (2) the time for onset of the reaction at the particular temperature, and (3) the time for completion of the reaction. This breakdown has several advantages: (1) The undercooling ΔT as expressed by Chaudron and Bénard[11] is effected by the cooling rate, and (2) the temperature and time for onset of reaction gives additional information on the reaction. Reactions will proceed at temperatures considerably higher than the ΔT at which reaction proceeds rapidly on direct cooling if sufficient time is allowed for the reaction to start.

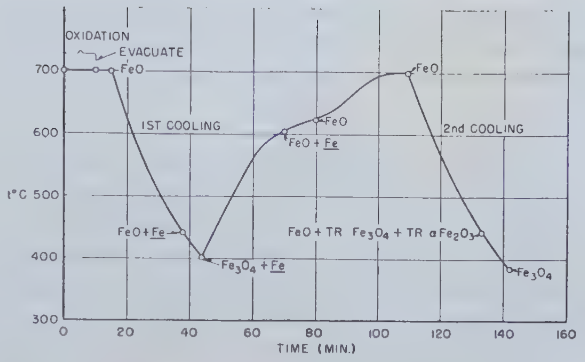

Fig. 6—Formation of Fe in reverse transformation.
Thick film (700°C 10 min, 1 cm O_2).

No method has been proposed which can study the kinetics of reactions occurring within the oxide film when present on a metal. However, the electron diffraction method can give useful information on the kinetics of the reaction, if we assume that the surface sampling is typical of the film as a whole. The method is limited also by the fact that the presence or absence of a second phase can only be determined when present to the extent of 5 to 10 pct.

Effect of Oxygen Pressure on the Direct Undercooling ΔT for Transformation: The atmosphere surrounding the specimen may affect the degree of undercooling ΔT and the rate of transformation in two ways. (1) The oxygen may oxidize the FeO to Fe_3O_4. This reaction is possible thermodynamically at temperatures up to 1000°C. The Fe_3O_4 thus formed gives a false picture that transformation had occurred internally. (2) The oxygen pressure may affect the nucleation and growth centers for Fe_3O_4 by its action on the number of vacancies in the FeO lattice.

We have studied the effect of low-oxygen pressures on the undercooling ΔT for a moderately thick film (500°C, 1 cm O_2, 1 min) and for a thick film (700°C, 1 cm O_2, 10 min). The moderately thick films are heated to 700°C before cooling, while the thick films are held at 600°C for 2 hr. The temperature for the start of transformation is used to

Table IV. Effect of Oxygen Pressure on FeO-Fe_3O_4 Transformation Temperature Cooled at Rate of 10°C per min

Oxygen Pressure, mm of Hg	Transformation Temperature, Start, °C
A. Initial Film (1 cm of O_2, 550°C and 11 min) Heated to 750°C	
1.6×10^{-3}	630
0.85×10^{-3}	604
0.5×10^{-3}	595
0.18×10^{-3}	574
0.015×10^{-3}	444
B. Initial Film (1 cm of O_2, 700° and 10 min) Heated to 600°C for 2 hr	
3×10^{-5}	502
1×10^{-5}	472
3×10^{-6}	300

Table V. Effect of Film Thickness on Time for Onset and Completion of Reverse Transformation at 500°C

Oxidation Conditions of Film	Vacuum Conditions During Experiment, mm of Hg	Time for Onset, Min	Time for Completion, Min
A. Vacuum formed oxide ($2x10^{-5}$ mm of Hg)	$2x10^{-5}$	No transformation as FeO is stable phase	
B. Thin film 305°C 1 min 1 mm ofO_2	$1x10^{-5}$	500 to 1,000	Less than 500
C. Thick film 700°C 10 min 1 cm of O_2	$1x10^{-5}$	75 70	25 20

evaluate ΔT. Table IV shows the results. Fe_3O_4 is observed to form at temperatures well above 570°C which indicates that the oxidation reaction is occurring.

For low-oxygen pressures where ΔT is positive, we cannot prove that the increase in ΔT for reaction is due to either the effects of the oxidation reaction or to the change in nucleation and growth factors in the formation of Fe_3O_4. In any case the transformation characteristics are sensitive to the oxygen pressure and this factor must be carefully controlled.

Effect of Film Thickness: Table V shows a comparison of the transformation factors of a vacuum-formed film with a thin oxide and a thick oxide film. The comparison is made at 500°C of the time for onset of transformation and time for completion of transformation. These and other experiments show that the transformation factors are strongly affected by the film thickness with the thin films being the most stable to decomposition. Fig. 5 shows a time-temperature-structure plot of part *B* of table V. The time scale is logarithmic.

Effect of Cooling Rate on Degree of Undercooling ΔT: Since Chaudron and Bénard[11] have indicated that the value of ΔT is one of the characteristic factors for reaction, it is of interest to study ΔT as a function of the cooling rate for a constant vacuum condition of $1x10^{-5}$ mm of Hg. If the thin film specimen shown in part *B* of table V is cooled very slowly, the transformation occurs at a temperature of about 500°C. However, the film transforms at 470°C when cooled at a rate of 5°C per min and at 418°C when cooled at 11°C per min. Similar results are observed with thick films.

Table VI. Effect of Temperature on the Time for Onset and Completion of the Reverse Transformation

Initial Oxidation 700°C, 10 min at 1 cm of O_2
Samples Cooled to Temperature at Rate of 11°C per min

Temp, °C	Time for Onset at Temperature, min		Time for Completion, min
1. Heated to 750°C before cooling. Vacuum, $2x10^{-5}$ mm of Hg			
540	95	α-Fe_2O_3 appears before Fe_3O_4	225
540	100	α-Fe_2O_3 appears before Fe_3O_4	1,270
500	46		50
500	75		25
500	70		30
475	10		30
475	20		20
470	15		10
420	0		5
390	0		4
2. Heated to 600°C for 5 min before cooling. Vacuum, $2x10^{-5}$ mm of Hg			
470	15		15
3. Heated to 600°C for 120 min before cooling. Vacuum, $2x10^{-5}$ mm of Hg			
470	20		20

These results have two explanations. First, the effect is one of time for nucleation to start at a given temperature, the slower cooling rates favoring the starting of the reaction at a higher temperature. Second, the effect is due to reaction with the oxygen or water vapor present in the vacuum which is a function of time and temperature. In general, we favor the former explanation.

Effect of Temperature on the Time for Onset and Completion of the Reverse Transformation: The relationships between the times for onset and completion of the decomposition are studied for several temperatures and a vacuum of $2x10^{-5}$ mm of Hg. The data are obtained by reheating successively this specimen to 750°C before cooling or to 600°C for 5 or 120 min before cooling. The specimens are cooled to the given temperature at a rate of 11°C per min. The time for onset and for completion is studied visually on the fluorescent screen. It is noticed that there is a trend in the data as a function of the number of cooling cycles. However, reproducible results are achieved after 10 coolings.

Table VI shows the results. The times noted are subject to the experimental errors inherent in observing the appearance or disappearance of a second phase by diffraction methods.

At temperatures above 500°C the reaction has a long induction period and the time for completion of the reaction is very long. However, at 420°C the transformation has a very short induction period and is complete in 5 min. These results are in essential agreement with the work of Chaudron and Forestier[9] on the decomposition of bulk samples. Also the results show the value of using the three factors to characterize a reaction of this type.

Effect of Composition of the Oxide on the Reverse Transformation: In a recent work, Chaudron and Bénard[11] have studied, using the thermomagnetic method, the effect of composition on (1) the temperature for onset of transformation and (2) the rate of the reverse transformation. Unfortunately details of the rate of cooling are not given.

It is of interest to note that Chaudron and Bénard's[11] curves show that FeO rich in oxygen has the lowest temperature (greatest ΔT) for onset of transformation and the largest rate of reaction.

In the presence of Fe and high vacua it is not possible for us to prepare and maintain FeO with oxygen concentrations higher than the eutectoid (76.85 pct Fe, Bénard[15]). A preliminary study of the composition effect can be made by comparing the transformation characteristics for two iron-oxygen ratios on the iron side of the FeO range of stability. These compositions are (1) FeO in equilibrium with Fe at 700°C (77.8 pct Fe) and (2) FeO in equilibrium with Fe at 600°C (77.2 pct Fe). To compare the results with those of Chaudron and Bénard[11] we have chosen to observe the temperature for onset of the transformation using a cooling rate of 11°C per min.

Table VII shows the results. The specimen of Puron is given an initial oxidation at 700°C for 10 min at 1 cm of O_2. To insure equilibrium with the iron the specimens are held at the temperatures of 700° and 600°C for 1 or 2 hr. An analysis of previous data[1] indicates that equilibrium is attained at 700°C in a few minutes and at 600°C in 2 hr.

It will be noticed in table VII that the temperature of onset of transformation decreases with the number of heating and cooling cycles until cycle 10 is reached. It is seen that cycles No. 10, 11 and 13 (sample held at 600°C) show a temperature for onset of transformation of 320° to 335°C while those held at 700°C (12 and 14) show a temperature of 372° to 378°C. The oxides richest in iron (700°C) show a higher temperature for onset of transformation and those specimens also require a somewhat greater temperature interval to complete the transformation than do the oxides somewhat poorer in iron (600°C).

Table VIII shows the results of the effect of composition on the time for onset and time for completion of the reverse transformation at a temperature of 450°C. It is seen that the oxide richest in iron nucleates a little more readily than the oxide a little poorer in iron. The time for completion of the reaction is approximately the same for both compositions. These results are in agreement with those shown in table VII.

The effect of composition on the temperature for onset or the time for onset of transformation are in general agreement with the observations of Chaudron and Bénard.[11] However, no agreement is found for the effect of composition on the rate of the transformation.

Criticism may be directed against both the electron diffraction and the thermomagnetic methods. First the electron diffraction method may not indicate the nature of the reaction in the bulk of the oxide. Also, due to the limitations on the rate of cooling, 11°C per min, the composition of Fe in the 700°C run may be somewhat lower than 77.8 pct. Second, we feel that the thermomagnetic method may not give the complete picture for the following reasons: (1) The magnetic separation of Fe_3O_4 from FeO may not be complete in the sense that small nuclei of Fe_3O_4 may remain within the FeO particles, and (2) the iron nuclei which form on cooling may be of different size and thus give a different magnetic behavior. The magnetic properties of Fe are known[22] to be a function of the particle size below 100Å. Since Fe nuclei are not usually observed, the size of the particles may be near the region where the magnetic properties depend upon the size.

Mechanism of the Reverse Transformation: Any mechanism suggested for the decomposition of FeO in oxide films when present on iron must explain the products and structures formed in the reaction and the kinetic observations. Two mechanisms may account for the fact that Fe is not usually observed during the transformation except in the initial cooling of thick oxide films: (1) The Fe crystallizes in extremely small particles of the order of 5 to 50Å in diam and these then grow very slowly giving incoherent diffraction patterns, and (2) supersaturation of Fe occurs in the FeO lattice which not only takes up some of the Fe but also permits the Fe to be transported to the metal interface forming new metal.

The following evidence favors the former mechanism: (1) The kinetics may be explained by a nucleation and growth process, (2) a micrographic study by Chaudron[23] of the decomposition of FeO on Fe shows Fe precipitating at the grain boundaries of the oxide and not at the metal interface, and (3) the appearance of a diffraction pattern of iron after cooling for the first time an oxide film after equilibrating with Fe at 700°C.

Table VII. Effect of Oxide Composition on Reverse Transformation Temperature

Initial Oxide Formed at 700°C. Vacuum, 3×10^{-6} mm of Hg

Cooling Cycle No.	Precooling Conditions, °C	Temperature for Onset, °C	Temperature for Completion, °C
4	2.6 hr at 700	460	398
7	2 hr at 700	402	315
10	2 hr at 600	320	290
11	1 hr at 600	335	290
12	2 hr at 700	378	325
13	1 hr at 600	335	290
14	1 hr at 700	372	325

The evidence favoring the diffusion mechanism is the recent unpublished work of Richardson[24] on the mechanism of reduction of the oxides on Fe between 700° and 900°C. Here, the Fe freed in the reaction, is transported through the oxide to form a new metal phase. However, this mechanism cannot interpret the kinetic data on the decomposition.

The formation of α-Fe_2O_3 in some of the decompositions is interesting since this reaction is also possible thermodynamically. It may indicate that a small amount of oxidation is occurring in the vacuum of the camera, especially of particles in poor contact with the oxide film.

The most plausible explanation of the reverse transformation is a process of nucleation and growth of Fe and Fe_3O_4 particles. Under certain conditions the nucleation and growth of Fe_3O_4 is the rate controlling process. However, the more usual case is that the Fe nuclei are controlling the rate of transformation for two reasons: (1) The Fe nuclei represent only 13 pct of the original oxide volume and are of a smaller size, requiring a larger amount of energy to form, and (2) interchange between FeO and Fe_3O_4 may occur readily due to similarity in lattice structures.

The theory of nucleation and growth has been developed by Volmer and Weber[25] and by Becker[26] and applied to metal systems by Mehl and Jetter.[27] A summary of the theory as applied to the decomposition of FeO will be given assuming that the nucleation and growth of Fe is the rate governing process. Similar equations would apply to a system in which the rate governing process is the nucleation and growth of Fe_3O_4.

The free energy required to form an Fe nucleus of radius, r; area, A; and volume, V; in the Fe_3O_4 film is given as the sum of two terms if no elastic stresses are present.

$$\Delta F = 4\pi\, r^2\sigma + 4/3\,\pi r^3\,\Delta f \qquad [1]$$

Table VIII. Effect of Oxide Composition on Time for Onset and Completion of Transformation

Initial Oxide 700°C, 10 min 1 cm of O_2. Vacuum, 3×10^{-6} mm Hg

Precooling Conditions	Time for Onset, min	Time for Completion, min
A. 700°C 1 hr		
Cooled to 458°C in 22 min Held at 450°C 77.8 pct Fe	128	30
B. 600°C 1 hr		
Cooled to 458°C in 18 min Held at 450°C 77.2 pct Fe	162	33

Here Δf refers to the free energy increase per unit volume and σ the interfacial energy.

The maximum value of

$$\Delta F = 16\pi\sigma / 3\Delta f \qquad [2]$$

for regions of radius

$$r_{\max} = - 2\sigma/\Delta f \qquad [3]$$

The rate of nucleation (N) of the iron crystals is given by

$$N = Ke - \frac{(\Delta F_{\max} + Q)}{RT} \qquad [4]$$

Here Q is the activation energy for the process of adding or removing one atom from the nucleus. Q is nearly independent of temperature, while $\Delta F_{\max}$ decreases with the degree of undercooling, since Δf increases with the degree of undercooling. The rate of nucleation is a maximum at a temperature $0 < T < T_e$ where $(\Delta F_{\max} + Q)/RT$ is a minimum. T_e is the equilibrium temperature.

Since the amount of Fe freed during the transformation is a function of the thickness, it is probable that the size of the nuclei which can form will depend upon the thickness for thin films. Above a certain thickness this effect will be small. By eq 3, the value of Δf must be larger for the nucleation of Fe in thin films than for thick films. Since Δf is a function of the degree of undercooling, ΔT, the reverse transformation occurs only at a temperature well below the equilibrium value.

The effect of composition is interesting in relation to the nucleation and growth theory. It may be expected that an oxide rich in Fe should nucleate more readily than for an oxide rich in oxygen. This is observed experimentally here and by Chaudron and Bénard.[11] The rate of nucleation and growth of Fe and Fe_3O_4 should not appear to be a strong function of the composition since the oxides after initial nucleation of Fe and Fe_3O_4 are of nearly the same composition if we assume that the first iron saturates the lattice rapidly.

Summary

Three problems are considered in this work: (1) The nature of the depressed transformation temperature for the $Fe_3O_4 + Fe \rightleftharpoons 4FeO$ reaction in extremely thin oxide films, (2) the nature of the transformation of Fe_3O_4 to FeO at or near 570°C, and (3) the nature and mechanism of the slow reverse transformation of FeO to Fe_3O_4 below 570°C.

Electron diffraction studies show that the forward and reverse transformations of $Fe_3O_4 + Fe \rightleftharpoons 4FeO$ may occur below 570°C for thin films and that FeO may exist as a result of thin film oxidation at temperatures as low as 400°C. This depressed transformation temperature is characteristic only of thin oxide films and subsequent vacuum oxidation during reheating of the specimens gives the normal or closer to normal transformation temperatures. It is to be noted also, that the lattice parameter of the initially formed oxide is greater than normal which indicates that the oxide is in a strained state. It is concluded that the depressed transformation may be due to the strained state of the Fe_3O_4 in attempting to match the repeat distance in the underlying Fe lattice.

Kinetic studies are made of the $Fe_3O_4 + Fe \rightleftharpoons 4FeO$ reaction at temperatures of 570° to 630°C for thin and thick films. A rapid reaction is found for thin films and a slow reaction for thick films. The mechanism of this transformation can be expressed by a simple diffusion picture of Fe ions diffusing through the FeO already formed to reduce the Fe_3O_4.

Studies on the reverse transformation $4FeO \rightleftharpoons Fe_3O_4 + Fe$ indicate a slow reaction for thin and thick films with a considerable degree of undercooling necessary for reaction. Three factors are used to characterize the transformation: (1) The temperature, (2) the time at this temperature for the onset of decomposition, and (3) the time at this temperature for completion of the reaction.

The kinetics of the transformation are studied as a function of time, temperature, and composition of the oxide. A process of nucleation and growth of Fe and Fe_3O_4 crystals in the oxide lattice is suggested as a possible mechanism for the reaction. Rate expressions are suggested following the theories of Volmer and Weber and of Becker. The free energy required to precipitate the small Fe or Fe_3O_4 nuclei is obtained by a large degree of undercooling.

References

[1] E. A. Gulbransen and R. Ruka: *Industrial and Engineering Chemistry.* (in press).

[2] H. R. Nelson: *Journal* Chem. Physics (1938) **6**, 606.

[3] R. Jackson and A. Q. Quarrell: Iron and Steel Institute. Special Report No. 24, (1939) 65-104.

[4] E. A. Gulbransen and J. W. Hickman: *Transactions* AIME (1947) **171**, 306; *Metals Technology* (Oct. 1946) TP 2068E.

[5] O. A. Tesche: Preprint No. 12, Fall Meeting, Amer. Soc. Metals. (1949).

[6] J. Bénard: *Journal* de Chemie Phys. et de Physico-Chim. Biolog. (1947) **44**, 266-268.

[7] G. Chaudron: *Compt. Rendu* (1921) **172**, 152.

[8] G. Chaudron: *Ann. de Chemie* (1921) **16** (9), 221.

[9] G. Chaudron and C. R. Forestier: *Acad. Sci.* (1924) **178**, 2173.

[10] J. Bénard and G. Chaudron: *Compt. Rendu* (1936) **202**, 1336.

[11] G. Chaudron and J. Bénard: Colloque Etat Solide, Paris, and *Bull.* Soc. Chim. France. D 88-90 (1949).

[12] J. Chipman and J. W. Murphy: *Industrial and Engineering Chemistry.* (1933) **25**, 319-327.

[13] L. S. Darken and R. W. Gurry: *Journal* A.C.S. (1946) **68**, 798.

[14] L. S. Darken and R. W. Gurry: *Journal* A.C.S. (1945) **67**, 1398-1412.

[15] J. Bénard: Colloque Etat Solide, Paris, and *Bull.* Soc. Chim. France. D 73-87 (1949).

[16] E. A. Gulbransen: *Journal* Applied Physics. (1945) **16**, 718-724.

[17] E. A. Gulbransen: *Review of Sci. Instruments.* (1947) **18**, 546-550.

[18] H. J. Goldschmidt: *Journal* Iron and Steel Institute. (1942) **146**, 157-180.

[19] E. A. Gulbransen: Unpublished Electron Microscope Studies.

[20] R. F. Mehl and E. L. McCandless: *Transactions* AIME (1937) **125**, 531; *Metals Technology* (Feb. 1937) TP 780C.

[21] J. Bénard: *Bull.* Soc. Chim., France. M 511-521 (1946).

[22] K. R. Dixit: *Physik. Ztschr.* (1938) **39**, 580-582.

[23] G. Chaudron: *Proceedings* Pittsburgh International Conference on Surface Reactions, p. 165-167 (1948). Corrosion Publishing Co., Pittsburgh, Pa.

[24] F. D. Richardson: Private Communication.

[25] M. Volmer and A. Weber: *Ztsch. Physik. Chem.* (1926) **119**, 277-301.

[26] R. Becker: *Ann. der Physik* (1938) **32** (5), 128-140.

[27] R. F. Mehl and L. K. Jetter: Symposium on Age Hardening of Metals. Amer. Soc. Metals (1939) 342-412.

aime NEWS

Annual Meeting Program Covers Wide Range of Metallurgical Subjects

The annual meeting of the American Institute of Mining and Metallurgical Engineers will be held at the Jefferson and Statler Hotels, St. Louis, Feb. 19 to 22, with the former as official headquarters. The Welcoming Luncheon, Smoker and Student Forum on Monday night, the Informal Dance, Tuesday night, and the Annual Banquet and President's Reception, Wednesday night, will be at the Jefferson. The Metals Branch and Petroleum Branch dinners on Tuesday night will be at the Statler. The Mining Branch, except for three sessions, at the Statler, will present its technical program at the Jefferson and the Metals and Petroleum Branches will hold their sessions at the Statler Hotel during the meeting.

The Council of Section Delegates will meet on Saturday and the Board of Directors will convene in general session on Sunday afternoon, at the Jefferson. The annual business meeting of the Institute will be on Tuesday afternoon. The Mineral Industry Education Div. will hold its usual Sunday sessions.

Whereas the technical program for Monday through Thursday still is in a state of flux and the meeting schedules shown here are tentative, there is a degree of fixation in that it has been necessary to assign rooms of appropriate seating capacities to sessions of anticipated attendances.

Metals Branch Activities

A Research in Progress Session of the Institute of Metals Div., such as proved so successful at the fall meeting, will be a feature of the annual meeting.

A feature of the Iron and Steel Div. program will be an all-day Symposium on Sulphur. While not completed, the following is a tentative lineup of the technical meetings.

Monday Morning—The Institute of Metals and Iron and Steel Divisions will each hold a joint technical session. For the Extractive Metallurgy Div. there will be two sessions: (1) Aluminum and Magnesium, and (2) Lead—Miscellaneous.

Monday Afternoon—The Institute of Metals and Iron and Steel Divisions will hold one session each. The IMD Membership Committee meets at 4:30 o'clock. Extractive Metallurgy Div. schedules a session: Zinc—Miscellaneous.

Tuesday Morning—Institute of Metals Div. and Iron and Steel Div. have one session each. The Howe Memorial Lecture will be delivered by J. R. Vilella, Research Laboratory, U. S. Steel Corporation of Delaware, at 11 o'clock. Extractive Metallurgy Div. has two sessions: (1) Titanium and Unusual Metals (continued in afternoon); (2) Symposium on Removal and Recovery of Zinc and Lead from Furnace Slag (continued in afternoon).

Tuesday Afternoon—Institute of Metals Div. and Iron and Steel Div. will hold one session each; and the Extractive Metallurgy Div. will continue its morning sessions.

Wednesday Morning—Institute of Metals Division will hold one session. The annual IMD lecture by G. Borelius, Royal Institute of Technology, Stockholm, Sweden, will be at 11 o'clock. The Iron and Steel Div. will have one session and the Extractive Metallurgy Div., two sessions: (1) Symposium on Electrolytic Zinc; (2) Copper—Cobalt—Miscellaneous.

Wednesday Afternoon—Institute of Metals Div. will have one session, another session will be held on Powder Metallurgy, and the Extractive Metallurgy Division will hold two sessions: (1) Symposium on Electrolytic Zinc; (2) Physical Chemistry of Extractive Metallurgy (continued Thursday morning and afternoon).

The Southwestern Section of the National Open Hearth Committee will hold its annual February meeting at the Lenox Hotel, followed by a dinner to which all Iron and Steel Div. members and their friends are invited.

Awards To Be Presented at the Annual Meeting

Charles F. Rand Medal to James Draper Francis.

William Lawrence Saunders Medal to Clyde Ewarts Weed.

Erskine Ramsey Medal to James B. Morrow.

Robert W. Hunt Medal to R. R. Webster and H. T. Clark.

C. H. Mathewson Gold Medal to C. S. Barrett.

Robert H. Richards Award to Frank R. Milliken.

Rossiter W. Raymond Memorial Award to A. J. Shaler.

J. E. Johnson, Jr. Award to Samuel Naismith.

Thursday Morning—Institute of Metals Div. and the Iron and Steel Div. have scheduled one session each. The Extractive Metallurgy Div. will hold one session: Physical Chemistry of Extractive Metallurgy.

Thursday Afternoon—The Metals schedule consists of one session for the Institute of Metals Div., a Powder Metallurgy seminar, and the concluding session of the EMD symposium on Physical Chemistry of Extractive Metallurgy.

Luncheons and Annual Dinner

Committee luncheons scheduled are:

Tuesday: Executive Committee, Institute of Metals Division.

Wednesday: Executive Committee, Extractive Metallurgy Division; Committee on Physical Chemistry of Steelmaking.

Thursday: Executive Committee, Iron and Steel Division; Powder Metallurgy Committee.

The Metals Branch dinner, preceded by a cocktail party, will be on **Tuesday** evening.

Woman's Auxiliary

The program of the Woman's Auxiliary includes their annual meeting on Tuesday morning, a round table discussion session on Wednesday morning and special social features that will be announced later.

Nominating Committee for AIME Officers in 1952

Names and addresses of the Nominating Committee for Institute officers for 1952 are given below, as provided in Article IX, Sec. 2, of the AIME bylaws. In each case, the name in parenthesis is that of the alternate, who will serve only in the absence of the principal at the meeting of the Committee, which will be held at St. Louis during the week of the Annual Meeting, Feb. 19 to 22, 1951.

Members designated by the Council of Section Delegates: W. L. Zeigler, general manager, Pend Oreille Mines and Metals Co., Metaline Falls, Wash. (Wallace G. Woolf, Box 209, Kellogg, Idaho); Henry T. Mudd, 1206 Pacific Mutual Bldg., Los Angeles 14, (James A. Kavenaugh, 950 N. Highland Ave., Los Angeles 38); Albert Mendelsohn, president and general manager, Cananea Consolidated Copper Co., Cananea, Son., Mexico (P. D. I. Honeyman, vice-president and general manager, Inspiration Consolidated Copper Co., Inspiration, Ariz.); Herbert M. Cooley, assistant metallurgical engineer, Bethlehem Steel Co., Box 2171, Tulsa 2, (P. P. Manion Jr., Stanolind Oil and Gas Co., Stanolind Bldg., Tulsa); Paul R. Turnbull, manager, drilling and production dept., La Gloria Corp., P.O. Box 779, Corpus Christi, Texas (M. D. Cooper, National Coal Assn., 5430 Aylesboro Ave., Pittsburgh 17); Philip D. Wilson, Lehman Bros., 1 William St., New York (James Douglas, Phelps Dodge Corp., 40 Wall St., New York 5); R. Schuhmann Jr., associate professor of process metallurgy, MIT, 77 Massachusetts Ave., Cambridge 39, Mass. (H. Rush Spedden, MIT, Cambridge 39, Mass.); Herbert R. Hanley, emeritus professor of metallurgy, Box 318, Rolla, Mo. (L. P. Davidson, Box 222, Monsanto, Ill.); Richard F. Miller, assistant to vice-president, research and technology, Carnegie-Illinois Steel Corp., 434 Fifth Ave., Pittsburgh 30 (John T. Ryan Jr., Mine Safety Appliances Co., 201 N. Braddock Ave., Pittsburgh 8); Harry M. St. John, superintendent, dept. 5, Crane Co., 4100 S. Kedzie Ave., Chicago 5 (Rudolph Tietig Jr., engineer, A. J. Boynton & Co., 58 E. Washington St., Chicago 2); E. D. Dickerman, 2251 S. Cook St., Denver 10 (C. L. Barker, 308 Jasmine St., Denver).

Members designated by the Branch Councils: S. J. Swainson, director mineral dressing laboratory, American Cyanamid Co., 1937 W. Main St., Stamford, Conn. (Veleair C. Smith, Kanawha Valley Bldg., Charleston, W. Va.); J. Murray Riddell, head, dept. of mining engineering, Michigan College of Mining and Technology, Box 144, Houghton, Mich. (Richard W. Smith, 1615 H St., N.W., Washington 6, D. C.); T. L. Joseph, assistant dean, Institute of Technology, University of Minn. School of Mines and Metallurgy, Minneapolis, Minn.; Lloyd E. Elkins, production research director, Stanolind Oil and Gas Co., P.O. Box 591, Tulsa 2, Okla. (R. C. Earlougher, 319 E. 4th St., Tulsa 3, Okla.)

Members designated by President McLaughlin: Clayton G. Ball, vice-president, Paul Weir Co., 20 No. Wacker Dr., Chicago 6, (Philip R. Bradley, Jr., president and general manager, Pacific Mining Co., 1022 Crocker Bldg., San Francisco); John R. Suman, vice-president and director, Standard Oil Co. (N. J.), 30 Rockefeller Plaza, New York 20, (Howard C. Pyle, president, Continental Consol. Corp., 1562 Razal Blvd., Glendale 7, Cal.); T. C. Federson, general superintendent, Bunker Hill Smelter, Box 29, Kellogg, Idaho, (John D. Sullivan, Battelle Memorial Institute, 505 King Ave., Columbus 1, Ohio).

The Committee will welcome suggestions for the official slate for 1952. The following offices are to be filled: President for 1952, President-elect (for 1953, two Vice-Presidents, and five other Directors. The terms of the following Directors expire in February, 1952; L. E. Young, A. B. Kinzel, Philip Kraft, H. W. Johnson, William J. Coulter, Erle V. Daveler, James L. Head, and George P. Swift. All are eligible for re-election.

Research In Progress Session Planned For Annual Meeting at St. Louis

The recent success scored at the IMD meeting in Chicago, guaranteed the continuation of the novel *Research In Progress Session* for the annual meeting in February. The past interest in this type of session indicates it may well become a regular feature of IMD meetings.

Abstracts for the *Research In Progress Session* for the annual meetings should be submitted to Thomas E. Lloyd, Editor, JOURNAL OF METALS, 29 West 39 St., New York 18, N. Y. by Dec. 18, and should be limited to about 150 words. The abstract should stress, without giving details of work, the project, line of work, and particularly its potential implications on future metallurgical, production, design, and equipment trends.

Business Meeting Scheduled

The Annual Business Meeting of the AIME will be held at the Hotel Jefferson, St. Louis, at 4 p.m. Tuesday, Feb. 20, 1951. Newly elected Directors and officers assume their duties at this meeting. A report of the financial condition of the Institute will be made, as well as reports of the principal officers and standing committees. All AIME members are invited to attend. Immediately afterward, at 5 p.m., the new Board will meet in executive session.

The Western Section, National Open Hearth Steel Committee, Iron and Steel Div., AIME, on a weekend trip to Las Vegas, Nev., visited plants of U. S. Limestone Corp. Thirty-three made the trip.

Engineering Groups Participate In Centennial Meeting and Exposition

Eleven American and one Canadian technical societies will participate in the international convocation to celebrate 100 years of engineering as an organized profession in the United States. This convocation, organized under *Centennial of Engineering, 1952, Inc.*, is designed to provide an opportunity for all engineers to exchange ideas and information. The American Society of Civil Engineers was formed in 1852, the first American engineering society.

Invitations have been extended to an additional 60 technical societies in this country and to appropriate societies of international scope, or of national scope in other countries. The international societies will be invited to hold their annual meetings in Chicago during the convocation from Sept. 3 to 13, 1952. Where it is not feasible for the societies of other countries to hold meetings in this country, it is hoped that they will send representatives to the convocation.

An important part of the celebration will be an exposition during July, August, and September, in 1952. It will be held at the Chicago Museum of Science and Industry. The show will be a pageant about America, how it grew and prospered over the years, and how it can continue to grow.

A permanent engineering exhibit will be built in the Museum, where it may be open to visitors in July, 1952, and during the years that follow.

Dues Payable Jan. 1, 1951

Pursuant to Article II, Section 2, of the bylaws of the AIME, notice is herby given that dues for the year 1951 are payable Jan. 1 as follows:

Members and Associate Members	*$20.00*
Junior Members for the first six years of Junior Membership	*12.00*
Junior Members, thereafter	*17.00*
Student Associates, including an annual subscription to a monthly journal	*4.50*
Student Associates, without journal subscription	*2.00*

Mailing of dues bills began in September and will be completed in December. Prompt payment will assure uninterrupted receipt of journals desired in 1951. If, for any reason, a bill is not received within a reasonable time after the last mailing date, Dec. 31, Institute headquarters should be notified.

25 Qualify for Legion of Honor

Just 25 AIME members qualify next year for the Legion of Honor, having been Institute members for 50 years. They are:

H. C. Boynton
Arthur C. Brinker
James F. Brophy
Donald G. Brown
George A. Camphuis
George L. Collord
Thomas Cox
J. V. N. Dorr
Lucien Eaton
John M. Fitzgerald
K. F. Goransson
B. Britton Gottsberger
Herbert R. Hanley
L. F. S. Holland
V. F. Stanley Low
W. T. MacDonald
E. A. Manners
Herbert A. Megraw
F. L. Morris
Horace Moses
Arthur C. Spencer
H. P. Townsend
Charles Henry White
Alexander N. Winchell
Lewis E. Young

They will be awarded a certificate and gold pin at the Annual Meeting, or later if they cannot be present on that occasion.

A. J. Shaler and C. S. Barrett Honored

A. J. Shaler, assistant professor on the MIT faculty, has been granted the Rossiter W. Raymond Memorial Award for 1951 for his paper: *"Seminar on the Kinetics of Sintering,"* published in the JOURNAL OF METALS, November 1949. The prize is given for the best paper published by an AIME member under 33 years old.

C. S. Barrett has been named as the first recipient of the recently authorized Mathewson Medal, which takes the place of the annual Institute of Metals Division award. The award is in recognition of the most notable written contribution to metallurgical science; it must have been published by the Institute as a Transactions paper in the three years preceding the granting of the award; and must have been presented at a meeting of the Institute of Metals Division. His paper was entitled *"Faults in the Structure of Copper-Silicon Alloys,"* and was published in the JOURNAL OF METALS for January, 1950.

AIME Bessemer Committee to Meet

The Bessemer Committee of the Iron and Steel Div, AIME, will hold an "off-the-record" meeting on Bessemer operating problems, Dec. 14, 1950, in the East Room of the Roosevelt Hotel, Pittsburgh, Pa. The tonnage of Bessemer steel is appreciable, both for duplexing and for Bessemer steel itself, and the meetings are of great value. The small attendance expected does not reflect upon the quality of the meetings, but rather on the limited number of Bessemer operators in the country. Any AIME Member who is interested in the program of the Bessemer meeting is invited to attend, in addition to those operators and metallurgists who normally attend these meetings.

The Bessemer Committee, under the chairmanship of Dan Loughrey, Supt. Open Hearth & Bessemer, Jones & Laughlin Steel Corp., Pittsburgh, is arranging a program that will be interesting and valuable to all persons interested in or operating Bessemer Converters. Serving on the Committee are: E. B. Speer, vice-chairman; S. J. Cresswell, S. J. Dougherty, H. C. Dunkle, K. L. Fetters, H. W. Graham, E. C. Penrod, E. B. Story, A. W. Thornton, F. L. Toy, and G. M. Yocom.

Topics that are expected to appear on the agenda are: Vessel linings and bottoms; Mixers; Iron Quality; Blowing; Use of oxygen for enriching the blast; Additions; Applications of acid Bessemer steel; Duplex process; Pouring practice; Quality and yield; Heating and soaking; and Dust control.

AIME Faces Deficit in 1950

Reviews of the financial position of the AIME in 1950, as made at recent meetings of the Directors, indicate that deficit of some $20,000 may be expected. The budget at the beginning of the year had been precariously balanced at $477,500, but in some instances income has been less than expected and expenses greater. Chief drop from expected income has been in advertising in the three journals, which had been budgeted at $125,000 and now promises to be about $105,000. Expense for the journals may be higher than expected, owing to increased printing and paper costs. The directory proved more expensive than anticipated. On the other hand, dues income has been higher than expected, and certain economies in administration and office practices have been attained.

Even with the publication of the directory this year, an expense not borne in 1949, the deficit promises to be reduced by some $50,000 from 1949 and by more than $60,000 from 1948.

IMD MEETS

Three days of technical meetings, climaxed by an annual dinner, were held by the AIME Institute of Metals Division during the 32nd National Metal Congress and Exposition, Oct. 23 to 27, in Chicago. Headquarters for the AIME activities were at the Sheraton Hotel, where some 450 registered for the AIME technical sessions.

Papers presented at the meeting dealt primarily with physical metallurgy (program and speakers were shown in JOURNAL OF METALS, October, pp. 1208 and 1209), and an unusual series of meetings were held on Research. Papers presented dealt with research projects not far enough along to warrant full scale summarizations, but upon which progress had been made. These Research in Progress sessions, arranged by Morris Cohen, Massachusetts Institute of Technology, vice-chairman of IMD Program Committee, may open a new type of session for the IMD meetings, bringing to the members a correlation of information that is helpful in other research.

Louis L. Thurstone, the Charles F. Grey Distin-

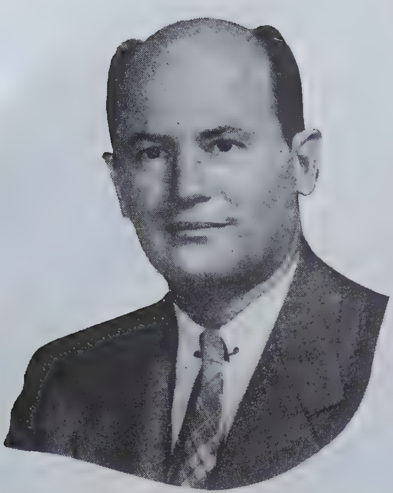
Morris Cohen, organizer of Research in Progress Session and the Panel Discussion Session.

Part of the speakers table (left) includes: L. L. Thurstone, guest speaker at the annual dinner; Maxwell Gensamer, IMD chairman and Toastmaster; A. E. Focke, ASM president, and W. M. Peirce, AIME Director. Below, another part of the table shows: Mr. Peirce, F. B. Foley, International Nickel Co.; A. B. Kinzel, AIME Director and President of Union Carbide and Carbon Research Laboratories, Inc., and E. O. Kirkendall, Secretary, AIME Metals Branch.

W. M. Peirce, New Jersey Zinc Co., Palmerton, Pa., and F. N. Rhines, Carnegie Institute of Technology, Pittsburgh.

H. M. Davis, Penn State College, State College, Pa.; J. C. Jones, Aluminum Transatlantic, Inc., New York; and Cyril Stanley Smith, Institute of Metals, University of Chicago.

IN CHICAGO

guished Service Professor of Psychology at University of Chicago, was the speaker at the annual dinner. Dr. Thurstone, speaking on: "Recent Studies of Intelligence and Personality," outlined the progress in educational work along the lines of psychological investigations, and illustrated many of the modern trends in thinking by educators in this field. M. Gensamer, chairman of IMD, was toastmaster at the dinner, and H. A. White, Chicago Section Chairman, introduced the speaker of the evening.

An informal panel discussion on precipitation hardening, arranged by Morris Cohen, had as experts B. L. Averbach, C. S. Barrett, W. L. Fink, A. H. Geisler, A. Guinier, J. H. Hollomon, R. F. Mehl, C. S. Smith, and C. Zener, playing before a full house. Discussions by the experts raised questions from the floor, and the popularity of the meeting tends to indicate a need for consideration of similar future panel groups. Following this meeting, an informal social meeting was held, with refreshments.

* * *

M. Gensamer, chairman of IMD and toastmaster at the Annual Dinner.

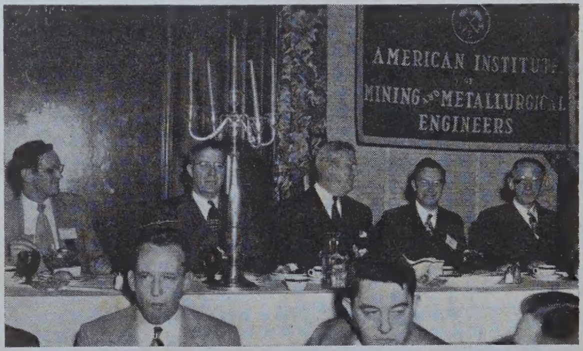
AMERICAN INSTITUTE OF MINING & METALLURGICAL ENGINEERS

At the speakers table, along with those shown at left, were: J. H. Reese, chairman of the Chicago Committee on Arrangements for the IMD meeting; H. K. Work, chairman of the AIME Iron and Steel Branch; Hjalmar Johnson, AIME Director; H. A. White, chairman of AIME Chicago Section; and Louis L. Thurstone, speaker.

R. E. Laub, Carnegie-Illinois Steel Corp., Gary; Hjalmar Johnson, Inland Steel Co., Chicago; Clyde Williams, Battelle Memorial Institute, Columbus, Ohio; and J. H. Reese, Revere Copper & Brass, Inc., Chicago.

R. H. Mehl, Carnegie Institute of Technology, Pittsburgh; and J. C. McDonald, Dow Chemical Co.

Members Automatically Become Affiliated With Local Sections

Many AIME members are not clear as to their affiliation with Local Sections of the Institute. In all, there are 43 Local Sections in the United States, and one each in the Philippines, Mexico, and Brazil. The only areas not included in Local Sections, as currently constituted, are New York State outside of a radius of 50 miles of New York City; a part of eastern Pennsylvania and southern Delaware, North and South Carolina, Iowa, Nebraska, North Dakota and the eastern part of South Dakota, and northern New Mexico.

An AIME member is automatically considered a member of the Local Section in whose territory he maintains a mailing address. Some Local Sections, however, have local dues, essentially to cover the cost of printing and mailing notices of meetings, and only those who pay these local dues are considered active members of the Section.

It happens that a member may be more interested in the programs of a neighboring Section, or may wish to receive notices of meetings of another Section. In such cases he may ask to join other Local Sections than his own. It is only necessary to write to the Secretary of the Section, whose name and address will be found on pages XXIV to XXXI of the 1950 Directory, and ask to be included in his mailing list.

FIELD TRIPS, 1951
AIME ANNUAL MEETING

Reservations will be limited to plant and transportation facilities. Reservations must be made immediately to assure a place on the trip. All trips will be on Friday, Feb. 23, and will take the entire day, except Trip No. 2, which will leave St. Louis 11:20 p.m. Thursday and return to St. Louis, Saturday, 7:25 a.m.

Trip No. 1 Lead Belt, Southeastern Missouri; mining, geology, and ore dressing; Bonne Terre and Flat River, Mo.

Trip No. 2 Tri-State Zinc District, Missouri, Kansas, Oklahoma; mining, geology, ore dressing, and lead smelting; Joplin, Mo., and Picher, Okla.

Trip No. 3 Zinc Smelters, horizontal retort and electrolytic smelting; Fairmont and Monsanto, Ill.

Trip No. 4 Midwest-Radiant Coal Mine and Washing Plant, Millstadt, Ill., and coking unit of Koppers Co., Granite City, Ill.

Trip No. 5 U. S. Bureau of Mines, synthetic fuels (oil from coal); Louisiana, Missouri.

Trip No. 6 Pittsburg Plate Glass Co., mine and plant (plate and safety glass); Crystal City, Mo.

F. N. Rhines Named Chairman Of IMD Auxiliary Publications Committee

The Auxiliary Publications Committee for the Institute of Metals Division has been appointed for the coming year. The committee consists of F. N. Rhines, Chairman; W. M. Baldwin, Jr.; C. S. Barrett; P. A. Beck; Morris Cohen; L. S. Darken; W. L. Fink; A. H. Geisler; B. W. Gonser; J. R. Low, Jr.; R. B. Mears; R. F. Mehl; C. S. Smith; T. A. Read; and J. F. Kuzmick. Members ex-officiis include M. Gensamer, Chairman, E. O. Kirkendall, Secretary, of Institute of Metals Division; and E. J. Kennedy, Jr., Secretary, AIME Technical Publications Committee.

Powder Metallurgists Meet in New York

Powder metallurgists in the New York area held an informal dinner and meeting on Oct. 4. Richard P. Seelig, chairman of the meeting, presented the Coffee speaker, George Cramer, a metallurgist at Oak Ridge. Mr. Cramer talked *"to the taxpayers present"* on powder metal activity in Oak Ridge and Los Alamos.

The speaker of the evening, E. Raymond Engstrand, American Sintered Alloys, Inc., Bethel, Conn., spoke on *"Metal Powders from the Fabricator's Point of View."* He described some of the difficulties of the producer in converting the metal powders supplied into parts. The talk resolved itself to how impossible it is to produce a perfect powder, and the speaker emphasized points where care must be exercised in handling powders and putting them to use.

Engineering Personnel Classified

Engineers Joint Control has recently completed a Survey of Selected Engineering Personnel made for the Dept. of Defense and handled by the American Society of Mechanical Engineers. Vol I of the survey outlines how the survey was made and the extent of the mailings in various localities, and Vol II shows definitions of occupational specialties in engineering. The purpose of the survey was to obtain a roster of senior engineers with their names and addresses, a record of each man's education, experience and competence; and definitions of engineering responsibilities.

AIME Directory Of Members

The Directory of Members of the AIME was sent to each Member, Associate Member, and Junior Member with the November issue of the magazine. While the cover of the Directory carries the name of the magazine, the complete roster of AIME members, regardless of Branch or Division affiliation, is contained in every Directory, regardless of its cover.

Proposed for Membership

Metals Branch AIME

Total AIME membership on Sept. 30, 1950, *was* 16,737; *in addition* 4,184 *Student Associates were enrolled.*

ADMISSIONS COMMITTEE

E. C. Meagher, Chairman; Albert J. Phillips, Vice-Chairman; George B. Corless, H. P. Croft, Lloyd C. Gibson, Ivan A. Given, F. W. Hanson, T. D. Jones, P. Malozemoff, Richard D. Mollison, and John Sherman.

Institute members are urged to review this list as soon as the issue is received and immediately to wire the Secretary's office, night message collect, if objection is offered to the admission of any applicant. Details of the objection should follow by mail. The Institute desires to extend its privileges to every person to whom it can be of service but does not desire to admit persons unless they are qualified.

In the following list C/S means change of status; R, reinstatement; M, Member; J, Junior Member; AM, Associate Member; S, Student Associate.

Colorado
Grand Junction—Son, Dorsey G. (M)

Illinois
Chicago—Gieselman, Richard F. (J) (C/S—S-J); Rosenqvist, Terkel N. (J); Witschey, Ray A. (M)
Hawey—Snow, Adolph I. (J)
Wilmette—Rudolphy, Edward C. (J)

Indiana
East Chicago—Kapitan, Josef S. (J); Seifko, Michael G. (M)
Warsaw—Bowen, Bernard D. (J) (C/S—S-J)

Massachusetts
Boston—Postlethwaite, Alan W. (J) (C/S—S-J)

Michigan
Dearborn—Cromwell, Dewitt P. (M)

Minnesota
Aurora—Morawski, Frederick P. (J) (C/S—S-J)

Missouri
Clayton—O'Meara, John (J) (C/S—S-J)
St. Louis—Donnell, Jess F. (M)

New Jersey
Asbury—Sjostrom, Robert A. (A)
Berkley Heights—Sloan, Arthur W. (M)
Englewood—Taylor, Neil R. (A)
South Orange—Grover, Clayton D. (M)

New York
Maspeth—Zysk, Edward D. (J) (C/S—S-J)
Hartsdale—Ydstie, Birger L. (J)
Larchmont—Marquis, Byron (M)
New York—Hambraeus, Gunnar A. (M); Nielsen, John P. (M) (C/S—A-M)

Ohio
Bowling Green—Winegartner, Edgar C. (J) (C/S—S-J)
Canton—Figeley, James G. (M)
Chagrin Falls—Peterson, Gustave A. (M)
Cleveland Heights—Manning, John T. (M)
Franklin—Gibbons, Vincent J. (M)
Lakewood—Varga, John Jr. (A)
Middletown—Komnenovich, Eli (M)

Oklahoma
Blackwell—Halfacre, Robert E. (J) (C/S—S-J)
Tulsa—Burke, John G. (M)

Oregon
Portland—Bates, James P. (M)

Pennsylvania
Duquesne—Wright, Ralston E. (M)
Haverford—Aksey, Alaettin M. (M) (C/S—A-M)
Homestead—Colledge, Floyd A. (M)
Monaca—Sevick, Joseph G. (J) (C/S—S-J)
Morgantown—Rodruan, Edgar A. (M)

Texas
El Paso—Howard, Edward E. (J)

Washington
Spokane—Hastings, Gordon R. (J)

Wisconsin
Madison—Monson, Leon A. (J) (C/S—S-J)

Australia
Newcastle—Bulter, Arthur K. (M)

Mexico
Mexico D. F.—Doerr, Karl P. (M) (C/S—A-M)

James L. Head

Library Board Elects Head Chairman

James L. Head, an AIME Director, has been elected chairman of the Library Board of United Engineering Trustees, which administers the Engineering Societies Library. He succeeds J. S. Thompson, who has just completed a two-year term. Frank T. Sisco, AIME, recently appointed as a member of the Board for a 4-year term ending in 1954, is chairman of the administrative committee of the Board, and James Douglas, also AIME, is on the budget committee.

All exchanges with the U.S.S.R. have been discontinued because of the irregular receipt of publications. Subscriptions have been placed for a few Soviet publications and the results are somewhat more satisfactory. Certain wanted publications from that country are unobtainable.

To the support of the library, the Founder Societies contributed $50,000. The AIME share for 1948 was about $12,400 and in 1949, $9300. However, about $3300 of this amount in each year was furnished by the James Douglas Library Fund, whose income is specially earmarked for this purpose. This left the net contribution by AIME in 1948 as $9114, and in 1949 $6049, or 59¢ and 37¢ per member, respectively.

Initiation Fee Payments

The $20 initiation fee required of applicants for Associate Membership and full membership in AIME may be paid in four annual instalments of $5 each. Junior Members do not have to pay any initiation fee; and application for such membership may be made at any time before one's 30th birthday anniversary. Junior Members may retain such status until their 33rd birthday anniversary, when they must become either Associate Members or Members. In either case they must pay the initiation fee; in $5 annual instalments if desired.